OPG's DEEP GEOLOGIC

REPOSITORY

FOR LOW & INTERMEDIATE LEVEL WASTE

Seismic Hazard Assessment

March 2011

Prepared by: AMEC Geomatrix, Inc.

NWMO DGR-TR-2011-20

amec

OPG's DEEP GEOLOGIC

REPOSITORY

FOR LOW & INTERMEDIATE LEVEL WASTE

Seismic Hazard Assessment

March 2011

Prepared by: AMEC Geomatrix, Inc.

NWMO DGR-TR-2011-20

THIS PAGE HAS BEEN LEFT BLANK INTENTIONALLY

Document History

Title:	Seismic Hazard Assessment		
Report Number:	NWMO DGR-TR-2011-20		
Revision:	R000	**Date:**	March 2011
AECOM Canada Ltd.			
Prepared by:	B. Youngs (AMEC Geomatrix, Inc.)		
Reviewed by:	G. Atkinson (University of Western Ontario)		
Approved by:	R.E.J. Leech		
Nuclear Waste Management Organization			
Reviewed by:	T. Lam		
Accepted by:	M. Jensen		

THIS PAGE HAS BEEN LEFT BLANK INTENTIONALLY

EXECUTIVE SUMMARY

This report develops design ground motions for Ontario Power Generation's (OPG) proposed Deep Geologic Repository (DGR) project at the Bruce nuclear site in the Municipality of Kincardine, Ontario. One important aspect of site evaluation is the assessment of the earthquake ground motions that could occur during the design/service life of the DGR. To provide adequate protection for the public and the environment, the DGR would be designed to withstand the effects of very rare events, including the occurrence of strong earthquake ground shaking at the site. A probabilistic seismic hazard assessment (PSHA) was conducted for the DGR that incorporates uncertainties in the models and parameters that affect seismic hazard. Guidance on conducting a PSHA, with the goal of capturing the knowledge of the informed scientific community regarding the inputs to the analysis, was provided in a landmark report by the Senior Seismic Hazard Advisory Committee (SSHAC). In the PSHA for the Bruce nuclear site, the interpretations of the larger scientific community were incorporated by way of review of the available literature, as well as correspondence with researchers to obtain unpublished data and observations in a SSHAC Level 2 process. The study for the Bruce nuclear site builds on both the 1997 PSHA sponsored by the Atomic Energy Control Board to characterize seismic hazards in southern Ontario and a recent PSHA conducted for the region surrounding the Darlington nuclear site for OPG.

In the PSHA for the Bruce nuclear site, future earthquakes that may affect the site are modeled using seismic sources. Seismic source characterization provides a probabilistic model for the rate of occurrence, spatial distribution, and size distribution of earthquakes within the region surrounding the site. The Bruce nuclear site lies in the stable continental region of eastern North America in an area of low, diffuse seismicity with no identified active faults. In such regions the primary data set used to develop a probabilistic model is the catalogue of regional earthquakes. The earthquake catalogue is limited by the duration of the sample (a few hundred years), and imperfect recording of past events, particularly in the period before the development of modern seismic monitoring networks. Thus, interpretations of other data, guided by scientific knowledge of the earthquake process, are used to extend the earthquake catalogue data to model the future occurrence of potentially damaging earthquakes in the site region. To do so, alternative models for the spatial distribution of future earthquakes are constructed based on interpretations of regions of the earth's crust that have homogeneous properties. These regions represent seismic sources in a PSHA.

The seismic source model developed for the Bruce nuclear site consists primarily of large regional seismic source zones used to model the occurrence of distributed earthquake activity. Uncertainty in characterizing the spatial distribution of future earthquakes within these sources was incorporated by the use of alternative source zone boundaries and spatial distribution models. In addition, the probabilistic model included a number of specific geologic/geophysical features that have been proposed in the scientific literature as potential active seismic sources. Most of these are located near the western end of Lake Ontario, but two of these, the Grenville Front tectonic zone and the Georgian Bay linear zone, extend closer to the site. A key uncertainty in the assessment of these potential local seismic sources is whether or not a source is seismogenic, defined as active and capable of generating moderate-to-large earthquakes. Multiple criteria, which include spatial association with seismicity and geologic evidence for brittle slip in the present stress/tectonic regime, are used to assess the probability that a source is seismogenic.

The results of the PSHA conducted for the Bruce nuclear site provide uniform hazard response spectra (UHRS) at the surface for a reference hard rock site. The UHRS were calculated for

annual exceedance frequencies (AEF) in the range of 10^{-2} to 10^{-8} (return periods of 100 to 10^{8} years). The regional source zones were found to be the dominant contributors to the hazard. The contribution of individual assessments to the uncertainty for various components in the seismic hazard computation was also examined. The results indicated that selection of the appropriate ground motion models is the largest contributor to the uncertainty in seismic hazard. The results of the PSHA are generally consistent with values published in the 2005 National Building Code of Canada (NBCC) when corrected to a common site condition and accounting for the differences in the selected ground motion models used in the two studies. The result of the PSHA indicate that the estimated ground motions at the surface on hard rock are expected to be less than 1.0g for annual exceedance frequencies of 10^{-5}, the reference case, and 10^{-6}, the extreme case. The following table summarized the results of the PSHA.

Annual Exceedance Frequency (AEF)	Peak Ground Acceleration on Hard Rock (%g)
1/1000	1.7
1/2500*	2.7
1/100,000	18.7
1/1,000,000	60.6

Note: * AEF for 2005 NBCC

Completion of the development of design ground motions involved translating the reference hard rock PSHA results to appropriate horizons within the proposed DGR in a manner that preserves the probabilistic levels assigned to each UHRS. A probabilistic model for site response was developed utilizing measured dynamic properties of the site geologic units. This model was then used to develop UHRS at the DGR level (depth 680 m) and at seven selected reference horizon levels between the surface and the repository. In addition UHRS were developed for the ground surface for three representative site conditions which reflect differences in the amount of surficial material that may be removed. These UHRS are provided for both horizontal and vertical motions.

The final task was to develop design time histories for the DGR and selected horizon levels. In order to represent the hazard with realistic earthquake motions, three earthquake scenarios were developed to represent the range of earthquakes contributing to the site hazard. Acceleration time histories were then spectrally matched to response spectra for these scenario earthquakes. The envelope of the response spectra for the three scenario earthquake time histories provides a good match to the DGR and horizon UHRS.

TABLE OF CONTENTS

LIST OF TABLES

Page

LIST OF FIGURES

Page

1. INTRODUCTION

Investigations are being conducted to confirm the suitability of the Bruce nuclear site in the Municipailty of Kincardine to safely host Ontario Power Generation's (OPG) proposed Deep Geologic Repository (DGR) for permanent storage of Low and Intermediate Level Waste (L&ILW). This report presents information for a seismic hazard assessment of, and the development of design ground motions for, the Bruce nuclear site.

1.1 Objectives

The scope of work for this study consisted of two tasks: (1) develop a seismic hazard model, and, (2) perform a probabilistic seismic hazard assessment (PSHA) to assess the ground shaking hazard at the Bruce nuclear site. A seismic hazard model was developed that involved compiling an earthquake catalogue for the region surrounding the site and identifying and characterising regional seismic source zones and local seismic sources. Hazard analyses were conducted for peak ground acceleration and response spectral accelerations covering the frequency range of importance.

The goal of all PSHAs should be to capture the state of knowledge of the informed scientific community regarding the inputs to the analysis. For the present study, the interpretations of the larger scientific community were incorporated through a review of the available literature, combined with correspondence with researchers to obtain unpublished data and observations. This study builds on the PSHA conducted for the Darlington nuclear site region for OPG. This study follows the guidance of the Senior Seismic Hazard Advisory Committee (SSHAC 1997), "Recommendations for Probabilistic Seismic Hazard Analysis: Guidance on Uncertainty and Use of Experts." Four levels of study for conducting a PSHA are defined by SSHAC (1997); required resources and the level of sophistication increase from Level 1 through to Level 4. A Level 2 PSHA was developed for this study in which a Technical Integrator (TI) team - the AMEC Geomatrix project team, led by Drs. Robert Youngs and Roseanne C. Perman - conducted a PSHA for the Bruce nuclear site based on all available information.

1.2 Document Structure

This report is organized into six parts, each of which addresses a separate aspect of demonstrating the feasibility of constructing a DGR at the Bruce nuclear site.

Chapter 1 – Introduction

This chapter presents the objectives of the study and describes the document structure.

Chapter 2 – General Site Description and Characteristics

This chapter gives a description of the Bruce nuclear site in terms of the location, tectonic setting, and regional seismicity. Included is a discussion of the use of earthquake catalogues in assessing earthquake occurrence rates.

Chapter 3 – Seismic Source Characteristics

This chapter describes the seismic source characterization used to assess the seismic hazard at the Bruce nuclear site. Types of uncertainties and the general logic tree structure used for seismic source characterization for the PSHA are described. Regional seismic source zones and local seismic sources are defined and characterised.

Chapter 4 – Ground Motion Models

This chapter describes the models used to characterise earthquake ground motions in the region and the modifying effect of the local geology at the Bruce nuclear site.

Chapter 5 – Probabilistic Seismic Hazard Analysis and Design Ground Motions

This chapter describes the results of the probabilistic seismic hazard analysis conducted for the Bruce nuclear site and the development of site ground-motion response spectra.

Chapter 6 – Conclusions

This chapter presents the study conclusions, based on the updated seismic hazard model for the Bruce nuclear site region.

2. GENERAL SITE DESCRIPTION AND CHARACTERISTICS

2.1 Site Location and Description

The Bruce nuclear site is located adjacent to the west shore of Lake Huron, in the Municipailty of Kincardine, Ontario. To assess the seismic hazard for this site, a study region has been defined between latitudes 38°N to 50°N and longitudes 65°W to 90°W (Figure 2.1). Seismic activity in the vicinity of the site is low, although it is higher to the east (Figure 2.1). The seismic sources to the east of the site have the greatest potential impact on the seismic hazard of the Bruce nuclear site.

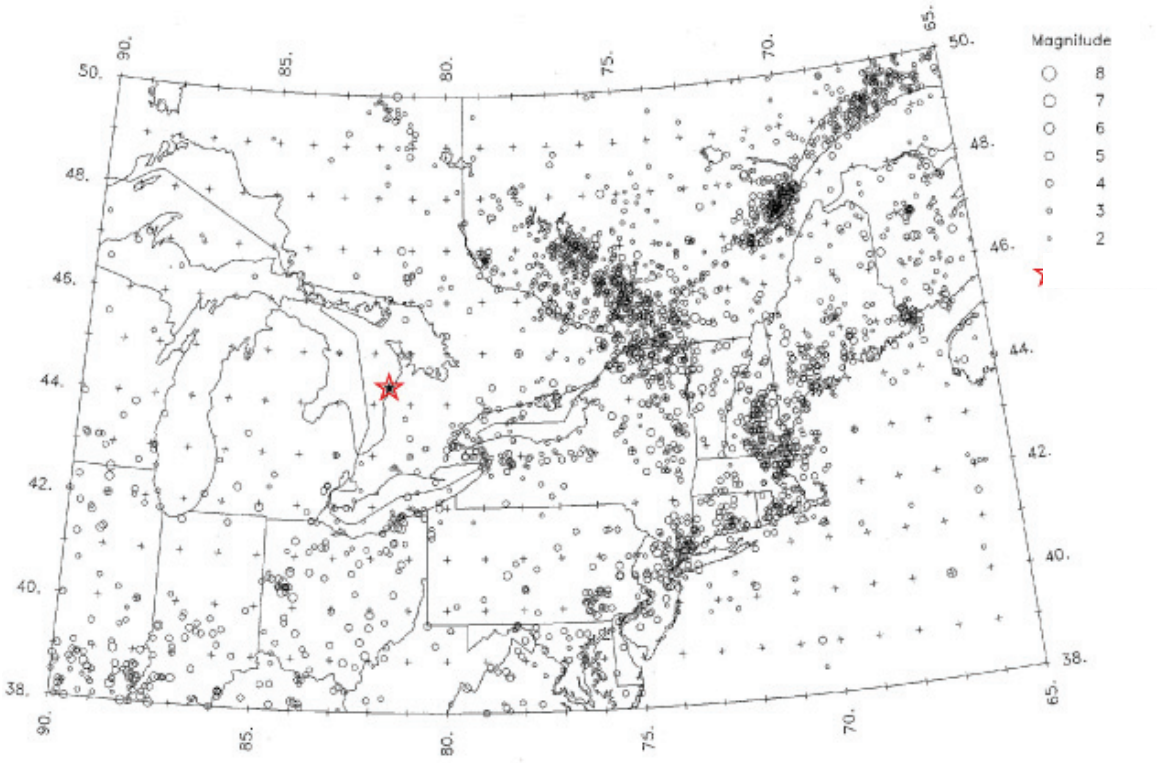

Figure 2.1: Location of Bruce Nuclear Site (star) and Study Region

2.2 Regional Structure and Geologic History

The Bruce nuclear site lies within the eastern Lake Huron region of southwestern Ontario, in the tectonically stable interior of the North American continent. The site is underlain by Middle Proterozoic Grenville basement (Bickford et al. 1986, Rankin et al. 1993, Johnston et al. 1994) and approximately 850 meters (m) of Paleozoic sediment strata that unconformably overly altered Precambrian granitic gneiss basement rocks (INTERA[1] 2011). The Paleozoic rocks range in age from Cambrian to Middle Devonian and consist primarily of limestone and shale deposited in shallow marine environments. Inferred basement within the study region includes

[1] Currently known as Geofirma Engineering Ltd.

crust from the Superior, Southern Granite-Rhyolite, and Grenville provinces, and the East Continent rift and Midcontinent rift (Figure 2.2). These units are covered by Paleozoic sediments structurally arranged in basins and arches (Figure 2.3) as a response to Paleozoic tectonic events, including the Penobscottian, Taconian, Salinian, Acadian, and Alleghenian orogenies (Figure 2.4 and Table 2.1).

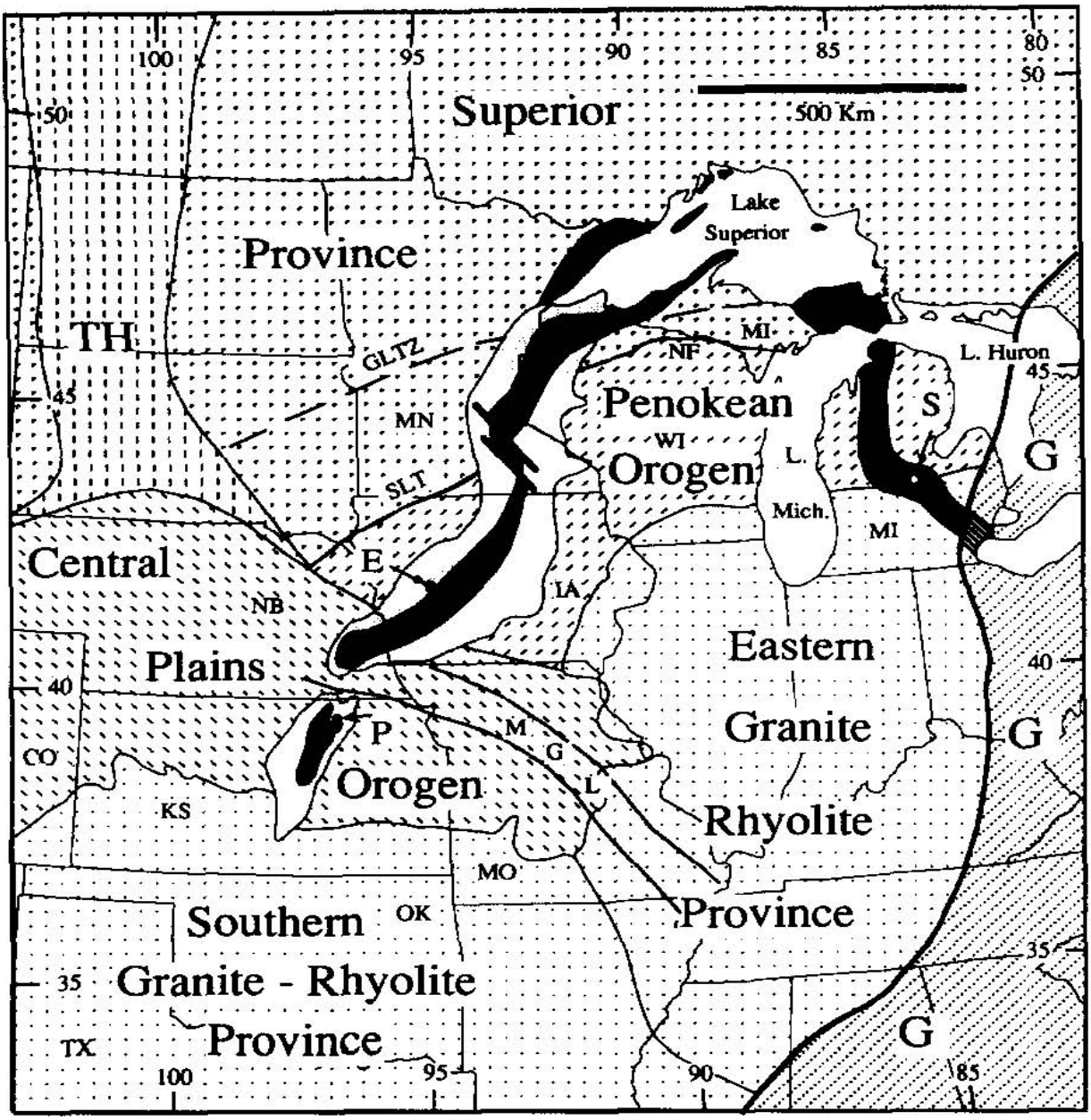

Notes: Location references include, E – Amoco-Eischeid drill hole, G – Grenville Province, GLTZ – Great Lakes tectonic zone, MGL – Missouri gravity low, NF – Niagara fault zone, P – Texaco-Poersch drill hole, S - McClure-Sparks drill hole, SLT – Spirit Lake trend, and TH – Trans-Hudson Orogen. Figure is from Van Schmus (1992).

Figure 2.2: Precambrian Basement Provinces

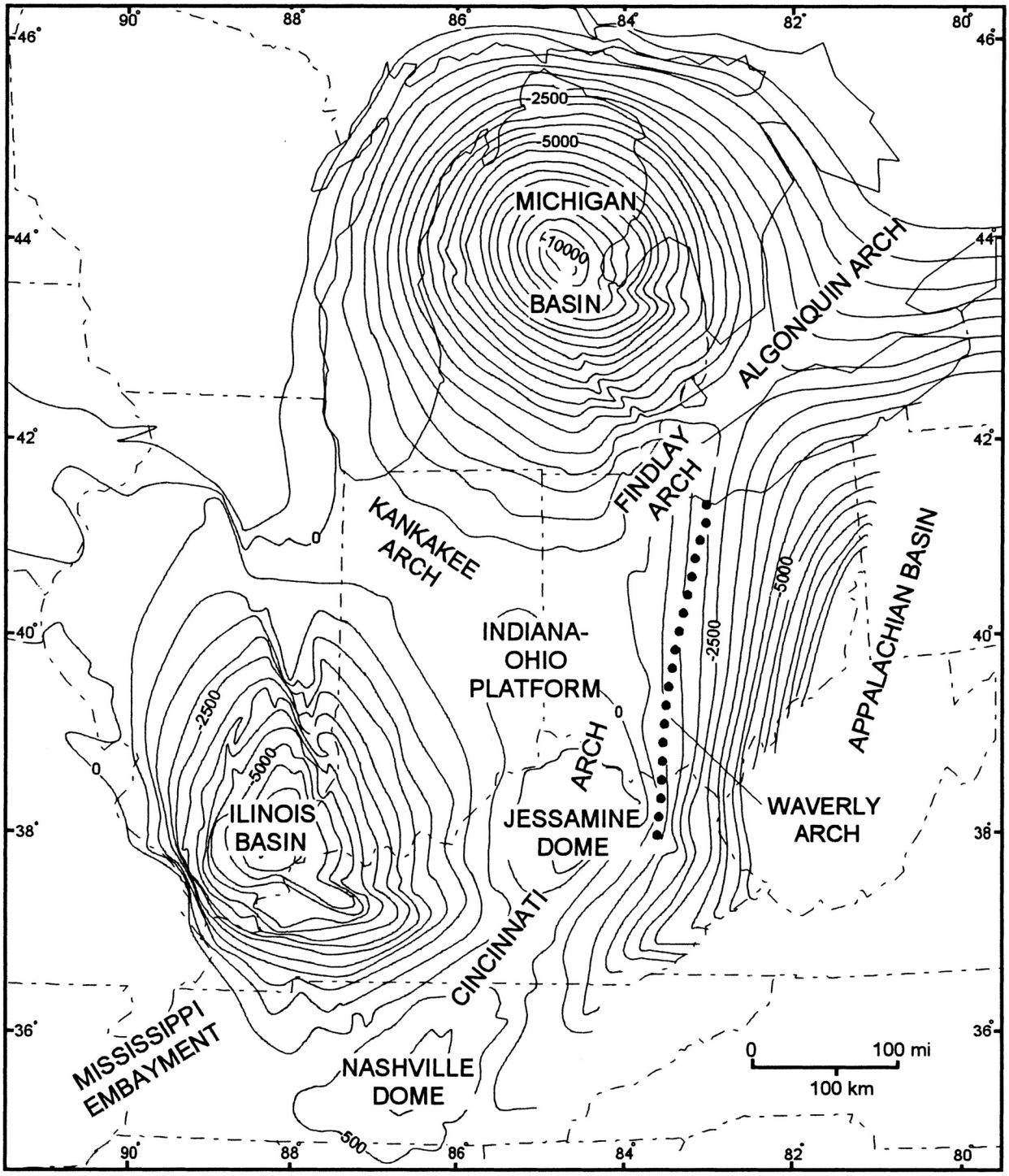

Note: Figure is from Root and Onasch (1999).

Figure 2.3: Paleozoic Basins and Arches

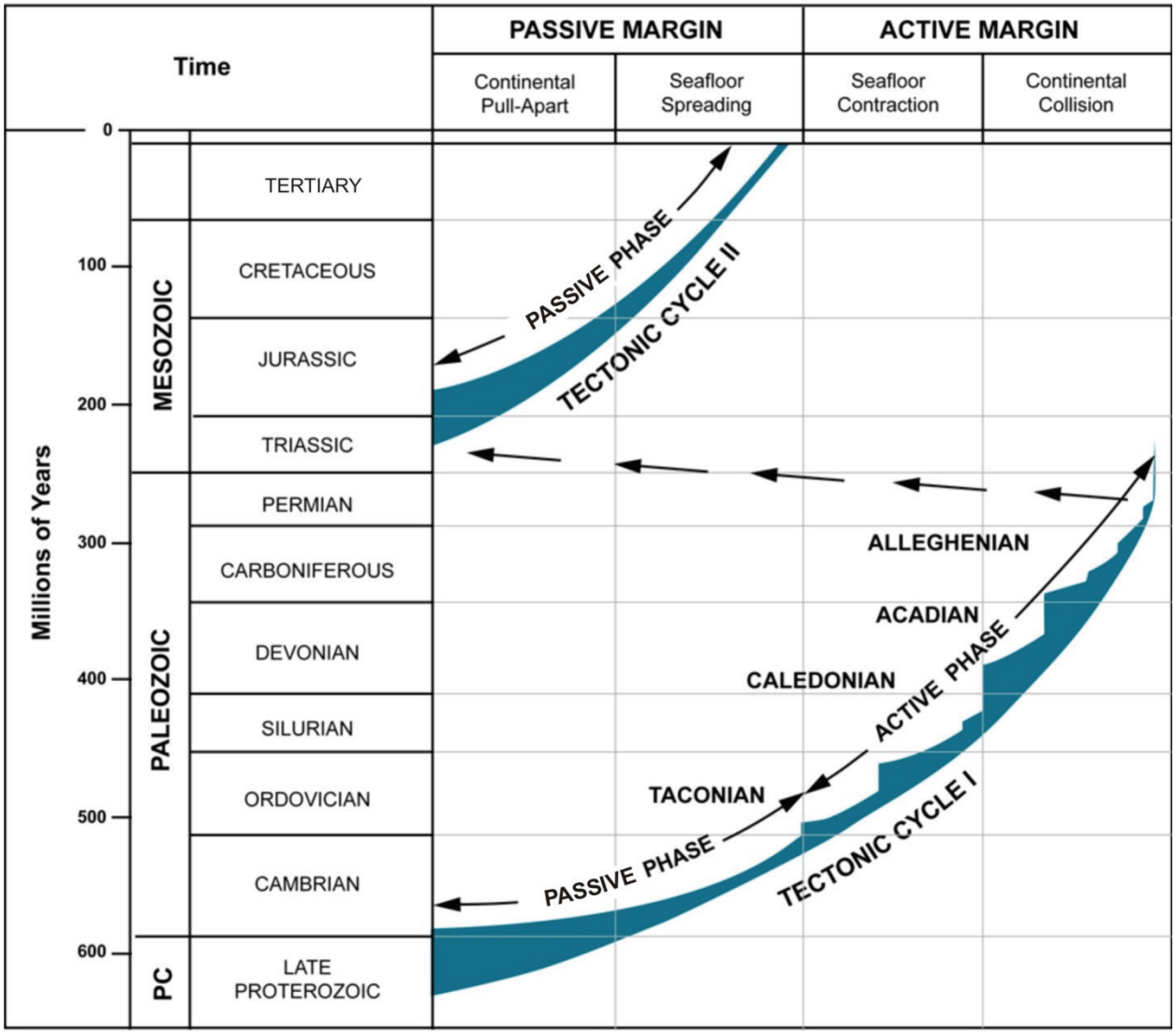

Note: Figure is modified from Sanford et al. (1985).

Figure 2.4: Phanerozoic Tectonic Cycles in the Appalachian Orogen

Table 2.1: Timetable of Tectonic Events in the Study Region

Era or Epoch	Time Interval	Tectonic Event	References
Neoarchean	2.7 Ga	**Kenoran Orogeny**—assembled terranes into the Superior province with collision between the Minnesota River terrane and the Wawa subprovince.	Hoffman 1988 Hoffman 1989 Van Schmus 1992
Paleoproterozoic	1.88–1.84 Ga	**Penokean Orogeny**—deforms supracrustal passive margin rocks of the Southern province.	Thurston et al. 1992b Cannon et al. 1991 Whitmeyer and Karlstrom 2007
Paleoproterozoic	1.6–1.8 Ga	**Central Plains Orogeny**—observed as basement lithologies in Nebraska and Kansas that are attributed to the Yavapai and Mazatzal orogenies exposed in the western United States.	Whitmeyer and Karlstrom 2007 Van Schmus 1992 Hoffman 1988 Hoffman 1989
Paleoproterozoic	1.74 Ga	**Plutons in CGB**—associated with Andean-style continental rocks.	White et al. 2000
Mesoproterozoic	1.5–1.23 Ga	**Granite Rhyolite Orogeny**—involved continental arc magmatism and the collision of juvenile rocks along the margin of Laurentia from Texas to Labrador.	Rivers and Corrigan 2000 Whitmeyer and Karlstrom 2007
Mesoproterozoic	Unknown	**East Continent Rift**—Mesoproterozoic rift of uncertain age located within the mid-continent and associated with the Fort Wayne rift of Indiana and Ohio.	Stark 1997
Mesoproterozoic	1.3–1.24 Ga	**Elzevirian Orogeny**—resulted from accretion of the Composite Arc Belt to the Central Gneiss Belt.	White et al. 2000 Carr et al. 2000
Mesoproterozoic	>1,165 Ma	**Amalgamation**—of the Frontenac-Adirondack Belt to the Composite Arc Belt boundary zone	White et al. 2000
Mesoproterozoic	1.19–1.11 Ga	**Collisional Shawanagan Phase**—extensional period, associated with anorthsite-magnerite-charnockite-granite plutonism, resulting in delamination from the orogenic collapse of overthickened crust.	Rivers 1997 Whitmeyer and Karlstrom 2007

Table 2.1: Timetable of Tectonic Events in the Study Region

Era or Epoch	Time Interval	Tectonic Event	References
Mesoproterozoic	1.1–1.0 Ga	**Midcontinent Rift**—arcuate aborted rift spanning from Kansas to Lake Superior and continuing southeast through Michigan.	Cannon et al. 1994
Neoproterozoic	1,090–980 Ma	**Ottawan Orogeny**—accreted rocks of the Frontenac-Adirondack Belt during the final continental collision of the Grenville orogeny.	Whitmeyer and Karlstrom 2007 White et al. 2000
Neoproterozoic	980–600 Ma	**Extension and denudation** following the end of orogenic activity.	Carr et al. 2000
Neoproterozoic	590 Ma	**Iapetan rifting**—initiated at Sutton Mountain triple junction.	Kumarapeli 1993 St. Seymour and Kumarapeli 1995 Kamo et al. 1995
Early Cambrian	550 Ma	**Rift-drift transition**—open marine sedimentation along the subsiding continental margin followed voluminous volcanism (554 Ma) interpreted as late stage rifting mmediately predating seafloor spreading	Kumarapeli 1993
Late Cambrian to Middle Ordovician	475 Ma (peak metamorphism)	**Penobscot Orogeny**—amalgamated composite terranes within island arcs of the Iapetus Ocean, now in the northern Appalachians. Resulted in basin-centered subsidence of the Michigan basin.	Murphy and Keppie 2005 Moench and Aleinikoff 2003 Howell and van der Pluijm 1999
Middle to Late Ordovician	480–445 Ma	**Taconic Orogeny**—accretion of island arcs to Laurentian margin from Labrador to Alabama, restricting the Appalachian basin from the oceans to the east. Associated with sinistral movement on NE-trending faults.	Faill 1997a Moench and Aleinikoff 2003 Murphy and Keppie 2005 Tremblay and Castonguay 2002
Late Ordovician to Early Devonian	430–410 Ma (peak metamorphism)	**Salinic Orogeny**—accretion of the Gander, Avalon, Nashoba, and Carolina terranes to Laurentia as a result of the collision between Laurentia and Avalonia and closure of	Murphy and Keppie 2005, Tremblay and Castonguay 2002

Table 2.1: Timetable of Tectonic Events in the Study Region

Era or Epoch	Time Interval	Tectonic Event	References
		the Iapetus Ocean.	
Devonian	385–375 Ma (peak metamorphism)	**Acadian Orogeny**—attributed to subduction along an Andean-type margin possibly overriding a plume and its swell. Resulted in siliclastic sedimentation in the Appalachian basin in the Middle to Late Devonian.	Murphy and Keppie 2005 Faill 1997b Tremblay et al. 2000 Tremblay and Castonguay 2002
Devonian	374 and 321 Ma (K-Ar ages of impact melt and breccias)	**Charlevoix Impact Crater**—impact structures crosscut faults within the St. Lawrence Rift and are associated with the Charlevoix seismic zone.	Tremblay et al. 2003
Late Carboniferous to Late Permian	330–265 Ma	**Alleghenian Orogeny**—terminal collision between Gondwana and Laurentia-Baltica that closed the Rheic Ocean and resulted in the formation of Pangea. Exhibited in the Northern Appalachians as relatively high-grade metamorphism of Taconic and Acadian crust and deformation of Appalachian deposits near the Hudson Valley.	Murphy and Keppie 2005 Faill 1998 Faure et al. 1996a Hatcher et al. 1989
Late Triassic to Middle Jurassic	197 – 170 Ma (age of dikes in Quebec)	**Opening of the Atlantic Ocean**—rifting associated with the breakup of Pangea.	Klitgord et al. 1988 Faure et al. 2006
Cretaceous	140–70 Ma	**Great Meteor Hotspot**—extension and uplift resulting in unroofing along the hot spot track.	Roden-Tice et al. 2009 Faure et al. 1996b
Tertiary and younger	50 Ma–present	**Contemporary Stress Regime**—ENE-WSW-directed compressional stress regime due to ridge push in the Atlantic Ocean.	Zoback et al. 1992

The Phanerozoic tectonic regime along the eastern margin of North America has been described in terms of two tectonic cycles, known as “Wilson cycles” (see Sanford et al. 1985). Three major tectonic events affected this region:

- Late Proterozoic/early Paleozoic rifting to form the Iapetus (proto-Atlantic) Ocean;
- Middle to late Paleozoic closure of the Iapetan Ocean basin, accompanied by subduction of Iapetan crust and multiple arc-continent and continent-continent collisional episodes of Appalachian mountain building; and

- Mesozoic rifting to form the present-day Atlantic Ocean (e.g., Klitgord et al. 1988, Hatcher et al. 1989, Milkereit et al. 1992).

It has been shown that, worldwide, the seismic potential of a stable continental region varies according to the degree of crustal extension that it experienced in the geologic past, and to a lesser extent, the age of the crust (Johnston et al. 1994). Three types of crust are identified in eastern North America:

- Unrifted—the craton and the Appalachian fold belt;
- Failed intracontinental rifts—the Ottawa and Saguenay aulacogens and the Reelfoot rift complex; and
- Rifted passive continental margin—the Atlantic passive margin produced by the present opening of the Atlantic Ocean in the late Mesozoic (Figure 2.5), and a relic passive margin produced by Iapetan rifting in the Late Proterozoic/early Paleozoic (Johnston et al. 1994).

The following subsections review the tectonic history and structural evolution of key features in the Bruce nuclear site region.

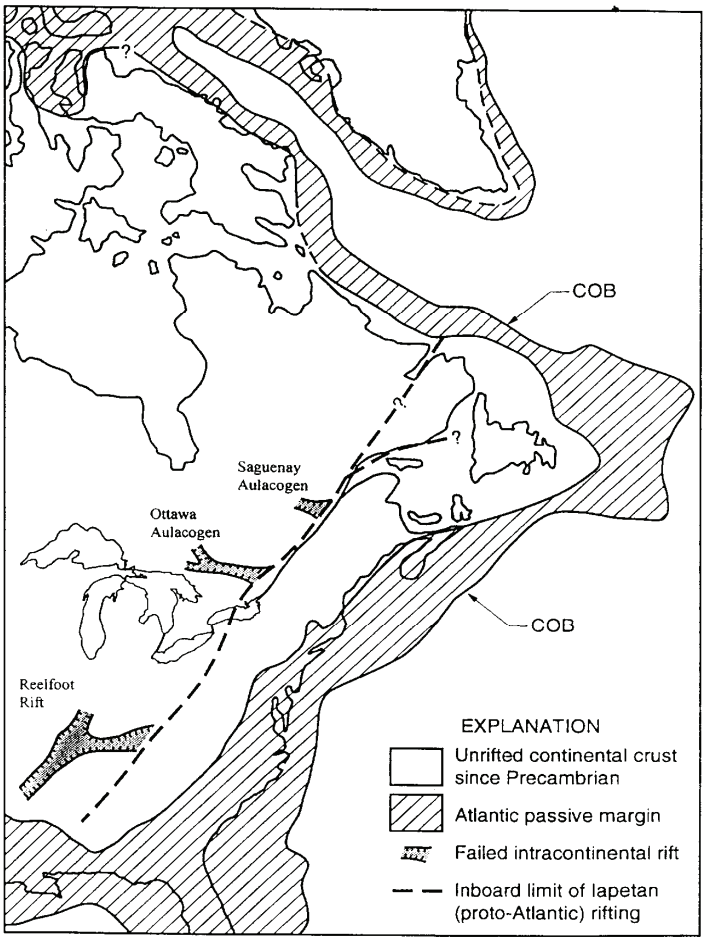

Notes: COB is continental/oceanic crust boundary. Figure is modified from Johnston (1995).

Figure 2.5: The Three Types of Seismogenic Continental Crust of Eastern North America

2.2.1 Superior Province

The earliest geologic history of the Bruce site region consists of the assembly of the Superior province (Table 2.1). The Superior province consists of greenstone belts with granitic plutonic rocks, granitic gneisses, and gneissic and migmatitic rocks dating from 3.6 to 2.6 billion years ago (Ga) (Van Schmus 1992). These lithologies are arranged in linear, fault-bounded subprovinces with distinctive rock types, ages, and metamorphic conditions (Thurston 1992a). Hoffman (1989) interpreted granite-greenstone belts as volcanic-plutonic island arcs, metasedimentary belts as accretionary prisms, plutonic belts as continental slivers within island arcs, and high-grade gneiss/granulite complexes as deeper erosion levels of other belt types. These belts were assembled progressively from north to south at approximately 2.7 Ga, during the oblique dextral transpressive Kenoran Orogeny.

Lithoprobe seismic reflection profiles 28, 29, 23, 24, 12, 12A, 25, 15, and 16A image north-dipping structures consistent with south-to-southeast vergent thrusting (Benn et al. 1994, Kellet et al. 1994). In subsequent Proterozoic tectonic events, the Superior province formed the lithospheric core during the assembly of the continent Laurentia (Hoffman 1988, 1989).

2.2.2 Southern Province

The Southern province consists of rocks initially deposited on the southern margin of the Superior province and deformed during the Penokean orogen (Figure 2.2). These rocks include siliceous, continental margin sedimentary rocks of the 2.4 – 2.2 Ga Huronian Supergroup, and deformed, rifted passive margin sequence of the 2.2 – 1.7 Ga Marquette Range Supergroup, overlain by a synorogenic foredeep sequence of the Animikie Group (Thurston 1992b). A poorly documented deformation event recorded in the Huronian Supergroup is thought to be younger than 2.2 Ga; however, much of the deformation in these deposits is attributed to the Penokean Orogeny. This event involved the collision of the an island arc (Cannon et al. 1991), with rocks of the Huronian Supergroup and Marquette Range Supergroup along the Niagara Fault between 1.88 and 1.86 Ga (Whitmeyer and Karlstrom 2007). Between 1.86 and 1.84 Ga, The Archean Marshfield terrane subsequently collided with a younger, north-vergent arc complex along the Eau Pleine shear zone (Whitmeyer and Karlstrom 2007, Cannon et al. 1991). These structural relationships were imaged in GLIMPCE (Great Lakes International Multidisciplinary Program on Crustal Evolution) seismic profile H (Figure 2.6) (Cannon et al. 1991). Post-tectonic granites intrude the Penokean orogenic belt and the Niagara fault zone, which pins the end of the collisional event at 1.83 Ga (Whitmeyer and Karlstrom 2007).

2.2.3 Granite Rhyolite Province

The Granite Rhyolite province consists of 1.47 – 1.37 Ga granite and felsic volcanic rocks of the midcontinent region (Van Schmus et al. 1996). Van Schmus (1992) interpreted these rocks as a veneer of supercrustal and shallow plutonic rocks that lie on Early Proterozoic crust of the Central Plains orogeny (a 1.8 – 1.6 Ga terrane to the west of the study region), from which they were derived by partial melting. Van Schmus et al. (1996) defined a northeast-southwest-trending Nd isotope boundary extending from southwestern Ontario to southeastern Oklahoma that separates Paleoproterozoic crust to the northwest and Mesoproterozoic (ca. 1.5 Ga) juvenile crust to the southeast. The Granite Rhyolite province was intruded by Mesoproterozoic “anorogenic” plutons, which extend from Colorado into Labrador (Van Schmus et al. 1996). There is increasing evidence for an orogenic link for the bimodal A-type granites involving continental arc magmatism and the collision of juvenile rocks along the margin of Laurentia. Rivers and Corrigan (2000) propose that a continental margin

magmatic arc existed along the southeastern margin of Laurentia from Texas to Labrador between 1,500 and 1,230 million years ago (Ma). Some of these rocks were incorporated into the Grenville province in subsequent tectonic events.

Few structural relationships are known about the Granite Rhyolite province. Consortium for Continental Reflection Profiling (COCORP) lines IL-1 in Illinois, IN-1 in Indiana, and the western portion of OH-1 in Ohio (Figure 2.6) image discontinuous, subhorizontal reflectors that can be traced laterally for up to 80 km, representing a layered assemblage as thick as 11 km (Pratt et al. 1989). Pratt et al. (1989) interpreted these reflectors as felsic igneous rocks underlain or intermixed with mafic igneous or sedimentary rocks. This discontinuous layering is absent in COCORP lines MO-1 and IL-2, which transect the Proterozoic caldera complexes of the St. Francois Mountains.

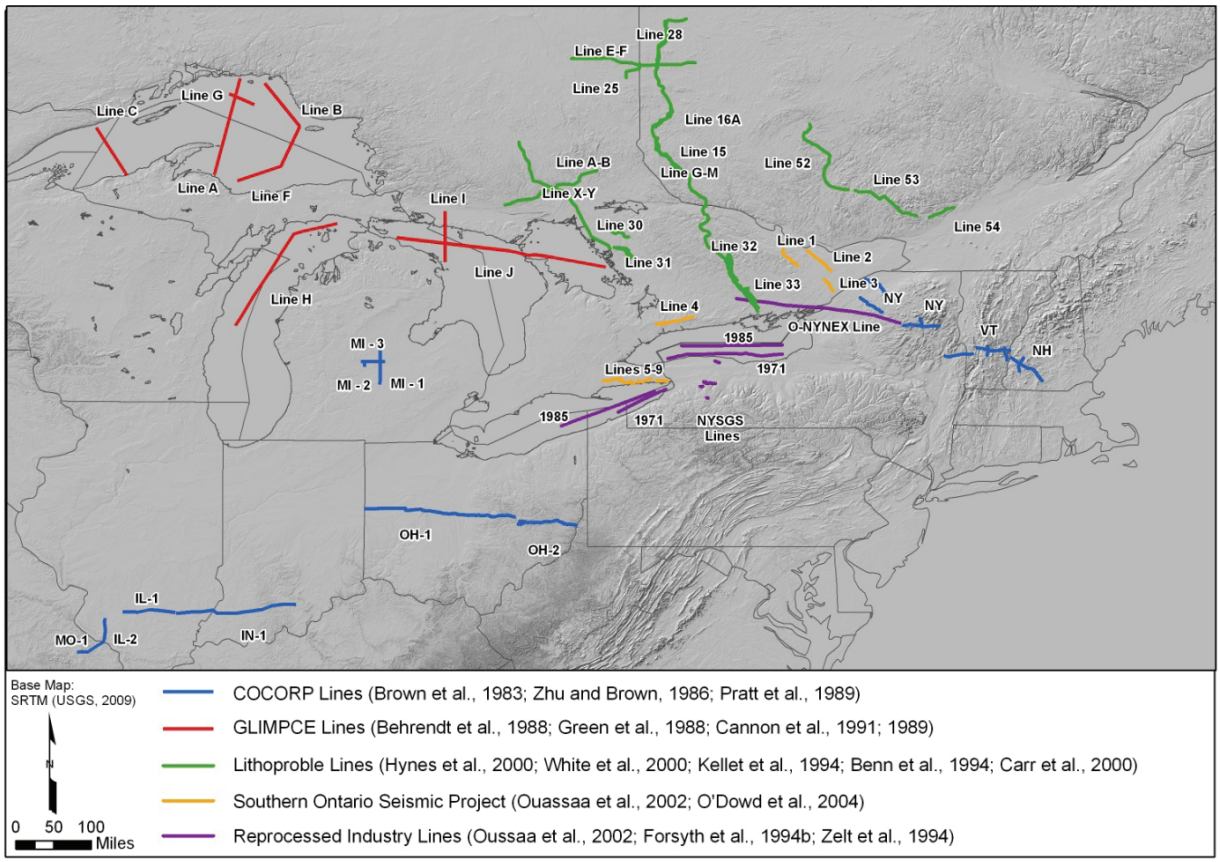

Figure 2.6: Locations of Seismic Profiles

2.2.4 East Continent and Midcontinent Rift Systems

Two major continental rifts developed along the eastern margin of Laurentia after emplacement of the Eastern Granite-Rhyolite province rocks. The first of these was the East Continent rift, which contains the northwest-trending Fort Wayne rift in western Ohio and eastern Indiana (Figure 2.7). Drahovzal et al. (1992) identified the East Continent Rift Basin (ECRB) based on: (1) presence of Middle Run formation (a lithic arenite interbedded with basalt); (2) association with the East Continent gravity high (ECGH), a northwest-trending

positive gravity anomaly that extends across Indiana, Michigan, Ohio, and Kentucky and is coincident with the Fort Wayne rift in Indiana and Ohio; and (3) magnetic anomalies coincident with gravity anomalies, suggesting deep-rooted bodies of mafic composition, possibly emplaced during rifting. The ECRB and Fort Wayne rift have uncertain Proterozoic ages based on a few age dates from drill core. Stark (1997) observed that the Fort Wayne rift and the ECRB contain a mafic basalt fill sequence on the north that is associated with the ECGH, and a southern depocenter filled with Proterozoic clastic rocks and minor volcanic flows. Baranoski et al. (2009) interpreted reprocessed data of COCORP line OH-1 (Figure 2.6) to include reflectors that indicate the Grenville collision and an end to the phase of rift basin subsidence.

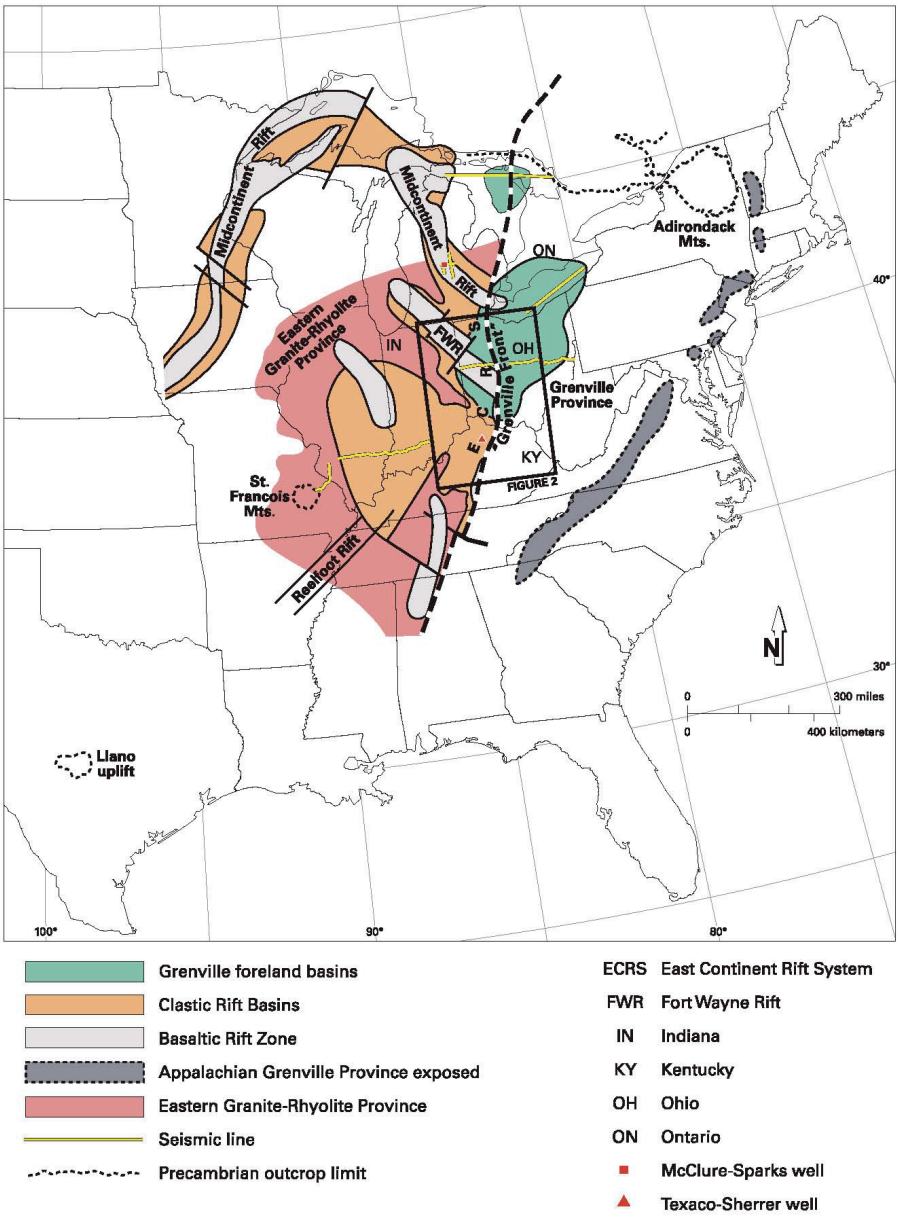

Note: Figure is from Baranoski et al. (2009).

Figure 2.7: Tectonic Elements of Eastern North America

The second major continental rift developed along the eastern margin of Laurentia after emplacement of the Eastern Granite-Rhyolite province rocks. It consists of the arcuate Midcontinent rift system (MRS) that extends from mid-Kansas to the Lake Superior region and then southeast across Michigan (Figure 2.2 and Figure 2.8). The arcuate MRS is coincident with the Midcontinent gravity high that extends from mid-Kansas to the Lake Superior region, the Mid-Michigan gravity high, and possibly portions of the ECGH from Ohio to Tennessee (Keller et al. 1983). The Midcontinent rift is interpreted as a relatively short-lived breakup of Laurentia with syn-rift volcanic and mafic intrusive rocks extruded between about 1.109 and 1.087 Ga, and younger post-rift sedimentary rocks deposited about 1.1 – 1.0 Ga (Van Schmus 1992).

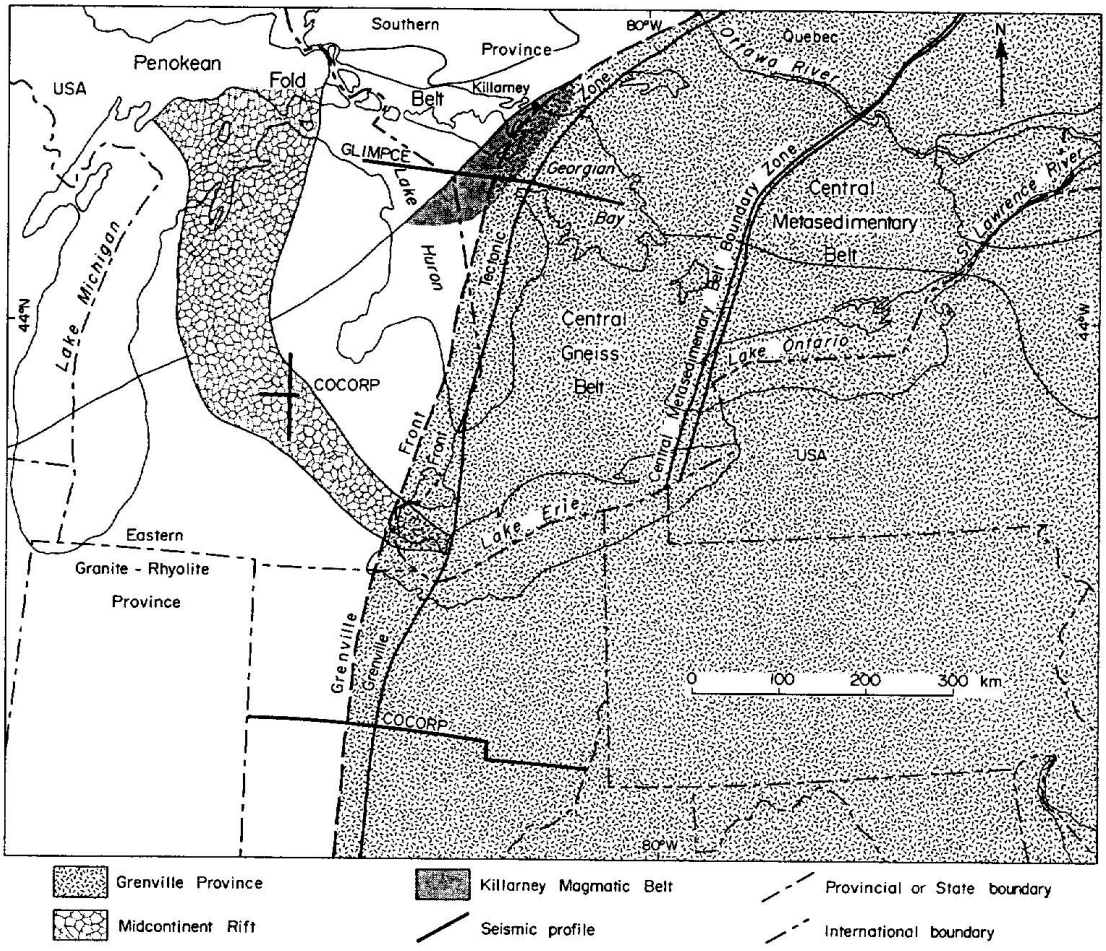

Note: Figure is from Easton and Carter (1995).

Figure 2.8: Principal Subdivisions of Precambrian Rocks in the Great Lakes Region

Compression associated with the Ottawan phase of the Grenville Orogen (1.09 – 1.025 Ga) aborted rifting and partially inverted the rift, particularly in the Lake Superior region. Cannon (1994) concludes that during compression, the southwest arm of the rift was closed about 30 km, the central graben area in the Lake Superior region was inverted, and the

southeast arm was dominated by strike-slip faulting. These structural relationships are documented in several deep seismic reflection profiles. COCORP lines MI-1, MI-2, and MI-3 (Figure 2.6), located in the center of the Michigan basin near the deep McClure-Sparks oil well, are interpreted to show a south-dipping rotated block (Zhu and Brown 1986). On GLIMPCE lines A, C, F the MRS can be recognized in the vicinity of Lake Superior (Behrendt 1988, Cannon et al. 1989) (Figure 2.6). A segmented rift structure with inverted, normal-faulted asymmetric half grabens separated by zones of accommodation (faults transverse to rift axis) is interpreted by Cannon et al. (1989).

The relative ages of these two rifting events are uncertain. Drahovzal et al. (1992) observed that the magnetic signature of the ECGH become less distinct east of the Grenville Front and that east-dipping thrust sheets overlying Middle Run formation in Kentucky indicate that the ECRB cannot be as young as Cambrian. The relative age of rifting in the ECRB could not be assessed, however, because of the unclear overthrust relationship between the Grenville Front and ECRB on COCORP line OH-1. Stark (1997) acknowledges that demonstrating an association between the MRS and ECRB requires additional research to resolve the inconsistent observations of basement lithology in northwestern Ohio. Baranoski et al. (2009) examined sequence stratigraphy, structural relationships, and geopotential field data but were unable to assess whether the Fort Wayne rift portion of the East Continent rift is coeval with the southeastern arm of the Midcontinent rift in Michigan.

2.2.5 Grenville Province

The Grenville Orogeny records the assembly of the Neoproterozoic supercontinent, Rodinia (Faill 1997a). The Grenville province consists of three general lithotectonic segments: (1) Laurentia and its pre-Grenvillian margin; (2) the Composite Arc Belt (CAB); and (3) the Frontenac-Adirondack Belt (Carr et al. 2000) (Figure 2.9). Laurentia and its pre-Grenvillian margin (L2 rocks depicted on Figure 2.9b) contain rocks of the Archean Superior province, Paleoproterozoic Southern province, and 1800 – 1350 Ma supracrustal and continental arc rocks (L3 rocks depicted on Figure 2.9b) of the Central Gneiss Belt (CGB) (Figure 2.9a; White et al. 2000). Widespread deformation, metamorphism, and magmatism recorded in these rocks at 1740 and 1450 Ma are attributed to Andean-style continental arcs (White et al. 2000) that may be related to Granite Rhyolite volcanism (Carr et al. 2000, Rivers and Corrigan 2000). The CAB (Figure 2.9b) contains allocthonous 1300 – 1250 Ma volcanic, plutonic, volcaniclastic, carbonate, and siliclastic rocks from various arcs, rifted arcs, and marginal basins amalgamated offshore by 1,240 Ma (White et al. 2000). The Frontenac-Adirondack Belt (Figure 2.9b) is composed of supracrustal rocks, orthogneiss assemblages, and anorthosites and anorthosite-mangerite- charnockite-granite that formed in continental crust or arc fragments and underwent granulite-amphibolite-facies deformation by 1170 Ma in a tectonic setting offshore of the pre-Laurentian margin (White et al. 2000).

The Elzevir Orogeny sutured the CAB to the eastern margin of Laurentia between 1.3 and 1.2 Ga, recorded as collision, deformation, and high-grade metamorphism (Carr et al. 2000, White et al. 2000). The Frontenac terrane and the Central Granulite Belt of the Adirondack highlands were amalgamated with the CAB by 1165 Ma as a result of crustal imbrications and stacking, forming the Central Metasedimentary Belt (CMB) (Figure 2.9a). Rocks of the CGB were reworked during this assembly, resulting in lithotectonic domains that are bounded by ductile shear zones assembled 1120 – 1040 Ma (White et al. 2000).

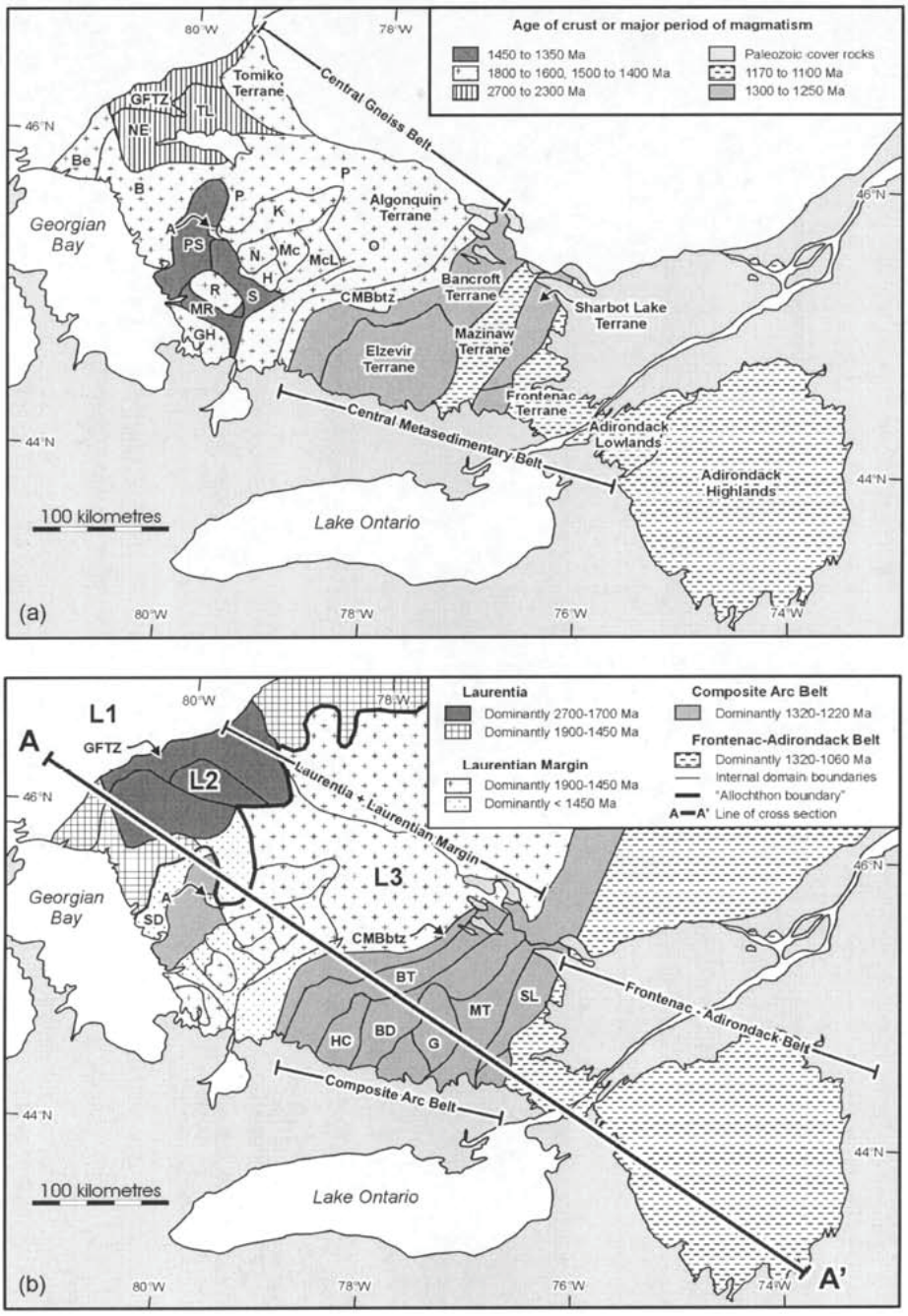

Notes: Domains indicated on maps above include, A, Ahmic domain; B, Britt domain; BD, Belmont domain; Be, Beverstone domain (part of Killarney magmatic belt); BT, Bancroft domain; CMBbtz, Central Metasedimentary Belt boundary thrust zone; G, Grimsthorpe domain; GFTZ, Grenville Front tectonic zone; GH, Go Home domain; H, Huntsville domain; HC, Harvey Cardiff Arch; K, Kiosk domain; Mc, McCraney domain; McL, McLintock domain; MR, Moon River domain; MT, Mazinaw terane; N, Novar domain; NE, Nepewassi domain; O, Opeongo domain; P, Powassan domain; PS, Parry Sound domain; R, Rosseau domain; S, Seguin domain; SD, Shawanaga domain; SL, Sharbot Lake domain; TL, Tilden Lake domain. Figure is from Carr et al. (2000).

Figure 2.9: Major Divisions and Structures of the Southwestern Grenville Province

Rivers (1997) defined the collisional Sawingian phase from abundant anorthosite-mangerite-charnockite-granite plutonism from 1.19 to 1.11 Ga. Whitmeyer and Karlstrom (2007) interpret a quiescent period between the Elzevir and Ottawan orogenies that is characterized by delamination and extensional collapse as a result of crustal thickening from plutonism. This extension occurred within the CGB as ductile extension along the Shawanaga shear zone (Figure 2.10) (White et al. 2000).

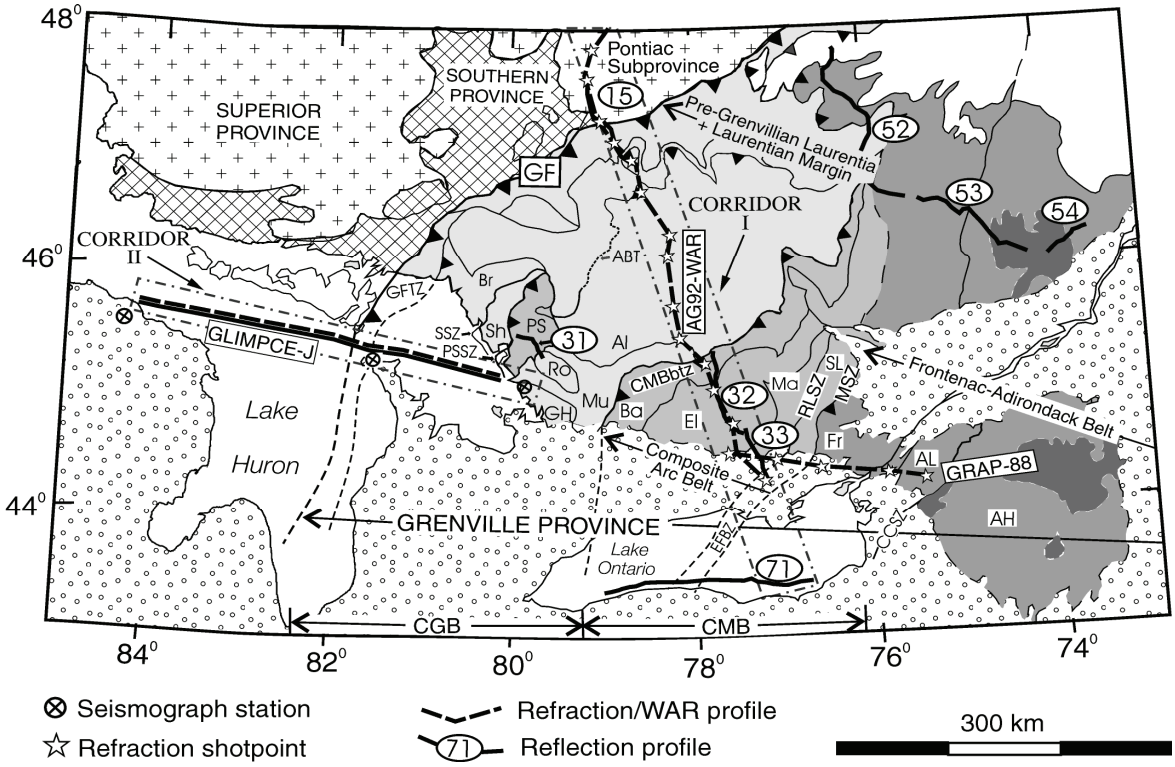

Notes: Corridor I – reflection line 15 (from AGT92), lines 31, 32, and 33 (from AGT90), and line 71 (Lake Ontario speculation data), as well as refraction – wide-angle reflection lines from the 1992 Abitibi–Grenville refraction – wide-angle reflection experiment (AG92-WAR), and the GRAP-88 experiment. Corridor II – seismic reflection and refraction – wide-angle reflection data from GLIMPCE line J. ABT, Allochthon Boundary Thrust; AH, Adirondack Highlands; AL, Adirondack Lowlands; Al, Algonquin domain; Ba, Bancroft terrane; Br, Britt domain; CGB, Central Gneiss Belt; CMB, Central Metasedimentary Belt; CMBbtz, Central Metasedimentary Belt boundary thrust zone; EFBZ, Elzevir–Frontenac boundary zone; El, Elzevir terrane; Fr, Frontenac terrane; GH, Go Home domain; GF, Grenville Front; GFTZ, Grenville Front Tectonic Zone; Ma, Mazinaw terrane; MSZ, Maberly shear zone; Mu, Muskoka domain; PS, Parry Sound domain; PSSZ, Parry Sound shear zone; RLSZ, Robertson Lake shear zone; Ro, Rousseau domain; Sh, Shawanaga domain; SL, Sharbot Lake domain; SSZ, Shawanaga shear zone. Figure is from White et al. (2000).

Figure 2.10: Seismic Cross-section of the Grenville Orogen

The 1.09 – 0.98 Ga Ottawan Orogeny renewed northwest-directed thrusting and imbrication of terranes as a result of a major collision with either the Amazonia, Rio de la Plata, and/or Kalahari cratons (Whitmeyer and Karlstrom 2007). These terranes were transported to the northwest on thrust systems of the CMB and thrust over rocks of the pre-Grenvillian Laurentian margin about 1120 – 980 Ma (some of these thrusts are exposed in the CGB). Domains of the Composite Arc and Frontenac-Adirondack belts formed at middle to upper crustal levels during the Grenvillian orogeny and exhibit complex fold geometry. Convergence between 1080 and

1040 Ma consisted of northwest-directed thrusting that resulted in substantial telescoping and thickening (White et al. 2000). Metamorphism peaked at 1.07 Ga and ended with emplacement of 0.96 Ga plutons in the Green Mountains of Vermont (Whitmeyer and Karlstrom 2007).

Post-orogenic denudation and cooling continued from 980 to 600 Ma (Carr et al. 2000) and was, in part, accommodated by distributed ductile strain. This ductile strain occurred within the CGB and on structures throughout the Grenville province, including the Grenville Front, the Robertson Lake shear zone, and the Carthage-Colton mylonite zone (Figure 2.10) (White et al. 2000). Postcollisional exhumation of overthickened crust may have uplifted rocks of the southeast CGB by at least 15 km relative to the northeast CMB (White et al. 2000). Exhumation of the Grenville Front was facilitated by partial melting and ductile flow due to high temperatures that persisted throughout the late stages of the orogeny, ensuring that late-stage normal or reverse faults would sole into the mid-crust (White et al. 2000).

Grenville-age terranes within the Appalachians have been interpreted as either rifted fragments accreted during Appalachian tectonic events, far-traveled terranes from west of the Granite Rhyolite province, or exotic terranes from West Africa or South America, which were accreted during Appalachian tectonic events (Whitmeyer and Karlstrom 2007).

The Grenville crustal structure is characterized by north-northeast-striking, relatively shallow east-southeast-dipping ductile thrust faults that developed at mid- to lower crustal depths during the Middle Proterozoic Grenville Orogeny (Green et al. 1988, Milkereit et al. 1992, Forsyth et al. 1994a, 1994b, Zelt et al. 1994). The following discussion characterizes important structural boundaries, including the Grenville Front tectonic zone, the Central Metasedimentary Belt boundary zone (CMBBZ), and the Composite Arc Belt boundary zone (CABBZ) (Figure 2.9a and 2.9b).

2.2.5.1 Grenville Front

In eastern Canada, the Grenville Front separates the Archean Superior province (more than 2.5 Ga) from much younger rocks of the Grenville Orogen (1.6 – 1.0 Ga) (Thurston 1992a). The Grenville Front tectonic zone (GFTZ) defines the northwest boundary of the Grenville province and extends through North America for approximately 1900 km. The GFTZ is interpreted from seismic reflection profiles: COCORP lines OH-1 and OH-2 in central Ohio (Pratt et al. 1989, Culotta et al. 1990) and GLIMPCE lines I and J in Lake Huron (Green et al. 1988, Mereu et al. 1990) (Figure 2.6). Green et al. (1988) interpreted the GFTZ as a 32 km wide, steeply dipping zone of east-dipping reflectors. After reprocessing these data, Mereu et al. (1990) interpreted these reflectors as mylonite zones associated with ductile faulting. Pratt et al. (1989) interpreted east-dipping parallel reflectors as the GFTZ in Ohio. Culotta et al. (1990) later synthesized these results and interpreted the GFTZ as a 50 km wide, 25- to 30-degree east-dipping zone penetrating to 25 km deep, attributing the west-dipping reflectors to the CMBBZ.

The location of the GFTZ has been interpreted in several alternative positions. In Michigan, Hinze et al. (1975) (Figure 2.11) interpreted areas of positive northeast-southwest-trending gravity and magnetic anomalies as characteristic of the Grenville province, consistent with the trend of anomalies of exposed Grenville province rocks in Ontario. In Ohio, Lucius and von Frese (1988) placed the GFTZ west of the Anorthosite Complex anomaly based on their model that this anomaly was uplifted from the deep crust during the Grenville orogeny. In a regional study, Atekwana (1996) characterized the Grenville province as having higher-amplitude and higher-frequency magnetic anomalies that trend northwest to north in Kentucky, Ohio, and

southeastern Michigan, as well as north-northeast in southwestern Ontario.
Easton and Carter (1995) interpreted the location of the GFTZ (Figure 2.8 and Figure 2.12) by combining seismic reflection profile data from COCORP lines OH-1 and GLIMPCE line J with drillhole data in southwestern Ontario.

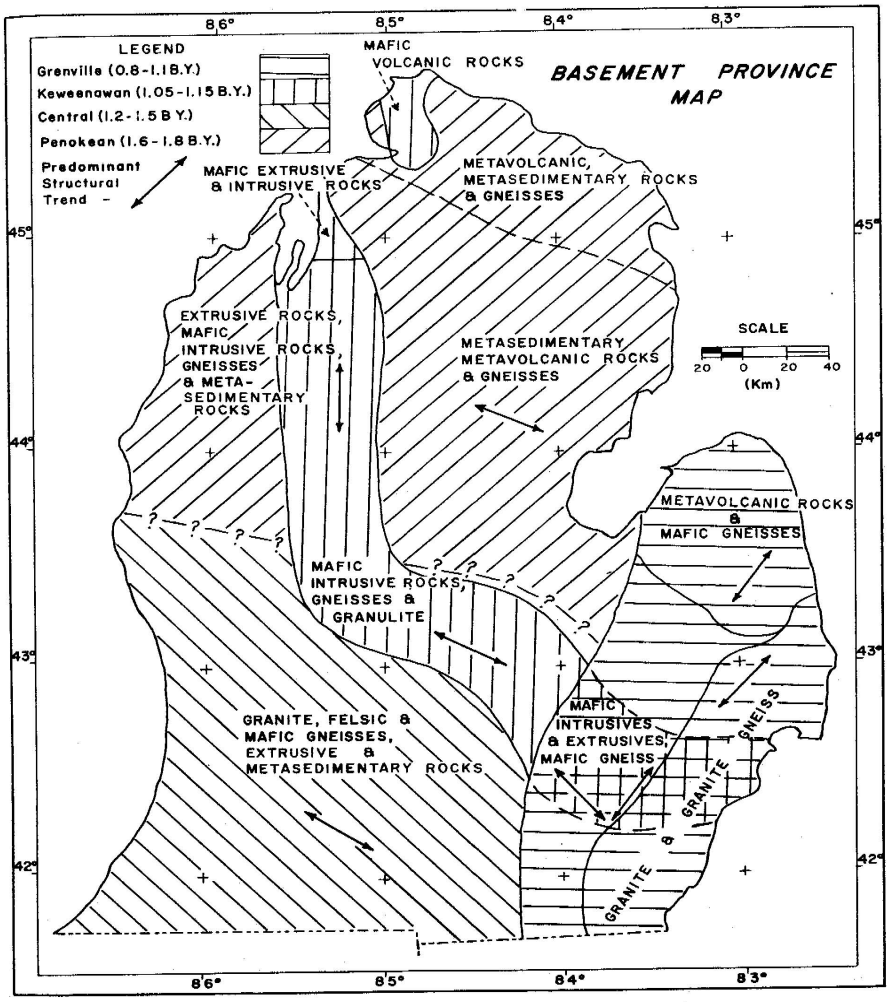

Note: Figure is from Hinze et al. (1975).

Figure 2.11: Basement Province Map of Southern Peninsula of Michigan

Easton and Carter (1995) identified lithotectonic domains within the basement of Ontario from aeromagnetic and gravity anomalies, drill core samples of basement rock, and seismic reflection profiles (Figure 2.12). In their interpretation, the GFTZ (Figure 2.8) is located east of the Killarney Magmatic Belt and extends to the south along the Detroit River through Michigan, consistent with the interpretation of geophysical anomalies by Lucius and von Freese (1988). Easton and Carter (1995) define a location of the GFTZ that is to the east of the location Hinze et al. (1975) interpreted in southeastern Michigan. Easton and Carter (1995) also considered the structural relationship between the Midcontinent rift and the Grenville Front. They observed that west to northwest-trending linear aeromagnetic anomalies of the Essex

domain (Figure 2.12) are along the strike of the east-trending gravity high of the Midcontinent rift in southeastern Michigan (Figure 2.11). Based on this information, Easton and Carter (1995) interpreted the Essex domain as either the metamorphosed fill rocks of the Midcontinent rift or, alternatively, as the eastern end of the rift overlain by Grenville thrust sheets.

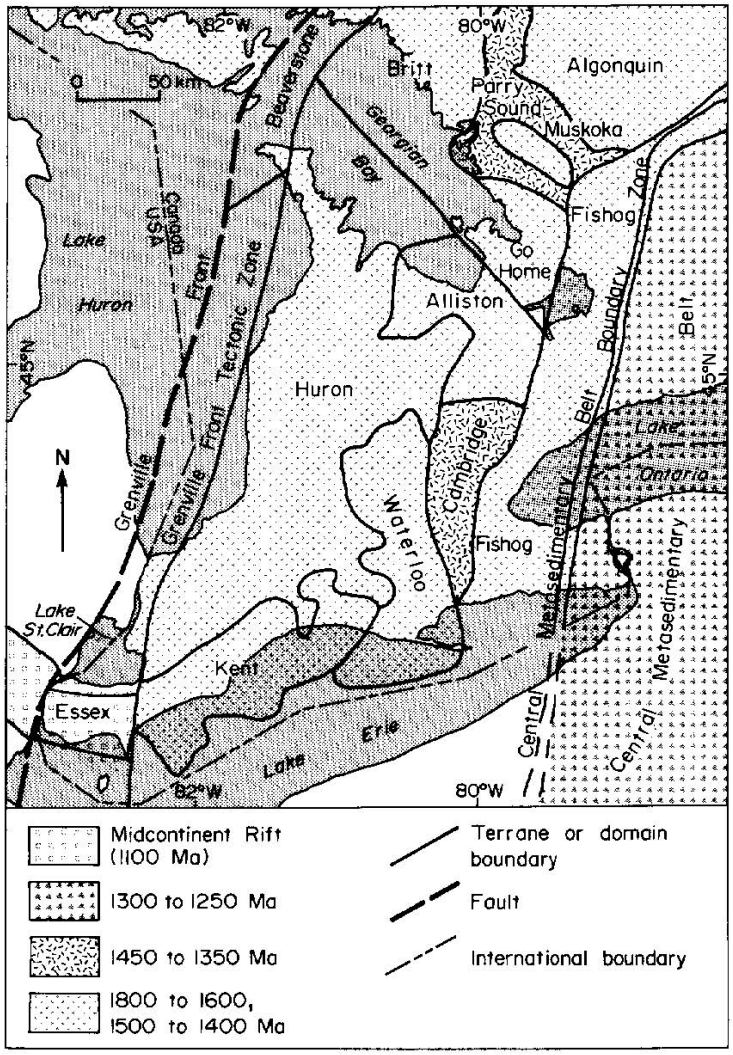

Note: Figure is from Easton and Carter (1995).

Figure 2.12: Lithotectonic Domains of the Grenville Province in Southwestern Ontario and Adjacent Areas

2.2.5.2 Central Metasedimentary Belt Boundary Zone

The CMBBZ defines the northwest boundary of the CAB (Carr et al. 2000) (Figure 2.9). Lithoprobe line 32 (Figure 2.6) images the northern edge of the CMBBZ across the Bancroft terrane into the Elzevir terrane (White et al. 1994). White et al. (1994) interpreted the Bancroft

terrane and the CMBBZ as the tectonized boundary between the CMB and the CGB (Figure 2.9). This tectonic zone is at least 30 km wide (up to 50 km wide surface expression); has an apparent southeast dip of 20 degrees in the Bancroft terrane, increasing to as steep as 40 degrees toward the CGB; and extends to at least 25 km in depth (White et al. 1994). This broad zone of ductile deformation and crustal stacking that characterize the CMBBZ, the Bancroft terrane, and their CGB footwall is interpreted as resulting from northwest-directed thrusting during the Ottawan Orogeny (1080 – 1040 Ma) (White et al. 2000). This structure overlies a wedge-shaped lower crustal zone that could have acted as a crustal wedge during the collision of the CMB and CGB, delaminating the CMB crust, or it could be autochtonous basement of the CGB underlying the allochthonous thrust sheets of the CMB (White et al. 1994).

A velocity culmination lies within the footwall of the CMBBZ, indicating that the CMBBZ is adjacent to velocity uplifts that suggest bulk relative upward transport of mid-crustal rocks across these zones (White et al. 2000). Carr et al. (2000) conclude that rocks of the CMBBZ and Bancroft terrane may have originated on the distal margin of pre-Grenvillian Laurentia, or they are allochthonous and were part of the CAB.

Seismic images interpreted by Milkereit et al. (1992) of the CMBBZ in Lakes Erie and Ontario provide evidence for ductile faults bounding imbricate thrust sheets on the western side of the boundary. The most western of the reflections maintains an approximately 30-degree easterly dip from beneath the Paleozoic cover to approximately 10 km depth, and flattens into a decollement extending to approximately 22 km depth. Many of the planar and listric reflections east of the CMBBZ border large-scale curvilinear reflection bands interpreted as either a sequence of folds successively truncated by later east-dipping faults or a sequence of ramp folds. Evidence of reactivation, either by late-phase Grenville extension or pre-Appalachian rifting, resulted in a local fault-bounded half graben in the eastern portion of the CMBBZ. Milkereit et al. (1992) attribute the formation of this basin to reversal of former thrust faults; they note that the top of the Trenton Group (Middle Ordovician) is not significantly deformed by this reactivated thrust fault.

Milkereit et al. (1992) interpolated the location of the CMBBZ between its location in Lakes Ontario and Erie and outcrops imaged by Lithoprobe lines 31 and 32 (Figure 2.6) using aeromagnetic data. The boundary is defined by higher amplitudes of magnetic anomalies along the western boundary of the CGB compared to lower values of the CMB. Subsequent work by Forsyth et al. (1994b) confirms that magnetic anomalies in west-central Lake Ontario coincide with a west-to-east, positive-to-negative change in the magnetic field. This transition coincides with a zone of east-dipping reflectors extrapolated from the end of the seismic section to beneath Lake Ontario. In the subsurface of Lake Erie, the CMBBZ also correlates with a change in magnetic signature from higher values west of the CMBBZ to lower values over the CMBBZ. On that basis, Forsyth et al. (1994a) traced the CMBBZ between Lakes Erie and Ontario (Figure 2.13).

Seismic data from line 4 (Figure 2.6) illustrates the complications in crustal geometry (O'Dowd et al. 2004). The CMBBZ consists of southeast-dipping reflections that truncate or overprint a subhorizontal band at approximately 21 km in depth. O'Dowd et al. (2004) performed cross-tip analysis and determined that reflectors of the CMBBZ have a strike of N13E and dip 25 degrees to the southeast. The deeper reflections have a strike of N65E and dip 20 degrees to the southeast. Comparing these results to recent aeromagnetic data, O'Dowd et al. (2004) revised the subsurface trace of the CMBBZ along the western edge of the Mississauga domain (Figure 2.15).

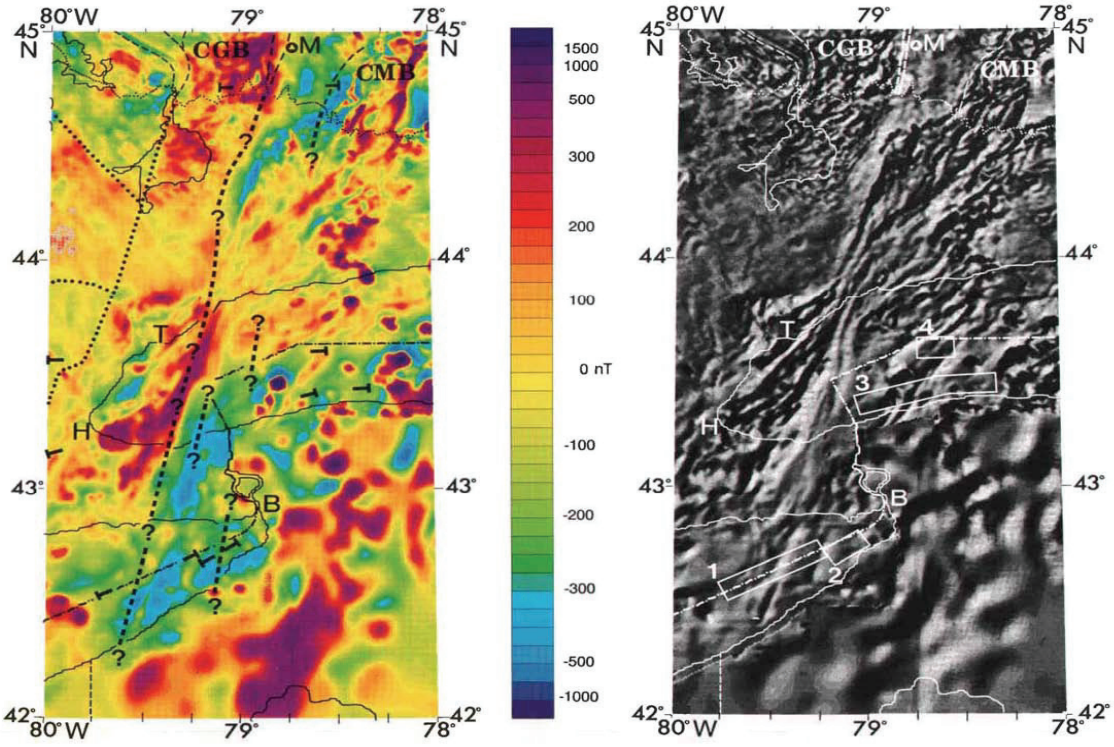

Notes: On left, dashed lines indicate magnetic trends coincident with interpreted boundary zone of the CMBBZ. Dotted lines are Grenville subdivisions; fine dotted line shows northern limit of Paleozoic cover. Location references include, B – Buffalo; M – Minden; T – Toronto; H – Hamilton; CGB – Central Gneiss Belt; CMB – Central Metasedimentary Belt. On right, rectangles 1, 2, 3, and 4 are locations of seismic profiles. The shaded relief image is illuminated from an apparent sun to the southeast. Figure is from Forsyth et al. (1994b).

Figure 2.13: Residual Total Magnetic Field and Shaded Relief Image and Location of CMBBZ

The structural style west of the CMBBZ changes significantly in Lake Erie. Forsyth et al. (1994b) observe westerly dipping mid-crustal reflections below and to the west of the CMBBZ. West-dipping mid- to deep crustal reflectors west of the CMBBZ were also observed in COCORP line OH-2 (Pratt et al. 1989) (Figure 2.6). Ouassaa et al. (2002) observed a change from east-dipping to west- or northwest-dipping reflectors in the center of line 6 (Figure 2.6). Hoehn (1991) reprocessed the seismic data from Lake Erie and interpreted the Akron Magnetic Boundary as a major suture within the Grenville province that separates east-dipping upper and middle crustal reflectors in the west from west-dipping mid-crustal reflectors in the east. Hoehn (1991) uses the terminology of Lidiak and Hinze (see Rankinet al. 1993) (Figure 2.14) and defines the Akron Magnetic Boundary as the eastern boundary of the eastern Midcontinent Magnetic Belt, a basement province between the CGB and CMB in the subsurface of Ohio and Lake Erie.

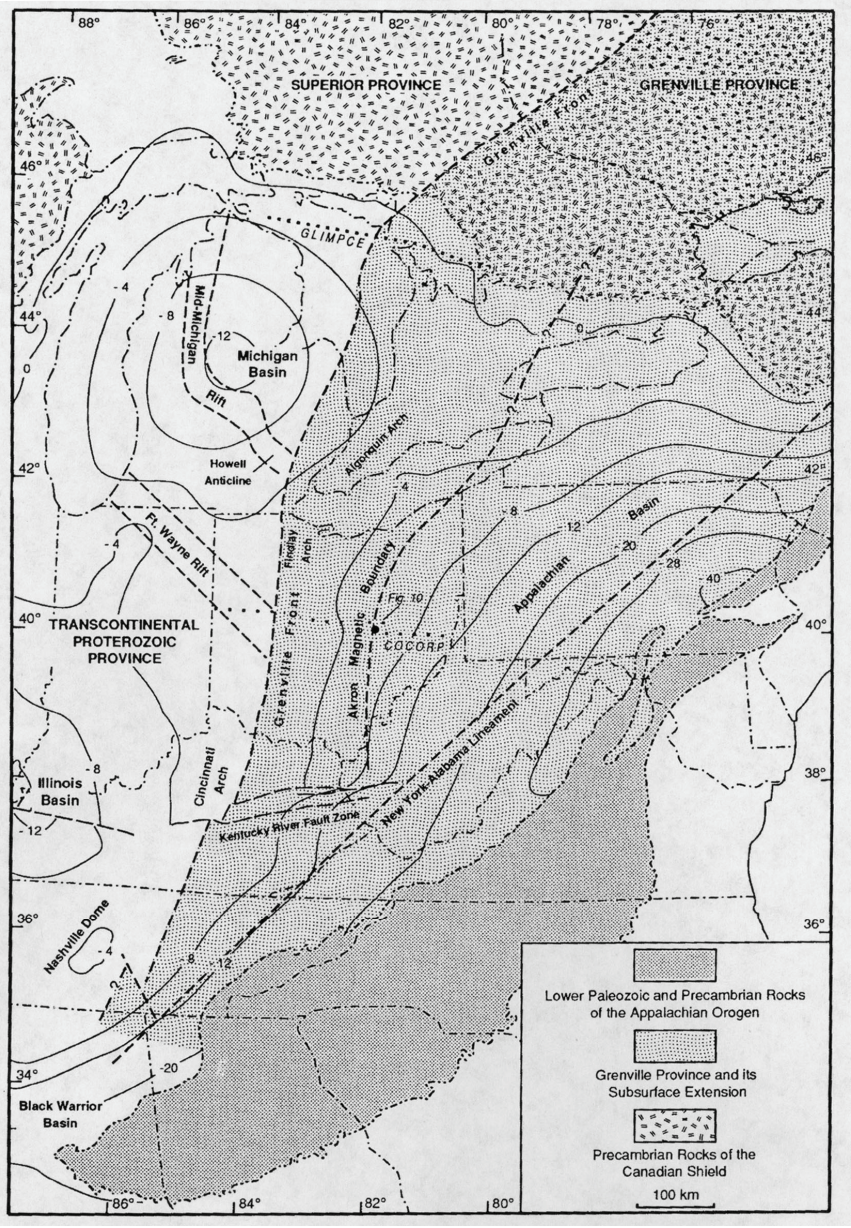

Notes: Heavy dashed lines are major basement structures. Note that northward continuation of the Akron Magnetic Boundary appears to coincide with the CMBBZ (See Figure 2.8, Figure 2.12, and Figure 2.13). Figure is from Rankin et al. (1993).

Figure 2.14: Basement Configuration Map and Regional Precambrian and Phanerozoic Structures in Part of Eastern North America

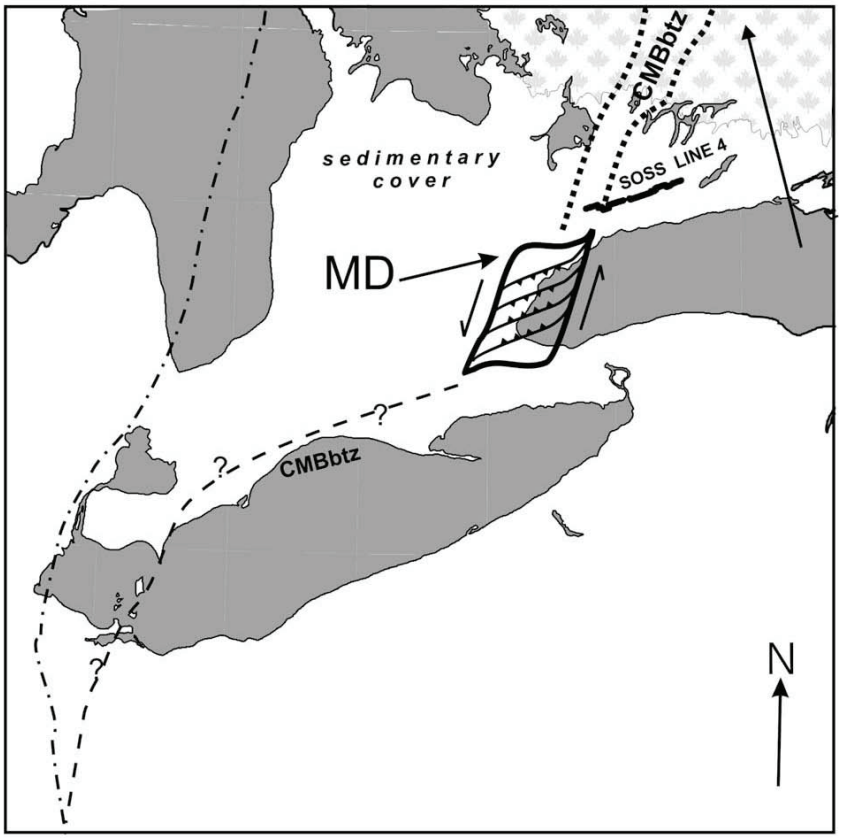

Notes: CMBbtz - Central Metasedimentary Belt boundary tectonic zone; MD - Mississauga domain. Figure is from O'Dowd et al. (2004).

Figure 2.15: Revised Location of the Central Metasedimentary Belt Boundary Zone

2.2.5.3 Composite Arc Belt Boundary Zone

The CABBZ (Ouassaa and Forsyth 2002) (Figure 2.16), also called the Elzevirian-Frontenac boundary zone (White et al. 2000), corresponds to the Sharbot Lake domain of Carr et al. (2000), who interpreted it as a rift arc. Continuation of the CABBZ into New York may correspond to the Clarendon-Linden fault system (Ouassaa and Forsyth 2002).

White et al. (2000) estimated that these three structures (the GFTZ, CMBBZ, and CABBZ) accommodated approximately 15 km of structural relief, as shown on deep seismic reflection profiles. Prominent north-northeast-trending geophysical anomalies associated with exposed Grenville structures extend southward beyond the Canadian Shield and beneath the unconformable lower Paleozoic cover rocks. Regional geologic maps (e.g., Ontario Geological Survey 1991) indicate that the overlying Paleozoic rocks are, with few exceptions, relatively flat-lying and laterally continuous, indicating that no large-scale major faulting has occurred in the region since they were deposited.

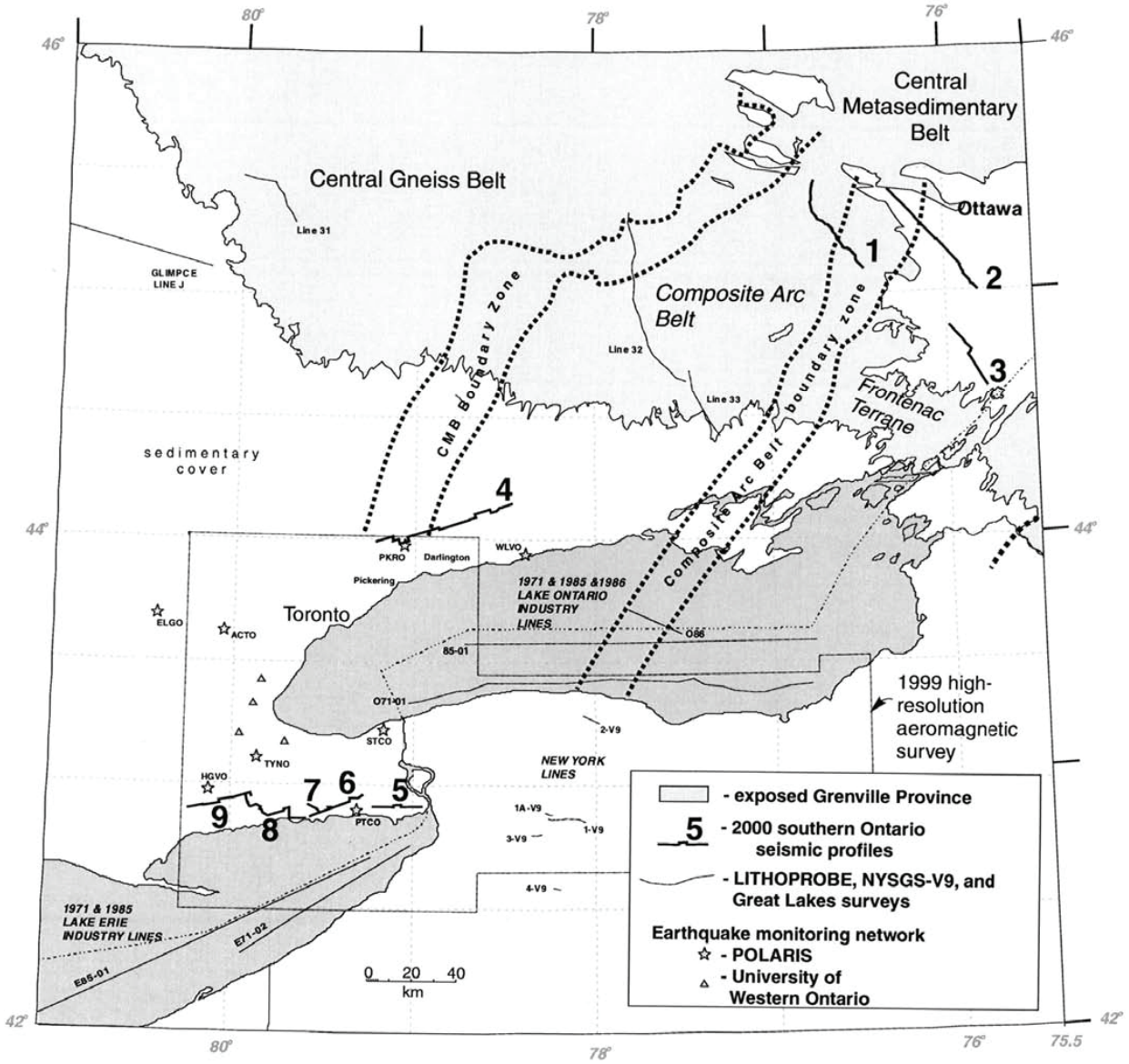

Note: Figure is from Ouassaa et al. (2002).

Figure 2.16: Location of Composite Arc Belt Boundary Zone

2.2.6 St. Lawrence Rift System

Crustal extension and rifting late in the Neoproterozoic and into the earliest Cambrian separated the Neoproterozoic supercontinent Rodina into East Gondwana, West Gondwana, and Laurentia (Figure 2.17) (Faill 1997a). In the study region, this rifting event resulted in the development of the St. Lawrence rift system (SLRS). The breakup of Rodinia spanned approximately 200 million years, with separation of East Gondwana from western Laurentia approximately 750 million years ago and rifting of eastern Laurentia from West Gondwana

resulting in the opening of several intervening oceans[2] (Figure 2.17) (Faill 1997a). A mantle plume initiated Iaptan rifting along the Sutton Mountain triple junction (Kumarapeli 1985) that resulted in the development of the St. Lawrence valley system and aulocogens of the Ottawa-Bonnechere and Saguenay grabens (Kumarapeli and Saull 1966; Kumarapeli 1985, 1993).

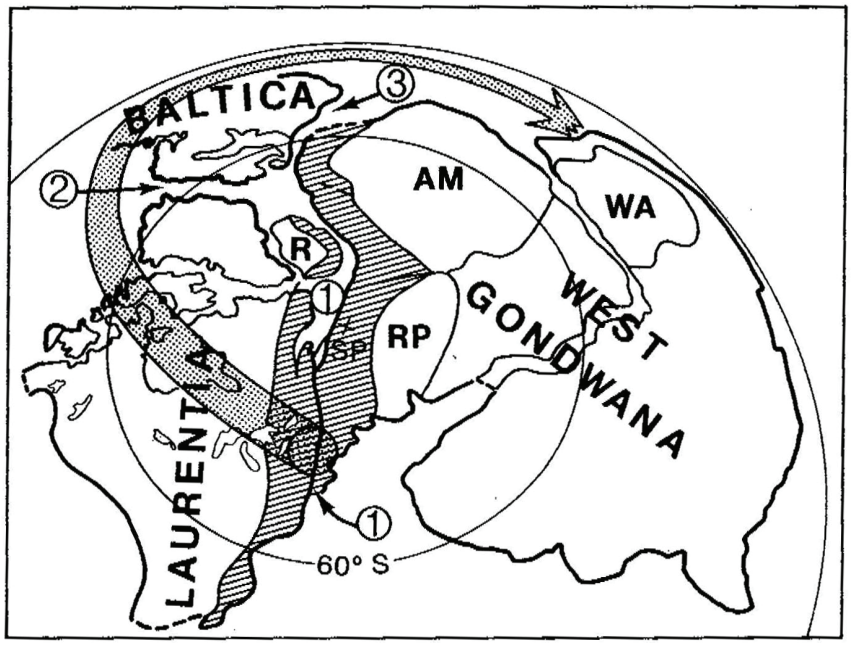

Notes: Numbers on figure refer to, 1 – Theic Ocean, 2- Iapetan Ocean, and 3 – Rheic Ocean. Letters on figure refer to, AM – Amazonia, RP – rio de la Plata, WA – Western Africa, R – Rockall platform, and SP – South Pole. Figure is from Faill (1997a).

Figure 2.17: Reconstruction of Rodinia at the End of the Neoproterozoic

Based on geochronological studies of the Sutton Mountain volcanics, Kumarapeli (1993) established the following sequence: rifting initiated at 590 Ma and continued for 35 million years; rifting ceased about 554 Ma after an outburst of alkaline to transitional basalts at the Sutton Mountain triple junction; a period of rift-facies clastic sedimentation followed until the rift-drift transition at 550 Ma. Kamo et al. (1995) confirmed that the Grenville dike swarm of the Ottawa graben is coeval with Sutton Mountain volcanism (500 Ma), implying that this swarm was emplaced within a relatively short time span at the onset of rifting. Major and trace element studies of the rocks confirm a mantle source consistent with plume activity (St. Seymour and Kumarapeli 1995, Abdel-Rahman and Kumarapeli 1998). Puffer (2002)

[2] The Iapetus Ocean was initially defined as the early Paleozoic ocean between Baltica and Laurentia (Greenland); the Theic Ocean was defined as the ocean between Laurentia and Gondwana; and the Rheic Ocean between Baltica and Gondwana (Figure 2.17). Faill (1997) emphasizes that the subsequent universal usage of Iapetus refers to the Paleozoic ocean off the Laurentia east margin and that sensu stricto the Iapetus Ocean was closed in the late Silurian Caledonia orogeny during the docking of Avalonia microcontinents with Laurentia. The remaining ocean that lay east of Avalonia is generally called Theic, leading Faill (1997) to recognize the Paleozoic ocean east of Laurentia as Theia. This discussion uses the terminology Iapetus as given by the authors cited, recognizing the distinction between these three Paleozoic oceans.

compiled a database of high field-strength elements for Late Neoproterozoic to early Paleozoic flood basalts revealing that super plume activity peaked at 550 Ma at the Sutton Mountain triple junction.

The SLRS comprises abundant large-scale normal faults displacing lower Paleozoic strata and underlying Grenville basement on the order of many hundreds of meters along the Ottawa, Champlain, St. Lawrence, and Saguenay river valleys (Figure 2.18) (Kumarapeli and Saull 1966). These extensional faults generally cut discordantly across Grenville-aged structures instead of reactivating them. The rift structures include zones of en-echelon faults parallel to the ancient margin, possible fracture zones transverse to the ancient margin, and two well-defined aulacogens (failed rifts)—the Ottawa and Saguenay grabens (fault-bounded troughs). The north-northeast-trending faults along both the Champlain and St. Lawrence river valleys, once attributed to a two-sided failed intracontinental rift, are now recognized as part of the southeast-facing Iapetan margin (Wheeler 1996a).

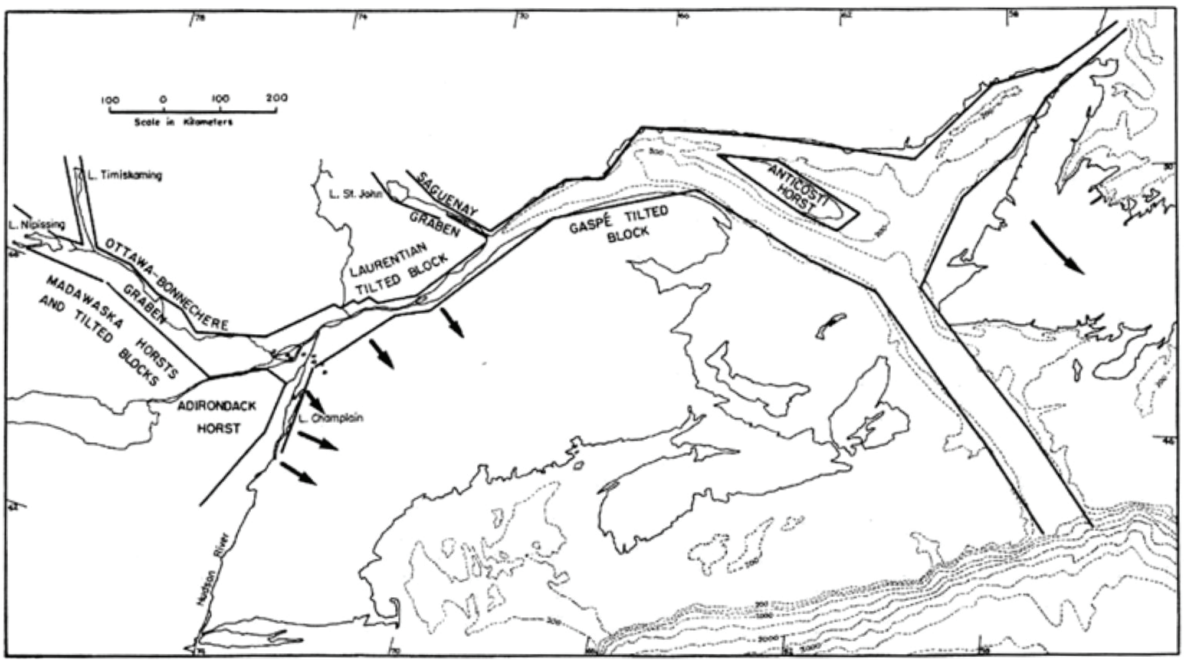

Note: Figure modified from Kumarapeli and Saull (1966)

Figure 2.18: Rift Zones of the St. Lawrence System

The SLRS provides evidence for multiple phases of reactivation. The St. Lawrence fault crosses the Devonian Charlevoix impact crater (Figure 2.19) without major deflection, suggesting post-impact reactivation (Lemieux et al. 2003). Faults within the Ottawa graben show three phases of reactivation consistent with the closure of the Iapetus Ocean, emplacement of Cretaceous dikes, and the post-Cretaceous stress field of North America (Rimando and Benn 2005). Faults in the southern portion of the rift provide evidence for northwest-southeast extension associated with the opening of the Iapetus Ocean; west-northwest/east-southeast compressions followed by minor north-northwest compressional events are associated with Appalachian thrusting; and, northeast-southwest

and north-northwest/south-southeast extension is associated with the opening of the Atlantic-Labrador Ocean. Northeast-southwest compression postdates these events (Rocher et al. 2003).

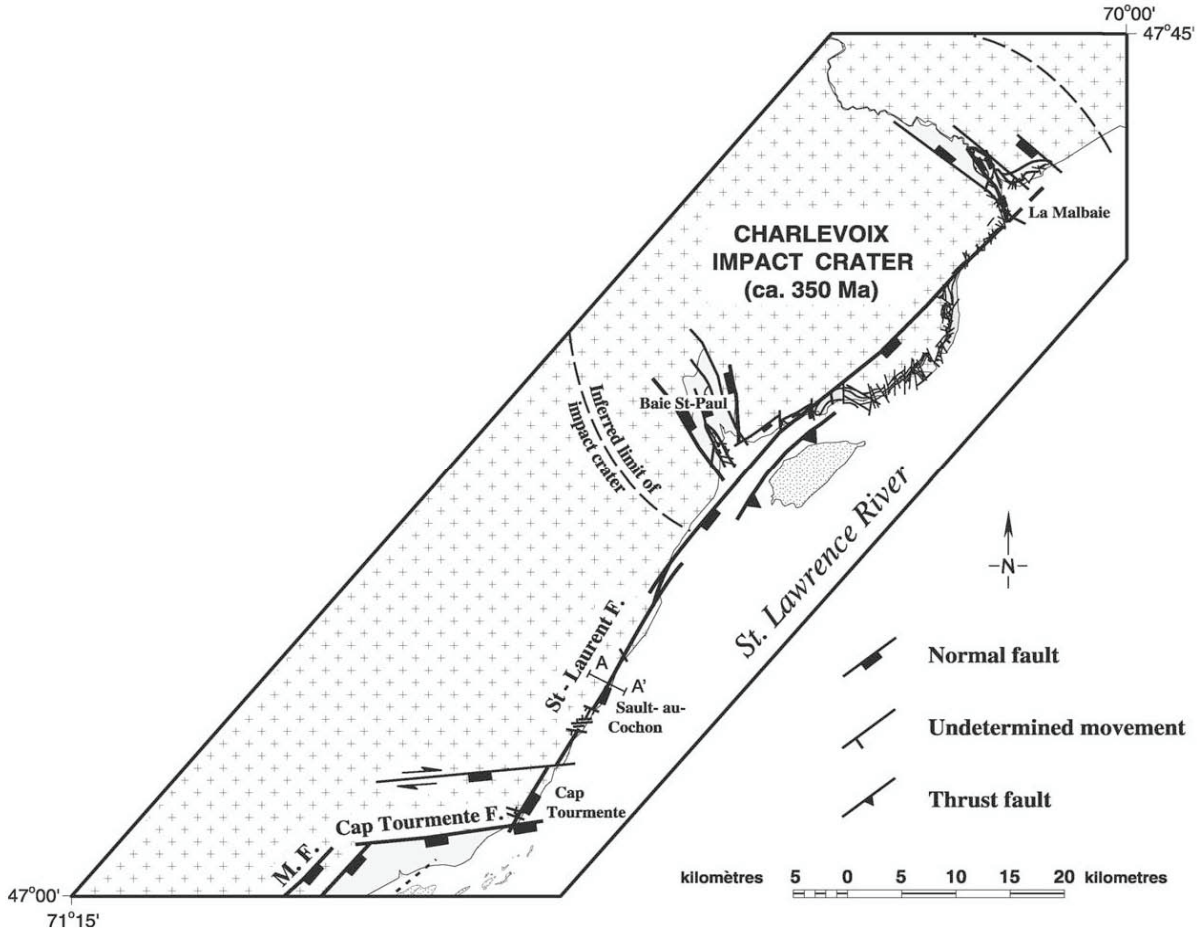

Note: Figure is from Tremblay et al. (2003)

Figure 2.19: Faulting in the Charlevoix Impact Crater

2.2.7 Intracratonic Basins

The four main Paleozoic structural units within the study region are the Michigan and Appalachian basins and the northwest-southeast-trending Algonquin and Findlay arches, which separate the basins (Figure 2.3). These structural features are present on structure contour maps of the Precambrian basement as subtle, contiguous features with a regional dip of less than one degree (Brigham 1971). The Michigan Basin is visible on these contours as a smooth, arcuate pattern, whereas contours within the Appalachian Basin have a triangular pattern (Brigham 1971).

The Michigan Basin is a circular intracratonic basin that subsided and was filled with marine sediments during the Paleozoic. These sediments dip gently toward the center of the basin

and away from the Algonquin arch (Sanford 1993). The Michigan Basin contains 4900 m of Paleozoic sedimentary rocks and at least 1500 m of Precambrian sedimentary rocks associated with the southeast arm of the Midcontinent rift system. Rifting was followed by thermal subsidence at 520 Ma, leading to an embryonic form of the Michigan Basin as a sag basin. Major subsidence began in the early Ordovician when the configuration as a circular basin was attained. The main structural grain of the basin is oriented northwest-southeast and is characterized by Paleozoic anticlines. The basin is tilted slightly asymmetrically to the north (Catacosinos et al. 1991).

The Appalachian Basin is elongate and sharply truncated by the Appalachian structural front to the east and attains a maximum depth of approximately 1100 m. Dips into the Appalachian Basin became steeper in the Late Ordovician and again in the Late Devonian (Brigham 1971). The Appalachian Basin formed as a single elongate basin in response to the Ordovician Taconic orogeny (Faill 1997a). By the Late Ordovician, orogenic activity confined the Appalachian Basin to its present geometry (Sanford 1993).

The northeast-trending, northeast-plunging Findlay Arch in western Ohio and southeast Michigan, and the northeast-trending, southwest-plunging Algonquin Arch in Canada separate the Michigan and Appalachian basins. The Findlay and Algonquin arches are part of the same feature, which was present in the Precambrian and remained a passive, positive feature as flanking basins settled. The present-day Findlay-Algonquin arch structure developed during episodes of subsidence that alternated on opposite sides of the arches. The axis of these arches migrated southeastward in response to encroachment of the Michigan Basin. The Findlay and Algonquin arches influenced Paleozoic sedimentary deposition into the Middle Devonian (Brigham 1971).

The Chatham Sag was formed by the mutual plunges of the Findlay and Algonquin arches and is first indicated in the Ordovician Trenton and Black River formations (Brigham 1971). The Chatham Sag is one of several major inlets into the Michigan Basin. This east-west-trending structure did not have a significant influence on sedimentation until the Late Silurian. The northern margin of the Chatham Sag is defined by the east-west-trending Electric fault (Brigham 1971), which deflects the nose of the Algonquin Arch to the west (see Section 2.4).

2.2.8 Penobscot Orogeny

Late Cambrian–Middle Ordovician Penobscottian orogeny amalgamated composite terranes within arcs of the Iapetus Ocean (Murphy and Keppie 2005) and therefore did not result in deformation within Laurentia. This tectonic event corresponds to low subsidence rates (Howell and van der Pluijm 1990) within a trough-shaped Michigan Basin (Howell and van der Pluijm 1999). These terranes were accreted to the Laurentian margin during the Taconic Orogeny (Moench and Aleinikoff 2003).

2.2.9 Taconic Orogeny

Magmatic arcs that developed in the Late Cambrian within the Theic Ocean were obducted to the Laurentian margin during the Middle to Late Ordovician Taconic Orogeny (Faill 1997a, Moench and Aleinikoff 2003). This widespread tectonic event occurred from Labrador to Alabama and is currently exposed in the southern Appalachians in the Piedmont and Great Valley allochthons and in western New England (Figure 2.20). Assemblages in the southern Appalachians contain complexes assembled in the Theic Ocean, whereas assemblages of western New England consist of two magmatic arcs: the Halwey arc of the Brompton-Cameron terrane and the Ammonoosuc arc of the Central Maine terrane (Faill 1997a). These arcs

developed from multiple accretionary events with changing polarity shortly before the closure of the Iapetus Ocean at 460 Ma (Moench and Aleinikoff 2003). This deformation produced north-south- to northeast-southwest-trending reverse conjugated brittle faults under a pure compressional stress regime late in the development of the orogeny (Faure et al. 2004). This Taconic compressional event also resulted in reactivation of Iapetan faults in the St. Lawrence lowlands as east-northeast/west-southwest dextral and northwest-southeast sinistral faults (Rocher et al. 2003, Faure et al. 2004). The Appalachian Basin developed in response to the Taconic orogeny and was expressed as a single elongate basin from Alabama to at least Quebec (Faill 1997b). The Michigan Basin experienced renewed subsidence (Howell and van der Pluijm 1990) and transitioned from basin-centered to eastward tilting (Howell and van der Pluijm 1999).

2.2.10 Salinic Orogeny

Late Ordovician-Silurian Salinic Orogeny accreted the Gander, Avalon, Nashoba, and Carolina terranes to Laurentia during the closure of the Iapetus Ocean during the Laurentia-Avalonia collision (Murphy and Keppie 2005). Silurian metamorphism (430-410 Ma) in the Northern Appalachians is attributed to retrograde metamorphism following the main compression event (Tremblay and Castonguay 2002). The event involved southeast-directed transport of Taconian crustal wedge followed by normal faulting (Saint-Joseph and Baie Verte-Brompton faults) and development of the fault-bounded sedimentary basins of the Connecticut Valley-Gaspé Trough (Tremblay and Castonguay 2002). Tremblay and Pinet (2005) attribute the late-stage extension to supracrustal extensional collapse due to late-stage delamination of the lithospheric mantle in a southeast-dipping subduction zone. Subsidence rates in the Michigan Basin are consistent with that of the Taconic Orogeny (Howell and van der Pluijm 1990) and correspond to a transition from eastward tilting to basin-centered morphology (Howell and van der Pluijm 1999).

2.2.11 Acadian Orogeny

The Devonian Acadian Orogeny has been attributed to either the collision of Avalonia with Laurentia or the accretion of the Meguma terrane; however, recent work indicates that the Meguma terrane is the passive margin on the southern margin of Avalonia (Murphy and Keppie 2005). Murphy and Keppie (2005) interpreted the Acadian Orogeny as forming along an Andean-type margin that possibly overrides a plume and swell. Acadian metamorphism is well dated as 385 – 375 Ma in the southern part of the Dunnage zone (Tremblay et al. 2000). Deformation from the Acadian Orogeny is expressed as east-southeast/west-northwest compression in a transpressional regime producing east-northeast/west-northwest dextral and northwest-southeast sinistral strike-slip faults that crosscut Taconian thrust faults in the Appalachians of Quebec and New Brunswick (Faure et al. 2004). This deformation also resulted in reactivation of Iapetan structures in the St. Lawrence lowlands (Faure et al. 2004, Rocher et al. 2003). The Acadian Orogeny is expressed in the Appalachian Basin as siliclastic sedimentation from the Middle to Late Devonian (Faill 1997b), with additional pulses of uplift occurring in the Early and Late Carboniferous. The morphology of the Michigan Basin transitioned from narrow basin-centered in the Early to Middle Devonian to broad basin-centered in the late Middle Devonian, and eastward tilting in the Late Devonian and Carboniferous (Howell and van der Pluijm 1999).

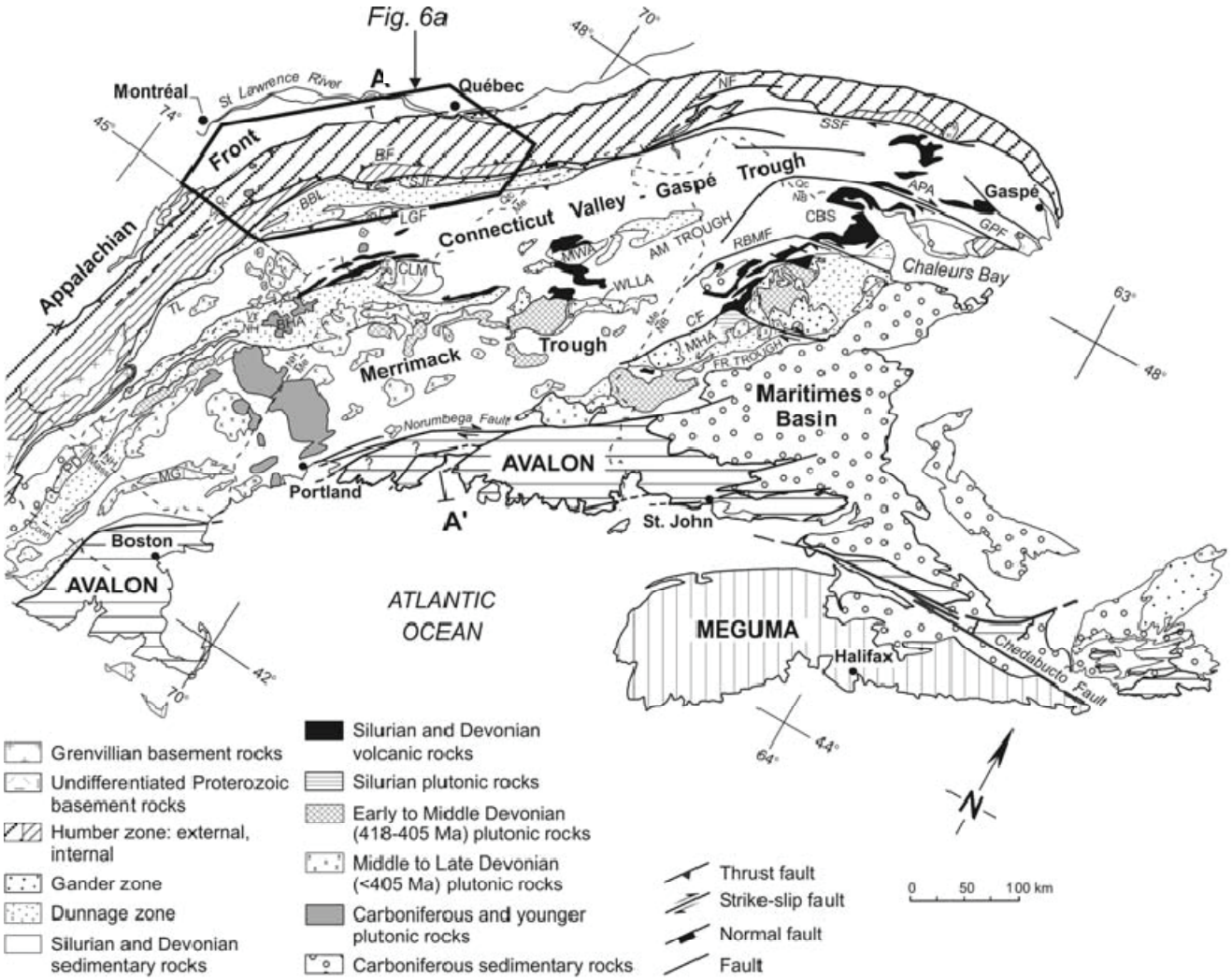

Notes: The major Silurian/Devonian sedimentary basins are the Connecticut Valley–Gaspe, Merrimack, Aroostook–Matapedia (AM) and Fredericton (Fr.) troughs. Basement rocks: CLM – Chain Lake Massif;MG–MassabesicGneiss; PD – Pelham Dome.Major anticlinoria and synclinoria: APA – Aroostook–Perc´e anticlinorium; CBS – Chaleurs Bay synclinorium; BHA – Bronson Hill Anticline; MHA – Miramichi Highlands Anticline; MWA – Munsungun– Winterville Anticline; WLLA – Weeksboro–Lunksoos Lake Anticline. Major faults: BBL – Baie Verte–Brompton Line; BF – Bennett fault; SJF – Saint-Joseph fault; LGF – LaGuadeloupe fault; TL – Taconic Line; NF – Neigette fault; SSF – Shickshock-Sud fault; GPF – Grand Pabos fault; RBMF – Rocky Brook–Millstream fault; CF – Catamaran fault. Line A–A' indicates the location of the structural profile of Figure 2. State boundaries: Conn – Connecticut; Mass – Massachussets; Me – Maine; NB – New Brunswick; NH – New Hamshire; Qc – Qu´ebec; Vt – Vermont. The boundary between Medial New England (Gander zone) and Composite Avalon is approximate (see question marks); see text for discussion. Figure is from Tremblay and Pinet (2005).

Figure 2.20: Terranes of the Northern Appalachians

2.2.12 Charlevoix Impact Crater

The Devonian Charlevoix impact crater is located on the north shore of the St. Lawrence River 100 km northeast of Quebec (Lemieux et al. 2003). The Devonian age is established from 321 and 372 Ma K-Ar dates on impact melt and breccia (Tremblay et al. 2003). The St. Lawrence fault crosses the Charlevoix impact crater without major trend deflection or fault

offsets within or at the boundaries of the Devonian impact structure (Figure 2.19). This observation suggests that impact-related faults did not significantly alter the orientation of pre-existing structures and that at least one episode of reactivation is younger than the impact structure, most probably concurrent with the opening of the Atlantic Ocean in the Mesozoic (Tremblay and Lemieux 2001, Lemieux et al. 2003).

2.2.13 Alleghenian Orogeny

There is general consensus that the Late Carboniferous–Permian Allegheny Orogeny was due to terminal collision between Gondwana and Laurentia-Baltica that closed the Rheic Ocean and resulted in the formation of Pangea (Murphy and Keppie 2005). The Alleghenian Orogeny produced decollement tectonism in the central and southern Appalachians along with early penetrative shortening, late low-angle thrusts, low-grade metamorphism, and transpressional shear zones. The northern Appalachians exhibit relatively high-grade metamorphism of Taconic and Acadian crust and deformation of Appalachian deposits near the Hudson Valley (Faill 1998). Brittle faults of the northern Appalachians exhibit three phases of compression: an early north-northwest/south-southeast compression, a north-northeast/south-southwest compression, and a late west-northwest/east-southeast compression (Faure et al. 1996a).

2.2.14 Opening of the Atlantic

Mesozoic rifting resulted in the breakup of Pangea. This rifting is associated with the separation of the North American and African plates and produced rift basins along the Atlantic seaboard that are situated landward of the hinge zone of the continental margin. This landward region experienced considerably less crustal thinning than did the region seaward of the hinge zone that includes the deeper marginal sedimentary basins (Klitgord et al. 1988). Faure et al. (2006) identified two phases of extension: an initial Late Triassic east-west extension related to the formation of rift basins in the Bay of Fundy and South Georgia and Early Jurassic east-southeast/west-northwest extension related to the central Atlantic rift system.

2.2.15 Cretaceous Volcanism and Extension

Cretaceous volcanism in eastern Canada and New England has been attributed either to intrusions along pre-existing zones of weakness (McHone 1996) or movement of the Great Meteor hotspot track (Crough 1981, Sleep 1990) beneath eastern North America.

Evidence for the hotspot consists of an alignment of mapped alkalic intrusions from the Monteregian Hills of Quebec to the Cretaceous seamounts of offshore New England (Zartman 1977). Morgan (1983) attributed the age distribution of these rocks to two hotspot tracks passing through New England at different times: the Verde hotspot track at 160 Ma and the Meteor hotspot at about 120 Ma. Duncan (1984) observed that radiometric ages for dredged volcanic rocks from seven of the New England seamounts increase in age from the southeast (82 Ma for the Nashville Seamount) to the northwest (103 Ma for the Bear Seamount). Subsequent mapping by Heaman and Kjarsgaard (2000) extended the Great Meteor hotspot track to the Rankin Inlet on the west side of James Bay by observing four periods of kimberlite magmatism along a northwest-southeast trend to Timiskaming.

After reviewing petrologic data, McHone (1996) observed that although a plume model fits the petrologic data, it does not fit the geographic age distribution of igneous activity. McHone (1996) concluded that lithospheric processes were necessary to start and stop the generations of

magma from the same source in the mantle, and he proposed that heterogeneous source areas coupled with tectonic reactivation of crustal structures could explain the distribution of these rocks. Results of a paleostress analysis of brittle faults in the Quebec Appalachians provide evidence for two distinct phases of Cretaceous extension: an initial geographically widespread northeast-southwest phase of extension and a later north-south phase of extension confined to southern Quebec (Faure et al. 1996b). Faure et al. (1996b) attributed this Cretaceous volcanism to continued fragmentation of Pangea. Early northeast- to east-northeast-oriented extension and associated magmatism between 140 and 90 Ma are correlated to rifting between Labrador and Greenland at approximately 140 Ma, to early breakup stages of the South Atlantic Ocean at 130 Ma, and to north-south-oriented extension and emplacement of dikes at 125 Ma, corresponding to the separation of Iberia from Newfoundland (Faure et al. 1996b).

Crough (1981) suggests that the passage of the hotspot caused a 600 km wide zone of epeirogeny in southeastern Canada and New England, resulting in erosion of at least 1 km in Montreal and as much as 6 to 7 km in New England. Recent thermochronology studies provide evidence for Late Cretaceous reactivation. Roden-Tice et al. (2000) see evidence for two periods of unroofing of the Adirondack Mountains from apatite fission track dating: Late Jurassic to Early Cretaceous (160 – 120 Ma) throughout the region and Early to Late Cretaceous (~110 – 80 Ma) in the southeast that must be explained by tectonic denudation processes. Roden-Tice (2000) support the hypothesis that this Early to Late Cretaceous uplift, contemporaneous with intrusion of the Monteregian Hills plutons, can be attributed to differential unroofing resulting from reverse reactivation of east-dipping normal faults.

Similar uplift ages were observed for the Hartford basin of Massachusetts and Connecticut, indicating that the basin is Cretaceous in age, not early Mesozoic (Roden-Tice and Wintsch 2002). Apatite fission track ages across the Norembega fault zone in southern coastal Maine reveal a 30 – 50-million-year discontinuity, suggesting that this fault shows 2 km of vertical offset in the Late Cretaceous (West and Roden-Tice 2003). Roden-Tice and Tice (2005) attribute the widespread unroofing during the Middle Jurassic to Late Cretaceous, accommodated by northwest-southeast extensional reactivation of faults in the Adirondacks and New Hampshire, to remnant heating from the Great Meteor hotspot track.

A remnant thermal anomaly is inferred to exist in the upper mantle and lower lithosphere, based on several geophysical studies. Travel-time inversions of teleseismic results from southern Ontario image a low-velocity corridor between 50 and 300 km that crosscuts regional structures of the Grenville province and Ottawa-Bonnechere graben (Rondenay et al. 2000). These results are attributed to a zone of contrasting thermal-compositional-anisotropic properties related to the Great Meteor hotspot (Rondenay et al. 2000). Subsequent work by Li et al. (2003) confirms the presence of a broad low-velocity layer in the upper mantle and attributes it to the Cretaceous hotspot. Crustal thickness and average VP/VS ratio maps for the area derived from teleseismic receiver functions illustrate thin crust northeast of the Ottawa-Bonnechere graben coincident with the Western Quebec seismic zone (Eaton et al. 2006).

2.3 Contemporary Stress and Neotectonic Setting

Southeastern Canada is included in a broad midplate compressive stress province that includes most of the central and eastern United States and possibly much of the western North Atlantic basin to within about 250 km of the mid-Atlantic ridge (Zoback et al. 1986). The stress field throughout this region is characterized by a nearly horizontal, northeast- through east-striking axis of maximum compressive stress (Zoback and Zoback 1991). The overall uniformity in the direction and relative magnitude of the midplate stress pattern suggests a far-field tectonic source, and ridge-push (due to accretion of oceanic crust along the mid-Atlantic ridge) is preferred over basal drag as the primary source of stress in the midplate region (Zoback and Zoback 1991).

Most earthquakes in this midplate stress province have strike-slip, oblique-reverse, or reverse fault mechanisms. Well-constrained focal mechanisms for earthquakes that have occurred in eastern North America in the past 25 years indicate primarily thrust (reverse) fault and/or strike-slip events (see, e.g., Zoback 1992, Adams and Bell 1991). Northwest- and northeast-trending faults are most favourably oriented for reactivation by reverse and/or strike-slip displacement, according to recent interpretations of the orientations of the contemporary regional stress components (Zoback 1992, Adams and Bell 1991, Adams 1995). Reverse faulting on planes striking other than northeast and northwest, however, is not precluded (Adams 1995). Equivocal evidence from within the seismogenic crust suggests that stress orientations may change with depth: shallower earthquakes (less than 10 km) tend to be more consistent with east-northeast compression, whereas deeper events tend to be less consistent (Adams and Bell 1991). The available data from eastern Canada indicate that deviatoric stresses throughout the shield generally exceed those necessary to generate earthquakes (Adams 1995). However, there is no evidence to suggest that particular regions are more likely to generate earthquakes based on the stress indicators (Adams 1995).

The seismicity of the Southern Great Lakes region has been studied in detail by Dineva et al. (2004) and Ma and Atkinson (2006). Dineva et al. (2004) relocated hypocenters from 106 earthquakes occurring during the period from 1990 to 2001 and identified several earthquake clusters. They report that these seismicity zones appear to correlate with areas where the regional magnetic data exhibit linear anomalies. According to Dineva et al. (2004), the proximity of the earthquake clusters to large bodies of water and the association with magnetic anomalies suggest that both surface water and pre-existing basement structures may play significant roles in controlling the occurrence of the seismicity. Ma and Atkinson (2006) analyzed focal depths for small-to-moderate earthquakes ($M_N \geq 2.8$) occurring from 1980 to 2004 in southern Ontario and northern New York. They found that virtually all of the earthquakes in the Lake Ontario region occurred with focal depths shallower than 8 km.

Adams and Basham (1991) have reported that most large historical and instrumental earthquakes in eastern Canada have occurred near Paleozoic or younger rift zones. This is similar to stable continental region earthquakes worldwide (Johnston et al. 1994). The Early Paleozoic SLRS, which is delineated by a persistent pattern of seismicity, is the postulated source of numerous large historical earthquakes in southeastern Canada (Adams and Basham 1991). Seismicity along this rift system is concentrated in a number of well-defined clusters, including the Ottawa River, Charlevoix, and lower St. Lawrence River

seismic zones, which are all separated by relatively aseismic regions. Fault slip in response to the current tectonic stress regime on pre-existing structures associated with the SLRS is believed to be the causal mechanism of this seismic activity (Adams and Bell 1991, Anglin 1984, Forsyth 1981). Focal mechanisms from historical earthquakes within these seismic zones indicate mainly thrust events occurring at depths of 5 to 25 km within the Grenville basement (Adams and Basham 1991).

The postulated northwestern boundary of the Late Proterozoic/Early Paleozoic Iapetan rifted margin (IRM) tectonic province is interpreted as the cratonward limit of large normal faults in the Iapetan passive margin that have some long-term potential for reactivation in the present compressional tectonic regime (Wheeler 1995). Wheeler (1995) has suggested that the Clarendon-Linden fault system (Figure 2.21) forms a segment of this western boundary. It is not known, however, whether normal slip congruent with Iapetan rifting occurred on this structure during the Late Proterozoic to Cambrian, and thus it cannot be defined unequivocally as an Iapetan structure (Wheeler 1996a). There is also deep seismic evidence suggesting that the western boundary of the Iapetan margin may lie farther to the west, along the Central CMBBZ (Figure 2.21) of the Grenville province (Milkereit et al. 1992). However, the thickness (approximately 43 km) and structure of Precambrian crust in this region do not suggest significant Iapetan extension (Forsyth et al. 1994a, b; Zelt et al. 1994).

The eastern boundary of the IRM is defined by a zone of intense thinning that separates highly attenuated Grenville crust to the southeast from extended but relatively intact crust to the northwest containing large Iapetan normal faults (Wheeler 1996b). Compressional reactivation of Iapetan normal faults is thought to play an important role in the seismic behaviour of eastern North America (e.g., the Charlevoix, Giles County, and Eastern Tennessee seismic zones) (See: Adams and Basham 1991, Johnston et al. 1985, Powell et al. 1994, Wheeler 1995).

West of the IRM lies the Precambrian Central Craton (Wheeler and Johnston 1992), which is composed of relatively flat-lying, Paleozoic platform sediments, overlying non-extended basement crust of the Grenville and Eastern Granite-Rhyolite provinces (Bickford et al. 1986, Van Schmus et al. 1996, Figure 2.2 and Figure 2.5). The rate of historical seismic activity in this region is low and appears typical of stable cratonic crust (Johnston et al. 1994). In general, seismic activity and the geologic conditions most associated with earthquake activity in the stable continental region of central and eastern North America increase toward the east, away from the Precambrian central craton and toward the rifted passive continental margin.

A neotectonic investigation of the Bruce nuclear site was conducted by Slattery (2011). The purpose of the investigation was to examine Quaternary deposits to look for evidence of paleoseismicity within a 50 km zone surrounding the Bruce site. Aerial photo interpretation, including examination of high resolution light detection and ranging (LiDAR) imagery, was used to assess the occurrence of neotectonic features and/or landforms. Potentially significant features were examined in detail through field-based inspection. Features observed, including offset beach ridges and contorted sedimentary bedding, were assessed to be a result of anthropomorphic, glacial, or syndepositional origin and not to be a result of neotectonic activity. No evidence of paleoliquefaction features or evidence of active faulting was observed within the area investigated.

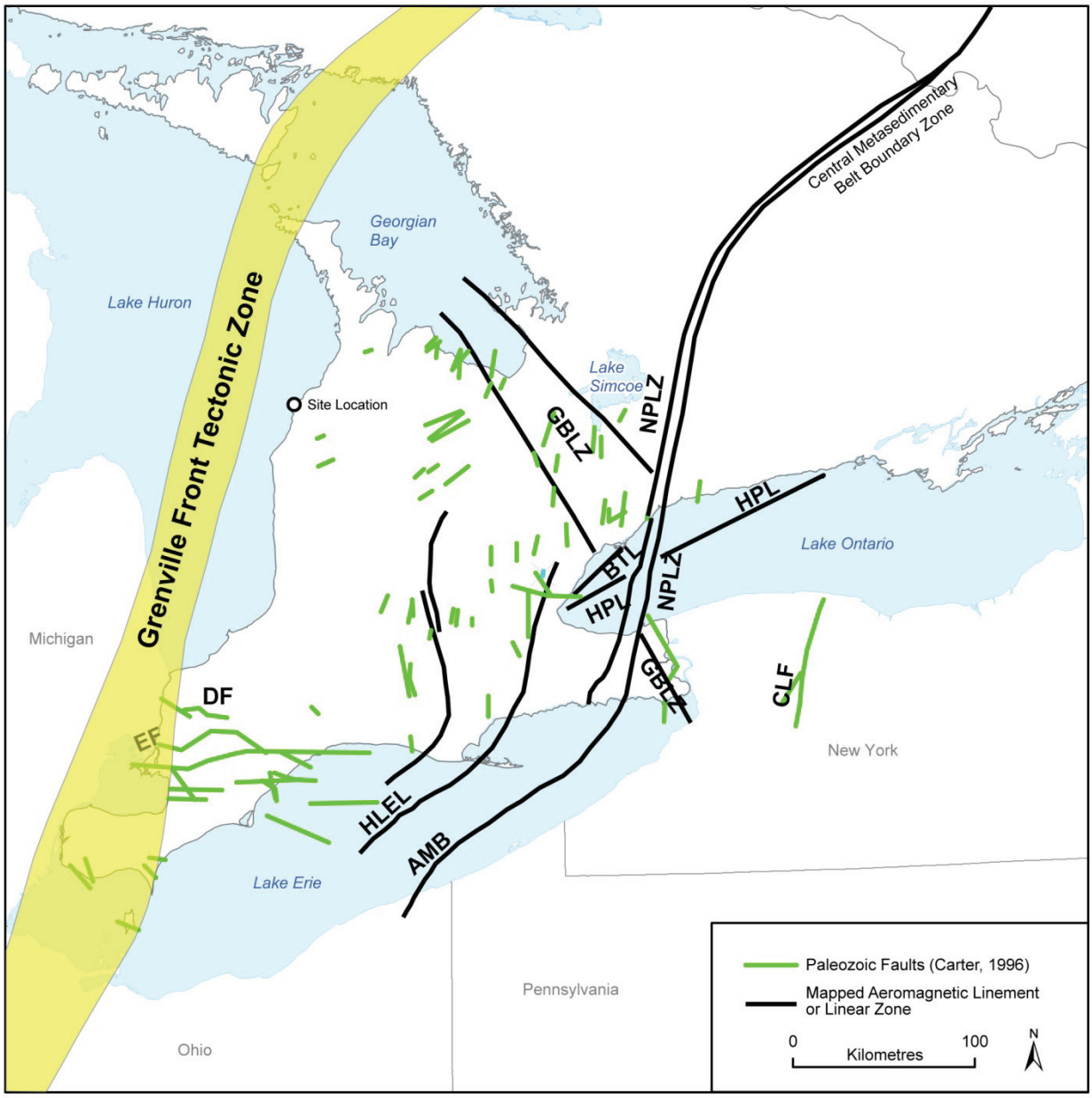

Note: Fault data is from Carter et al. (1996) and Armstrong and Carter (2006). Areomagnetic lineaments are after Carter and Easton (1990), Easton and Carter (1995), Wallach et al. (1998), Jacobi and Fountain (1993). CMBBZ: Central Metasedimentary Belt Boundary Zone; AMB: Akron Magnetic Boundary; NPLZ: Niagara– Pickering Linear Zone; HLEL: Hamilton– Lake Erie Lineament; BTL: Burlington–Toronto Lineament; HPL: Hamilton– Presqu'ile Lineament; GBLZ: Georgian Bay Linear Zone; EF: Electric fault; DF: Dawn fault; CLF: Clarendon – Linden fault (modified from Boyce and Morris 2002).

Figure 2.21: Structural Subdivisions of Precambrian Basement with Faults, Aeromagnetic Lineaments and Lithotectonic Domain Boundaries

2.3.1 Glacial Adjustments

Postglacial rebound or glacial isostatic adjustment (GIA) is the response of the solid earth to changing surface loads brought on by the waxing and waning of large-scale ice sheets and

glaciers. Tilting of relic lake shorelines, changes to modern lake levels, changes to surface gravity observations and secular movements (slow, systematic, persistent crustal motion over time) are manifestations of land uplift and subsidence brought about by GIA (Sella et al. 2007). GIA is also suspected as a cause of deformation within continental plates and may be a trigger of seismicity in eastern North America (Wu and Johnston 2000, Mazzotti and Adams 2005).

Late Cenozoic crustal deformation related to glacial processes is recognized in the southern Ontario region. The Laurentide ice sheet was the last of several great ice sheets to cover parts of Ontario during the Quaternary period (Barnett 1992). Differential uplift and tilting of the entire Lake Ontario basin has been attributed to postglacial isostatic rebound related to the removal of the Laurentide ice sheet (Martini and Bowlby 1991). A review of GIA and the implications for glacially induced faulting and nuclear repositories was recently published (Lund and Naslund 2009), in which the authors describe observations and numerical models used to study various aspects of these phenomena. Glacially induced faulting has been recorded almost exclusively in regions of low to moderate seismicity, generally where there has been no evidence of surface rupture during historical time, and all examples have involved reactivation of existing faults and fractures. Almost all of the large (i.e., kilometre-scale) faults generally accepted currently as being glacially induced are located in northern Fennoscandia (i.e., the region of Finland, Sweden, and Norway). Lund and Naslund (2009) state that current models of the process of faulting due to GIA are not mature enough to accurately predict the location and magnitude of future faulting events. They note that efforts are underway to include more complex processes in the faulting models, such as poroelastic effects, strain-release effects and local geological conditions.

The rates and uncertainties on seismic moment and deformation in eastern Canada, including a comparison of seismic strain rates with GIA predictions for the region, are described by Mazzotti and Adams (2005). They note that the differences between estimated rebound-induced strain rates and seismic strain rates suggests that only a very small percentage of the elastic GIA deformation leaks into plastic deformation to produce earthquakes. They also state that while models of GIA adjustments can in theory be used to predict three-dimensional velocity, strain and stress fields in the lithosphere, in practice the models are quite sensitive to the model inputs (e.g., ice load history, ambient tectonic stress, viscosity of the mantle), leading to significant variations in results.

Recent observations of GIA from global positioning system (GPS) velocity field data indicate that the hinge line marking the approximate boundary between regions of vertical rebound to the north and subsidence to the south in eastern North America lies close to the Bruce nuclear site (Sella et al. 2007). The residual velocity field indicates subsidence (1 to 2 mm/yr) throughout most of the site region to the south and uplift to the north, which achieves a maximum (~10 mm/yr) near Hudson Bay, the site of thickest ice at the last glacial maximum.

Studies of fluctuating water levels in the Great Lakes region indicate that these resulted from climate changes, as well as from the pattern of GIA-related uplift (Larsen 1985). The erosional and depositional terraces studied along the shores of Lakes Huron and Michigan were left at progressively higher altitudes northward, reflecting differences in the rates of rebound from south to north (Larsen 1985).

Bedrock pop-up structures are elongate anticlinal features that form at the bedrock surface by buckling under horizontal compression. They have been documented throughout southern Ontario, and most can be shown unequivocally to be postglacial, and thus neotectonic (e.g., Wallach 1990, Rutty and Cruden 1993, McFall 1993, Jacobi et al. 2007). Pop-ups generally appear as narrow ridges with open fractures located along their crests, and some

exhibit an en-echelon geometry (Rutty and Cruden 1993). The formation of pop-ups in this region can be attributed in most cases to the retreat of the Laurentide ice sheet and the reduction of the vertical component of crustal stress. Jacobi et al. (2007) investigated a popup field on the floor of western Lake Ontario. They report that the popups formed throughout late and postglacial time during the past 20,000 years, following the last glacial maximum. The earliest set of popups investigated trend west-northwest, and do not parallel major geophysical or structural linear zones in the region, suggesting that they developed in response to glacial rebound-induced stress. Younger popups form an irregular pattern with several orientations of axes. Jacobi et al. (2007) suggest that recently formed popups are likely a response to reduced glacial stress combined with far-field tectonic stresses.

2.4 Local Geologic Setting

The Bruce nuclear site is located on the eastern shore of Lake Huron between the northeastern edge of the Michigan basin and the northwestern edge of the Algonquin arch (Figure 2.3). The site is underlain by approximately 850 m of limestone, dolostone, shale, and evaporites ranging in age from Upper Cambrian to Middle Devonian (INTERA 2011). Descriptions of these sediments and their depositional history are included in the Regional Geology Report (AECOM AND ITASCA CANADA 2011), a supporting technical report prepared as part of the Phase 1 Geosynthesis Program for the Bruce nuclear site.

A model of regional-scale networks of east-west-trending and northeast-southwest-trending fractures and faults were postulated by Sanford et al. (1985) in southwestern Ontario. They proposed that these fractures developed during Iapetan rifting and suggested that subsequent compressional and extensional tectonic regimes during the Phanerozoic periodically reactivated these fractures. The reactivation occurred through uplift of the basement-cored arches marginal to the Paleozoic sedimentary basins, as well as through small-scale differential vertical displacement across the fracture/fault-bounded blocks. Using a large multiparameter geophysical and subsurface geological database, including newly processed data, Boyce and Morris (2002) investigated the relation between Precambrian basement structures and the occurrence of Paleozoic faults in southern Ontario. Their mapping indicates that regional basement magnetic trends in southern Ontario are systematically related to fracture patterns that occur within the overlying Paleozoic sedimentary rocks, which suggests reactivation and upward propagation of basement faults and fractures into overlying cover strata.

Well-defined aeromagnetic anomalies interpreted to represent deep-seated Precambrian ductile structures occur beneath the Paleozoic cover rocks underlying the western Lake Ontario region and extend northwestward into Georgian Bay (Figure 2.21). Although deep seismic data collected across some of these structures in Lakes Erie and Ontario suggest that they have been tectonically stable since early Paleozoic times (e.g., Forsyth et al. 1994a, b; Milkereit et al. 1992), some have been identified as potentially active features based on the locations of nearby faults and fractures observed in outcrops of Precambrian and Paleozoic bedrock (Wallach and Mohajer 1990). Eyles et al. (1993) have presented evidence suggesting that relict drainage systems that cut across the lower Paleozoic rocks in the western Lake Ontario region have been controlled in part by reactivation of some of the Precambrian structures associated with these geophysical lineaments.

Structural features that could be possible seismic sources have been investigated and are incorporated into the seismic hazard analysis for the Bruce nuclear. These sources, which include the Grenville Front tectonic zone, Georgian Bay linear zone, Niagara-Pickering linear zone, Clarendon-Linden fault system and Hamilton-Presqu'ile lineament (Figure 2.22), are

described in Section 3.3. Other notable structural features identified in the region are described below.

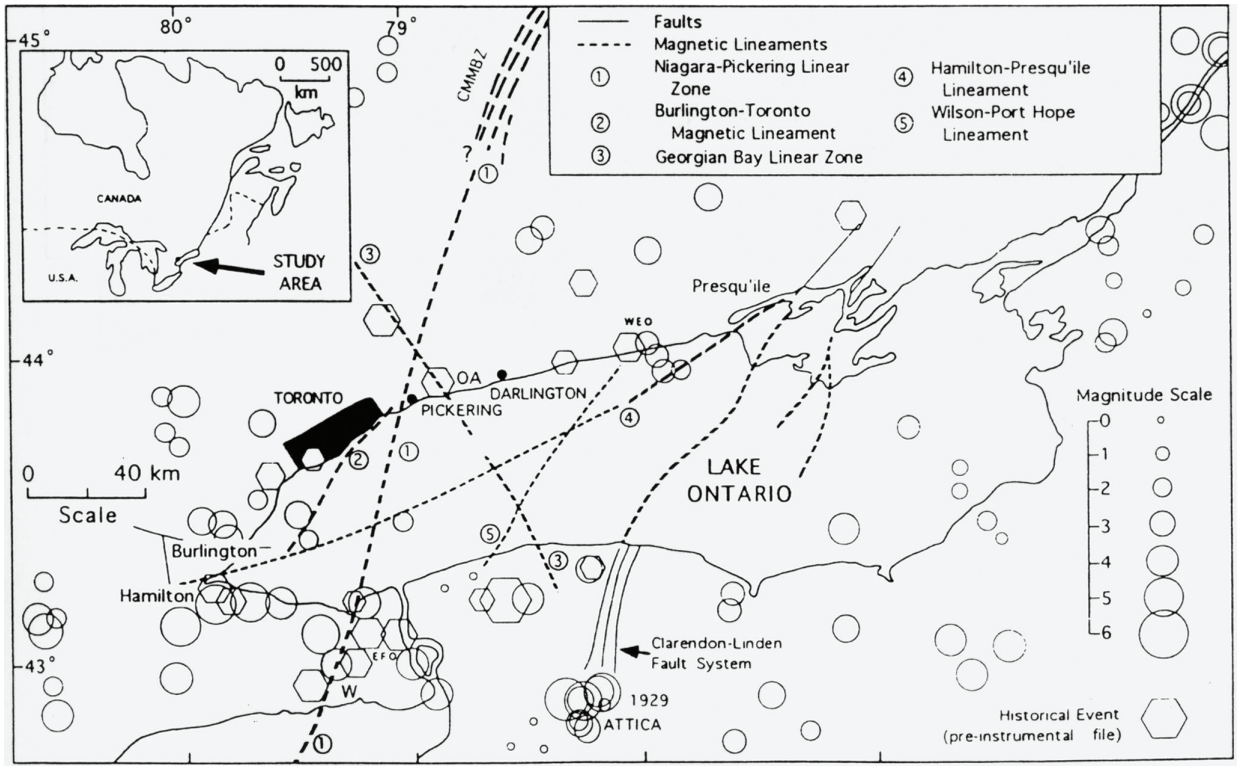

Note: Figure from McQuest Marine (1995)

Figure 2.22: Known and Postulated Structural Features of Lake Ontario

2.4.1 Erie–Georgian Bay Lineament

This lineament was identified and named by Boyce and Morris (2002), who recognized it as part of a linear zone of mapped northeast-trending aeromagnetic lineaments in southern Ontario (2-23). Reprocessing and digital image enhancement was used by Boyce and Morris (2002), along with existing regional gravity and aeromagnetic data sets to facilitate lineament mapping. The Erie–Georgian Bay Lineament (EGBL) is the westernmost of a series of parallel "en echelon" lineaments that include the Hamilton-Lake Erie lineament (HLEL) and the prominent Niagara-Pickering linear zone that bounds the series of northeast-trending lineaments on the east (Boyce and Morris 2002). Citing the work of previous investigators (e.g., Wallach and Mohajer 1990), Boyce and Morris (2002) suggest that these northeast-trending lineaments may be associated with reactivated basement faults that are related to Grenville-age terrane boundaries.

Paleozoic faults mapped in southern Ontario by Carter et al. (1996) are approximately parallel to, but not coincident with, the EGBL. The Paleozoic faults are interpreted to reflect the structural grain of the Precambrian basement rocks (Carter et al. 1996).

A cluster of seismic events was recorded over a section of this lineament by a small seismic telemetry network from July 1980 to August 1984 (Mereu et al. 1986). The earthquakes were mainly in the magnitude 1 – 2 range, although there were also three felt events with magnitudes larger than 3. All of these events were in the vicinity of the Gobles oil field and had hypocenters near the depth of the producing stratigraphic horizon. The events appeared to be associated with at least two active faults oriented almost perpendicular to each other. Mereu et al. (1986) concluded that the earthquakes were induced or triggered by fluids pumped into and out of wells during secondary recovery activities in the Gobles oil field.

2.4.2 Erie-Huron Linear Zone

This lineament was recognized and named by Boyce and Morris (2002) as a broad (>80 km) belt of low-amplitude, linear and curvilinear magnetic anomalies that extend from eastern Lake Huron south toward western and central Lake Erie (Figure 2.23). Lineaments within the Erie-Huron Linear Zone (EHLZ) have a north-northwest strike and are approximately parallel with the GBLZ. The northwest-trending magnetic lineaments in southern Ontario have similar trends to larger-scale, northwest-trending basement geophysical lineaments in the eastern United States, and, thus, may record transform faults formed initially during Iapetan rifting also.

A cluster of earthquakes has been recorded at the south end of this linear zone. Boyce and Morris (2002) note that these events are coincident with the west-east-trending Electric fault (described below), which is a Paleozoic fault that is reported to appear as a distinct topographic lineament in satellite imagery. In the vicinity of the EHLZ, however, Boyce and Morris (2002) note that the earthquake cluster may be artificially induced, as the Electric fault system is associated with several producing oil and gas fields.

2.4.3 Hamilton–Lake Erie Lineament

The Hamilton–Lake Erie lineament was identified and named by Wallach et al. (1998) as approximately parallel to, and about 50 km west of, the Niagara-Pickering linear zone. Wallach et al. (1998) suggest that the parallelism and proximity of the Hamilton-Lake Erie Lineament (HLEL) to the Niagara-Pickering linear zone suggests that the two might be part of the same fault zone.

Boyce and Morris (2002) recognize the HLEL as part of a linear zone of mapped northeast-trending aeromagnetic lineaments that include the EGBL and Niagara-Pickering linear zone (Figure 2.23). Boyce and Morris (2002) also recognize a well-defined elliptical gravity low that corresponds with a zone of low magnetic intensity that is bounded by the EGBL and HLEL and records a distinct lithotectonic domain.

2.4.4 Electric Fault and Dawn Fault

The east-west-trending Electric fault (Figure 2.21) is located on the northern margin of the Chatham sag and deflects the nose of the Algonquin arch to the west. The Electric fault is a south-side-down normal fault with a maximum observed vertical displacement on the Precambrian surface of approximately 93 m (Brigham 1971). The Electric fault had recurrent displacement in the Paleozoic; it displaces structure contours on the top of the uppermost Late Silurian Bass Island Group and the base of the lower Middle Devonian Detroit River Group, but does not offset the base of the overlying Dundee Limestone (Brigham 1971).

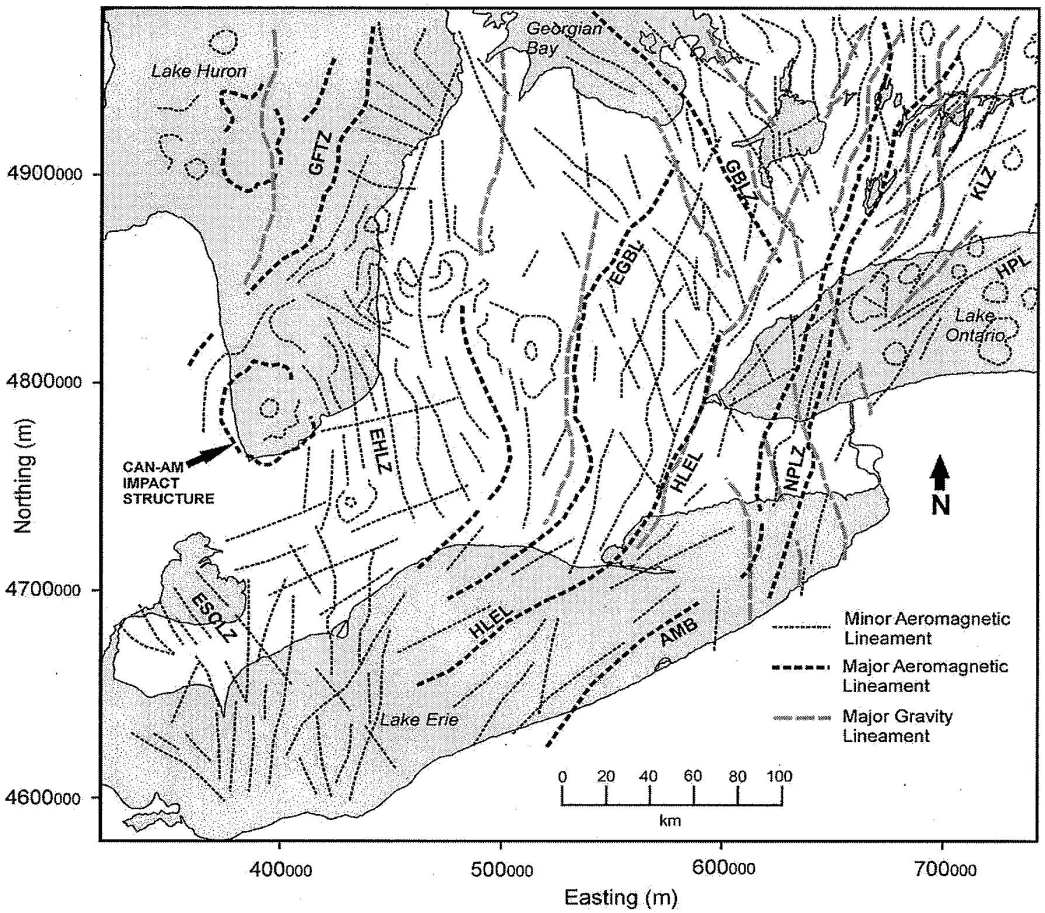

Notes: Abbreviations are as in Figure 2.21, except EGBL: Erie - Georgian Bay lineament, GFTZ: Grenville Front tectonic zone, EHLZ: Erie - Huron linear zone, KLZ: Kawartha linear zone, and ESCLZ: Erie - St. Clair linear zone. Figure is from Boyce and Morris (2002).

Figure 2.23: Interpreted Aeromagnetic and Gravity Lineaments in Southern Ontario

A nontectonic origin for Holocene fault movement on the Electric fault was postulated by Cumming and Al-Aasm (1999) from an analysis of porewater isotope chemistry from cores in the St. Clair River delta. Differences in porewater mixing and displacement rates between boreholes may result from vertical movement along the Electric fault due to collapse related to the dissolution of Salina salt beds within the southern, downthrown block of the fault. Although no faulting or fracturing is visible in cores, microscale faulting may have occurred, increasing secondary hydraulic conductivity (Cumming and Al-Aasm 1999).

The Dawn fault (Figure 2.21) is an east-west-trending fault that has been identified in borings and with geophysical data. The fault is a south-side-down normal fault with a maximum observed vertical displacement of approximately 60 m (Brigham 1971). The Dawn fault displaces the base but not the top of the lower Devonian Detroit River Group.

Boyce and Morris (2002) speculate that the Electric and other east-west-trending faults in southwestern Ontario are related to the Mesozoic St. Lawrence Valley system rifting that occurred in the Mesozoic. However, the absence of displacements by the Electric and Dawn faults of units younger than the lower Middle Devonian Detroit River Group does not support this hypothesis.

2.5 Seismicity

Characterization of the seismicity of the region surrounding the Bruce nuclear site forms an essential part of the assessment of the seismic hazard. The primary means of characterization of the seismicity is use of the earthquake catalogue. The earthquake catalogue is used to assess earthquake occurrence rates and as part of the assessment of maximum magnitudes for earthquake sources. This section describes the development and processing of the earthquake catalogue.

2.5.1 Development of Earthquake Catalogue

The earthquake catalogue was developed for the region extending from latitude 38ºN 50ºN and longitude 65º W to 90º W. The primary source of data for the project catalogue is the Seismic Hazard Earthquake Epicenter File (SHEEF) developed by the Geological Survey of Canada (GSC) (Halchuk 2009). The GSC SHEEF catalogue was compiled for use in the 2005 Fourth Generation Seismic Hazard Maps of Canada. The catalogue was updated by the GSC to include earthquakes through the end of 2007. The GSC SHEEF catalogue has been supplemented for this study by downloading earthquake data for 2008 from the National Earthquake Data Base (NEDB) of Canada (accessed on October 14, 2009).

The secondary source of earthquake data was the catalogue compiled by the U.S. Geological Survey for development of the U.S. National Seismic Hazard Maps (Petersen et al. 2008). This catalogue consists of earthquake data through the end of 2006. The USGS national hazard mapping catalogue was supplemented for the years 2007 and 2008 by data from the Advanced National Seismic Systems (ANSS) online catalogue (accessed on October 23, 2009). The USGS national catalogue was then merged with the GSC SHEEF catalogue and duplicates were removed. Preference was given to the GSC SHEEF catalogue when selecting parameters for earthquakes north of the Canada-United States border, and to the USGS catalogue for earthquakes south of the Canada-United States border.

The most important data for characterizing the size of earthquakes in the pre-instrumental period (prior to about 1920) is the level of shaking intensity. Shaking-intensity data for earthquakes in the combined catalogue were obtained from two primary sources: Smith (1962, 1966) and the NCEER-91 catalogue (Seeber and Armbruster 1991). These data are used to develop the unified moment magnitudes for the earthquakes as described in Section 2.5.2. Additional historical earthquakes were compiled from Metzger et al. (2000) and OPG (2001).

The resulting earthquake catalogue data was then supplemented by data for specific earthquakes provided in Ma and Atkinson (2006); Ma and Eaton (2007); Ma et al. (2008); Lamontagne and Ranalli (1997); Dineva et al. (2004); Du et al. (2003); Faust et al. (1997); Fujita and Sleep (1991); and Ruff et al. (1994). Nontectonic events identified in Fujita and Sleep (1991); Ma et al. (2008); Seeber and Armbruster (1993); Pomeroy et al. (1976); and the ANSS and NEDB blast lists were then removed from the catalogue.

2.5.2 Conversion to Moment Magnitude

The magnitude scale used in the GSC is Nuttli magnitude, M_N; the scale used in the USGS catalogue is the equivalent body-wave magnitude, m_{bLg}; and the scale used in modern ground-motion models is moment magnitude, **M**. In order to provide consistency between the earthquake occurrence parameters and the ground motion assessment in the PSHA for the

nuclear site, a unified moment-magnitude estimate was developed for each earthquake magnitude.

2.5.2.1 Direct Estimates of Moment Magnitude

Direct estimates of seismic moment were obtained from the literature for a limited number of events. The data sources were Street and Turcotte (1977); Boore and Atkinson (1987); Du et al. (2003); Atkinson and Boore (2006); Johnston (1996a, 1996b); Bent (1992, 1996); the St. Louis University Earthquake Center website; and the Harvard Moment Tensor Catalog.

Three studies provided approximate moment magnitudes for earthquakes in the study region. Boatwright (1994) inverted vertical recordings from the Eastern Canadian Telemetered Network to obtain estimates of earthquake source spectra, including seismic moment. Figure 2.24 compares Boatwright's (1994) estimates of moment magnitude with moment magnitudes obtained from standard waveform inversion. The moment-magnitude values obtained by Boatwright (1994) are close to reported moment magnitudes for values of **M** below 3.5 and tend to slightly underestimate the value of **M** at larger values. A locally weighted, least-squares fit, to the data shown on Figure 2.24 was used to correct the moment magnitudes reported in Boatwright (1994) to values of **M** used in this study.

Macheridas (2002) developed estimates of moment magnitudes for northeastern U.S. earthquakes using a coda wave technique. Figure 2.25 compares her estimates with moment magnitudes obtained from standard waveform inversion. The moment-magnitude values obtained by Macheridas (2002) are close to reported moment magnitudes, albeit with considerable scatter. A least-squares fit to the data shown on Figure 2.25 was used to correct the moment magnitudes reported in Macheridas (2002) to values of **M** used in this study.

Atkinson (2004) developed estimates of moment magnitudes for eastern Canada earthquakes based on analysis of Fourier spectra. Figure 2.26 compares her estimates with moment magnitudes obtained from standard waveform inversion. The moment-magnitude values obtained by Atkinson (2004) are close to reported moment magnitudes for values of **M** above magnitude 4, overestimating **M** by about 0.2 units for smaller values. A locally weighted least-squares fit to the data shown on Figure 2.26 was used to correct the moment magnitudes reported in Atkinson (2004) to values of **M** used in this study.

2.5.2.2 Conversion from Other Size Measures

Moment-magnitude estimates for the remaining earthquakes in the catalogue were based on empirical relationships between the available size measures and **M**.

The GSC SHEEF catalogue reports values of local magnitude, M_L, for most of the earthquakes in the historical period (prior to about 1920). However, comparison of these magnitudes with values of maximum intensity reported in Smith (1962, 1966) suggests that these values of M_L are based on the relationship $M_L = \frac{2}{3} I_0 + 1$ developed by Gutenberg and Richter (1958) for California earthquakes. Therefore, a more direct estimate of **M** was made by developing an empirical relationship between I_0 and **M**. Figure 2.27 shows the data set of earthquakes with reported values of I_0 and **M**. This data set includes earthquakes with values of **M** estimated from the data in Boatwright (1994); Macheridas (2002); and Atkinson (2004). Shown on Figure 2.27 is the relationship between I_0 and **M** developed by Johnston (1996b) using a worldwide data set of stable continental region (SCR) earthquakes, primarily for values of I_0 5 and larger. The Johnston (1996b) relationship overestimates the values of **M** at intensities less than 8.

The red curve shows the locally weighted least-squares fit to the data used to provide estimated values of **M** from I_0.

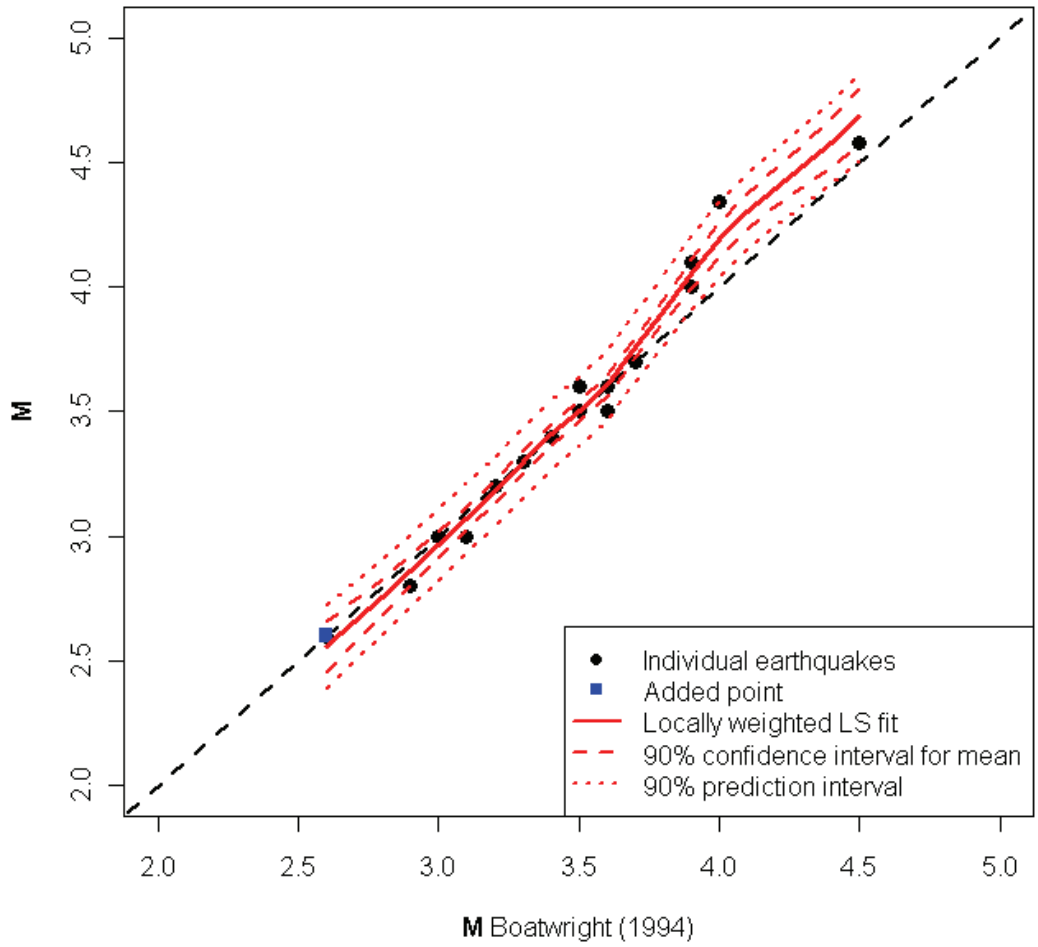

Notes: Moment magnitude estimates are from Boatwright (1994). Red curves indicate relationship used to adjust M_Boatwright to values of M used in this study.

Figure 2.24: Comparison of Moment Magnitude Estimates with Reported Values of M

The other size measure used for historical earthquakes is the natural log of the felt area (lnFA). Figure 2.28 compares the available data for earthquakes with reported values of lnFA and **M** with the relationship developed by Johnston (1996b). The limited data are consistent with the Johnston (1996) relationship and were used to develop values of **M**.

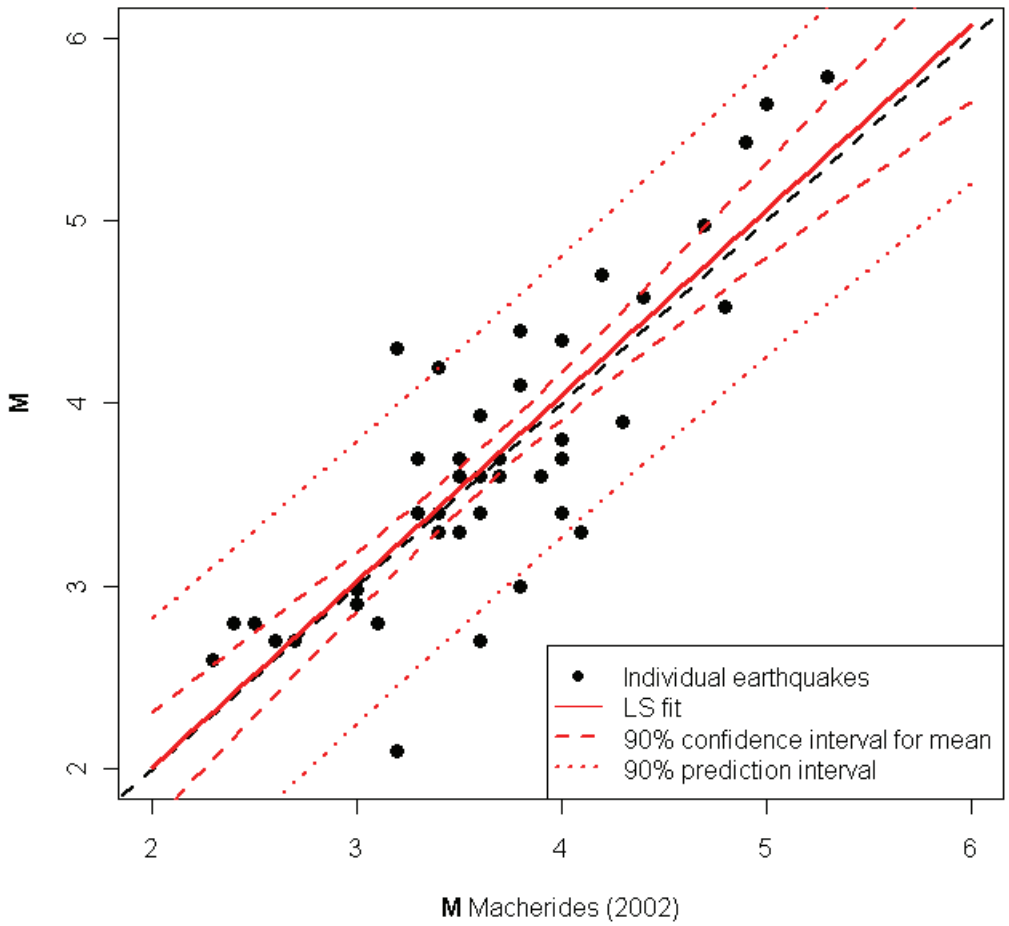

Notes: Moment magnitude estimates are from Macheridas (2002). Red curves indicate relationship used to adjust M_Macheridas to values of M used in this study.

Figure 2.25: Comparison of Moment Magnitude Estimates with Reported Values of M

The majority of earthquake magnitudes reported in the GSC SHEEF catalogue are in the body-wave M_N magnitude scale. Relationships between M_N and **M** have been developed by Atkinson and Boore (1995) and Sonley and Atkinson (2005). The M_N-**M** data shown on the figure were assembled by Bent (2010). As suggested by Bent (2010), a simple relationship of the form **M** = M_N + C provides as good a fit as the other published relationships within the range of the data. Bent (2010) also reports an apparent change in the scaling between M_N and **M** that occurs for the years after about 1995, such that the constant offset changes from about -0.4 to about –0.5. The M_N-**M** data were analysed, and the change in scaling from -0.41 to -0.57 was determined to be statistically significant. Therefore, the conversion from M_N to **M** used for the project catalogue consisted of **M** = M_N – 0.41 for years before 1998 and **M** = M_N – 0.57 for 1998 and after, with a standard error of 0.18 magnitude units.

The other body-wave magnitudes reported for earthquakes in the catalogue are in the m_{bLg} scale. This scale is generally similar to the M_N scale but is typically based on recordings on a different type of instrument. Figure 2.29 compares the available m_{bLg}-**M** data from the project catalogue with two published relationships and the M_N-**M** conversion used in this study. The relationship developed by Johnston (1996a) appears more consistent with the data, thus it was used to develop estimates of **M** from reported values of m_{bLg}.

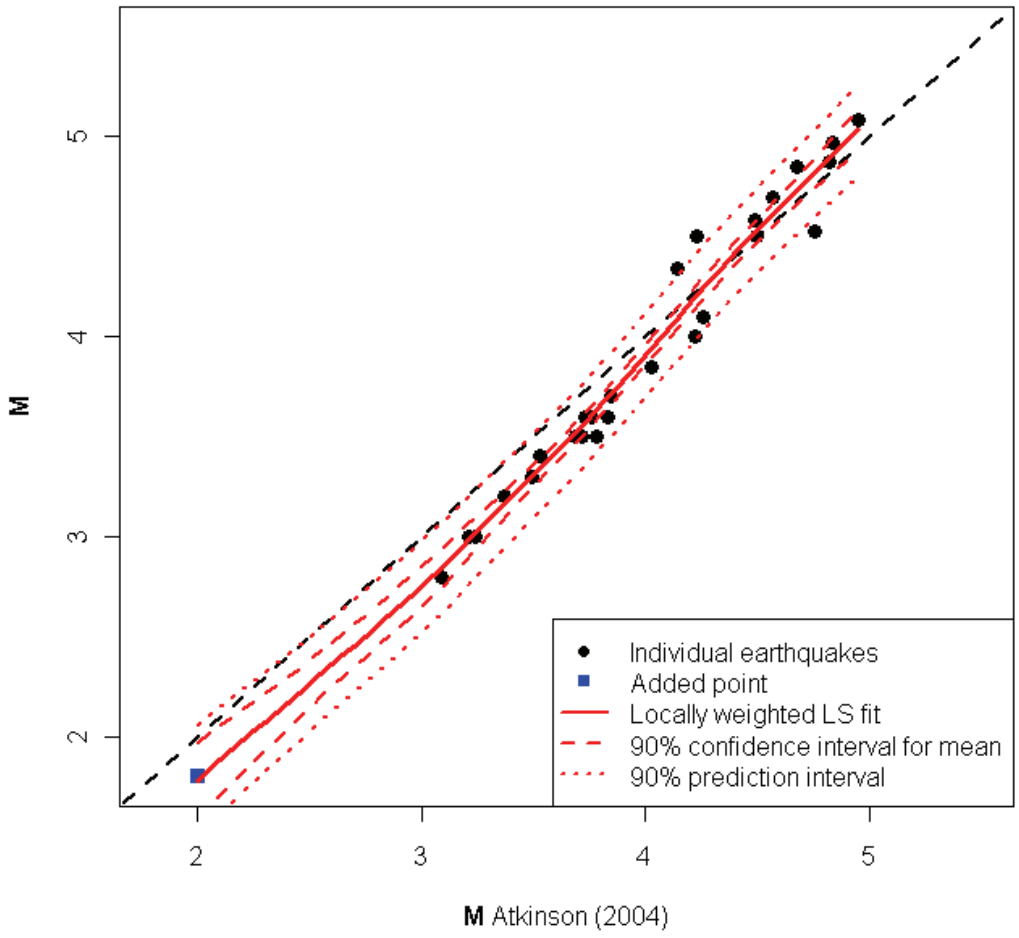

Notes: Moment magnitude estimates are from Atkinson (2004). Red curves indicate relationship used to adjust M_Atkinson to values of M used in this study.

Figure 2.26: Comparison of Moment Magnitude Estimates with Reported Values of M

The earthquake catalogue contains three other magnitude measures: local magnitude M_L, coda magnitude M_C and duration magnitude M_D. Figure 2.30 compares the available M_L-**M** data pairs from the project catalogue to the relationship published by Johnston (1996a). The data do not appear consistent with the Johnston (1996a) M_L-**M** relationship. Therefore, the least-squares fit to the data shown on Figure 2.30 was used to develop estimates of **M** from M_L. Figure 2.31 compares M_C and M_D magnitudes to M_N magnitudes for earthquakes in the project catalogue. These magnitudes appear to be equivalent to M_N, and the M_N to **M** conversion developed above for the years before 1998 was used to estimate **M** from M_C and M_D magnitudes.

Finally, Johnston et al. (1994) report values of **M** for several earthquakes in the project catalogue developed from empirical relationships between the area with various shaking intensity isoseismals and moment magnitude. These magnitudes and their uncertainties were adopted for use in the project catalogue.

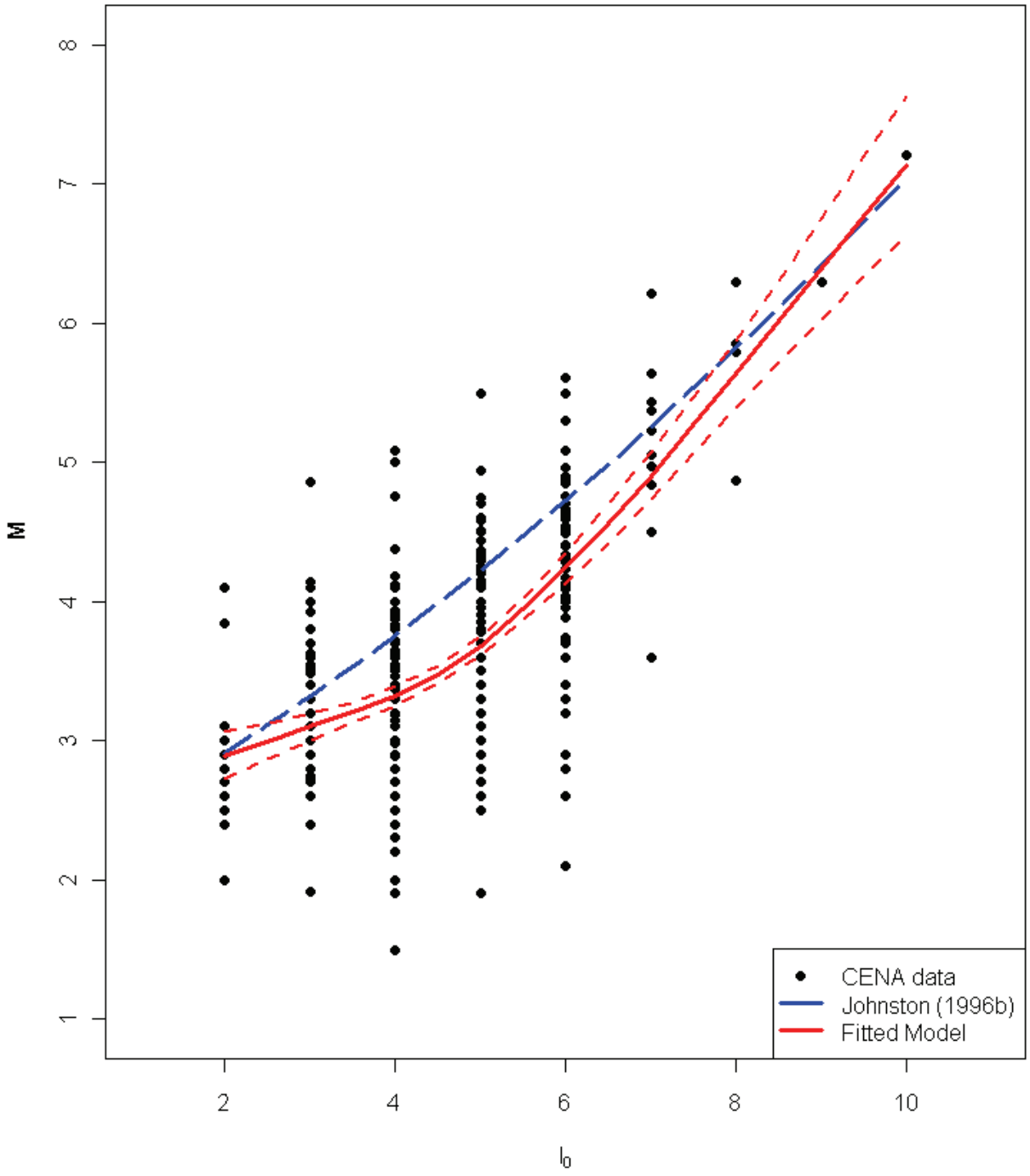

Note: Also shown is the relationship developed by Johnston (1996b) from a world wide dataset of stable continental earthquakes.

Figure 2.27: Conversion from Maximum Intensity, I_0 to M Developed for this Study

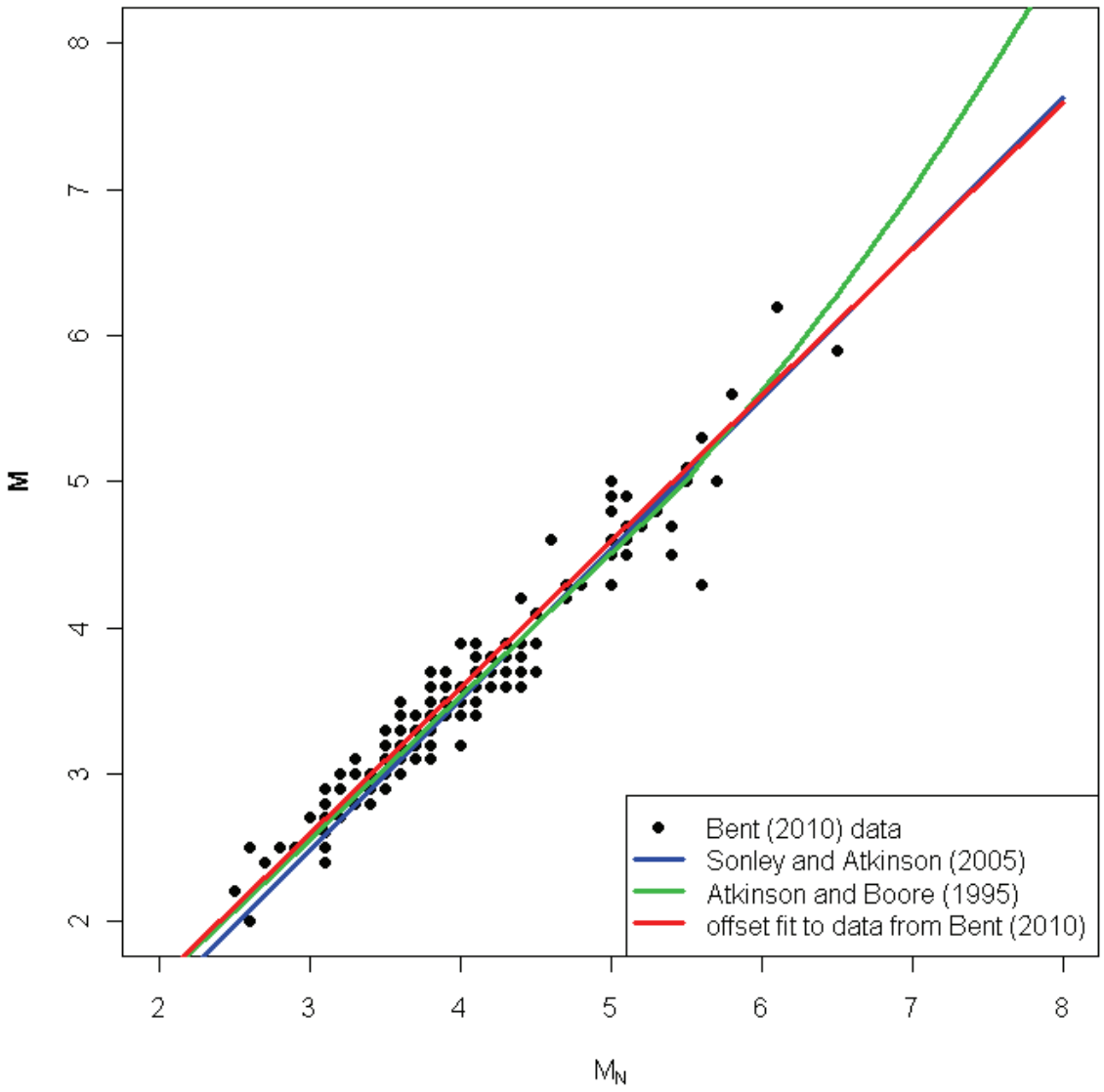

Notes: MN-M data were assembled by Bent (2010). Data are shown for years prior to 1998.

Figure 2.28: Comparison of Relationships Between MN and M

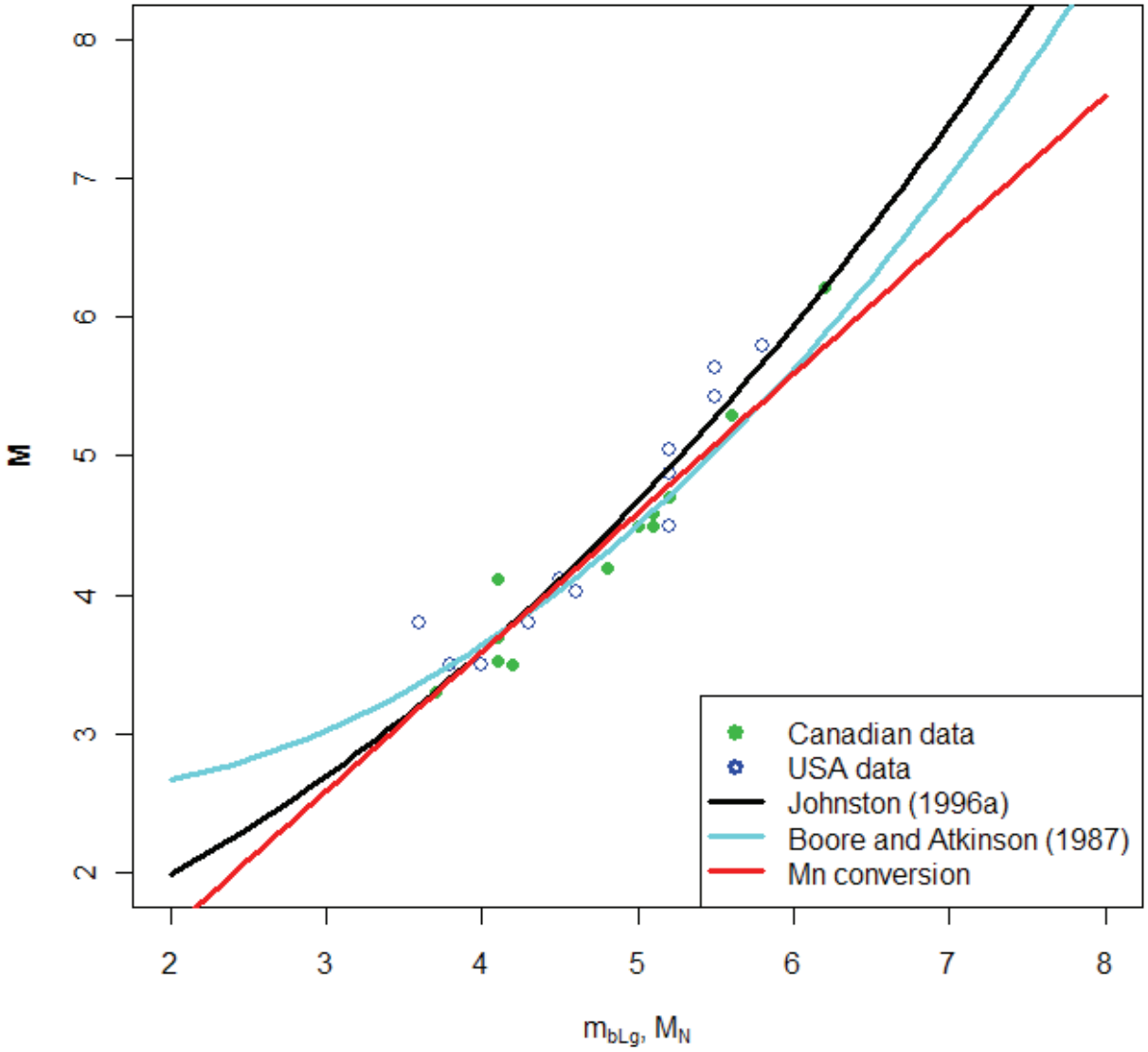

Notes: Curves indicate the relationships of Boore and Atkinson (1987) and Johnston (1996a). Also shown is the M_N conversion developed in this study.

Figure 2.29: Comparison of Project Data for m_{bLg} Versus M

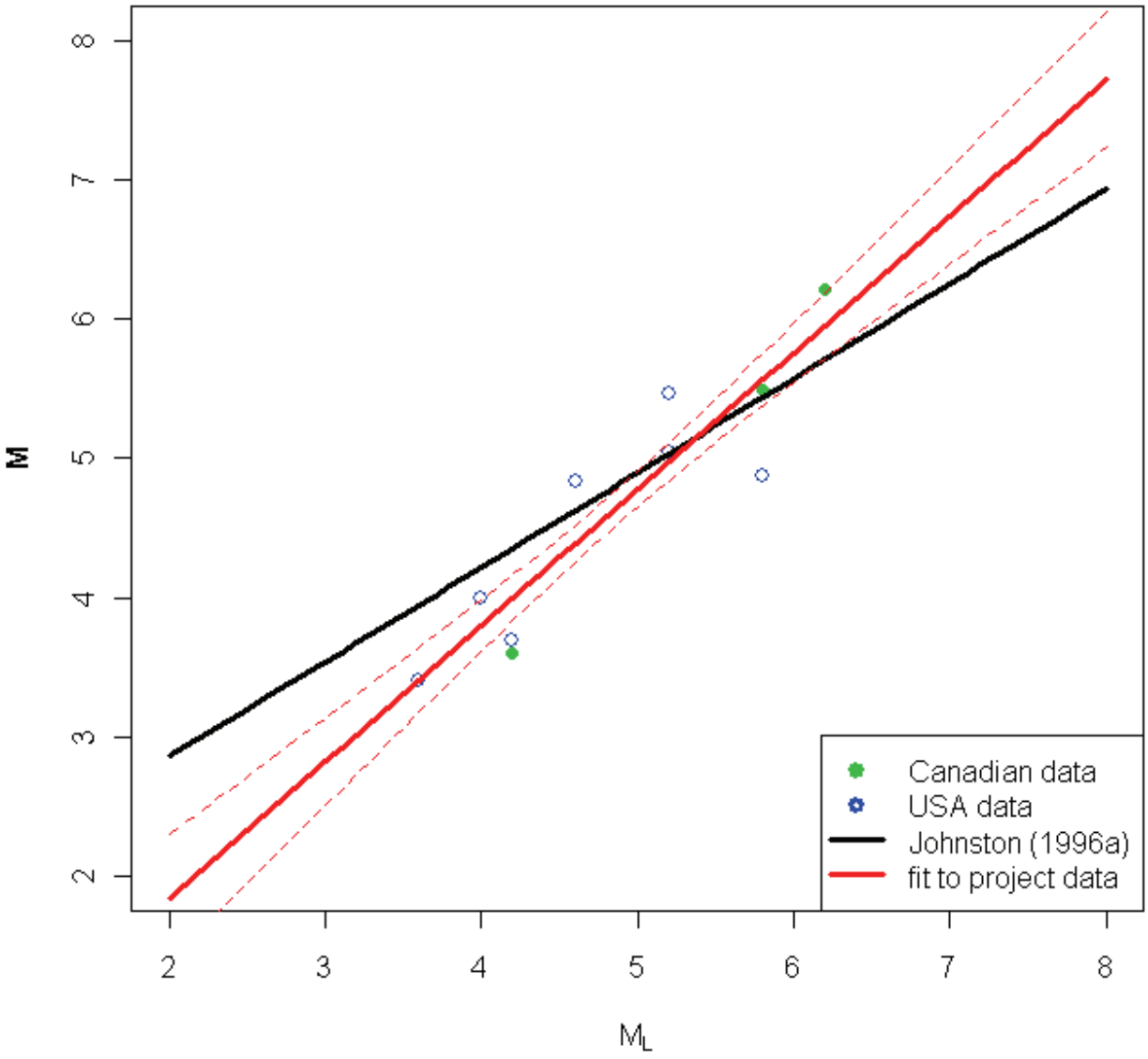

Notes: The red curve shows the fit to the project data used to develop the project catalogue, developed by Johnston (1996a).

Figure 2.30: Comparison of Project M_L-M Data to Relationship

2.5.2.3 Uniform Magnitude Scale

A uniform moment magnitude was computed for all events using the formulation presented in EPRI-SOG (1988). The appropriate conversion relations are applied to each earthquake in the catalogue to obtain a value of **M** and its prediction uncertainty σ_P given by the equation:

$$\sigma_P = \sqrt{\sigma_{res}^2 + \sigma_{E[M|X]}^2} \tag{2.1}$$

where $\sigma_{E[M|X]}$ is the uncertainty in the mean of **M** given the value of the independent variable X and σ_{res} is the residual standard error. These values are either computed from the regression analyses described above or taken from the published relationships used in the conversion. If a measured value of **M** is available for an event, it is taken as the expected value of **M,** and a standard deviation of 0.1 is assigned as an average uncertainty in estimating **M** unless one is given in the data source.

For the majority of events, the value of **M** is estimated from the other available size measures. Given multiple measures of the earthquake size, the expected value and variance of **M** are calculated as in EPRI-SOG (1988) using Equations 2-2 and 2-3:

$$E\left[\mathbf{M} \mid \underline{\hat{X}}\right] = \left\{ \sum_i \frac{\sigma_P^2\left[\mathbf{M} \mid \underline{\hat{X}}\right]}{\sigma_P^2\left[\mathbf{M} \mid \hat{X}_i\right]} \cdot E\left[\mathbf{M} \mid \hat{X}_i\right] \right\} + (r-1) \cdot \beta \cdot \sigma_P^2\left[\mathbf{M} \mid \underline{\hat{X}}\right] \tag{2.2}$$

$$\sigma_P^2\left[\mathbf{M} \mid \underline{\hat{X}}\right] = \left\{ \sum_i \frac{1}{\sigma_P^2\left[\mathbf{M} \mid \hat{X}_i\right]} \right\}^{-1} \tag{2.3}$$

where $\underline{\hat{X}}$ is the vector of different earthquake size measures, $\hat{X}_i$ is a single member of $\underline{\hat{X}}$, r is the number of earthquake size measures and β =bln(10). The b-value was set at an initial estimate of 1.0. After one pass through the process of assessing completeness and seismicity parameters, an average b-value near 0.9 was determined.

As discussed in EPRI-SOG (1988), uncertainty in the magnitude estimates and its propagation through the magnitude conversion process introduces a bias in the estimated earthquake occurrence rates. This bias is corrected by using an adjusted magnitude **M*** for each earthquake and then computing the earthquake recurrence parameters by maximum likelihood using earthquake counts in terms of **M***. The adjusted magnitude is defined by the relationship

$$M^* = M - \beta\sigma_{M|M\,instrumental}^2 / 2 \tag{2.4}$$

when **M** is based on instrumentally recorded moment magnitudes and by the relationship

$$M^* = M + \beta\sigma_{M|X}^2 / 2 \tag{2.5}$$

when **M** is based on other size measures X, such as maximum intensity I_0 or other magnitude measures, such as M_N. The change in sign in the correction term from negative in Equation 2.4 to positive in Equation (2.5) reflects the effects of the uncertainty in the conversion from size measure X to **M**.

The resulting earthquake catalogue for the project region is listed in Appendix A and is shown on Figure 2.1.

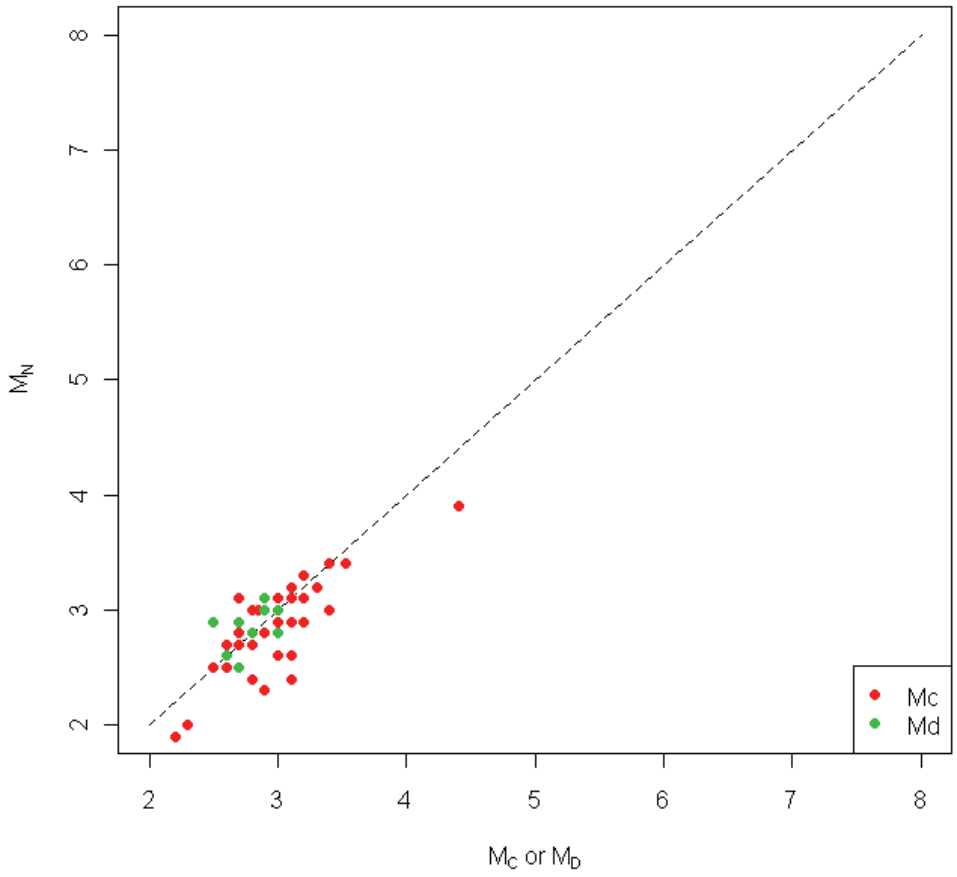

Note: Dashed line indicates a one-to-one relationship.

Figure 2.31: Comparison of M_D and M_C with M_N for Project Data

2.5.3 Identification of Independent Earthquakes

The PSHA formulation used to assess the earthquake hazard at the Bruce nuclear site is based on the Poisson model for the occurrence of independent earthquakes. Therefore, dependent earthquakes (foreshocks and aftershocks) must be identified and not included in the earthquake statistics. Dependent earthquakes were identified by applying the declustering algorithm developed by EPRI-SOG (1988). The standard method of creating a catalogue of independent earthquakes developed by Gardner and Knopoff (1974) is to remove all smaller earthquakes within a fixed time and distance window about a large earthquake. In contrast, the approach developed by EPRI-SOG (1988) is to perform a statistical test of the rate of earthquakes in the immediate time and distance interval about a large earthquake. If the rate of earthquakes is significantly higher than a background rate in the local neighborhood of the main event, then earthquakes are removed until the rate becomes consistent with the background rate. The dependent earthquakes identified with this procedure are indicated in the earthquake catalogue listed in Appendix A.

2.5.4 Earthquake Catalogue Completeness

Assessment of earthquake occurrence rates requires an evaluation of the completeness of the earthquake catalogue. The standard technique for maximum likelihood estimation of earthquake rates (e.g., Weichert 1980) is to use only the earthquake counts within the assessed period of complete reporting in the earthquake catalogue. EPRI-SOG (1988) extended the maximum likelihood approach to incorporate data from both the period of complete catalogue reporting and the period of incomplete catalogue reporting. For the period of incomplete reporting, a probability of detection, P^D, is defined that represented the probability that the occurrence of an earthquake would ultimately be recorded in the earthquake catalogue for the region. EPRI-SOG (1988) provided estimates of P^D for the central and eastern United States and southeastern Canada. Figure 2.32 shows the EPRI-SOG (1988) catalogue completeness regions that cover the study area.

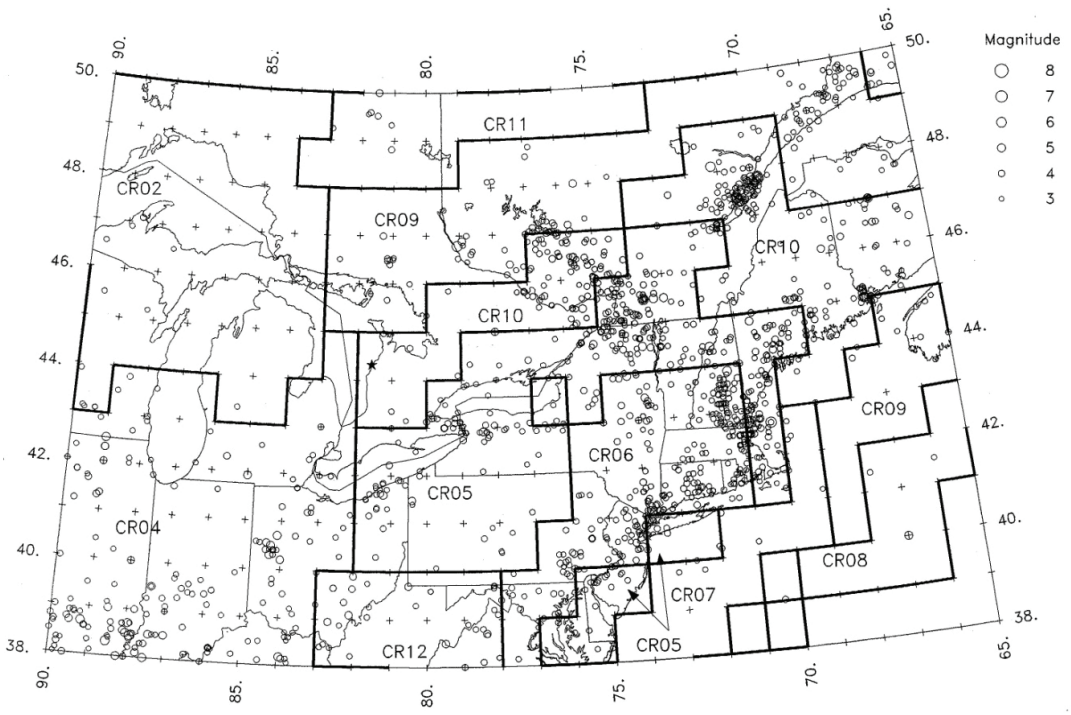

Note: Earthquake catalogue is from Electric Power Research Institute (EPRI 1988).

Figure 2.32: Catalogue Completeness Regions in the Project Study Area

The values of P^D were reassessed for completeness regions 2, 4, 5, 6, 9, 10, and 11 using the updated earthquake catalogue and the EPRI-SOG (1988) computer program EQPARAM. Consistent with the software application, the magnitude bins were set at a width of 0.6 magnitude units, starting at **M*** 3.3. Examination of the results indicated that fitting a truncated exponential model to the full magnitude range from **M** 3.3 to 7.5 resulted in an underprediction of the observed rates for the larger-magnitude earthquakes. The EPRI-SOG (1988) approach provided for the ability to assign relative weights to the various magnitude intervals in fitting the truncated exponential model to the observed data. The departure from

the truncated exponential model at larger magnitudes may by due to a possible excess of magnitudes in the lowest magnitude interval, 3.3 ≤ **M*** < 3.9. This magnitude interval is most affected by the nonlinear I_0 to **M** conversion. Therefore, the weight assigned to this interval was reduced from 1.0 to values of 0.1 and 0.01.

The resulting models of catalogue completeness produced reasonable fits to the observed rates of the larger earthquakes that are important to the assessment of the seismic hazard. Comparisons between the observed and predicted seismicity rates are provided in Section 3.4. Two earthquake catalogue completeness models were carried forward into the PSHA analysis: Model A is based on a weight of 0.1 assigned to data in the magnitude interval 3.3 ≤ **M*** < 3.9 when fitting earthquake occurrence relationships, and Model B is based on a weight of 0.01 assigned to data in the magnitude interval 3.3 ≤ **M*** < 3.9. The resulting values of P^D for models A and B are listed in Table 2.2 and Table 2.3, respectively.

Table 2.2: Probability of Earthquake Detection for Model A (Weight of 0.1 on Magnitude Interval 3.3 ≤ M* < 3.9)

Magnitude Interval	Probability of Detection, P^D for Time Period:						
	1625 to 1780	1780 to 1860	1860 to 1910	1910 to 1950	1950 to 1975	1975 to 2009	Equivalent Period of Completeness (years)
Completeness Region 2							
3.3 ≤ **M*** < 3.9			0.993	1	1	1	148.7
3.9 ≤ **M*** < 4.5			0.993	1	1	1	148.7
4.5 ≤ **M*** < 5.1			0.993	1	1	1	148.7
5.1 ≤ **M*** < 5.7			0.998	1	1	1	148.9
5.7 ≤ **M*** < 6.3			0.999	1	1	1	149.0
6.3 ≤ **M*** < 6.9			1	1	1	1	149.0
6.9 ≤ **M***			1	1	1	1	149.0
Completeness Region 4							
3.3 ≤ **M*** < 3.9			0.996	1	1	1	148.8
3.9 ≤ **M*** < 4.5			0.996	1	1	1	148.8
4.5 ≤ **M*** < 5.1		0.847	1	1	1	1	216.8
5.1 ≤ **M*** < 5.7		0.99	1	1	1	1	228.2
5.7 ≤ **M*** < 6.3		0.99	1	1	1	1	228.2
6.3 ≤ **M*** < 6.9		0.99	1	1	1	1	228.2
6.9 ≤ **M***		0.997	1	1	1	1	228.8
Completeness Region 5							
3.3 ≤ **M*** < 3.9		0.664	1	1	1	1	202.1
3.9 ≤ **M*** < 4.5		0.742	1	1	1	1	208.4
4.5 ≤ **M*** < 5.1	0.419	0.806	1	1	1	1	278.4
5.1 ≤ **M*** < 5.7	0.967	0.971	1	1	1	1	376.6

Table 2.2: Probability of Earthquake Detection for Model A (Weight of 0.1 on Magnitude Interval 3.3 ≤ M* < 3.9)

Magnitude Interval	Probability of Detection, P^D for Time Period:						
	1625 to 1780	1780 to 1860	1860 to 1910	1910 to 1950	1950 to 1975	1975 to 2009	Equivalent Period of Completeness (years)
5.7 ≤ **M*** < 6.3	0.993	0.993	1	1	1	1	382.4
6.3 ≤ **M*** < 6.9	1	1	1	1	1	1	384.0
6.9 ≤ **M***	1	1	1	1	1	1	384.0
Completeness Region 6							
3.3 ≤ **M*** < 3.9		0.765	1	1	1	1	210.2
3.9 ≤ **M*** < 4.5		0.765	1	1	1	1	210.2
4.5 ≤ **M*** < 5.1	0.375	0.946	1	1	1	1	282.8
5.1 ≤ **M*** < 5.7	0.877	1	1	1	1	1	364.9
5.7 ≤ **M*** < 6.3	0.977	1	1	1	1	1	380.4
6.3 ≤ **M*** < 6.9	0.995	1	1	1	1	1	383.2
6.9 ≤ **M***	0.999	1	1	1	1	1	383.8
Completeness Region 7							
3.3 ≤ **M*** < 3.9			0.307	0.532	0.951	1	94.4
3.9 ≤ **M*** < 4.5			0.546	0.918	1	1	123.0
4.5 ≤ **M*** < 5.1		0.475	0.925	0.984	1	1	182.6
5.1 ≤ **M*** < 5.7		0.957	0.991	1	1	1	225.1
5.7 ≤ **M*** < 6.3		0.996	1	1	1	1	228.7
6.3 ≤ **M*** < 6.9		1	1	1	1	1	229.0
6.9 ≤ **M***		1	1	1	1	1	229.0
Completeness Region 8							
3.3 ≤ **M*** < 3.9					0.485	1	46.1
3.9 ≤ **M*** < 4.5					0.807	1	54.2
4.5 ≤ **M*** < 5.1					0.963	1	58.1
5.1 ≤ **M*** < 5.7				0.805	1	1	91.2
5.7 ≤ **M*** < 6.3				0.975	1	1	98.0
6.3 ≤ **M*** < 6.9				1	1	1	99.0
6.9 ≤ **M***				1	1	1	99.0
Completeness Region 9							
3.3 ≤ **M*** < 3.9				0.984	1	1	98.4
3.9 ≤ **M*** < 4.5			0.988	0.995	1	1	148.2
4.5 ≤ **M*** < 5.1			0.952	0.995	1	1	146.4

Table 2.2: Probability of Earthquake Detection for Model A (Weight of 0.1 on Magnitude Interval 3.3 ≤ M* < 3.9)

Magnitude Interval	Probability of Detection, P^D for Time Period:						
	1625 to 1780	1780 to 1860	1860 to 1910	1910 to 1950	1950 to 1975	1975 to 2009	Equivalent Period of Completeness (years)
5.1 ≤ **M*** < 5.7			0.971	0.995	1	1	147.4
5.7 ≤ **M*** < 6.3			0.992	1	1	1	148.6
6.3 ≤ **M*** < 6.9			0.998	1	1	1	148.9
6.9 ≤ **M***			0.999	1	1	1	149.0
Completeness Region 10							
3.3 ≤ **M*** < 3.9			0.789	1	1	1	138.5
3.9 ≤ **M*** < 4.5			0.789	1	1	1	138.5
4.5 ≤ **M*** < 5.1		0	0.811	1	1	1	139.6
5.1 ≤ **M*** < 5.7	0	0.29	0.926	1	1	1	168.5
5.7 ≤ **M*** < 6.3	0	0.687	1	1	1	1	204.0
6.3 ≤ **M*** < 6.9	0.392	0.93	1	1	1	1	284.2
6.9 ≤ **M***	0.955	0.98	1	1	1	1	375.4
Completeness Region 11							
3.3 ≤ **M*** < 3.9					0.968	0.995	58.0
3.9 ≤ **M*** < 4.5					1	1	59.0
4.5 ≤ **M*** < 5.1				1	1	1	99.0
5.1 ≤ **M*** < 5.7				1	1	1	99.0
5.7 ≤ **M*** < 6.3				1	1	1	99.0
6.3 ≤ **M*** < 6.9				1	1	1	99.0
6.9 ≤ **M***				1	1	1	99.0
Completeness Region 12							
3.3 ≤ **M*** < 3.9		0	0.303	0.754	1	1	104.3
3.9 ≤ **M*** < 4.5		0.435	0.881	0.995	1	1	177.7
4.5 ≤ **M*** < 5.1	0.327	0.82	0.99	1	1	1	264.8
5.1 ≤ **M*** < 5.7	0.763	0.935	0.99	1	1	1	341.6
5.7 ≤ **M*** < 6.3	0.952	0.987	1	1	1	1	375.5
6.3 ≤ **M*** < 6.9	0.984	1	1	1	1	1	381.5
6.9 ≤ **M***	0.984	1	1	1	1	1	381.5

Table 2.3: Probability of Earthquake Detection for Model B (Weight of 0.01 on Magnitude Interval 3.3 ≤ M* < 3.9)

Magnitude Interval	Probability of Detection, P^D for Time Period:						
	1625 to 1780	1780 to 1860	1860 to 1910	1910 to 1950	1950 to 1975	1975 to 2009	Equivalent Period of Completeness (years)
Completeness Region 2							
3.3 ≤ **M*** < 3.9			0.987	0.987	1	1	147.8
3.9 ≤ **M*** < 4.5			0.987	0.987	1	1	147.8
4.5 ≤ **M*** < 5.1			0.987	0.994	1	1	148.1
5.1 ≤ **M*** < 5.7			0.996	0.998	1	1	148.7
5.7 ≤ **M*** < 6.3			0.998	0.999	1	1	148.9
6.3 ≤ **M*** < 6.9			0.999	1	1	1	149.0
6.9 ≤ **M***			1	1	1	1	149.0
Completeness Region 4							
3.3 ≤ **M*** < 3.9			0.996	1	1	1	148.8
3.9 ≤ **M*** < 4.5			0.996	1	1	1	148.8
4.5 ≤ **M*** < 5.1		0.85	1	1	1	1	217.0
5.1 ≤ **M*** < 5.7		0.99	1	1	1	1	228.2
5.7 ≤ **M*** < 6.3		0.99	1	1	1	1	228.2
6.3 ≤ **M*** < 6.9		0.99	1	1	1	1	228.2
6.9 ≤ **M***		0.997	1	1	1	1	228.8
Completeness Region 5							
3.3 ≤ **M*** < 3.9		0.724	0.985	1	1	1	206.2
3.9 ≤ **M*** < 4.5		0.724	0.985	1	1	1	206.2
4.5 ≤ **M*** < 5.1	0.415	0.799	1	1	1	1	277.2
5.1 ≤ **M*** < 5.7	0.96	0.97	1	1	1	1	375.4
5.7 ≤ **M*** < 6.3	0.992	0.992	1	1	1	1	382.1
6.3 ≤ **M*** < 6.9	1	1	1	1	1	1	384.0
6.9 ≤ **M***	1	1	1	1	1	1	384.0
Completeness Region 6							
3.3 ≤ **M*** < 3.9		0.773	1	1	1	1	210.8
3.9 ≤ **M*** < 4.5		0.773	1	1	1	1	210.8
4.5 ≤ **M*** < 5.1	0.385	0.949	1	1	1	1	284.6
5.1 ≤ **M*** < 5.7	0.88	1	1	1	1	1	365.4
5.7 ≤ **M*** < 6.3	0.977	1	1	1	1	1	380.4
6.3 ≤ **M*** < 6.9	0.995	1	1	1	1	1	383.2

Table 2.3: Probability of Earthquake Detection for Model B (Weight of 0.01 on Magnitude Interval 3.3 ≤ M* < 3.9)

Magnitude Interval	Probability of Detection, P^D for Time Period:						
	1625 to 1780	1780 to 1860	1860 to 1910	1910 to 1950	1950 to 1975	1975 to 2009	Equivalent Period of Completeness (years)
6.9 ≤ **M***	0.999	1	1	1	1	1	383.8
Completeness Region 7							
3.3 ≤ **M*** < 3.9			0.307	0.532	0.951	1	94.4
3.9 ≤ **M*** < 4.5			0.546	0.918	1	1	123.0
4.5 ≤ **M*** < 5.1		0.475	0.925	0.984	1	1	182.6
5.1 ≤ **M*** < 5.7		0.957	0.991	1	1	1	225.1
5.7 ≤ **M*** < 6.3		0.996	1	1	1	1	228.7
6.3 ≤ **M*** < 6.9		1	1	1	1	1	229.0
6.9 ≤ **M***		1	1	1	1	1	229.0
Completeness Region 8							
3.3 ≤ **M*** < 3.9					0.485	1	46.1
3.9 ≤ **M*** < 4.5					0.807	1	54.2
4.5 ≤ **M*** < 5.1					0.963	1	58.1
5.1 ≤ **M*** < 5.7				0.805	1	1	91.2
5.7 ≤ **M*** < 6.3				0.975	1	1	98.0
6.3 ≤ **M*** < 6.9				1	1	1	99.0
6.9 ≤ **M***				1	1	1	99.0
Completeness Region 9							
3.3 ≤ **M*** < 3.9				0.998	1	1	98.9
3.9 ≤ **M*** < 4.5			0.999	1	1	1	149.0
4.5 ≤ **M*** < 5.1			0.961	1	1	1	147.1
5.1 ≤ **M*** < 5.7			0.975	1	1	1	147.8
5.7 ≤ **M*** < 6.3			0.993	1	1	1	148.7
6.3 ≤ **M*** < 6.9			0.998	1	1	1	148.9
6.9 ≤ **M***			0.999	1	1	1	149.0
Completeness Region 10							
3.3 ≤ **M*** < 3.9			0.806	1	1	1	139.3
3.9 ≤ **M*** < 4.5			0.806	1	1	1	139.3
4.5 ≤ **M*** < 5.1		0	0.817	1	1	1	139.9
5.1 ≤ **M*** < 5.7	0	0.293	0.925	1	1	1	168.7
5.7 ≤ **M*** < 6.3	0	0.69	1	1	1	1	204.2

Table 2.3: Probability of Earthquake Detection for Model B (Weight of 0.01 on Magnitude Interval 3.3 ≤ M* < 3.9)

Magnitude Interval	Probability of Detection, P^D for Time Period:						
	1625 to 1780	1780 to 1860	1860 to 1910	1910 to 1950	1950 to 1975	1975 to 2009	Equivalent Period of Completeness (years)
6.3 ≤ **M*** < 6.9	0.351	0.923	1	1	1	1	277.2
6.9 ≤ **M***	0.93	0.977	1	1	1	1	371.3
Completeness Region 11							
3.3 ≤ **M*** < 3.9					0.996	0.999	58.9
3.9 ≤ **M*** < 4.5					1	1	59.0
4.5 ≤ **M*** < 5.1				1	1	1	99.0
5.1 ≤ **M*** < 5.7				1	1	1	99.0
5.7 ≤ **M*** < 6.3				1	1	1	99.0
6.3 ≤ **M*** < 6.9				1	1	1	99.0
6.9 ≤ **M***				1	1	1	99.0
Completeness Region 12							
3.3 ≤ **M*** < 3.9		0	0.303	0.754	1	1	104.3
3.9 ≤ **M*** < 4.5		0.435	0.881	0.995	1	1	177.7
4.5 ≤ **M*** < 5.1	0.327	0.82	0.99	1	1	1	264.8
5.1 ≤ **M*** < 5.7	0.763	0.935	0.99	1	1	1	341.6
5.7 ≤ **M*** < 6.3	0.952	0.987	1	1	1	1	375.5
6.3 ≤ **M*** < 6.9	0.984	1	1	1	1	1	381.5
6.9 ≤ **M***	0.984	1	1	1	1	1	381.5

3. SEISMIC SOURCE CHARACTERIZATION

A seismic source characterization (SSC) model was developed that characterises all seismic sources (areal source zones and fault sources) that could be of significance to the hazard at the Bruce nuclear site.

3.1 Types of Uncertainties and Logic Tree Structure

Types of uncertainties (i.e., aleatory and epistemic) and the general logic tree structure used for seismic source characterization for the probabilistic seismic hazard assessment (PSHA) are described in this section.

3.1.1 Aleatory and Epistemic Uncertainty

A key focus of this study is to identify and quantify the uncertainties associated with seismic source characteristics, thus fully incorporating the current knowledge and uncertainties into the hazard analysis. As discussed in the Senior Seismic Hazard Analysis Committee's Recommendations for Probabilistic Seismic Hazard Analysis (SSHAC 1997), PSHA incorporates both aleatory uncertainty and epistemic uncertainty. Aleatory uncertainty (or variability) is the natural randomness in a process, and epistemic uncertainty is the scientific uncertainty in the process due to limited data and knowledge. Examples of aleatory uncertainty are variation in the peak ground motion of individual recordings about a median ground-motion relationship, and the location and magnitude of the next earthquake. Examples of epistemic uncertainty are alternative models for ground motion estimation and the long-term rate of slip on a particular fault.

In concept, epistemic uncertainties are potentially reducible with additional data, while aleatory uncertainties are irreducible. For example, a fault's slip rate and its associated uncertainties could be quantified at a particular point in time, followed by a program of field data collection and interpretation, followed in turn by another assessment of uncertainty. If properly quantified in the first place, the second assessment should result in slip rate estimates that lie entirely within the first range of assessments. Further, the second assessment range of possible slip rate values may be narrower or the relative weights on the central and outlying estimates may have changed. Thus one way to mitigate the potential for large fluctuations in seismic hazard estimates over time is to properly quantify epistemic uncertainties. The present study was carried out with that goal in mind.

Significant advances in the development of the methodology for quantifying epistemic uncertainty in seismic hazard have been made during the past decades (SSHAC 1997). These advances involve the development and weighting of alternative interpretations of seismic source characteristics to provide a structured characterization of epistemic uncertainty suitable for seismic hazard computation. For a PSHA, the weighted alternative interpretations are typically expressed in logic trees.

A logic tree consists of a series of nodes and branches that describe the alternative models or parameter values or both. At each node, there is a set of branches that represent the range of alternative credible models or parameter values. The branch weights must sum to unity at each node. The weights on the branches of logic trees reflect scientific judgments in the relative confidence in the alternative models and should be consistent with the knowledge and understanding of the informed scientific community.

Epistemic uncertainty is the result of limited data (often very limited). In seismic hazard analyses, evaluating the alternative models involves considering alternative simplified physical models, data from analogous regions, and empirical observations. These are subjective. In some cases, uncertainties are developed from formal statistical assessment of fitting models to data (e.g., recurrence rate and b-value parameters obtained from fitting the truncated exponential recurrence model to recorded seismicity).

Each pathway through the composite (across all sources) logic trees represents a complete interpretation of the seismic sources of the site for which an aleatory seismic hazard curve is computed. Each pathway is associated with a probability equal to the product of the conditional probabilities of all the branches along the way. The result of computing the hazard for all pathways is a family of hazard curves, each with an associated weight, representing the full aleatory variability and epistemic uncertainty in the hazard at a site.

3.1.2 Logic Trees

The uncertainty assessment in this study is performed using a logic tree methodology. The logic tree formulation for seismic hazard analysis (Coppersmith and Youngs 1986, EPRI 1988) involves first setting out the sequence of assessments that must be made in order to perform the analysis and then addressing the uncertainties in each of these assessments in a sequential manner. Thus the methodology provides a convenient approach for breaking a large, complex assessment into a sequence of smaller, simpler components that can be more easily addressed.

The general structure of the logic tree used in this study is shown on Figure 3.1. The logic tree is composed of a series of nodes and branches. Each node represents an assessment of a state of nature or an input parameter value that must be made to perform the analysis. Each branch leading from the node represents one possible discrete alternative for the state of nature or parameter value being addressed. If the variable in question is continuous, it can be discretised at a suitable increment. The branches at each node are intended to represent mutually exclusive and collectively exhaustive states of the input parameter. In practice, a sufficient number of branches are placed at a given node to adequately represent the uncertainty in the parameter estimation.

Probabilities assigned to each branch represent the relative likelihood or degree of belief that the branch represents the correct value or state of the input parameter. These probabilities are assessed conditional on the assumption that all the branches leading to that node represent the true state of the preceding parameters. Because they are conditional probabilities for an assumed mutually exclusive and collectively exhaustive set of values, the sum of the conditional probabilities at each node is unity. The probabilities are usually based on scientific judgments because the available data are too limited to allow for objective statistical analysis, and because scientific judgment is needed to weigh alternative interpretations of the available data. The logic tree approach simplifies these assessments because the uncertainty in a single parameter is considered individually with all other assessments leading up to that parameter assessment assumed to be known with certainty. Thus the nodes of the logic tree are sequenced to provide for the conditional aspects or dependencies among the parameters and to provide a logical progression of assumptions from the general to the specific in defining the input parameters for an evaluation.

In most cases, the probabilities (relative weights) assigned to the branches at a node are in units of tenths unless there is a basis for finer-scale resolution. The weights represent one of two types of probability assessments. In the first, the branches at a node of the logic tree

define the range of possible parameter values, and the associated weights assigned to the branches define the probability distribution. For example, an estimate of the slip rate on a fault is uncertain because of uncertainties in the amount of displacement of a particular geologic unit across the fault and the age of the unit. The resulting slip rate is usually represented by a preferred value and a range of higher and lower values, similar to a normal or lognormal statistical distribution.

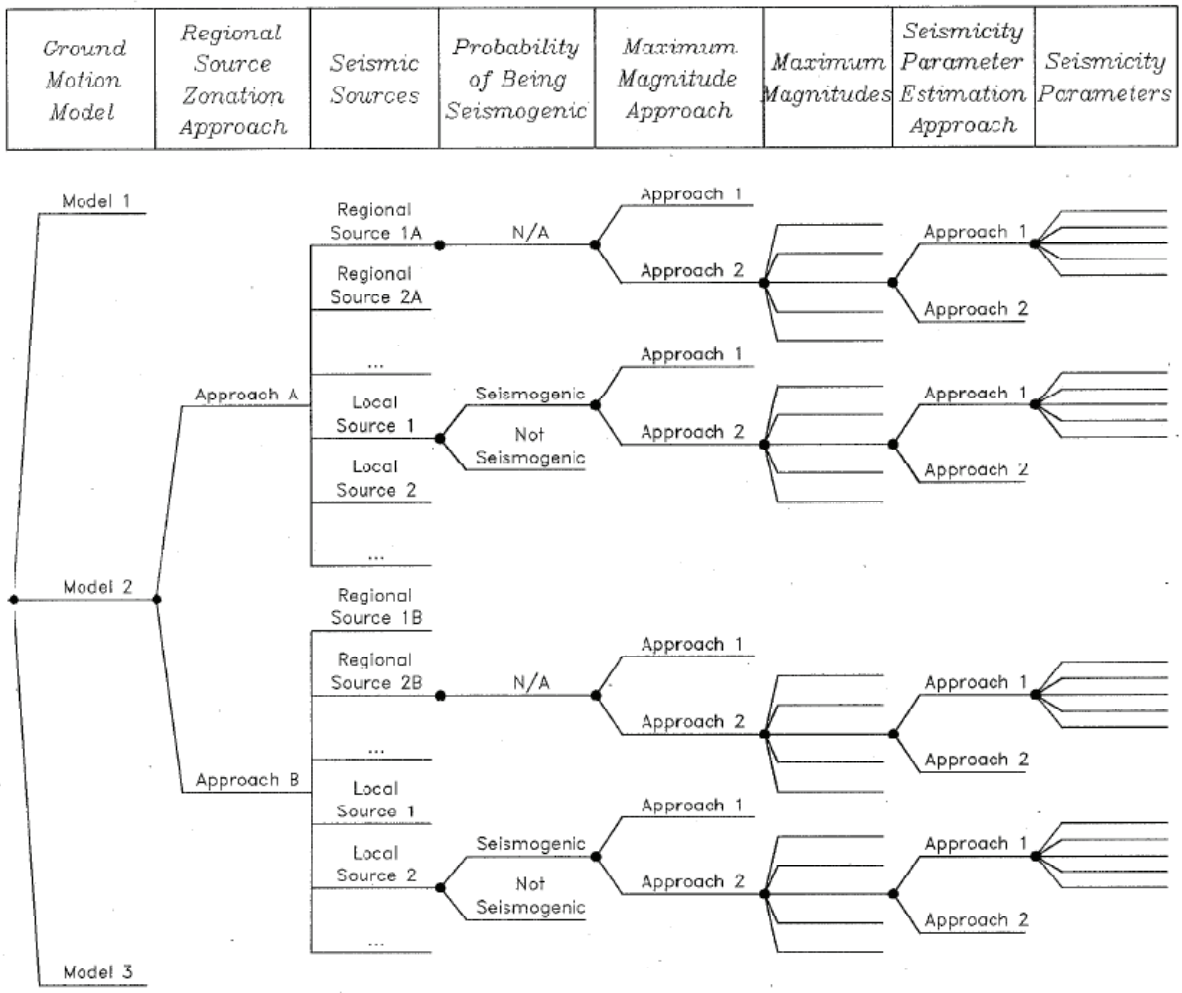

Figure 3.1: General Logic Tree Structure Used in PSHA

In some instances, this type of uncertainty in parameter assessment can be estimated using formal statistical techniques. In these cases, continuous parameter distributions developed from statistical estimation procedures can be discretised for use in a logic tree formulation. Such an approach will be used to develop discrete distributions for earthquake recurrence parameters and maximum magnitudes in Section 5.

A second type of probability assessment to which logic trees are particularly well suited involves indicating a relative preference for, or degree of belief in, two (or more) alternative hypotheses. For example, the sense of slip on a fault may be uncertain; two possible

alternatives might be strike-slip or reverse-slip. Based on the pertinent data, a relative preference for these alternatives can be expressed by the logic tree weights. A very strong preference for one over the other is usually represented by weights such as 0.9 and 0.1 for the two alternatives. If there is no preference for either hypothesis, they are assigned equal weights (0.5 and 0.5 for two hypotheses). Increasing the weight assigned to one of the alternatives from 0.5 to 0.9 (or more) reflects an increasing preference for that alternative, given the available data. Because the relative weights are ultimately scientific judgments based on available information, it is important to document the data and interpretations that led to the assessment of parameter values and to the assignment of relative weights in order that the process can be reviewed by others.

Figure 3.1 lays out the logic tree structure that will be used in this PSHA. The logic tree is schematic in that only the general levels of the logic tree are indicated. The first level of the logic tree addresses the uncertainty in defining the appropriate ground-motion attenuation model. Although uncertainty in identifying and characterizing seismic sources is the focus of this study, the uncertainty in ground motion characterization will be included in the analysis in order to indicate its relative importance in the overall uncertainty in the seismic hazard.

The second level of the generalised logic tree addresses the uncertainty in the appropriate approach for regional seismic source zonation. The importance of this level of the logic tree is that alternative approaches to regional seismic zonation may lead to the definition of different seismic sources. Section 3.2 discusses the various methods that have been used to identify seismic sources in the region and describes the basis for the seismic sources.

At this point the logic tree is expanded into subtrees, one for each seismic source identified following a particular zonation approach. (The vertical line without a node [dot] on Figure 3.1 denotes summation of the hazard from multiple independent sources.) Two types of seismic sources are defined in this study: regional areal sources and local sources. The regional sources are identified by 1A and 1B to indicate that different sources may be defined using different zonation approaches. The local sources are all given the same designation to indicate that their definition is independent of the regional zonation approach.

The next level of uncertainty addressed is the likelihood that the individual local sources are “seismogenic” (this term is defined in Section 3.2.1). If a local source is seismogenic, then it is considered a discrete seismic source in addition to the regional source zone. If not, then only the regional source zone is present. This assessment is only applied to the local sources, the regional source zones are considered to be seismogenic with certainty (probability 1.0).

The final four levels of the logic tree address the assessment of maximum magnitude and seismicity rate parameters. For each there is an assessment of the appropriate approach and then an assessment of the parameters following the selected approach. The approaches that will be used for assessment of maximum magnitude and seismicity rate parameters are discussed in Section 5.

3.2 Regional Seismic Sources

The logic structure used to define the relationships among regional seismic sources in the site region is given in the logic tree shown on Figure 3.2. The first assessment looks at three alternative approaches to defining the models for the spatial distribution of future seismicity: (1) seismic source zones based primarily on geologic and tectonic bases (Plates 1 through 24); (2) seismic source zones developed by the Geological Survey of Canada (Adams and Halchuck 2003, Figure 3.3 and Plate 25) that enclose zones of elevated

seismicity; and (3) a zoneless approach based on smoothing observed seismicity without imposed source zone boundaries (Plate 26). The geologic/tectonically based source zones (Plates 1 through 24) are derived primarily on the basis of mapped or interpreted major tectonic features and have potential differences in seismicity (earthquake recurrence rate and maximum earthquake magnitude) from those of adjoining source zones. The geologic and tectonic bases for source zonation are strongly favoured (0.8) over the alternatives that are based on clusters of seismicity (0.2) because they subdivide the region into zones with more uniform crustal characteristics. Defining sources as areas of uniform seismicity rate is not necessary because the techniques used for seismicity modeling can allow for spatially varying rates within a source (see Section 3.4). Thus it is judged that a geologic or tectonic basis is more relevant for identifying regions of crust with homogeneous characteristics. The seismicity-based approaches use the pattern of observed seismicity in a literal sense to define the future pattern of earthquakes.

A key difference between these methodologies is the degree to which the spatial pattern of observed seismicity (both historical and instrumentally recorded earthquakes) provides an indication of the locations of future seismicity. The methodology used for spatial smoothing of seismicity is one that smoothes both the rate of activity (a-value of the earthquake recurrence relationship) and the b-value. The advantages of this approach are that it does not require an interpretation of the boundaries of sources (i.e., the spatial density differences of seismicity are evaluated automatically as part of the procedure) and there is flexibility in the degree to which the seismicity is smoothed. The zoneless smoothing approach is equally weighted (0.1) with the seismicity zones approach (0.1).

The second level of the logic tree addresses the basis for zonation, given the geologic/tectonic approach for regional source modeling. For the geologic/tectonic approach, the boundary between the St. Lawrence rift system (SLRS) and lapetan rifted margin (IRM) is judged to be significant to defining regional sources. The weight of 0.8 for IRM separate from the SLRS is based on the expression of rift faults. Normal faults of the SLRS are expressed at the surface and provide evidence for multiple stages of reactivation (Tremblay et al. 2003, Rocher et al. 2003, Lemieux et al. 2003, Rimando and Benn 2005). The IRM seismotectonic zone has also experienced extension associated with lower Cambrian rifting; however, these faults are inferred to exist beneath Appalachian thrust sheets (Wheeler 1995).

The third level of the logic tree (Figure 3.2) addresses whether the Grenville province is included in the Central Craton. The presence of pervasive structural fabric associated with the Grenville province postdating the Superior and Southern provinces is the basis for assigning a weight of 0.6 to the logic tree branch of separate Grenville and Central Craton provinces.

The fourth level of the logic tree (Figure 3.2) addresses the location of the IRM boundary with the Southern Grenville (SGR) source zone. This boundary is judged to be significant to defining regional sources, as the seismogenic potential of a stable continental region is known to vary significantly according to the degree of extension it experienced in the past (e.g., Johnston et al. 1994). As discussed in Section 3.2.1.4, alternative locations are considered: one proposed for this study (designated WAU, for Western Adirondack Uplift); one proposed by Wheeler (1995); and one proposed by Milkereit et al. (1992) (designated CMBBZ, for Central Metasedimentary Belt boundary zone). The weights assigned in Section 3.2 are 0.5, 0.4 and 0.1, respectively. For the CMBBZ alternative, two alternative domain boundaries (eastern and western) are assigned equal weight (CMBBZ East and CMBBZ West). The western boundary is based on the presence of the Mississauga domain as recognised by O'Dowd et al. (2004).

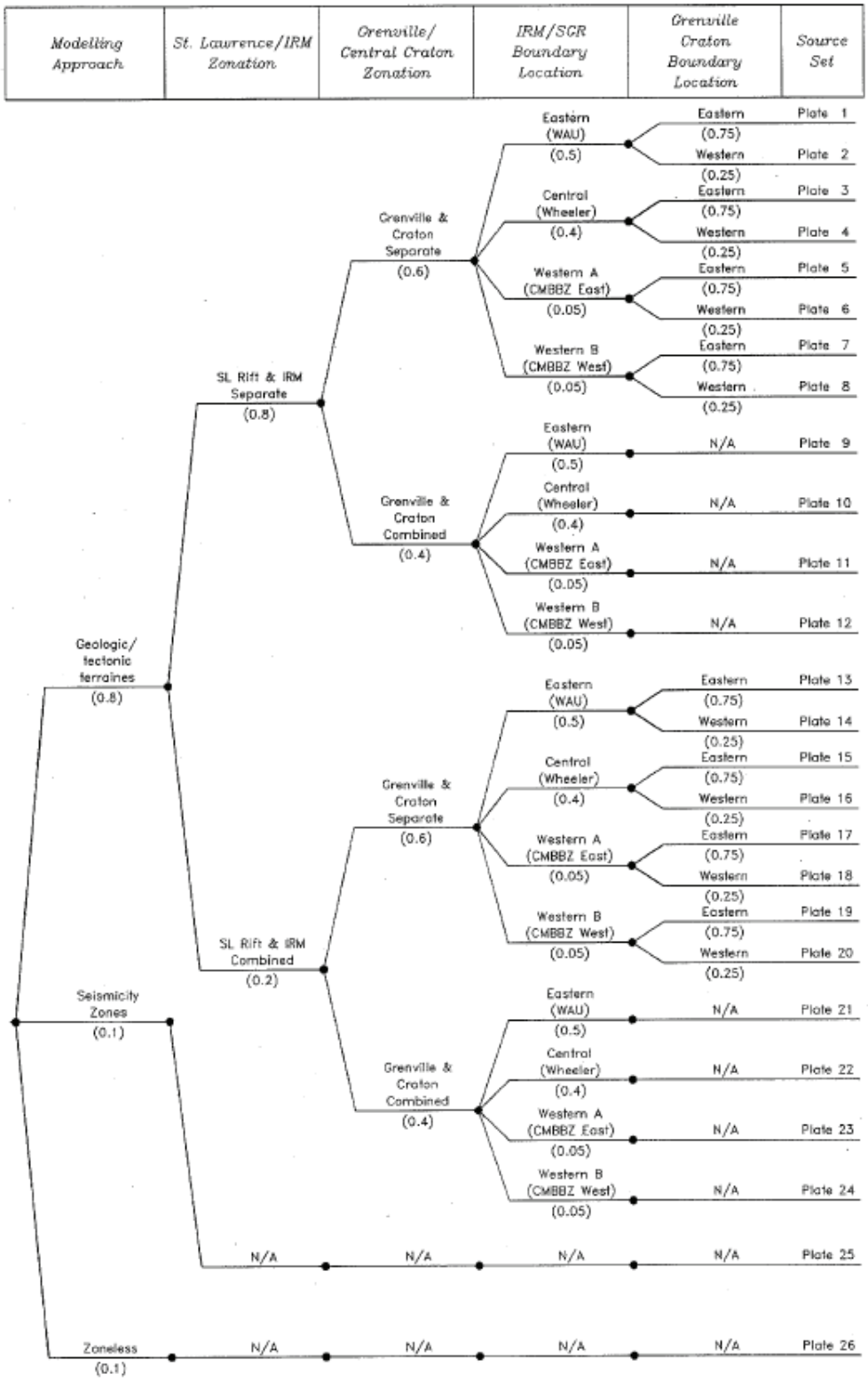

Figure 3.2: Logic Tree for Regional Sources

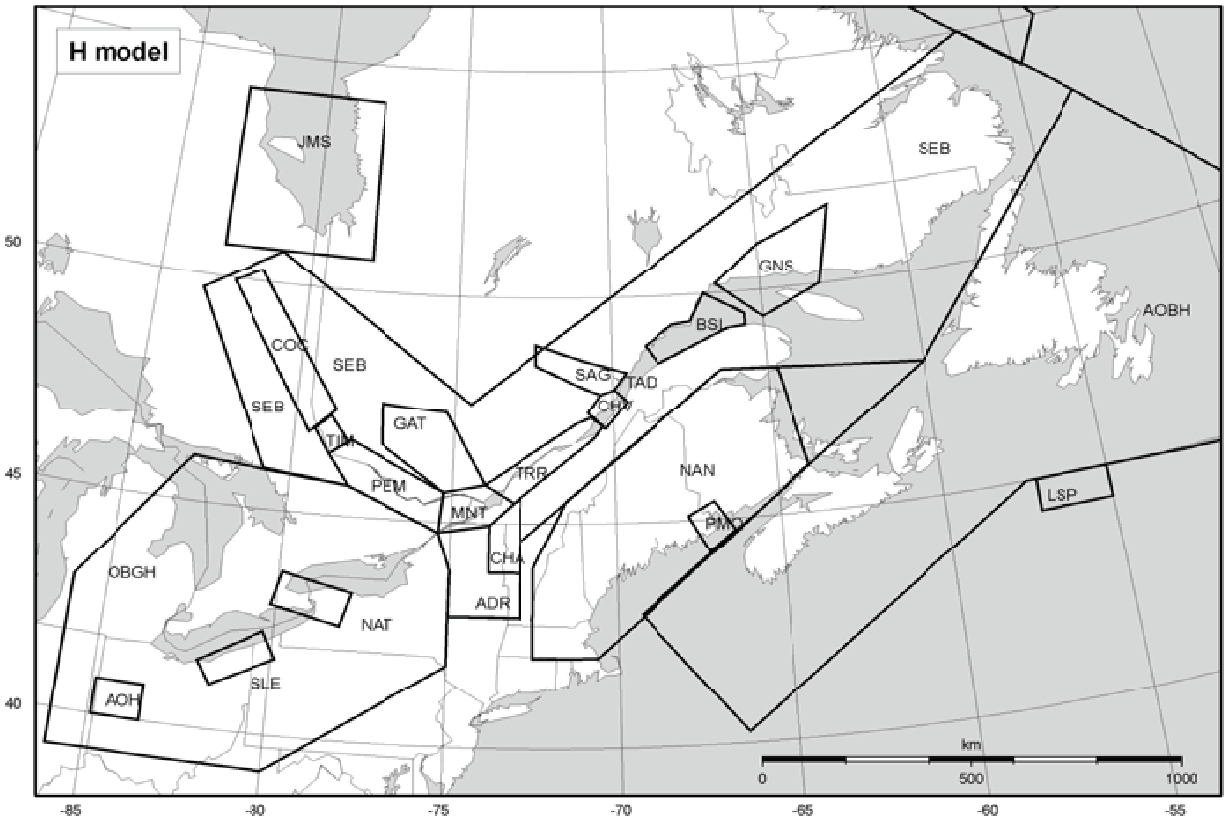

Notes: Source zones indicated include, ADR: Northern Adirondacks, AOBH: Atlantic Offshore Background, AOH: Anna Ohio, BSL: Bas Saint Laurent, CHA: Champlain, CHV: Charlevoix, COC: Cochrane, GAT: Gatineau, GNS: Gulf of St. Lawrence-North Shore, JMS: James Bay, LSP: Laurentian Slope, MNT: Montreal, NAN: Northern Appalachians, NAT: Niagara Attica, OBGH: Ontario Background (H model), PEM: Pembroke, PMQ: Passamaquoddy Bay, SAG: Saguenay, SEB: Southeast Canada Background, SLE: South Shore Lake Erie, TAD: Tadoussac, TIM: Timiskaming, TRR: Trois-Rivieres. Figure is from Adams and Halchuck (2003).

Figure 3.3: GSC Source Zone Map for Model H

The fifth assessment in the logic tree (Figure 3.2) considers alternative locations of the Grenville/Central Craton boundary in southeastern Michigan, southwestern Ontario, and northwestern Ohio defined by Easton and Carter (1995) and Hinze et al. (1975). Easton and Carter (1995) interpreted the location of the Grenville Front tectonic zone (GFTZ) based on geopotential field data, lithological drill cores, and seismic reflection profiles (Figure 2.8). Using the interpreted location of line J of Great Lakes International Multidisciplinary Program on Crustal Evolution (GLIMPCE) as a control point in the area of Lake Huron, they located the GFTZ to the east of the Killarney Magmatic Belt and extending along the Detroit River through Michigan. This location of the GFTZ is consistent with interpretations by Lucius and von Freese (1988) of geophysical anomalies, seismic reflection lines in Lake Erie by Forsyth et al. (1994a), and COCORP line OH-1 by Pratt et al. (1989) and Culotta et al. (1990). The placement of the GFTZ by Easton and Carter (1995) is to the east of the location defined by Hinze et al. (1975) in southeastern Michigan. Hinze et al. (1975) based their interpreted location (Figure 2.11) on the distinction between areas of positive northeast-southwest-trending gravity and magnetic anomalies characteristic of the Grenville province. Easton and Carter (1995) question the assignment of these anomalies to the

Grenville province. The eastern boundary as defined by Easton and Carter (1995) is weighted 0.75, and the western boundary as defined by Hinze et al. (1975) is weighted 0.25.

The final column of the logic tree indicates the various seismic sources that exist given the combination of branches leading to each end point. The plate number that shows the configuration of a given set of seismic sources is indicated. The relative weight associated with a specific combination of assessments is the product of the probabilities on all of the branches. For example, Plate 1 illustrates that the St. Lawrence rift is separated from the IRM by the eastern IRM boundary, and the Grenville province is separated from the Central Craton by the eastern Grenville boundary. (Note that local seismic sources are superimposed on these regional source zones, based on the probability of their being seismogenic).

The logic tree shown on Figure 3.2 lists only those regional sources that are affected by the alternative interpretations considered in the tree. The hazard analysis is conducted using all of the sources shown on Plates 1 through 25. For each of these sources, the assessment of seismicity parameters follows the logic tree format presented in Section 3.4.

In all cases the regional source zones are assumed to be seismogenic with a probability of 1.0. This is because the regional sources include a large region spatially and are likely to include at least one fault (although unknown) capable of generating a moment magnitude (**M**) rating of **M** > 5 earthquake. Because the regional sources exist everywhere in the study region, there is a finite potential for earthquake occurrence everywhere in the study region.

3.2.1 Geologic/Tectonic Seismic Source Zones

Regional source zones for the Bruce nuclear site based on geology and tectonics are shown on Plates 1 through 24. These sources are described below, beginning with the zone in which the Bruce nuclear site is located.

3.2.1.1 Southern/Northern Grenville Source Zones

The Grenville (SGR and NGR) source zones represent non-extended crust of the Precambrian Central Craton of North America (Wheeler and Johnston 1992). Both zones are characterised by sparse and diffuse seismicity. Basement within the two zones consists of rocks deformed during the Proterozoic Grenville orogen, which occurred over a period of about 200 million years (m.y.) between about 1160 and 970 Ma (Rivers et al. 1989).

The Grenville Front tectonic zone (GFTZ), which is associated with northwest-directed ductile thrusting, marks the western boundary to the Grenville source zones. The GFTZ is a major feature that traverses the Canadian Shield for more than 1,000 km, crossing Georgian Bay and Lake Huron and extending into central Ohio. This feature is located within about 50 km of the Bruce nuclear site. Although the GFTZ is assessed to have a very low probability (0.01) of activity in the study region, for completeness it is considered a local seismic source and is described in Section 3.3.2.

3.2.1.2 Central Craton Source Zone

The Central Craton source zone (CC) comprises non-extended Precambrian crust assigned to several basement provinces. From north to south these include portions of the Superior, Southern (Penokean orogen), Grenville and Eastern Granite-Rhyolite provinces (see Figure 2.2). As described in Section 2.2, the ages of the rocks in these basement provinces

range from about 3.6 to 1.5 Ga. The Midcontinent rift system (see Section 2.2.4) is located within the CC source zone. Low rates of seismicity characterize the CC source zone.

3.2.1.3 St. Lawrence Rift System Source Zone

The St. Lawrence rift system (SLRS) source zone encompasses a terrane of known and inferred normal faults that formed parallel to the passive margin of Laurentia during the Late Proterozoic–Early Paleozoic opening of the Iapetus Ocean (e.g., Wheeler 1995, 1996b). Compressional reactivation of favourably oriented Iapetan faults has been postulated as the causal mechanism for several seismically active regions in eastern North America, including Charlevoix and the lower St. Lawrence Valley, Quebec (Adams and Basham 1991).

The 1925 Charlevoix event (**M** 6.2; Bent 1992) is considered by Adams et al. (1995) to be the paradigm earthquake for the St. Lawrence source zone, although they acknowledge that the great depth extent of seismicity and the length of the faults suggest much larger earthquakes are possible. The Charlevoix region (CHV on Figure 3.3) hosts several large-magnitude historical earthquakes: M ~7 1663; M ~6 1790; M ~6 1860; M ~6.5 1870; and M_s 6.2 ± 0.3 1925 (Lamontagne and Ranalli 1997, 1996).

Doig (1990) inferred a variable recurrence rate for the Charlevoix seismic zone from silt layers in lakes due to earthquake-induced landslides. Some silt layers in the section were correlated with historic earthquakes from 1638, 1663, 1791, 1870 and 1925. From 320 B.C. to A.D. 800, Doig (1991) determined a 120-year recurrence interval, 270 years between 800 A.D. and 1500 A.D., and 75 years from A.D. 1500 to the present. Filion et al. (1991) interpreted two earthquake induced landslides by dating tree rings in the base of flow materials of dammed lakes along the Riviere du Gouffree located within the Charlevoix seismic zone. Tuttle and Atkinson (2010) and Tuttle (2006) provide evidence for three Holocene paleoearthquakes in Charlevoix with M ≥ 6.2, including at least two prehistoric episodes at 5,000 and 10,000 years ago. The absence of liquefaction features to the south in the Trois-Rivières seismic zone of the GSC H model (TRR on Figure 3.3) suggests that large-magnitude events in Charlevoix are spatially stationary.

Within the Charlevoix seismic zone, focal mechanisms for earthquakes of magnitude ≥3 show reverse faulting; smaller-magnitude earthquakes indicate some strike-slip and normal faulting. This information led Lamontagne and Ranalli (1997) to suggest that local stress conditions affect rupture style. The distribution of spatially clustered events (doublets and triplets) within the Charlevoix seismic zone indicate that very few events have occurred on the same fractures with similar focal mechanisms, implying that these fault zones occur in highly fractured rocks (Lamontagne and Ranalli 1997). Hypcentral depths for the Charlevoix seismic zone occur as deep as 29 km, although most earthquakes occur between 8 and 15 km (Lamontagne and Ranalli 1996). Comparing this depth distribution to rheological models of the region, Lamontagne and Ranalli (1996) attribute earthquakes in the Charlevoix seismic zone to a brittle-ductile transition deeper than 25 km, corresponding to higher than average geotherms, onset of ductility for hydrated feldspar at about 350°C, high pore-fluid pressure and a low friction coefficient, possibly related to unhealed zones of intense fracturing.

Lamontagne et al. (2003) reviewed the seismotectonic characteristics of a region they refer to as the lower St. Lawrence seismic zone (BSL on Figure 3.3), in which a moderate earthquake of magnitude M_N 5.1 occurred under the St. Lawrence River in 1999. This localised zone of seismicity occurs within the Precambrian basement where intersecting faults of different orientations may be weakened by crustal fluid at depth, hydrostatic pressure, or fault gauge.

Emplacement of the Sept-Iles layered igneous complex may have further fractured this portion of crust (Lamontagne et al. 2003).

Saguenay and Ottawa Grabens

In southeastern Canada, the IRM is associated with two failed arms, or aulacogens, that formed transverse to the faulted edge of the ancient continental margin. These aulacogens are oriented at a high angle to the Iapetan margin and extend into the unrifted (non-extended) craton of Grenville crust. They comprise the Saguenay and Ottawa grabens, which are defined by zones of approximately east-west-trending normal faults extending into the Canadian Shield. The normal faults comprising these aulacogens have not undergone significant total extension; however, their dimensions and earthquake depths are likely similar to those of the Iapetan margin (Adams et al. 1996).

The Ottawa graben extends for approximately 700 km into the Canadian Shield (Kumarapeli and Saull 1966, Kumarapeli 1985, 1993) from the Sutton Mountains salient of the central Appalachian orogen (Rankin 1976; Plate 1). The graben is inferred to extend eastward beneath the Appalachian thrust sheets for approximately 30 km (Kumarapeli 1993). Alkalic intrusions within the Ottawa graben yield an early Cambrian age (approximately 565 Ma; Kumarapeli 1985). A tholeiitic diabase dike swarm associated with the graben is dated at 590 Ma, implying that the initiation of rifting was a Late Proterozoic event (Kumarapeli 1985). The faults defining the Ottawa graben generally strike west-northwest and offset Silurian strata (Forsyth 1981). In addition, a Late Jurassic kimberlite dike occurs at the western end of the rift (Poole et al. 1970).

Adams et al. (1996) consider the 1935 Timiskaming (**M** 6.2) event, which occurred at a depth of 10 km near the Quebec-Ontario border, the paradigm earthquake for the Ottawa graben. Aylsworth et al. (2000) attributed widespread landsliding and irregular subsidence along the Ottawa River to two paleoearthquakes occurring at about 7,060 and 4,550 BP that could be as large as the 1663 Charlevoix (>M 7) event. Doig (1991) interprets two paleo events from earthquake induced landslide sediments within lakes near the 1935 Timiskaming event.

Results of the 1982 Canadian Consortium for Crustal Reconnaissance Using Seismic Techniques (COCRUST) long-range seismic refraction experiment show a sharp, step-like displacement of the Moho beneath the south shoulder of the Ottawa graben, confirming the deep-seated nature of its faults and penetration of mantle melts into the crust (Mereu et al. 1986). Furthermore, the COCRUST surveys show a poorly defined Moho at unusually shallow depths beneath the graben (Mereu et al. 1986).

The Saguenay graben also represents a failed arm of the Iapetan passive margin (Kumarapeli 1985) and extends into the Canadian Shield for approximately 300 km from the St. Lawrence Valley (Figure 3.3). The graben margins are defined by approximately east-west-striking faults; their extent and geometry at depth are unknown (DuBerger et al. 1991). Syn-rift carbonatite complexes dated at 565 Ma imply an early Cambrian age of the graben (Kumarapeli 1985). Some of the graben-bounding faults offset Ordovician limestone by as much as 500 m and are marked by prominent topographic scarps having 100 – 300 m of relief (DuBerger et al. 1991). Unlike the Ottawa aulacogen, there is no evidence for Mesozoic reactivation in the Saguenay graben. The paradigm earthquake for the Saguenay graben is the 1988 Saguenay (**M** 5.9) event, which occurred at a depth of 27 km (Adams et al. 1996). Seismicity in the region was very low prior to this event (DuBerger et al. 1991). Doig (1998) determined a recurrence interval ranging from 350 to

1000 years based on evidence of earthquake-induced landslide deposits within lakes near the epicenter of the 1988 earthquake.

Southwestward Extension

Various authors have postulated a southwesterly midcontinent extension (i.e., aulacogen) of the SLRS, which is now recognised as a remnant of the IRM (Wheeler 1996a). For example, Adams and Basham (1989) postulated such an extension in the region of the New Madrid rift in the central United States, although they later retracted this speculation, citing a lack of evidence (Adams and Basham 1991). However, to allow for this hypothesis, we consider possible local evidence for a southwesterly extension of the rift system in the southern Great Lakes region.

Grier (1995) reported that brittle faulting occurs on a series of north-northeast- and northeast-trending faults along the upper St. Lawrence Valley, from Kingston to Cornwall. The faults in this region generally exhibit offsets of up to tens of meters, and show variable slip directions (Grier 1995). However, the amount and timing of brittle deformation on these faults and their relationship with the much larger faults along the St. Lawrence Valley north of Cornwall are unknown (Grier 1995).

Gauthier and Benn (1996) identified two prominent northeast-striking faults on the Frontenac arch in northern New York State. These faults are associated with brittle deformation and are interpreted to be reactivated Grenville ductile structures (Gauthier and Benn 1996). The recognition of these structures led Gauthier and Benn (1996) to suggest that other northeast-southwest-trending lineaments along the upper St. Lawrence River may correspond to reactivated basement structures, which may form a possible structural linkage between Lake Ontario and the St. Lawrence rift.

In an abstract, Wallach and Thomas (1996) suggested that the Carthage-Colton mylonite zone, a sinuous, ductile structure separating the Frontenac and Central Granulite blocks within the Grenville province, denotes the southern limit of the St. Lawrence fault zone (i.e., rift). Wallach and Thomas (1996) further suggested that the features in the South Ontario structural zone, which lie approximately along the southwest projection of the Carthage-Colton mylonite zone, represent brittle reactivation of this originally ductile Grenville structure.

Faure et al. (2006) performed paleostress analysis of mesoscopic faults and emplacement of Jurassic dikes in Quebec and New Brunswick and concluded that although Atlantic rifting was a widespread extension event, it extended as far as 400 km into the plate. Preexisting late Proterozoic, Taconic, Acadian, and Alleghenian structures within this zone were reactivated during the opening of the Atlantic Ocean and are kinematically linked to faults bounding Mesozoic basins.

Deep seismic data collected along and across the Ottawa River (e.g., Mereu et al. 1986) show crustal-scale extension on the approximately east-west-trending, high-angle faults within the Ottawa aulacogen. Similarly, seismic profiles collected across the St. Lawrence Valley and the northern Appalachian front indicate step-faulting of the Grenville basement, with displacements ranging from 200 to 1,000 m, extending eastward beneath the Appalachian thrust sheets (St.-Julien et al. 1983). The deep seismic data collected in Lakes Ontario and Erie (e.g., Milkereit et al. 1992, Forsyth et al. 1994a, 1994b, Zelt et al. 1994, White et al. 1994) do not show any high-angle extensional structures or extensional deformation on the scale of the Ottawa graben faults or the St. Lawrence Valley faults, providing very strong evidence that a failed rift arm does not extend into the lake. The well-documented, high-angle Iapetan faults

that cut Grenville basement along the St. Lawrence, Champlain, Ottawa, and Saguenay river valleys exhibit offsets of the lower Paleozoic rocks on the order of many hundreds of meters (e.g., Kumarapeli 1985, DuBerger 1991), whereas faulted lower Paleozoic rocks in the northeastern Lake Ontario region (e.g., Grier 1995) generally exhibit maximum offsets on the order of several tens of meters. Furthermore, unlike the Ottawa, Saguenay, Champlain, and St. Lawrence river valleys, the postulated southwesterly extension of the rift system is not delineated by elevated and persistent seismicity.

3.2.1.4 Iapetan Rifted Margin Source Zone

The Iapetan Rifted Margin (IRM) source zone extends northeast-southwest across the entire study area and encompasses a terrane of known and inferred normal faults that formed parallel to the passive margin of Laurentia during the Late Proterozoic-Early Paleozoic opening of the Iapetus Ocean (e.g., Wheeler 1995, 1996b). Compressional reactivation of favourably oriented Iapetan faults has been postulated as the causal mechanism for several seismically active regions in eastern North America, including Charlevoix and the lower St. Lawrence Valley, Quebec (Adams and Basham 1991); Giles County, Virginia (Bollinger and Wheeler 1988); and eastern Tennessee (Powell et al. 1994, Wheeler 1995).

Iapetan normal faults likely decrease in size, abundance, and slip gradually and irregularly northwestward into the North American craton over a distance of perhaps 100 - 200 km (Bollinger and Wheeler 1988). The northwest boundary to Iapetan normal faults is based on the northwesternmost locations of known Iapetan faults, both seismic and currently aseismic (Wheeler 1995). This boundary coincides approximately with the northwestward transition from a more seismically active continental rim to a generally less active cratonic interior. The northwestern boundary of the IRM includes the Clarendon-Linden fault system as defined by Wheeler (1995). The location of the Wheeler (1995) boundary is also reflected in the 2008 update of the U.S. national seismic hazard maps (Petersen et al. 2008).

Milkereit et al. (1992) have suggested that the CMBBZ, which lies approximately 100 km to the west of the Clarendon-Linden fault system (see Figure 2.21), displays characteristics of an Iapetan structure. (The CMBBZ is described by O'Dowd et al. [2004] as a 10 to 20 km wide zone of intense structural deformation within the Grenville orogen of southeastern Canada.) A Middle to Late Proterozoic half graben imaged from deep seismic reflection data collected across the CMBBZ in eastern Lake Erie was interpreted to be the result of either pre-Appalachian (i.e., Iapetan) continental rifting or terminal collapse of the Grenville orogen. This feature involved extensional reactivation of a gently east-dipping Grenville-age thrust fault in the CMBBZ, as opposed to cutting discordantly through the gently east-dipping boundary zone (Milkereit et al. 1992). At the data resolution scale, the seismic data indicate that the lower Paleozoic sediments overlying this half graben are not significantly deformed (Milkereit et al. 1992).

In view of the uncertainty associated with the location of the western boundary of the IRM source zone, we make an assessment of the significance of the IRM/SGR source zone boundary. Johnston et al. (1994) note that in stable continental regions worldwide, Precambrian rifts, such as the midcontinent rift system, are considered to be incorporated into the craton and do not localise seismicity above background seismicity levels. Iapetan rifting occurred from very late Proterozoic to the earliest Paleozoic (Johnston et al. 1994); thus Iapetan rifted crust is considered a Paleozoic domain by Johnston et al. (1994).

There is widespread acceptance by the scientific community of the important differences between rifted (or extended) and nonrifted crust with respect to seismic hazard.

Johnston et al. (1994) characterised the seismic potential of rifted vs. unrifted crust in eastern North America using a seismic activity rate normalised to a given unit area of crust. They concluded that the normalised rates for rifted crust in eastern North America are nearly twice those of unrifted crust. Worldwide, normalised rates for rifted crust exceed those for unrifted crust by a factor of 4 at **M** > 5, increasing to a factor of 8 at **M** > 6 (Johnston et al. 1994). This implies that the western boundary of the IRM, and in fact all of the intact Iapetan rifted crust, is significant in terms of seismic hazard.

Based on the foregoing information, we consider three alternatives for the position of the northwestern boundary of the IRM source zone: (1) the regional IRM boundary as substantially defined by Wheeler (1995) and Petersen et al. (2008; see Plate 1a); (2) the CMBBZ as suggested by Milkereit et al. (1992; Plate 2a); and (3) the western limit of known Iapetan normal faults in the Adirondack uplift (Plate 3a). For the CMBBZ boundary, two alternatives in the vicinity of western Lake Erie are considered to be equally credible: (1) a boundary on the west that is based on the existence of the Mississauga domain as recognised by O'Dowd et al. (2004) and (2) an eastern boundary that does not include this domain. A low weight (0.1) is assigned to the CMBBZ's representing the northwest boundary of Iapetan rifting, based on the following:

- Absence of large-scale, high-angle, down-to-the-east step faults cutting through the gently east-dipping Grenville reflectors in the seismic data;
- Thickness (approximately 43 km) of the Grenville crust adjacent to the CMBBZ (Zelt et al. 1994, Forsyth et al. 1994a);
- Well-documented occurrences of post-orogenic extension due to collapse in the Grenville Orogen within the Canadian Shield (e.g., van der Pluijm and Carlson 1989); and
- Absence of significant early Paleozoic normal slip overlying the half graben imaged in Lake Erie.

We assign a weight of 0.5 to the boundary lying along the western flank of the Adirondack uplift, and a weight of 0.4 to the boundary as defined by Wheeler (1995). The western Adirondack boundary is given slightly higher weight because it marks the limit of known Iapetan faults in the Lake Ontario region, and the Clarendon-Linden fault system cannot be shown unequivocally to be an Iapetan structure.

3.2.1.5 Extended Continental Crust Source Zone

The Extended Continental Crust (ECC) source zone consists of continental crust that most recently experienced significant extension during Mesozoic rifting associated with the separation of the North American and African plates (Plate 1a). This zone includes exposed rift basins along the Atlantic seaboard that are situated landward of the hinge zone of the continental margin. This region experienced considerably less crustal thinning than did the region seaward of the hinge zone that includes the deeper marginal sedimentary basins (Klitgord et al. 1988). The boundaries of this zone generally coincide with the boundaries of the western part of the Eastern Seaboard Domain as defined by Johnston et al. (1994; see Figure 2.5). This domain includes Paleozoic basement of part of the eastern United States as well as the eastern continental shelf. The western boundary of this domain generally follows the western edge of the Triassic-Jurassic onshore basins or the boundaries of the structural blocks in which they occur (Klitgord et al. (1988). As shown by Johnston et al. (1994), this zone also includes Paleozoic basins in the northern Appalachians that resulted from post-Acadian transtensional deformation.

The eastern boundary of this zone is defined by a basement hinge zone that separates shallow platforms from deep marginal sedimentary basins in a series of parallel half graben structures that deepen seaward. At the hinge zone, basement deepens steeply to the east by a series of down-dropped fault blocks from about 2 to 4 km depth to over 8 km depth (Klitgord et al. 1988). The character of block faulting at the hinge zone varies along the margin and may reflect the influence of older crustal structure on the Mesozoic rifting (Klitgord et al. 1988). Half graben structures with seaward-dipping border faults are observed at the Georges Bank hinge zone, whereas faulted blocks with landward-dipping faults form the hinge zone in the Baltimore Canyon trough (Klitgord et al. 1988, Trehu et al. 1989).

Seismicity within the ECC source zone is not randomly distributed, but tends to be clustered with intervening areas exhibiting low seismicity. The largest historical events within this zone are the earthquakes of 1755 (Cape Ann, M ~ 6.2), 1884 (Rockaway Beach/New York City, body-wave magnitude m_b = 5.2), and 1737 (New York City, m_b = 5.2).

3.2.1.6 Northern Appalachians Source Zone

The Northern Appalachians (NAZ) source zone consists of a variety of Paleozoic terranes assembled in the Taconic, Salinian, and Acadian orogenies and deformed by these events and the subsequent Alleghenian orogeny, opening of the Atlantic Ocean, and the Great Meteor Hotspot (see Table 2.1). Normal faulting in the late stages of the Salinian orogeny (Tremblay and Castonguay 2002), extensional reactivation of the Ammonoosuc Fault in the Mesozoic (Moench and Aleinikoff 2003), and the Norembega fault zone in the Late Cretaceous (West and Roden-Tice 2003) indicate that this zone has experienced multiple phases of extension. The Northern Appalachians is a separate tectonic block built in the Taconic and Acadian orogenies, separately from the central and southern Appalachians and is therefore separated from the ECC source zone. The terranes of the Northern Appalachians overrode the Iapetan passive margin along an east-dipping zone of detachment (Grenvillian ramp), seen as a major lateral velocity change that reaches a depth of about 25 km in the source zone (Hughes and Luetgert 1991). This structure has not been identified as a source of recorded seismicity. As noted by Adams et al. (1995), all earthquakes in this zone with known depths are relatively shallow (less than 10 km).

3.2.1.7 Great Meteor Hotspot Source Zone

The Great Meteor Hotspot (GMH) source zone is adopted from the Gatineau (GAT) source zone of the GSC (Adams et al. 1996, Adams and Halchuck 2003). Adams and Basham (1991) have suggested that the band of seismicity north of the Ottawa River within the Western Quebec seismic zone is due to crustal fractures that formed as the North American plate rode over a Cretaceous hotspot (Crough 1981). As discussed in Section 2.2.15, various interpretations exist regarding the role of the hotspot and its role in Late Cretaceous extension.

Regardless of the exact timing and mechanism, the hotspot track continues to influence rates of seismicity. The GMH has been associated with clusters of midcrustal seismicity by Ma and Eaton (2007). Ma and Atkinson (2006) attribute the wide hypocentral depth distribution (2 - 25 km) for events in the western Quebec seismic zone to faults of through-going crustal extent or of varying depths in the crust and note that the clustering of focal depths at 5, 8, 12, 15 and 22 km and may reflect layering in seismogenic properties within the crust. Subsequent work by Ma and Eaton (2007) noted that shallow events with depths less than 8 km are randomly distributed with reverse mechanisms attributed to glacial isostatic adjustment, earthquakes with intermediate depths define a linear band of earthquakes, and deep earthquakes (greater than 17 km in depth) are localized as clusters at Timiskaming, Maniwaki, Mont Laurier, and

Adirondack. Crustal thickness maps derived by Eaton et al. (2006) from teleseismic analysis and results of regional seismic refraction surveys image the hotspot track northeast of the Ottawa-Bonnechere graben as minima on these maps. The thinnest crust (34.5 - 37.0 km) coincides with the elevated seismicity rates of the Western Quebec seismic zone, northeast of the Ottawa Bonnechere graben. These observations led Ma and Eaton (2007) to propose that the Western Quebec seismic zone represents blind intrusions associated with entrapment of mantle-derived melt in the crust between the area emplaced with kimberlitic dikes and the Monteregian intrusions.

3.2.2 Seismicity-Based Source Zones

A second approach to defining regional source zones is to delineate areas with relatively uniform seismicity. Seismic hazard maps for Canada and adjacent parts of the United States were prepared by the Geological Survey of Canada as part of the Canadian National Earthquake Hazards Program (Adams and Halchuk 2003). Both aleatory and epistemic uncertainties are incorporated into the new maps, the fourth generation of seismic hazard maps of Canada. For eastern Canada, two models are used in Adams and Halchuk (2003). The H model uses relatively small source zones drawn around historical seismicity clusters, and the R model establishes larger, regional source zones. Since the tectonic elements used to develop the R model are all considered in the geologic/tectonic source zones described above, only the H model is used in this study (Plate 25). In this model, the seismicity zones represent areas of uniform seismicity rate. Smaller zones are drawn about small clusters and larger zones are drawn about more elongated clusters of seismicity. Some consideration is given to geology and tectonics in connecting individual centers of clustered seismicity along the axis of the St. Lawrence rift and Ottawa graben.

3.2.3 Zoneless Model of Seismicity-Based Source Zones

The zoneless approach is based on a similar concept to the seismicity based model (Section 3.2.2): the pattern of recorded seismicity is the single most important factor controlling the rate and spatial distribution of future earthquakes in the region. The difference is that instead of defining zones of uniform seismicity (i.e., small zones of higher seismic activity embedded in large zones of lower activity), a nonparametric spatial smoothing process is used to define the spatial variation of activity rate (a-value) and b-value over the entire region. The methodology was developed by EPRI (1988) and was used to assess earthquake catalogue completeness in Section 2.5.4. The region is divided into cells of one degree longitude and latitude. The seismicity parameters (a- and b-value) for each cell are estimated from the earthquakes that have occurred within the cell using a penalised likelihood methodology that imposes a degree of smooth variation across the entire region.

The penalised likelihood approach compares the seismicity parameters estimated in a cell with the average of the parameters in the neighbouring cells. Large changes in the rate of activity or b-value compared to the neighbouring cells require a large amount of data within the cell. Cells with little data receive seismicity parameters that are similar to those in the neighbouring cells. The zoneless model developed for the Bruce nuclear PSHA covers the region shown on Plate 26. A low degree of smoothing (small penalty function) was applied to the a-value, allowing for rapid changes in seismicity rates across the region. A greater degree of smoothing was applied to the b-value estimation, reflecting the concept that large changes in b-value are not expected with stable continental regions.

3.3 Local Seismic Sources

Two local seismic sources are potentially active within a 100 km radius of the Bruce nuclear site: the GFTZ and the Georgian Bay linear zone (GBLZ) (see Figure 2.21). Five additional seismic sources more than 100 km distant from the Bruce nuclear are also included in the seismic hazard analysis. The characteristics of these sources are described below and alternative geometries are shown on Plates 27 and 28. Some of these sources have a very low assessed probability of activity and, therefore, minimal influence on seismic hazard in the Bruce nuclear site region. However, each of these local sources has been identified as being potentially significant by other researchers and therefore is included in the PSHA for completeness.

3.3.1 Seismogenic Potential

A key uncertainty in the assessment of local features is whether individual faults, lineaments, and other interpreted tectonic features are seismogenic. Seismogenic in this context is defined as capable of generating moderate-to-large earthquakes ($M_N > 5$). Uncertainty in this assessment, which is specific to each local seismic source, is represented by the relative probabilities on the yes and no branches of the logic tree. In the hazard analysis, the “yes” branch means that the fault or lineament will be treated as a source that localises seismicity; the “no” branch means that the fault or lineament will not localise seismicity above the levels of the regional source zone within which it lies. In all cases, the regional seismic source zones are assumed to be seismogenic with a probability of 1.0. This is because the regional sources include a large region spatially and likely include at least one fault (although unknown) capable of generating an M > 5 earthquake. Because the regional sources exist everywhere in the study region, there is a finite potential for earthquake occurrence everywhere in the study region. The definition of local sources can, therefore, include the manner in which future seismicity might be localised along particular tectonic features. The probability that any given tectonic feature is seismogenic varies as a function of evidence for its activity, as discussed below.

The approach used in this analysis to quantify explicitly the probability of being seismogenic is essentially the same as that used for the EPRI seismic hazard analysis for the eastern United States (EPRI 1988). The assessment follows three basic steps:

- Identify diagnostic criteria for assessing seismogenic potential and evaluating their relative value;
- Evaluate individual tectonic features relative to the criteria; and
- Combine the feature-specific evaluation of the criteria with the relative value of the criteria to arrive at the probability that the tectonic feature is seismogenic (note that in the EPRI study, this was termed the “probability of activity”).

Below, we first define and rate the criteria, followed by a discussion of the procedure for evaluating the probability of being seismogenic. This is followed by the evaluation of the seismic potential of local sources.

3.3.1.1 Criteria for Assessing Seismogenic Potential

Given the importance of this component of the source characterization to the hazard analysis, it is useful to define explicitly the criteria that are used to assess whether a tectonic feature or lineament is seismogenic, and to define the relative value that each criterion has in making the evaluation. “Relative value,” in this sense, is an expression of the resolving power that a particular criterion - and its associated data - has in determining whether a tectonic feature is

seismogenic. A criterion that provides a high resolving power (i.e., provides a strong indication that a feature is seismogenic) is therefore assigned a high relative weight. For example, if a tectonic feature is spatially associated with several $M_N > 5$ earthquakes in the historical record, it would have a high potential for being seismogenic (that is, capable of generating $M_N > 5$ earthquakes in the future). Some criteria may be less diagnostic and have a relatively low resolving power for determining whether a tectonic feature is seismogenic. An example of such a criterion might be evidence that the tectonic feature has undergone multiple episodes of reactivation during its geologic history. Studies of earthquake occurrence within stable continental regions worldwide have suggested that observed moderate-to-large earthquakes commonly have been associated with multiply reactivated structures (Johnston et al. 1994). However, these studies also have concluded that there are many more such tectonic features not associated with observed earthquakes than ones that are associated, suggesting that this is not an effective diagnostic criterion.

The criteria discussed below are judged to be diagnostic types of information that would indicate whether a fault is capable of generating $M_N > 5$ earthquakes in the future. These criteria are best suited for potential sources with unclear evidence of activity, but would not be used if certain evidence is well documented. For example, if a fault has been causally (not just spatially) associated with large-magnitude historical earthquakes or shows unequivocal evidence of repeated late Quaternary displacements (as would an active fault in a plate-boundary tectonic setting), then that fault would be considered seismogenic with a probability of 1.0. If, however, these most diagnostic criteria are not present for a particular tectonic feature, then there exist uncertainties in the seismogenic potential of that feature. This uncertainty is expressed by the probability that the feature is seismogenic and will be less than 1.0. The criteria and their relative diagnostic value are explained below.

Spatial Association with $M_N > 5$ Seismicity

The first criterion is the spatial association of a tectonic feature (e.g., fault or lineament) with observed moderate-to-large earthquakes that have occurred historically or during the instrumental period. Note that this is not a causal association (which would clearly indicate that the feature is seismogenic), but merely the spatial distribution of observed earthquakes relative to the feature of interest. We define spatial association as being an alignment of seismicity along the length of a substantial portion of a given feature (i.e., a fault or lineament). For general application, the spatial association is made in two dimensions only (map view) because reliable hypocenter data are not generally available. Uncertainties associated with this criterion stem from the fact that, in low-activity environments, the historical record is short relative to the recurrence intervals of large earthquakes. As a result, the occurrence of only a single historical event or the absence of large observed events is not uncommon. In addition, it is difficult to associate older historical events with a particular feature because of uncertainties in epicenter location; sometimes even instrumentally located events are not easily associated with known faults. If available, other information, including focal depth and focal mechanisms, is considered in the final assessment of the seismogenic potential of a given feature. This is applied on a case-by-case basis because these data generally are not available for most of the features being considered in this analysis. (See the discussion below on using feature-specific data sets to "update" the assessment of seismogenic potential.)

Spatial Association with $M_N < 5$ Seismicity

The second criterion is the spatial association of a tectonic feature with small-magnitude ($2 > M_N < 5$) seismicity. Again, we define spatial association as an alignment of seismicity along the length of a substantial portion of a given tectonic feature. It is common for

seismogenic faults to be associated with small-magnitude seismicity; however, the association of a fault or lineament with such events does not necessarily indicate that the feature can also generate larger events.

To illustrate the notion of a "spatial association" of seismicity with a tectonic feature, we present on Figure 3.4 a range of assessments for an idealised linear tectonic feature and idealised "observed" seismicity. The feature C displays a clear association with seismicity aligned along its entire length. In this example the trend in the seismicity is consistent with the trend of the feature, and the feature is assessed to be spatially associated with seismicity with a probability of 1.0. In the example, both historical and instrumental events are present, suggesting persistence through time and little chance that the spatial association with older historical events is merely a matter of the coincidence of poor locations. The feature A on Figure 3.4 has a single recorded event in close proximity to it, and although other earthquakes occur in its vicinity, they show no tendency to align themselves along the feature. Thus feature A on Figure 3.4 is assessed to have a low probability (0.1) of spatial association with seismicity.

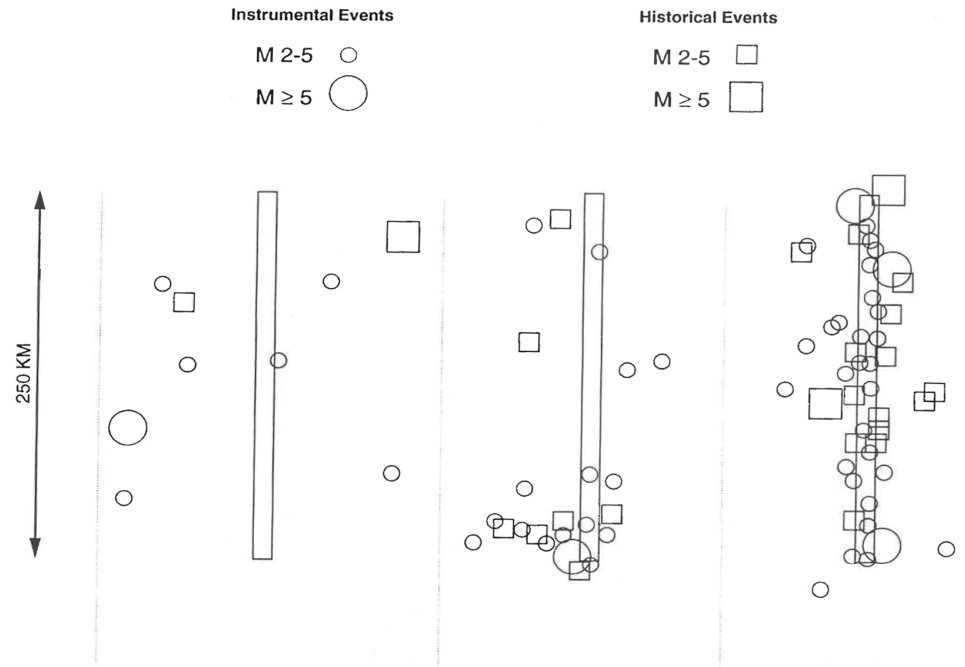

Figure 3.4: Examples of Spatial Association with Seismicity

The other example presented on Figure 3.4 further illustrates the definition of spatial association. Seismicity in the vicinity of feature B on Figure 3.4 occurs primarily near one end. This cluster, however, is part of a trend of seismicity that is perpendicular to the feature and

extends away from the feature. Seismicity that occurs near the remaining portion of the feature is scattered and cannot be distinguished from random background activity. This feature is assessed to have a probability of 0.2 of being spatially associated with seismicity because the trend in the seismicity is not consistent with the trend of the feature.

For two or more features that are proximal to one another, or that intersect, we assume that the seismicity in their vicinity can be associated with any of the features, i.e., a single seismicity cluster that is proximal to, say, three features is considered in the individual assessments of each of the features.

Multiple Episodes of Reactivation

The third criterion is geologic evidence for multiple episodes of reactivation. A fault that exhibits evidence for brittle slip during distinctly different geologic time periods/tectonic phases might be an indication that that structure is a persistent zone of weakness in the crust. For example, in their global study of the association of M > 4.5 earthquakes with various tectonic features, Johnston et al. (1994) found that several of the moderate-to-large earthquakes that have occurred in stable continental regions have been associated with intracratonic rifts that have experienced multiple episodes of reactivation. Admittedly, however, they also found that there are many rifts displaying such evidence of reactivation that have not been associated with seismicity. Uncertainties in applying this criterion arise from the lack of, or uncertainties in, crosscutting relationships of brittle structures and recognizing different types of cogenetic displacement (e.g., normal faults in the hanging wall of a thrust fault). A structure reactivated in the present-day northeast-southwest-oriented compressional stress field would also show evidence of activation during a previous phase of deformation.

Brittle Slip in Present Stress Regime

The fourth criterion is geologic evidence for brittle slip that is kinematically consistent with the present tectonic stress regime. Clearly, faults and other features associated with ductile deformation reflect a deformation episode that occurred at a tectonic level below the seismogenic zone of the crust. Therefore, we are only considering tectonic features associated with brittle deformation. We consider compressional deformation, i.e., strike-slip, reverse, or oblique reverse faulting, to be an indication of slip within the present-day regional stress field. Further, we assume that the axis of maximum horizontal compression is in the northeastern quadrant in the study region. Seismogenic faults, by definition, are favourably oriented relative to tectonic stresses because earthquakes are a manifestation of the release of tectonic stresses. However, in the absence of other evidence, determination of how favourably a fault is oriented involves knowledge of the three-dimensional geometry of the fault, the orientations of the principle stress directions, and the rheological properties of the rocks (Zoback 1992).

Crustal Extent

Because of the rupture dimensions associated with large earthquakes, most seismogenic faults extend through the seismogenic crust (i.e., depths of 10 – 20 km). The fifth criterion expresses the degree to which knowledge of the downdip crustal extent of a fault provides an indication of whether it is seismogenic. Evidence for expression in the deep crust might include large geophysical anomalies and gradients, the identification of a feature in deep seismic data, and geologic/tectonic interpretations of the role that a tectonic feature represents (e.g., continental rift faults). Crustal-scale extent is not considered an exclusively sufficient condition for assessing seismogenic potential. That is, seismogenic tectonic features would be

expected to extend to seismogenic depths, but the mere fact that a feature extends to these depths does not provide much assurance that it is in fact seismogenic. This conclusion is supported in many geologic environments, such as in much of the eastern United States, where abundant, large, crustal-scale faults exist, but relatively few are believed to be seismogenic. These features are merely the vestiges of previous tectonic deformation episodes.

3.3.1.2 Additional Criteria

The criteria discussed above generally are applicable to the tectonic features in the Bruce nuclear site region because of the available databases. However, additional data of potential use to the evaluation of seismogenic potential may be available locally if special studies have been conducted. For example, local seismic networks may provide information on the spatial distribution of microseismicity ($M_N < 2$), or geologic studies may identify evidence for geologically recent faulting or evidence for paleoseismic shaking (e.g., paleoliquefaction evidence). These observations, although not generally applicable to all local sources, are important to certain local sources and must be taken into account in arriving at the probability of the feature's being seismogenic. The additional criteria are discussed here, and the procedure for "updating" the assessment to include feature-specific additional data is discussed in the following section.

As defined above, the criteria for "spatial association with seismicity" are based on a two-dimensional (map view) association between observed seismicity and the tectonic feature. In some cases, additional seismologic data may exist that could affect the assessment. These data include information on the hypocentral distribution (such that the three-dimensional geometry of the feature can be correlated with seismicity or the crustal extent of the feature assessed); focal mechanisms that indicate whether the orientation of the focal planes is consistent with the feature of interest; stress tensors that may or may not be consistent with the kinematic indicators on the feature of interest; the spatial pattern of microseismicity ($M_N < 2$); and the spatial pattern of aftershock sequences that define the geometry of coseismic rupture planes.

An additional consideration is geologic evidence for Quaternary tectonic displacement. The Quaternary geologic record spans a much longer period than the historical record, and typically includes evidence of large earthquakes that rupture the surface. In plate-boundary tectonic environments, this criterion is the primary means of assessing whether particular faults are active. Uncertainties in using this criterion in eastern North America come from uncertainties in dating the age of slip and discerning whether displacements are tectonic or other in origin. Given the common occurrence of geologically young glacial features and postglacial pop-up structures in the Great Lakes region, the identification of young tectonic deformation requires considerable care. In evaluating this criterion for a given fault or lineament, we consider both the geologic evidence for recency of deformation associated with that feature, and the likelihood that the evidence represents seismotectonic or other deformation.

3.3.1.3 Procedure for Calculating Probability of Being Seismogenic

The diagnostic value of the five seismogenic criteria is shown in Table 3.1 in terms of the conditional probability that a feature is seismogenic given a specific set of observations. The table is laid out in the form of a matrix containing the 32 possible combinations of observing the criteria or lack of criteria when considering a specific tectonic feature. Each box in the matrix represents one possible set of observations for a tectonic feature. The number in the

box represents the conditional probability that the feature is seismogenic given the specific set of observations. The table is arranged such that the upper left-hand corner is the most favourable case for the feature's being seismogenic (i.e., all five criteria are observed), and the lower right-hand corner is the least favourable case for the feature's being seismogenic (i.e., all of the criteria are observed to be absent). The criteria are arranged in order of decreasing diagnostic ability from left to right and from top to bottom.

Table 3.1: Conditional Probabilities of Being Seismogenic as a Function of Observed Criteria

				Multiple Reactivations							
				Yes				No			
				Brittle Slip				Brittle Slip			
				Yes		No		Yes		No	
				Deep Crustal Extent		Deep Crustal Extent		Deep Crustal Extent		Deep Crustal Extent	
				Yes	**No**	**Yes**	**No**	**Yes**	**No**	**Yes**	**No**
Spatial Association $M_N \geq 5$	Yes	Spatial Association $2 \leq M_N < 5$	Yes	0.95	0.94	0.93	0.92	0.91	0.90	0.87	0.85
			No	0.90	0.89	0.88	0.88	0.86	0.85	0.82	0.80
	No	Spatial Association $2 \leq M_N < 5$	Yes	0.70	0.68	0.57	0.55	0.52	0.50	0.42	0.40
			No	0.10	0.08	0.05	0.02	0.01	0.005	0.002	<0.001

The procedure used to assess the conditional probabilities is to first assess the values at the extremes (i.e., the four corners). For example, in the case where all of the criteria are observed to apply with certainty to a given feature (upper left-hand corner), the probability that these observations indicate that the feature is seismogenic is judged to be very high (0.95). The reason it is not certainty (1.0) stems from the fact that these observations do not demonstrate unequivocally a causal relationship between the feature and earthquakes. In the case where none of the three geologic criteria are observed for a given feature, yet the feature is spatially associated unequivocally with both large- and small-magnitude seismicity (upper right-hand corner), the probability that the feature is seismogenic is also judged to be very high (0.85).

The bottom row of the matrix in Table 3.1 contains the cases where no spatial association of a tectonic feature with small-magnitude or moderate-to-large earthquakes is observed. The lower right-hand corner is the case where none of the geologic criteria are observed to be present. In this instance, it is judged very unlikely (probability <0.001) that the feature is a localiser of seismicity. Again, the probability is not set to certainty (0) because of our imperfect knowledge of the processes controlling the occurrence of earthquakes in eastern North America. In the case where a feature exhibits unequivocally all of the geologic criteria but shows no spatial association with earthquakes (lower left-hand box), the probability of the feature's being seismogenic is judged to be only 0.1. This probability reflects our judgment that, in the low-strain tectonic environment of eastern North America, the geologic criteria alone are not strong indicators of the potential of a feature to generate future earthquakes.

This is indirectly supported by the widespread occurrence of known geologic structures in the region that have not been associated with historical or instrumental seismicity.

The next stage in assessing the conditional probabilities of being seismogenic is to consider the relative importance of adding (or subtracting) the observation of one of the criteria. Considering the top row of Table 3.1 (spatial association of both moderate-to-large and small earthquakes with a feature), the diagnostic power of observing that the feature has deep crustal extent (an increase in conditional probability from 0.85 to 0.87) is judged to be less than the diagnostic power of observing brittle slip (an increase in conditional probability from 0.85 to 0.90), and the diagnostic power of observing multiple reactivations is judged to be greater (an increase in conditional probability from 0.85 to 0.92). Deep crustal extent is judged to be the least diagnostic of the three geologic criteria because some moderate-sized earthquakes have occurred in stable continental crust at depths shallower than 10 km. An example is the 1986 magnitude 5 Leroy, Ohio, earthquake, which occurred at a depth of about 6 km in Precambrian basement rocks (Seeber and Armbruster 1993). The same relative importance of the three geologic criteria is used to complete the assessments for the top row and to assess the intermediate conditional probabilities along the bottom row.

The left-hand and right-hand columns illustrate the relative importance of observed spatial association with moderate-to-large and small-magnitude seismicity. The assigned conditional probabilities reflect the judgment that a spatial association with moderate-to-large seismicity is more important than a spatial association with small-magnitude seismicity. The assigned probabilities also signify our judgment that spatial association with seismicity is much more diagnostic of seismic potential than the three geologic criteria. The remaining conditional probabilities within the interior of Table 3.1 were assigned by interpolating between values along the table margins.

The evaluation of the probability that an individual feature is seismogenic is performed by assessing the degree to which each of the five criteria is judged to apply. For example, the following list shows the assessments for a hypothetical feature.

Criterion:	**Probability:**
Association $M_N > 5$	0.1
Association $M_N < 5$	0.4
Multiple reactivation	0.3
Brittle slip	0.6
Crustal extent	0.7
Probability of being seismogenic	**0.29**

The five probabilities listed above indicate the degree to which each criterion is judged to apply to the feature. These probabilities provide a basis for assigning the likelihood that the observed criteria match one of the 32 possible conditions in Table 3.1. The calculation procedure is illustrated in Table 3.2. Each of the five criteria has two possible states: being observed to apply (yes) or being observed not to apply (no). The probabilities listed above are the probabilities that each criterion is observed (yes), as indicated in Table 3.2. One minus these values equals the probabilities that the criteria are not observed. Assuming that the probabilities assigned to observing the five criteria are independent, then the joint probability of a particular set of observed criteria is obtained by multiplying the five individual probabilities. For example, the likelihood that all five criteria are observed is 0.1×0.4×0.3×0.6×0.7 = 0.0050 (first row of Table 3.2), and the likelihood that none of the criteria are observed is (1 0.1)×(1 0.4)×(1-0.3)×(1–0.6)×(1–0.7) = 0.0454 (last row of Table 3.2). The unconditional

assessment of the probability that the feature is seismogenic is made by multiplying the likelihood that a particular set of criteria is observed by the conditional probability that the feature is seismogenic (Table 3.1) and summing the result over all 32 possible sets of observations (last column of Table 3.2). The result for the example feature is 0.29.

By disaggregating the assessment this way into its component parts, the technical basis for the assessment is made clear. It should be noted, however, that although the assessment is made more explicit by dissecting it into its component parts, the assessment of the probability of the feature's being seismogenic is still one that involves professional judgment. The technical basis for the assessments is given for each feature in the following section.

As discussed above, in some cases additional data may exist for certain tectonic features (e.g., focal mechanisms, geologic evidence for Quaternary tectonic slip). In those cases, the probability of being seismogenic that is calculated for the feature—based on the five general criteria—is "updated" to account for the additional information. For example, in the example given above, the tectonic feature is assessed to have a probability of 0.29 of being seismogenic based on the five general criteria. Suppose that, in addition, a local seismic network has shown that microseismicity is aligned along a significant portion of the tectonic feature, and focal mechanisms for several earthquakes in proximity to the feature indicate that one nodal plane is parallel to the feature. This additional information would lend further support to the seismogenic potential of the feature. The additional criteria are used in a formal Bayesian update of the probability that the feature is seismogenic. The probability of 0.29 assessed from the five primary criteria is considered the "prior" assessment, $P'(S)$. The "posterior" probability, $P''(S|C)$, given the observation of criteria, C, is given by Bayes's Theorem:

$$P''(S|C) = \frac{P(C|S) \times P'(S)}{P(C|S) \times P'(S) + P(C|\overline{S}) \times P'(\overline{S})} \tag{3.1}$$

where $P(C|S)$ is the likelihood (probability) of observing criteria C given that the feature is seismogenic, $P(C|\overline{S})$ is the likelihood of observing criteria C given that the feature is not seismogenic, and $P(\overline{S})$ is the prior probability that the feature is not seismogenic $[P'(\overline{S}) = 1 - P'(S)]$.

Table 3.2: Example Calculation of the Probability a Feature Is Seismogenic

Assoc. $M_N \geq 5$		Assoc. $M_N < 5$		Reactivation		Brittle Slip		Deep Crustal Extent		Comb. Prob. of State*	Cond. Prob. of Seis.**	Prob. of Seis.***
State	Prob.	State	Prob.	State	Prob.	State	Prob.	State	Prob.			
Yes	0.1	Yes	0.4	Yes	0.3	Yes	0.6	Yes	0.7	0.0050	0.95	0.0048
Yes	0.1	Yes	0.4	Yes	0.3	Yes	0.6	No	0.3	0.0022	.094	0.0021
Yes	0.1	Yes	0.4	Yes	0.3	No	0.4	Yes	0.7	0.0034	0.93	0.0032
Yes	0.1	Yes	0.4	Yes	0.3	No	0.4	No	0.3	0.0014	0.92	0.0013

Assoc. $M_N \geq 5$		Assoc. $M_N < 5$		Reactivation		Brittle Slip		Deep Crustal Extent		Comb. Prob. of State*	Cond. Prob. of Seis.**	Prob. of Seis.***
State	Prob.	State	Prob.	State	Prob.	State	Prob.	State	Prob.			
Yes	0.1	Yes	0.4	No	0.7	Yes	0.6	Yes	0.7	0.0118	0.91	0.0107
Yes	0.1	Yes	0.4	No	0.7	Yes	0.6	No	0.3	0.0050	0.90	0.0045
Yes	0.1	Yes	0.4	No	0.7	No	0.4	Yes	0.7	0.0078	0.87	0.0068
Yes	0.1	Yes	0.4	No	0.7	No	0.4	No	0.3	0.0034	0.85	0.0029
Yes	0.1	No	0.6	Yes	0.3	Yes	0.6	Yes	0.7	0.0076	0.90	0.0068
Yes	0.1	No	0.6	Yes	0.3	Yes	0.6	No	0.3	0.0032	0.89	0.0028
Yes	0.1	No	0.6	Yes	0.3	No	0.4	Yes	0.7	0.0050	0.88	0.0044
Yes	0.1	No	0.6	Yes	0.3	No	0.4	No	0.3	0.0022	0.87	0.0019
Yes	0.1	No	0.6	No	0.7	Yes	0.6	Yes	0.7	0.0176	0.86	0.0151
Yes	0.1	No	0.6	No	0.7	Yes	0.6	No	0.3	0.0076	0.85	0.0065
Yes	0.1	No	0.6	No	0.7	No	0.4	Yes	0.7	0.0118	0.82	0.0097
Yes	0.1	No	0.6	No	0.7	No	0.4	No	0.3	0.0050	0.80	0.0040
No	0.9	Yes	0.4	Yes	0.3	Yes	0.6	Yes	0.7	0.454	0.70	0.0318
No	0.9	Yes	0.4	Yes	0.3	Yes	0.6	No	0.3	0.0194	0.68	0.0132
No	0.9	Yes	0.4	Yes	0.3	No	0.4	Yes	0.7	0.0302	0.57	0.0172
No	0.9	Yes	0.4	Yes	0.3	No	0.4	No	0.3	0.0130	0.55	0.0072
No	0.9	Yes	0.4	No	0.7	Yes	0.6	Yes	0.7	0.1058	0.52	0.0550
No	0.9	Yes	0.4	No	0.7	Yes	0.6	No	0.3	0.0454	0.50	0.0227
No	0.9	Yes	0.4	No	0.7	No	0.4	Yes	0.7	0.0706	0.42	0.0297
No	0.9	Yes	0.4	No	0.7	No	0.4	No	0.3	0.0302	0.40	0.0121
No	0.9	No	0.6	Yes	0.3	Yes	0.6	Yes	0.7	0.0680	0.10	0.0068
No	0.9	No	0.6	Yes	0.3	Yes	0.6	Yes	0.3	0.0292	0.08	0.0023
No	0.9	No	0.6	Yes	0.3	No	0.4	Yes	0.7	0.0454	0.05	0.0023
No	0.9	No	0.6	Yes	0.3	No	0.4	No	0.3	0.0194	0.02	0.0004
No	0.9	No	0.6	No	0.7	Yes	0.6	Yes	0.7	0.15886	0.01	0.0016
No	0.9	No	0.6	No	0.7	Yes	0.6	No	0.3	0.0680	0.005	0.0003
No	0.9	No	0.6	No	0.7	No	0.4	Yes	0.7	0.1058	0.002	0.0002
No	0.9	No	0.6	No	0.7	Yes	0.6	No	0.3	0.0454	0.001	0.0000
									Sum	**1.0000**	**Sum**	**0.2903**

Notes:

* Probability of combined state of criteria equal to product of probabilities for each of the criteria.
** Conditional probability of being seismogenic from Table 3.1.
*** Product of probability of combined state and conditional probability of being seismogenic. Sum is the unconditional probability of being seismogenic.

If the relative likelihood of observing a criterion when a feature is seismogenic compared to when it is not is defined as $RL(C) = P(C|S) / P(C|\overline{S})$, then Equation (3.1) can be rewritten as

$$P''(S|C) = \frac{RL(C) \times P'(S)}{RL(C) \times P'(S) + \{1 - P(S)\}} \tag{3.2}$$

If one judges that it is twice as likely that the criteria will be observed for a seismogenic feature as for a nonseismogenic feature, then P"(S | C) = (2·0.29)/(2·0.29+[1–0.29]) = 0.45. It should be noted that the use of Equation (3.2) assumes that the probability of observing the additional criteria, given that the feature is not active, is not zero; that is, the additional criteria are not perfectly diagnostic. If they were, then P(C | S) would equal zero and the posterior probability would be 1.0 by Equation (3.1).

The assessments for the local sources described below are summarised in Table 3.3 and Table 3.4.

Table 3.3: Summary of Assessments for Local Sources within 100 km of Site

Source (alternative weight)	Spatial Association $M_N \geq 5$ Seismicity	Spatial Association M_N 2–5 Seismicity	Geologic Evidence for Multiple Episodes of Reactivation	Geologic Evidence for Brittle Slip in Present Stress/ Tectonic Regime	Extends to Seismogenic Depths (10–20 km)	Probability of Being Seismogenic P(S)
Georgian Bay Linear Zone Truncated (GBLZ-ET) (0.67)	0	0.1	0.1	0.1	0.1	0.05
Extending into New York State (GBLZ-E) (0.33)	0.1	0.1	0.1	0.1	0.1	0.12
Grenville Front Tectonic Zone Eastern Location (GFTZ-E) (0.5)	0	0	0.2	0.1	1	0.01
Western Location (GFTZ-W) (0.5)	0	0	0.2	0.1	1	0.01

Table 3.4: Summary of Assessments for Local Sources ≥ 100 km from Site

Source (alternative weight)	Spatial Association $M_N \geq 5$ Seismicity	Spatial Association M_N 2–5 Seismicity	Geologic Evidence for Multiple Episodes of Reactivation	Geologic Evidence for Brittle Slip in Present Stress/ Tectonic Regime	Extends to Seismogenic Depths (10–20 km)	Probability of Being Seismogenic P(S)
Niagara-Pickering Linear Zone w/o Akron Magnetic Boundary (NPLZ) (0.67)	0	0.1	0.5	0.2	1	0.08
w/ Akron Magnetic Boundary (NPLZ-AMB) (0.33)	0.2	0.25	0.5	0.2	1	0.3 increased to 0.35 based on additional information
Wilson–Port Hope Lineament	0	0.1	0.4	0.1	0.2	0.06
Hamilton-Presqu'ile Lineament	0	0.15	0.2	0.1	0.5	0.08
Clarendon-Linden Fault System	0.1	0.25	1	0.1	0.6	0.25 increased to 0.4 based on additional information
Mississauga Magnetic Domain Seismic Zone	0	0.3	0.4	0.1	0.9	0.16

3.3.2 Grenville Front Tectonic Zone

The Grenville Front tectonic zone (GFTZ) marks the boundary between the weakly deformed rocks of the Superior structural province (age 2.5 gigayears, or Gyr) and the highly deformed, much younger rocks of the Grenville province (age 1.0 Gyr; Mereu et al. 1986). The Grenville Front is a major tectonic feature exposed on the Canadian Shield and has a length of approximately 1,900 km. Evidence has been presented that suggests the Grenville Front was a result of a continent-to-continent collision process (Mereu et al. 1986). Geophysical and geologic data indicate that the Grenville Front is highly variable in its character along the length of the orogen (Kellett et al. 1994).

Aeromagnetic lineaments in southern Ontario were mapped by Boyce and Morris (2002) using an image-enhanced first vertical derivative map (see Figure 2.23). The GFTZ is one of several major northeast-trending aeromagnetic lineaments that record the presence of a Grenville-age terrane boundary. Other prominent northeast-trending lineaments recognised include the Erie-Georgian Bay lineament (located about 100 km to the east of the Bruce nuclear site) and the Niagara-Pickering linear zone that crosses the western end of Lake Ontario.

Carr et al. (2000) examined a geologic transect across the Grenville orogen in southern Ontario and New York using seismic reflection and geologic data. They described the GFTZ as the northwest limit of Grenvillian brittle-ductile deformation and an area of ductile thrusting from 1,020 to 980 Ma. The GFTZ may have been part of a compressional system that rooted in the mid-lower crust. Subsequently, the area cooled and was exhumed and overprinted by younger faults up until about 600 Ma.

An analysis involving seismic refraction tomography and data from the 1992 Lithoprobe Abitibi-Grenville Seismic Refraction Experiment was conducted by Winardhi and Mereu (1997). Their work provided constraints on the crustal thickness and the nature of the crust-mantle transition across the Grenville Front in the region directly to the northeast of Lake Huron. The GFTZ is imaged as a southeast-dipping region of anomalous velocity gradients that extend down to the Moho. The character of the Moho varies from a sharp discontinuity south of the Grenville Front to a more diffuse transitional boundary to the north of the front. The Moho depth is shallowest (34 km) on the north side of the exposed Grenville Front and is generally deeper (39 – 43 km) to the south; also, the crust to the south of the front is 4 - 5 km thicker than that to the north.

A seismic reflection line approximately 300 km long was located perpendicular to the Grenville Front north of Lake Ontario as part of 1982 experiments by COCRUST (Mereu et al. 1986). Results from the survey indicate a change in the character of the velocity gradient within the crust, as well as significant thickening of the crust by at least 5 km at depth in the vicinity of the Grenville Front. GLIMPCE deep seismic reflection data included an east-west-trending profile across Lake Huron and Georgian Bay (Green et al. 1988). This line shows evidence for a major crustal shear zone along the Grenville Front.

The deep structure of the Grenville Front in western Quebec was examined by Kellet et al. (1994) using line 15 of the Lithoprobe Abitibi-Grenville transects, integrated with aeromagnetic, magnetotelluric, and geologic mapping data. Kellet et al. (1994) compared the characteristics of the Grenville Front in their study area with the results of the studies using deep seismic reflection data across the front in central Ontario (GLIMPCE line, described by Green et al. [1988]), and central Ohio (COCORP line, described by Culotta et al. [1990], also above). The crustal structures revealed by each of these profiles were quite different, and Kellet et al. (1994) therefore state that the Grenville Front is highly variable in its character along the orogen.

Seismogenic Potential: The following table summarises the assessment of the seismogenic potential of the Grenville Front tectonic lineament. The individual assessments are listed below.

Criterion:	**Probability:**
Association with $M_N \geq 5$ seismicity	0
Association with $2 \leq M_N < 5$ seismicity	0
Evidence for reactivation	0.2
Slip favourable w/present stress regime	0.1
Seismogenic crustal extent	1
Probability of being seismogenic	**0.01**

There are no earthquakes having magnitudes greater than 5 within more than 250 km of the GFTZ; therefore, a probability of zero is assigned to the GFTZ associated with this level of seismicity. The level of small-magnitude seismicity within about 100 km of the feature is extremely low. Near the south end of the Erie-Huron linear zone (see Figure 2.23), a cluster of

earthquakes was recorded that Boyce and Morris (2002) interpret as coincident with the west-east-trending Electric fault (see Figure 2.21). However, Boyce and Morris (2002) note that the earthquake cluster is likely to be artificially induced, as the Electric fault system is associated with several producing oil and gas fields. Based on the lack of an alignment of seismicity associated with the GFTZ, a probability of zero is assigned to the criteria of association with small-magnitude seismicity.

The Grenville Front is described by Carr et al. (2000) as likely originating from ca. 1,000 Ma thrust fault that was overprinted by younger faults up until about 600 Ma. Multiple episodes of reactivation along the GFTZ have not been identified in southern Ontario. Where the GFTZ extends into the subsurface of Ohio, however, a younger fault with recurrent displacement through the latest Silurian is recognised. The recurring displacement on the Bowling Green fault is attributed by Onasch and Kahle (1991) to the GFTZ, which served to localise the release of stress in the craton.

The Bowling Green fault has been mapped in the subsurface of Ohio and Michigan. The fault is approximately 190 km in length and has three recognised segments (the northern segment is also known as the Lucas-Monroe monocline/fault). The central segment of the Bowling Green fault is well studied because of quarry exposures and is essentially coincident with the GFTZ and the Findlay Arch (see Figure 2.3). The fault displaces the Precambrian unconformity surface west-side-down (Baranoski 2002) and has had at least six episodes of displacement through the Middle Silurian (Hauser 1996). As exposed in the Waterville quarry in southern Lucas County, the fault is a 10 m wide near-vertical zone of highly sheared rock striking N10° to 20°W, with secondary faulting extending out 10 – 90 m on either side (Onasch and Kahle 1991). Onasch and Kahle (1991) speculate that adjacent fault-parallel, east-dipping thrust faults having maximum displacements of less than 5 m are consistent with the contemporary stress field, and if related to contemporary stresses, the Bowling Green fault is Late Cretaceous or younger. Onasch and Kahle (1991) suggest that the location of the fault and recurrent displacement through latest Silurian on the fault are controlled by the Grenville Front and Paleozoic orogenic activity to the east, including possibly the Carboniferous to Permian Alleghenian event. Based on these data, a weight of 0.2 is assigned to the criteria of geologic evidence for multiple episodes of reactivation.

There is no documented evidence for Quaternary deformation on the Bowling Green fault. Given the evidence for possible post-Alleghenian thrust faulting, however, the possibility that the fault—and consequently the GFTZ—is active cannot be ruled out. Therefore, the geologic evidence for brittle slip in the present tectonic stress regime is assigned a weight of 0.1.

Deep seismic reflection and refraction profile data clearly indicate that the GFTZ extends down to the Moho (Winardhi and Mereu 1997, Mereu et al. 1986, Kellett et al. 1994). Given this deep crustal structure, a very high probability (1.0) is assigned to the GFTZ's extending to seismogenic depths.

Given the assessments above, the probability that the GFTZ is seismogenic is 0.01.

3.3.3 Georgian Bay Linear Zone

The Georgian Bay linear zone (GBLZ) was identified by Wallach and Mohajer (1990) on the basis of parallel, discontinuous, linear aeromagnetic, and gravity anomalies. The feature is an approximately 50 km wide zone extending from the northeast corner of Georgian Bay to possibly as far south as western New York state (see Figure 2.22). The linear zone is approximately coincident with the straight east coast of Georgian Bay. Wallach (1990)

interpreted the differently expressed lineaments of the GBLZ as a major Precambrian structural zone. The location of the GBLZ can be interpreted on the GLIMPCE line J seismic reflection profile between shots 700 and 1000. At this approximate location, Green et al. (1988) imaged strong, east-dipping reflections to depths of approximately 30 km. These reflections coincide with the wide belt of ductile strain associated with the GFTZ as it deepens to the east (Green et al. 1988). A physiographic lineament along the trend of the GBLZ was interpreted by Sanford et al. (1985) as a fault block boundary, tectonically active at least during the early Paleozoic. The Laurentian channel, a pre-glacial outlet of the upper Great Lakes to the St. Lawrence River (Eyles et al. 1993), also lies along the trend of the GBLZ.

Based on interpretations of aeromagnetic and gravity data in southern Ontario, Roest (1995) reported the existence of the GBLZ to be very questionable. Using an image-enhanced first vertical derivative map, however, Boyce and Morris (2002) mapped aeromagnetic lineaments in the region and identified the GBLZ as the most prominent northwest magnetic trend in the region. Boyce and Morris (2002) noted that first vertical derivative filtering significantly improves the resolution of this feature, although they also state that the northwest-trending lineaments are generally lower in amplitude and less prominent than northeast-trending lineaments. The origin of the northwest-trending magnetic boundaries such as the GBLZ is not well established but may record extension into the midcontinent of transform faults formed initially during Iapetan rifting. Boyce and Morris (2002) show the GBLZ as extending from Georgian Bay to north of Lake Ontario, where it appears to be truncated by the Niagara-Pickering lineament northwest of Pickering.

Wallach and Mohajer (1990) reported that a zone of earthquakes trending north-northwest extends from western New York State to near the northeast corner of Georgian Bay and outlines a linear belt that lies within and parallels the elements of the GBLZ. Among these earthquakes are the 1857 Lockport event (~M 5.0), which has since been relocated southwest of Buffalo and downgraded to M ~ 4, and the 1929 Attica event (m_b 5.2), which occurred near the intersection of the GBLZ and the Clarendon-Linden fault system. Two mesoscopic brittle faults observed in lower Paleozoic rocks in the vicinity of the GBLZ are thought to be associated with this feature (Wallach and Mohajer 1990). These faults are oriented approximately parallel to the zone and have normal displacement, with one dipping 75 degrees northeast and the other dipping 75 degrees southwest (Wallach and Mohajer 1990).

Seismogenic Potential: There are uncertainties associated with whether the GBLZ extends south into the subsurface below Lake Ontario. Because whether the linear zone is truncated affects the assessment of seismogenic potential, two separate assessments are made for the GBLZ: (1) the linear zone is truncated by the Niagara-Pickering lineament to the north of Lake Ontario, and (2) the linear zone extends south into New York. Based on the available data, particularly the work of Boyce and Morris (2002), we consider the likelihood that the GBLZ is truncated to be twice that of the alternative that it extends into New York State.

The following lists summarise the assessments of the seismogenic potential of the GBLZ. The individual assessments are discussed below.

Assuming truncation at the Niagara-Pickering Lineament:

Criterion:	**Probability:**
Association with $M_N \geq 5$ seismicity	0
Association with $2 \leq M_N < 5$ seismicity	0.1

Evidence for reactivation	0.1
Slip favourable w/present stress regime	0.1
Seismogenic crustal extent	0.1
Probability of being seismogenic	**0.05**

Assuming extension into New York State:

Criterion:	**Probability:**
Association with $M_N \geq 5$ seismicity	0.1
Association with $2 \leq M_N < 5$ seismicity	0.1
Evidence for reactivation	0.1
Slip favourable w/present stress regime	0.1
Seismogenic crustal extent	0.1
Probability of being seismogenic	**0.12**

The 1929 m_b 5.2 Attica, New York, earthquake is located at the southeast end of the GBLZ, and most interpretations associate this event with the Clarendon-Linden fault system (Herrmann 1978, Seeber and Armbruster 1993, Tuttle et al. 2002). However, given the error (less than 50 km) associated with the epicentral location of the Attica event, it could be associated with the GBLZ. There is also uncertainty in the epicentral location and magnitude of the 1857 Lockport event: the most recent interpretation revises its magnitude downward and places it southwest of Buffalo; its previous location placed it within the GBLZ. When the GBLZ is assumed to extend into New York State, given the possibility of a spatial association with the 1929 Attica event, we assign a very low probability (0.1) to the GBLZ associated with $m_b \geq 5$ seismicity. In light of the recent reinterpretation of the 1857 Lockport event, we do not consider it to be spatially associated with this zone. When the GBLZ is assumed to be truncated, there is no association with $m_b \geq 5$ seismicity.

Wallach and Mohajer (1990) reported that at least eight small-magnitude earthquakes, both historical and instrumentally recorded events, define a line that extends along the GBLZ from northwestern New York State to the northeastern corner of Georgian Bay. Several small-magnitude events are located within the mapped trace of the GBLZ in the Lake Ontario vicinity, and numerous others occur adjacent and proximal to it in the northeast. The northwest-trending gravity gradient south of Lake Ontario near the Clarendon-Linden fault system appears to be spatially associated with some seismicity. However, the small-magnitude seismicity that is spatially associated with the GBLZ occurs as small, isolated clusters in parts of the zone, does not define a continuous alignment along it, and consists of relatively few events such that the number of events within the zone is not greatly different from that occurring outside of it. Given the rather weak spatial association of some events with this feature and the absence of a linear alignment along it, a very low probability (0.1) is assigned to the GBLZ associated with small-magnitude seismicity.

There are no data to directly evaluate the downdip extent of the GBLZ. Furthermore, unlike the Niagara-Pickering linear zone and the Clarendon-Linden fault system (described below), no major tectonic boundary has been defined by Rankin et al. (1993) that is spatially coincident with this feature. The relatively weak, discontinuous geophysical expression of the GBLZ suggests it is not a prominent crustal structure. The northwest-trending transfer zones among the north-south-striking Clarendon-Linden faults could be considered analogous to hypothesised features that compose the GBLZ. However, these northwest-trending structures

occur in the Paleozoic cover, and do not unequivocally extend to seismogenic depths. Given the weak geophysical expression of this feature relative to the other geophysical lineaments in the region, and its discontinuous nature, we assign a low probability (0.1) to the GBLZ's extending to seismogenic depths.

Wallach (1995) reported that a northwest-trending linear feature, several hundred meters long was recognised in the glacio-lacustrine sediments of Georgian Bay. This feature occurs parallel to the GBLZ and was interpreted as resulting from degassing or dewatering, which suggests the presence of an open fracture or active fault. While the orientation of this feature is considered favourable for reactivation in the current tectonic stress regime, there is no evidence that the feature is accompanied by brittle tectonic displacement. Given the uncertainty in the origin of this feature and the ambiguous association of this feature with the GBLZ, we assign a very low probability (0.1) to the GBLZ's having evidence for brittle slip consistent with the contemporary tectonic stress regime.

Wallach and Mohajer (1990) reported evidence of brittle deformation in both the Precambrian and Paleozoic rocks within the GBLZ. Two small-displacement northwest-striking normal faults, whose ages are unknown, occur in lower Paleozoic rocks along the trend of the GBLZ and are postulated to be associated with it (Wallach and Mohajer 1990). There is no evidence indicating a structural association of these local outcrop-scale faults with the postulated basement structures underlying the GBLZ, other than the similarity in their trends. Small-displacement faults occur in the lower Paleozoic rocks throughout southern Ontario; these structures have not been studied systematically to determine whether they are anomalous in the vicinity of the GBLZ.

The northwest-trending fault zones associated with the Clarendon-Linden fault system were active in the Ordovician, Silurian and Devonian (Jacobi and Fountain 2002), and it is possible that these faults could be considered analogous to hypothesised structures in the GBLZ. Eyles et al. (1993) suggested that the position of the Laurentian channel, a northwest-trending pre-glacial outlet between Georgian Bay and Lake Ontario, is controlled by a basement structure, i.e., the GBLZ. The foregoing information is considered possible evidence of reactivation of hypothesised structures that compose the GBLZ. However, given the geophysical evidence suggesting that the GBLZ is not a Grenville crustal structure (e.g., Boyce and Morris 2002), we assign a very low probability (0.1) to the GBLZ's having multiple episodes of reactivation.

Considering all of the information above, the probability that the truncated GBLZ is seismogenic is 0.05. If the feature extends into New York State, we arrive at a probability of 0.12 that the GBLZ is seismogenic.

3.3.4 Niagara-Pickering Linear Zone

The Niagara-Pickering linear zone (NPLZ) is a north-northeast-trending feature defined by a prominent linear aeromagnetic anomaly, a less well-defined Bouguer gravity anomaly, and linear physiographic features (Wallach and Mohajer 1990). This linear zone is the most prominent northeast-trending magnetic boundary identified in the region by Boyce and Morris (2002) in their mapping of aeromagnetic lineaments using image-enhanced first vertical derivative maps. The NPLZ is reported by some (e.g., Easton and Carter 1995, Wallach et al. 1998) to coincide with the southward projection of the CMBBZ, which is exposed in the Grenville province and extends southward from the Canadian Shield. Based on deep seismic reflection profiling, however, O'Dowd et al. (2004) propose that the buried extension of the CMBBZ is located along the western shoreline of Lake Ontario, west of the Mississauga

domain (see Figure 2.15), and therefore is not coincident with the NPLZ. South of Lake Ontario, the magnetic anomaly associated with the NPLZ is postulated to connect with the Akron magnetic boundary (Wallach 1990, Mohajer 1993).

The depth to the magnetic sources along strike of the NPLZ gradually increases from 2 km in the north to 4 km in the south, consistent with the southward thickening of the Paleozoic cover (Roest 1995). Roest (1995) reports that the magnetic field data indicate that the Niagara-Pickering magnetic lineament is not an isolated feature. He describes it as a series of more or less en-echelon, curvilinear anomalies within a zone (i.e., the CMBBZ) that widens to the north and south of the northern Lake Ontario shoreline. Roest (1995) also reports that it is not the highest-amplitude anomaly over Lake Ontario, and that the associated gravity signature is relatively subtle.

Wallach (1995) reports that outcrop-scale faults and fractures within Grenvillian and upper Middle Ordovician rocks within and adjacent to the NPLZ/CMBBZ provide unequivocal evidence for three separate phases of brittle reverse, normal, and strike-slip faulting along the NPLZ/CMBBZ and a zone at least 30 km wide to the east. However, Wallach (1995) does not report on the amount or timing of faulting or the full extent of the area affected. Wallach (1995) also reports evidence of macro-scale faulting along the NPLZ/CMBBZ, based on an apparent right-lateral separation of lower Paleozoic rocks shown on a bedrock geology map of Ontario (Ontario Geological Survey 1991). Wallach and Mohajer (1990) suggest that the possible spatial association of historical earthquakes with the NPLZ, including the 1853 modified Mercalli (MM) intensity V event and possibly the 1873 MM intensity VI event, may indicate that the NPLZ may be seismically active.

Mereu et al. (2002) report that in the western Lake Ontario area, the earthquake pattern from the Southern Ontario Seismic Network is significantly different from the past earthquake patterns obtained when the instrument coverage was poor. Based on analyses by O'Dowd et al. who also cite the work by Mereu et al. (2002), seismicity trends and implied basement faults are oblique to and offset from the NPLZ (O'Dowd et al. 2004).
Dineva et al. (2004) relocate hypocenters from earthquakes occurring between 1990 and 2001 that delineate clusters of events beneath Lake Ontario. They report that their clusters A and B cross the Niagara-Pickering lineament, but the trends of the clusters are rotated by about 30 degrees and thus do not appear to be associated with the NPLZ.

Seismogenic Potential: There are uncertainties associated with whether the NPLZ is structurally related to the Akron magnetic boundary. Because this possibility affects the assessment of seismogenic potential, two separate assessments are made for the NPLZ: (1) no association with the Akron magnetic boundary, and (2) an association with the Akron magnetic boundary.

It has been postulated that the CMBBZ/NPLZ and the Akron magnetic boundary may represent the same Grenville terrane boundary, based on similarities in their magnetic attributes (Rankin et al. 1993) and the observation that the lineaments appear to curve towards one another (Wallach 1995). Wallach (1995) notes that the apparent curvature evident in the magnetic field map also is evident on the gravity map of the region. Rankin et al. (1993) have interpreted the Akron magnetic boundary as a major Grenville terrane boundary, and they have mapped the northern extension of the Akron magnetic boundary north of Lake Erie as a continuous feature that appears to coincide with the CMBBZ (Figure 2.14).
Carter and Easton (1990) and Easton (1992), however, have not interpreted the magnetic features as representing the same structural boundary. Carter and Easton (1990) used both magnetic and limited borehole data in southern Ontario to extend the CMBBZ beneath the

Paleozoic cover as far south as northeastern Pennsylvania (Figure 2.8 and Figure 2.12). Forsyth et al. (1994a) also used structural constraints, along with magnetic data, to interpret the southerly continuation of the CMBBZ beneath western Lake Ontario and eastern Lake Erie and into northeastern Pennsylvania (Figure 2.13), approximately coincident with the interpretation of Carter and Easton (1990).

O'Dowd et al. (2004) state that the Niagara-Pickering lineament ends abruptly south of Lake Ontario and interpret the CMBBZ to be located along a magnetic high near the western end of Lake Erie (see the discussion below of the Mississauga magnetic domain source zone). The Akron magnetic boundary is distinct from the NPLZ on the map of interpreted aeromagnetic and gravity lineaments developed by Boyce and Morris (2002).

Based on the available data, we consider the likelihood of the model that considers the CMBBZ and the Akron magnetic boundary to not be the same tectonic feature to be twice that of the model that says they are the same tectonic feature. In the case where the two features are assumed to be connected (i.e., the same tectonic feature), the geometry of the Akron magnetic boundary is assumed to be consistent with the geometry of the NPLZ/CMBBZ as imaged in the deep seismic data (e.g., White et al. 1994).

The following lists summarise the assessments of the seismogenic potential of the NPLZ. The individual assessments are characterised below.

Assuming no association with the Akron Lineament:

Criterion:	**Probability:**
Association with $M_N \geq 5$ seismicity	0
Association with $2 \leq M_N < 5$ seismicity	0.1
Evidence for reactivation	0.5
Slip favourable w/present stress regime	0.2
Seismogenic crustal extent	1.0
Probability of being seismogenic	**0.08**

Assuming an association with the Akron magnetic Lineament:

Criterion:	**Probability:**
Association with MN ≥ 5 seismicity	0.2
Association with $2 \leq M_N < 5$ seismicity	0.25
Evidence for reactivation	0.5
Slip favourable w/present stress regime	0.2
Seismogenic crustal extent	1.0
Probability of being seismogenic	**0.30**

The 1929 m_b 5.2 Attica, New York, event and the 1986 m_{bLg} 5 Leroy, Ohio, event are the only known m_b 5 earthquakes in the region that could have occurred on the NPLZ. The epicentral location of the Attica event is well constrained and lies 80 km to the southeast of the NPLZ. Given the error in the epicentral location of the Attica event (less than 50 km), it cannot be associated with the NPLZ. The Leroy event is located well over 100 km from the NPLZ. When the NPLZ and the Akron magnetic boundary are not connected, a probability of zero is assigned to the NPLZ associated with M > 5 seismicity. The epicentral location of the m_{bLg} 5 Leroy event is well constrained and appears to be spatially associated with the Akron magnetic boundary (Seeber and Armbruster 1993, 1995). Two additional $m_b > 5$ events (one historical,

the other recorded) occur proximal to the Akron magnetic boundary in southern Ohio (Plate 11). Therefore, when a connection between the NPLZ and the Akron magnetic boundary is assumed, a low probability (0.2) is assigned to the NPLZ's being associated with $m_b > 5$ seismicity.

A cluster of historical and instrumentally recorded small-magnitude seismicity occurs in the Niagara Falls area, between Lakes Ontario and Erie. Very few of the events within this cluster are spatially coincident with the NPLZ. Along the northern portion of the NPLZ, seismicity is much more diffuse, and even fewer instrumentally recorded small-magnitude events occur in the vicinity of the mapped trace of the NPLZ/CMBBZ. Deep seismic data (e.g., Forsyth et al. 1994a) indicate that the CMBBZ is a gently east-dipping structure. Considering this geometry and the depth distribution of earthquakes in the western Lake Ontario region, events located near the surface trace that occur deeper than about 5 km are likely not associated with this feature. East of the mapped trace (i.e., downdip), seismicity is diffuse and cannot be distinguished from random background activity. For the case when there is no connection between the NPLZ and the Akron magnetic boundary, we assign a very low probability (0.1) to the NPLZ associated with small-magnitude seismicity. This assessment reflects the observation that very few events are spatially associated with the NPLZ, and there is no associated linear alignment of small-magnitude seismicity along it.

A relatively dense cluster of small-magnitude seismicity occurs in the vicinity of the Akron magnetic boundary. A number of these events, both historical and recorded, are aligned along the trend of the feature. Since the associated seismicity forms an alignment along only a small portion of the entire feature, however, we assign a low probability (0.25) to the NPLZ's being associated with small-magnitude seismicity.

Deep seismic reflection profiles collected across the CMBBZ in Lakes Erie and Ontario show that this gently east-dipping feature extends to the lower crust. Further, the CMBBZ is a profound feature in the magnetic data, suggesting a deep crustal structure. Therefore, a very high probability (1.0) is assigned to the NPLZ/CMBBZ's extending to seismogenic depths.

Evidence for brittle slip on the NPLZ in the contemporary tectonic stress regime consists of the mesoscale brittle reverse and strike-slip faults along the CMBBZ/NPLZ reported by Wallach (1995), and an apparent right-lateral separation of the upper Middle Ordovician rocks at Lake Scugog shown on the bedrock geology map of southern Ontario (Ontario Geological Survey 1991). The apparent right-lateral separation at Lake Scugog is not compelling evidence of brittle faulting. Much of the regional bedrock distribution was determined from water well records, and data coverage in this area is very limited (Eyles et al. 1993). Further, there is no corresponding right-lateral offset in the Middle Ordovician outcrop belt to the north (Ontario Geological Survey 1991). Hence the mapped bedrock distribution, if true, could be explained simply by glacial erosion.

Sanford (1993) examined the Middle Ordovician rocks along the Precambrian/Paleozoic contact at the western boundary of the CMBBZ and found no evidence of brittle faulting at this location. Sanford (1993) did document normal faulting at several locations to the east of this area. The faults were predominantly northwest-striking and generally exhibited vertical offsets of less than one meter. Sanford (1993) noted minor northwest-striking strike-slip faults at one location and a normal fault with a vertical displacement of several tens of meters at another location. Sanford (1995) and McQuest Marine (1995) also interpreted possible faults beneath Lake Ontario in the vicinity of the intersection between the NPLZ and the Hamilton-Presqu'ile lineament. However, these interpreted faults are oriented approximately parallel to the

Hamilton-Presqu'ile lineament, and therefore, we consider an association of these features with the NPLZ to be unlikely.

Lewis et al. (1995) documented numerous small-displacement (0.5 m) normal faults in this area; however, these structures were limited to a package of stratified sediment and did not penetrate bedrock. Lewis et al. (1995) suggest the structures may have formed due to differential settling of the underlying sediments. Lewis et al. also documented numerous sediment depressions in the vicinity of the NPLZ, the margins of which resemble monoclines. These features were attributed to sediment drape into a depression, rather than displacement of sediment after deposition, based on continuous and undisturbed reflection data. The depressions could not be correlated to deeper sedimentological or bedrock features, which strongly suggests a nontectonic origin (Lewis et al. 1995). Lewis et al. (1995) note that these features are widely distributed in the basin and are spatially unrelated to the various underlying geophysical lineaments. Based on the available evidence, which includes the local reverse and strike-slip faults in the Middle Ordovician rocks reported by Wallach (1995) and the minor strike-slip faults in the vicinity of the NPLZ documented by Sanford (1993), we assign a low probability (0.2) to the NPLZ's having evidence of brittle slip in the present tectonic stress regime.

Wallach (1990, 1995) reports observations of outcrop scale structures in both Precambrian and Paleozoic rocks and suggests that the NPLZ/CMBBZ has undergone several episodes of brittle reactivation. Deep seismic reflection data collected in eastern Lake Erie indicate that the CMBBZ was reactivated once in extension (Milkereit et al. 1992). Eyles et al. (1993) present evidence suggesting a possible relationship between the CMBBZ and a relict drainage system cut across the lower Paleozoic cover in the western Lake Ontario region. Eyles et al. (1993) suggest that the position of a northeast-trending channel on the Niagara Peninsula, along with another northeast-trending channel north of Lake Ontario, indicates the upwards propagation of fractures associated with reactivation of the CMBBZ. Wallach and Mohajer (1990) also note that northeast-trending linear lakes and swamps parallel the CMBBZ/NPLZ.

Sanford (1993) and Rutty and Cruden (1993) documented surface lineaments trending north-northeast as well as northeast and northwest along the CMBBZ/NPLZ in both the lower Paleozoic rocks and the exposed Grenville rocks. The origin of the north-northeast-trending surface lineaments is questionable, and it is not known whether they are geographically limited to the CMBBZ/NPLZ (Sanford 1993, Rutty and Cruden 1993). North-northeast-trending joints and fractures have been documented in numerous other areas around Lake Ontario (e.g., McFall 1993, Mohajer et al. 1992). Rutty and Cruden (1993) also report that northwest-trending pop-ups are the only neotectonic structures present within the Paleozoic rocks immediately south of the exposed CMBBZ, and their orientations suggest they are genetically unrelated to recent reactivation of the CMBBZ.

From the deep seismic data it is clear that the CMBBZ has undergone at least one episode of reactivation. The spatial association of the relict Paleozoic drainages and the CMBBZ also suggests possible reactivation, though it is not as compelling as the seismic data. It is not clear whether the local brittle faulting in the Grenvillian and lower Paleozoic rocks reported by Wallach (1995) and Sanford (1993) is associated with reactivation of the CMBBZ or other processes, such as isostatic depression and rebound. Sanford (1993) suggests that periodic uplift of the regional basement-cored arches during the various Phanerozoic compressional and extensional tectonic regimes could be responsible for the small-scale deformation observed in the lower Paleozoic rocks throughout the southern Ontario region. Small-scale faulting occurs throughout the Ordovician outcrop belt north of Lake Ontario, and these fault structures have not been systematically analyzed to determine whether they are anomalous in

the vicinity of the NPLZ. Considering the foregoing information, we assign a moderate probability (0.5) to the NPLZ/CMBBZ's having evidence of multiple episodes of reactivation.

We arrive at a probability of 0.08 that the NPLZ is seismogenic. If a connection between the NPLZ and the Akron magnetic boundary is assumed, we arrive at a probability of 0.30 that the NPLZ is seismogenic; this assessment is updated to a probability of 0.35, however, based on the following additional information.

Additional Information: Additional information exists that is pertinent to the assessment of the seismogenic potential of the NPLZ. Aftershock hypocenters of the 1986 m_{bLg} 5 Leroy, Ohio, event suggest a northeast-striking vertical rupture about 1 km across, and place the event at a depth of about 6 km within the Grenville basement (Seeber and Armbruster 1993, 1995). This orientation is parallel to the trend of the Akron magnetic boundary and lends support to the possibility that the earthquake was associated with the feature. Fault plane solutions suggest a right-lateral motion, which is consistent with the northeast-southwest orientation of horizontal compression in the regional stress field (Seeber and Armbruster 1993, 1995).

If the NPLZ/CMBBZ and the Akron magnetic boundary are assumed to be a single source, the geometry of the feature is assumed to be consistent with the geometry of the CMBBZ as determined from deep seismic data (e.g., White et al. 1994, Forsyth et al. 1994a). These data indicate that the north-northeast-trending CMBBZ comprises gently east-dipping structures (White et al. 1994). Focal mechanisms for the Leroy event yield a northeast-striking vertical plane, which is not consistent with the geometry of the CMBBZ. In our judgment, the relative likelihood of observing an inconsistent focal mechanism for a given seismogenic feature compared to a given nonseismogenic feature is estimated to be 1.25:1.

Given the additional information and using Equation (3.2), the probability that the NPLZ is seismogenic is updated from 0.30 to 0.35 when an association with the Akron magnetic boundary is assumed.

3.3.5 Wilson–Port Hope Magnetic Lineament

The northeast-trending Wilson–Port Hope magnetic lineament extends for approximately 80 km across central Lake Ontario, from Port Hope, Ontario, in the north, to Wilson, New York, in the south (Mohajer 1993, McQuest Marine 1995, see Figure 2.22). It lies between and subparallel to the NPLZ and the Clarendon-Linden fault system, along the trend of a system of prominent subsurface fractures in the Lake Erie–Niagara Falls area identified by Sanford et al. (1985) and McQuest Marine (1995). Mohajer (1993) shows the Wilson-Port Hope lineament as comprising three discontinuous, slightly curvilinear segments. McQuest Marine (1995) suggests this feature may correspond to a Precambrian basement structure. Although recent seismic reflection data do not reveal any faults along this lineament, McQuest Marine (1995) concluded that evidence from other studies (e.g., Sanford et al. 1985) suggests that the Wilson–Port Hope lineament may be a currently active fault. Dineva et al. (2004) relocate hypocenters from earthquakes occurring between 1990 and 2001 that delineate clusters of events beneath Lake Ontario. The closest cluster of earthquakes they recognise near the Wilson-Port Hope magnetic lineament is their cluster C, which is parallel to the Clarendon-Linden fault system but is shifted slightly to the southeast by about 4 km.

Seismogenic Potential: The following list summarises the assessment of the seismogenic potential of the Wilson–Port Hope lineament. The individual assessments are described below.

Criterion:	Probability:
Association with $M_N > 5$ seismicity	0
Association with $2 < M_N < 5$ seismicity	0.1
Evidence for reactivation	0.4
Slip favourable w/present stress regime	0.1
Seismogenic crustal extent	0.2
Probability of being seismogenic	**0.06**

Both of the known $m_b \geq 5$ earthquakes in the region (1929 m_b 5.2 Attica, New York, and 1986 m_{bLg} 5 Leroy, Ohio) are located more than 50 km away from the Wilson–Port Hope lineament. Similarly, the relocated epicenter of the 1857 event lies approximately 75 km southwest of the lineament. Considering that the errors in the epicentral locations of these events are less than 50 km, a probability of zero is assigned to the Wilson–Port Hope lineament associated with $M_N \geq 5$ seismicity.

There is no obvious spatial association of the Wilson–Port Hope lineament with small-magnitude seismicity. A few events have occurred near the northern end of the lineament, however, and could be projected onto it. Several events also have occurred near the intersection of this lineament with the GBLZ, and these events could be associated with either feature. Based on the scarcity of events that have occurred near the Wilson–Port Hope lineament and the lack of an alignment of events along this feature, we assign a very low probability (0.1) to the Wilson-Port Hope lineament's being associated with small-magnitude seismicity.

It is not known whether this magnetic feature corresponds to an actual structure in the Grenville basement or whether it simply reflects variable basement lithology. It does not appear to be defined by truncated, offset potential field anomalies; rather, it appears to be defined by a narrow, linear, positive anomaly. Although its trend is subparallel to other known Grenville structures in the region, a structure corresponding to this anomaly is not readily apparent in the data of Forsyth et al. (1994a). Therefore, a low probability (0.2) is assigned to the Wilson–Port Hope lineament's extending to seismogenic depths.

Seismic reflection data collected across the Wilson–Port Hope lineament in southern Lake Ontario do not reveal the presence of any faults in the lake bottom (McQuest Marine 1995). Side-scan sonar lines collected across this lineament reveal dark linear features, some of which are interpreted as anchor scours, and segmented dark marks that are interpreted to be possible degassing marks along fractures (McQuest Marine 1995). The distribution of these features does not suggest a spatial association with the lineament. McQuest Marine (1995) also reports that a system of open fractures at least 40 km long occurs roughly perpendicular to the southern end of the Wilson–Port Hope lineament, based on sediment-water-chemical relationships. However, the relationship between the inferred open fracture system and the Wilson–Port Hope lineament is ambiguous, and no explanation is offered by McQuest Marine (1995). Given the lack of clear evidence for brittle faulting on the Wilson–Port Hope lineament, but considering the possibility that the lake-bottom features identified by McQuest Marine (1995) represent slip at depth and are associated with the Wilson–Port Hope lineament, we assign a very low probability (0.1) to the Wilson–Port Hope lineament's having evidence for brittle slip consistent with the present-day regional stress regime.

There is no evidence that the Wilson–Port Hope lineament has undergone multiple episodes of reactivation. Therefore, we assign a moderate probability of 0.4 to reflect the judgment that fewer structures display evidence of multiple reactivations than those that display evidence of no reactivation.

Based on the above assessments, the probability that the Wilson–Port Hope lineament is seismogenic is 0.06.

3.3.6 Hamilton-Presqu'ile Lineament

The Hamilton-Presqu'ile lineament strikes east-northeast and extends for approximately 200 km, from near the western shore of Lake Ontario to Prince Edward County in the northeast (Ontario Geological Survey 1991; see Figure 2.21). This feature was recognised by McFall and Allam (1991) as a discontinuous aeromagnetic lineament in the Precambrian basement beneath Lake Ontario, and was later classified as a subsurface fault by the Ontario Geological Survey (1991). McQuest Marine (1995) reported that four faults, displacing lake-bottom sediments estimated to be about 11,000 years old and bedrock, can be seen in airgun seismic reflection profiles collected across this feature in the vicinity of the intersection of the Hamilton-Presqu'ile lineament with the NPLZ. The interpreted faults are northeast-striking and predominantly north-dipping and have apparent throws of up to 7 m.

Sanford (1995) also interpreted numerous small-displacement northeast-trending fractures affecting the Paleozoic bedrock and post-Paleozoic sediments in this area from sleeve airgun profiles. Lewis et al. (1995) interpreted several small-displacement (0.5 m) normal faults in the same general area of western Lake Ontario. The interpreted faults occur in acoustically stratified sediment also estimated to be about 11 ka, and Lewis et al. (1995) suggest that differential settling of the underlying sediment could be responsible for the features. Lewis et al. (1995) also documented numerous sediment depressions in this area, and the margins of some of these depressions resemble monoclines. These features were attributed to sediment drape into a depression rather than displacement of sediment after deposition, based on continuous and undisturbed reflection data (Lewis et al. 1995). The depressions could not be correlated to deeper sedimentological or bedrock features, which strongly suggests a nontectonic origin (Lewis et al. 1995).

Thomas et al. (1993) noted that the Hamilton-Presqu'ile lineament lies parallel to and just north of the northern margin of the postulated southwest extension of the SLRS as illustrated by Adams and Basham (1989). Thomas et al. (1993) thus interpreted this structure to represent either the northern boundary of the St. Lawrence rift extension or one of a series of faults within a rift zone wider than previously envisaged. It should be noted that, at the intersection of the Hamilton-Presqu'ile lineament with the Niagara-Pickering linear zone, the east-west-trending magnetic lineament associated with the Hamilton-Presqu'ile lineament appears to be truncated by the north-northeast-trending Niagara-Pickering magnetic lineament.

Dineva et al. (2004) relocated hypocenters from earthquakes occurring between 1990 and 2001 that delineate clusters of events beneath Lake Ontario. Their clusters A, B, and C are situated close to the Hamilton-Presqu'ile lineament, but neither the orientation of clusters nor the hypothetical line connecting clusters A and B are parallel to this lineament (Dineva et al. 2004).

Seismogenic Potential: The following list summarises the assessment of the seismogenic potential of the Hamilton-Presqu'ile lineament.

Criterion:	**Probability:**
Association with $M_N \geq 5$ seismicity	0
Association with $2 \leq M_N < 5$ seismicity	0.15
Evidence for reactivation	0.2

Slip favourable w/present stress regime	0.1
Seismogenic crustal extent	0.5
Probability of being seismogenic	**0.08**

Both of the known $M_N \geq 5$ earthquakes in the region occur well over 50 km away from the Hamilton-Presqu'ile lineament. Given that the error in the epicentral locations of these events is less than 50 km, we assign a probability of zero to the Hamilton-Presqu'ile lineament associated with $M_N \geq 5$ seismicity.

Mohajer (1993) reported that at least 10 small-magnitude earthquakes (historical and instrumentally recorded events) are possibly associated with the Hamilton-Presqu'ile lineament. Seven of these earthquakes occur at or near the intersection of the Mississauga magnetic domain seismic zone (described below) and the Hamilton-Presqu'ile lineament, and three of the events can be associated with either feature (Mohajer 1993). Seismicity that could be spatially associated with the Hamilton-Presqu'ile lineament is relatively scattered and does not form an alignment along the feature. A weak cluster occurs near the eastern end of the Hamilton-Presqu'ile lineament, which is proximal to the Wilson–Port Hope lineament and could be associated with either structure. Given the scarcity of events proximal to this feature and the absence of an alignment of seismicity along it, we assign a low probability (0.15) to the Hamilton-Presqu'ile lineament's being associated with small-magnitude seismicity.

There are no data to directly evaluate the downdip geometry and extent of the Hamilton-Presqu'ile lineament. However, based on its mapped length (200 km) and the 40 m of displaced Paleozoic rocks across this feature, a moderate probability (0.5) is assigned to the feature's extending to seismogenic depths.

Evidence for brittle slip in the present stress regime consists of the displaced Paleozoic rocks across the eastern end of the lineament and the interpreted faults on the lake bottom (e.g., McQuest Marine 1995, Sanford 1995). The faults interpreted from seismic reflection data of McQuest Marine (1995) exhibit a downwards decrease in displacement, which suggests they are not tectonic structures. Further, the vertical exaggeration of the cross section is over 60 times, which grossly distorts the actual relief of the reflectors. Sanford (1995) interpreted numerous apparent block faults affecting bedrock and overlying post-Paleozoic sediments along the trend of the Hamilton-Presqu'ile lineament in western Lake Ontario. However, the timing and sense of movement on these structures could not be precisely established (Sanford 1995). Although the northeast orientation of the faults interpreted by McQuest Marine (1995) is considered favourable for reactivation in the present tectonic stress field, their normal sense of displacement is not consistent with northeast-southwest-oriented compression. Furthermore, their apparent downdip decrease in offset strongly suggests a nontectonic origin. The normal sense of displacement of the Paleozoic rocks across the east end of the lineament also is considered inconsistent with regional northeast-oriented compression. The origin, age, and sense of displacement of the features interpreted by Sanford (1995) are questionable; however, their orientations suggest a possible association with the Hamilton-Presqu'ile lineament. Based on the available evidence, we assign a very low probability (0.1) to the Hamilton-Presqu'ile lineament's having evidence of brittle faulting compatible with the present-day regional tectonic stress regime.

McFall and Allam (1991) originally defined this structure on the basis of aeromagnetic data, which implies that it lies within the Grenville basement because the overlying Paleozoic cover has relatively no magnetic signal (McFall 1993). Ordovician rocks displaced 40 m down to the north across the eastern end of the Hamilton-Presqu'ile lineament are considered potential evidence for an episode of reactivation of this structure. Additional evidence of brittle

reactivation of the Hamilton-Presqu'ile lineament consists of the interpreted lake-bottom faults along the trend of the lineament in western Lake Ontario. Sanford (1995) interpreted block faulting of the Ordovician rocks in this area and suggested that some of these faults may have moved in post-Paleozoic time. It is unknown, however, whether these structures are associated with the Hamilton-Presqu'ile lineament. None of the faults interpreted by Sanford (1995) can be shown unequivocally to displace the recent lake-bottom sediments. Based on this information, a low probability (0.2) is assigned to the Hamilton-Presqu'ile lineament's having evidence of multiple episodes of reactivation.

Based on the above assessment, we arrive at a probability of 0.08 that the Hamilton-Presqu'ile lineament is seismogenic.

3.3.7 Clarendon-Linden Fault System

The Clarendon-Linden fault system is a broad zone of small faults with small displacements in the lower Paleozoic bedrock. The fault system is at least 77 km long and 7 – 17 km wide; it is spatially coincident with a north-trending geophysical (combined aeromagnetic and gravity) lineament within the basement rock (Fakundiny and Pomeroy 2002). The fault system may extend for approximately 150 km from just north of the Pennsylvania border (Jacobi and Fountain 1993) to the north shore of Lake Ontario (Hutchinson et al. 1979; see Figure 2.22). Closely spaced, small-offset step faults characterise the Clarendon-Linden fault system in outcrops of Devonian rocks (Jacobi and Fountain 1993, 2002). By integrating surface stratigraphy, structure, soil gas and lineaments, Jacobi and Fountain (2002) could recognise the location of as many as 10 parallel, segmented faults across the fault system in southwestern New York state. The main strand of the Clarendon-Linden fault system is highly segmented, steeply east-dipping in the north and west-dipping in the south, and displays a maximum vertical displacement of about 80 m (Jacobi and Fountain 1993). Cumulative offset across the Clarendon-Linden fault system is as high as ~170 m, based on well log, outcrop, and seismic data (Jacobi and Fountain 2002). Forsyth et al. (1994b) have suggested that the Clarendon-Linden fault system is part of a wider zone of small Paleozoic faults that lie above the crestal area of a northeast-trending Precambrian bedrock high, termed the Iroquoian high. Crone and Wheeler (2000) identify the Clarendon-Linden fault zone in New York as a Class C tectonic feature.

Deep seismic reflection data suggest that the Clarendon-Linden fault system is coincident with structures associated with the Elzevir-Frontenac terrane boundary zone of the Grenville province (Forsyth et al. 1994b). Seismic reflection profiles clearly show the gently east-dipping ductile thrusts of the Elzevir-Frontenac boundary zone extending up to the Precambrian/Paleozoic contact in the region of the Clarendon-Linden fault system (Forsyth et al. 1994, Jacobi and Fountain 2002). The Salmon River fault, which is exposed approximately 30 km north of Lake Ontario, is believed to be the northern extension of the Clarendon-Linden fault system (McFall 1993).

Farther north, the projection of the Clarendon-Linden fault system and Salmon River faults coincide with the Robertson Lake mylonite zone in the Canadian Shield (McFall 1993). The surface continuity of inferred faults constituting the Clarendon-Linden fault system is not strongly supported by the reprocessed seismic data examined by Ouassaa and Forsyth (2002). From this same study it was noted that north- to northeast-trending curvilinear magnetic and gravity anomalies parallel, but are not restricted to, the principal trend of the postulated Clarendon-Linden fault system (Ouassaa and Forsyth 2002).

Dineva et al. (2004) relocate hypocenters from earthquakes occurring between 1990 and 2001 that delineate clusters of events beneath Lake Ontario. They report that their cluster C is parallel to the Clarendon-Linden fault system but shifted slightly to the southeast by about 4 km. During the 1990–2001 recording period for their analysis, Dineva et al. (2004) note that little seismic activity occurred along the Clarendon-Linden fault system, with only two events near the southern end.

A paleoliquefaction study of the Clarendon-Linden fault system was conducted by Tuttle et al. (2002); their investigations indicated a lack of earthquake-induced liquefaction features in geologic units that suggest the fault system did not generate large M >6 earthquakes during the past 12,000 years. Tuttle et al. (2002) conclude that the fault system could have produced small and moderate earthquakes, but probably not large events during the Late Wisconsinan and Holocene.

The Clarendon-Linden fault system probably represents brittle reactivation of a major Grenville structure (Hutchinson et al. 1979, Seeber and Armbruster 1995). The detailed map pattern of the Clarendon-Linden fault system shows that the north-south-trending faults comprise numerous short segments connected by oblique northwest-trending transfer faults, similar to those in rift settings (Jacobi and Fountain 2002). Culotta et al. (1990) have correlated the Clarendon-Linden fault system with a continental-scale magnetic lineament, the Amish anomaly, which extends from New York to Alabama (Culotta et al. 1990). This feature is interpreted as a major Grenville terrane boundary that separates the Elzevir and Frontenac tectonic blocks (Culotta et al. 1990). Wheeler (1995) placed the northwestern boundary of the Iapetan rifted margin along the Clarendon-Linden fault system, which implies it is a potentially seismogenic structure. The probability of this lineament's being seismogenic is 0.25.

Seismogenic Potential: The following list summarises the assessment of the seismogenic potential of the Clarendon-Linden fault system. The individual assessments are described below.

Criterion:	**Probability:**
Association with $M_N \geq 5$ seismicity	0.1
Association with $2 \leq M_N < 5$ seismicity	0.25
Evidence for reactivation	1.0
Slip favourable w/present stress regime	0.1
Seismogenic crustal extent	0.6
Probability of being seismogenic	**0.25**

The Clarendon-Linden fault system is associated with a well-defined cluster of seismicity, which is referred to as the Attica seismic zone (Seeber and Armbruster 1995). This zone contains the 1929 m_b 5.2 Attica earthquake, numerous natural small-magnitude events, and several induced events associated with salt brine recovery at Dale, New York (Fletcher and Sykes 1977). Seeber and Armbruster (1995) suggest it also is possible that the 1929 event may have been artificially triggered, as the brine fields in Dale were already active in 1929. Seismicity appears to be spatially associated and possibly aligned with the gravity gradient that marks the approximate location of the Clarendon-Linden fault system. However, while seismicity does appear to be spatially associated with a segment of the Clarendon-Linden fault system, it does not form an alignment along a significant portion of the structure. Given the observation that the 1929 Attica earthquake occurred within 50 km of the Clarendon-Linden fault system and is the only known $m_b \geq 5$ event in the area, a low

probability (0.1) is assigned to the Clarendon-Linden fault system associated with $m_b \geq 5$ seismicity.

Based on the cluster of small-magnitude seismicity that is spatially associated and partially aligned with a short segment of the Clarendon-Linden fault system, but that does not form a continuous alignment along the length of the feature, a relatively low probability (0.25) is assigned to the Clarendon-Linden fault system's being associated with small-magnitude seismicity.

Deep seismic reflection profiles and geophysical data suggest that the Clarendon-Linden fault system is associated with basement structures that extend to seismogenic depths (Forsyth et al. 1994b; Culotta et al. 1990). Although these basement structures cannot be directly linked to individual Clarendon-Linden faults, the available evidence suggests that a structural linkage between the features is likely. We therefore assign a moderate probability (0.6) to the Clarendon-Linden fault system's extending to seismogenic depths.

There is no clear evidence of brittle slip on the Clarendon-Linden fault system during the present tectonic stress regime. Jacobi and Fountain (1993) report that gas seeps along the southern part of Clarendon-Linden fault system were initiated during or shortly after the 1988 Saguenay (m_{bLg} 6.5) earthquake. The source of the gas seeps was inferred to be Devonian shales at a depth of about 300 m (Jacobi and Fountain 1993). Jacobi and Fountain (1993) suggest that fractures within the fault zone were opened as a local response to the Saguenay event. While the opening of fractures and the emission of deep gases from the Clarendon-Linden fault system suggests recent activity, there is no evidence to suggest that this activity was accompanied by brittle tectonic displacement at depth. There is no evidence of recent tectonic deformation at the ground surface. Based on the foregoing information, a very low probability (0.1) is assigned to the Clarendon-Linden fault system's having evidence of brittle slip in the present-day regional tectonic stress regime.

Well data indicate that the Clarendon-Linden fault system was reactivated twice during the Paleozoic, once in extension and once in compression (Van Tyne 1975). From Early to Middle Ordovician time, the Clarendon-Linden fault system was periodically active as a normal fault while its post-Devonian sense of displacement was reverse (Van Tyne 1975, Jacobi and Fountain 1993). Jacobi and Fountain (2002) have also presented seismic reflection data that indicate multiple periods of Paleozoic reactivation of the Clarendon-Linden fault system. Based on this information, a very high probability (1.0) is assigned to the Clarendon-Linden fault system's having multiple episodes of reactivation.

Based on our assessment, we arrive at the probability of 0.25 that the Clarendon-Linden fault system is seismogenic. Given the additional information described below, however, the probability is updated to 0.40.

Additional Information: Additional information exists regarding the seismogenic potential of the Clarendon-Linden fault zone. Herrmann (1978) reported that focal mechanism studies of two shallow (2 – 3 km) earthquakes in 1966 and 1967 in the Attica area suggested that seismicity occurs along approximately north-northeast-trending Clarendon-Linden faults. The 1966 event (m_b = 4.6) yielded solutions with one nodal plane striking north-northeast and dipping steeply to the east, and a second striking west-northwest and dipping steeply to the south. If the north-northeast solution is accepted, then the fault motion was primarily right-lateral strike-slip with a reverse component. The 1967 event (m_b = 4.4) yielded solutions with one nodal plane striking north-northeast and dipping steeply to the east, and a second west-northwest-striking plane dipping moderately to the south. Again, accepting the

north-northeast solution indicates right-lateral and reverse slip on the fault. Herrmann (1978) selected the north-northeast nodal plane as the most likely fault plane solution, in light of the well log data (Van Tyne 1975) indicating north-northeast-trending Clarendon-Linden faults. He noted, however, that the west-northwest trend could not be totally discounted.

The focal mechanisms derived from these two events yield solutions that are consistent with the geometry (both strike and dip) of the Clarendon-Linden faults as determined from both geologic and seismic data. We judge that it is twice as likely that a consistent focal mechanism will be observed for a given seismogenic feature than for a given nonseismogenic feature (relative likelihood 2:1).

Considering this additional information and using Equation (3.2), the probability that the Clarendon-Linden fault system is seismogenic is updated from 0.25 to 0.40.

3.3.8 Mississauga Magnetic Domain Seismic Zone

This local source zone is named after the Mississauga domain identified by O'Dowd et al. (2004) on the basis of magnetic anomalies expressed in the subsurface of western Lake Ontario (see Figure 2.15). The source corresponds with the southern part of a major lithotectonic domain defined within the Precambrian basement rocks by Easton and Carter (1995) and named the Fishog domain (see Figure 2.12).

The Mississauga magnetic domain source is approximately coincident with magnetic lineaments described by Thomas et al. (1993) and Mohajer (1993). Thomas et al. (1993) identified a magnetic lineament extending for at least 65 km from Burlington to Toronto, offshore of and parallel to the northeast-trending coastline of western Lake Ontario (see Figure 2.22). This lineament, known as the Burlington-Toronto magnetic lineament (Thomas et al. 1993), and a parallel magnetic lineament to the west together form a 20 km wide zone termed by Mohajer (1993) as the Toronto-Hamilton seismic zone. Mohajer (1993) reported that more than 80 percent of the best-located earthquakes in the western Lake Ontario region are confined to the Toronto-Hamilton seismic zone. Thomas et al. (1993) interpreted anomalous lake-bottom features (i.e., dark linear patterns and plumose structures) and bedrock pop-ups observed in the vicinity of the Burlington-Toronto magnetic lineament as evidence of neotectonic activity.

Mereu et al. (2002) report that in the western Lake Ontario area, the earthquake pattern from the Southern Ontario Seismic Network is significantly different from the past earthquake patterns obtained when the instrument coverage was poor. The new, post-1991 pattern indicates that most of the events are confined to the lake or just to the southeast of the lake. The investigators believe that water may be playing a major role in the cause of seismicity in the region, perhaps related to water flows along fissures below the lake.

Dineva et al. (2004) relocate hypocenters from earthquakes occurring between 1990 and 2001 that delineate clusters of events beneath Lake Ontario. The correlation of these events to linear trends in magnetic data or linear physiographic features indicates that these events are offset to the southeast by about 7 – 8 km (cluster A) or 30 km (cluster B) from the Toronto-Hamilton seismic zone of Mohajer (1993).

Seismogenic Potential: The following list summarises the assessment of whether the Mississauga magnetic domain seismic zone is seismogenic. The individual assessments are described below.

Criterion:	**Probability:**
Association with $M_N \geq 5$ seismicity	0
Association with $2 \leq M_N < 5$ seismicity	0.3
Seismogenic crustal extent	0.9
Slip favourable w/present stress regime	0.1
Evidence for reactivation	0.4
Probability of being seismogenic	**0.16**

The only known historical $M_N > 5$ earthquakes in the region are the 1929 m_b 5.2 Attica, New York, event and the 1986 m_{bLg} 5 Leroy, Ohio, event. The 1857 **M** ~ 5 Lockport, New York, event also occurs in the region; however, there is uncertainty as to both its epicentral location and magnitude. Seeber and Armbruster (1993) recently relocated the 1857 event southwest of Buffalo, along the south shore of Lake Erie. Previous interpretations placed this event near Lockport, in upper New York state. In addition to its relocated epicenter, Seeber and Armbruster (1993) revised the magnitude of the Lockport event to **M** 4.

The locations of both the Leroy and Attica earthquakes are well constrained, and the error in their epicentral locations is less than 50 km (Seeber and Armbruster 1993). Both events occur well over 50 km away from the Mississauga magnetic domain seismic zone, and therefore a probability of zero is assigned to the Mississauga magnetic domain seismic zone associated with $M_N > 5$ seismicity.

There is a concentration of small-magnitude seismicity in the western Lake Ontario region relative to the surrounding areas. The depth distribution of instrumentally recorded earthquakes in this region indicates that more than half of the events are located at depths of 5 – 20 km (Mohajer 1993). Mohajer (1993) reports that 8 of the best instrumentally located earthquakes in this region are spatially associated with the Burlington-Toronto magnetic lineament, and that at least 13 earthquakes are spatially associated with the lineament that defines the western boundary of the zone. However, three of the events associated with the Burlington-Toronto magnetic lineament are just as likely to be associated with the Hamilton-Presqu'ile fault, which intersects the zone to the south (Mohajer 1993). Earthquakes within the Mississauga magnetic domain seismic zone form small clusters that lie partially on and adjacent to the mapped traces of the zone-bounding lineaments. Seismicity within the south-central part of the zone appears to trend north-south, oblique to the northeast trend of the zone. The Southern Ontario Seismic Network (Mereu et al. 1996) has recorded nine events ($m_b > 1$) within the southern part of the zone since the network began operation in 1991. A number of these events form a northeast-trending alignment that lies within and approximately parallel to the southern part of the Mississauga magnetic domain seismic zone.

As discussed in Section 2.2, improved station coverage has resulted in a concentration of epicenters in a 32 km trend of seismicity near the Hamilton area (Asmis et al. 2001). O'Dowd et al. (2004) have suggested that this cluster of earthquakes in western Lake Ontario appear to be aligned parallel to the east-northeast-trending magnetic anomalies that characterise the surrounding rock, and they propose a revised location for the CMBBZ that trends parallel to and west of the shoreline of Lake Ontario, instead of across western Lake Ontario, as was previously interpreted by some. Despite the potential viability of this interpretation, small-magnitude seismicity is found in the vicinity of the Mississauga magnetic domain seismic zone and must be included in the assessment of its seismogenic potential.

Given the concentration of small-magnitude seismicity in this region, and the partial alignment of seismicity along the south-central part of the Mississauga magnetic domain seismic zone,

we assign low-to-moderate probability (0.3) to the Mississauga magnetic domain seismic zone's being associated with small-magnitude seismicity. Mohajer (1993) has also recorded small-magnitude seismicity in the area.

It is unknown whether the Mississauga magnetic domain seismic zone is correlative to a structure at depth. Deep seismic data collected in Lake Ontario (e.g., Forsyth et al. 1994a) did not cross this feature. Eyles et al. (1993) suggest that the zone coincides with the Fishog-Cambridge terrane boundary within the Grenville basement, though Carter and Easton (1990) interpret this boundary to lie considerably west of Lake Ontario. Instrumentally recorded seismicity within the Toronto-Hamilton seismic zone does extend to a depth of about 20 km (Mohajer 1993). Given the prominent magnetic signature of the feature and the deep extent of the seismicity, a very high probability (0.9) is assigned the Mississauga magnetic domain seismic zone's extending to seismogenic depths.

There is no clear geologic evidence for brittle tectonic faulting within the Mississauga magnetic domain seismic zone in the present tectonic stress regime. Although west-northwest-trending pop-up structures in the vicinity of the Burlington-Toronto magnetic lineament indicate buckling of strata on the bedrock surface consistent with the contemporary northeast-oriented horizontal compressive stress, these features are not considered to be spatially or structurally associated with the Mississauga magnetic domain seismic zone. Lewis et al. (1995) have shown that these features are widely distributed on the flanks of the Lake Ontario basin and are spatially unrelated to the Burlington-Toronto magnetic lineament and the various other geophysical lineaments beneath the lake. Thomas et al. (1993) also observed plumose structures and dark linear features on the bottom of western Lake Ontario and interpreted these features as indicators of neotectonic activity. They suggested that the plumose structures represent the surface expression of fracture or fault propagation, and that the dark linear patterns result from structurally controlled gas injections into the lake-bottom sediments (Thomas et al. 1993). While processes of this type could indicate the presence of open joints or fractures in the underlying bedrock, they would not necessarily imply recent brittle tectonic faulting. Lewis et al. (1995) have reported that the distribution and character of both the linear patterns and plumose structures do not fully support tectonic origins for the features. Furthermore, Lewis et al. (1995) have suggested anthropogenic origins for both sets of features, namely, the plumose structures represent anchor drag marks, and the dark linear patterns may represent steamship ash debris trains. Considering the lack of clear evidence for brittle tectonic faulting within the Mississauga magnetic domain seismic zone, we assign a very low probability (0.1) to this criterion.

No direct data can be used to assess whether multiple episodes of brittle reactivation occurred in the Mississauga magnetic domain seismic zone. However, the zone appears to be coincident with a major terrane boundary, and, based on other studies it is judged that such boundaries can be associated with multiple episodes of reactivation. Therefore, we assign a moderate probability of 0.4 to reflect this judgment.

Based on our assessment, we arrive at the probability of 0.16 that the Mississauga magnetic domain seismic zone is seismogenic (See Section 3.2.1 for calculation procedure).

3.4 Seismicity Parameter Characterization for Seismic Sources

The approaches used to model the seismicity parameters are discussed below. The parameters necessary are the maximum magnitude of earthquakes that can occur associated with each source and the parameters that define the rate of occurrence and size distribution of future earthquakes.

3.4.1 Maximum Magnitude

The primary approach used for assessing the maximum magnitude for a seismic source is the Bayesian approach developed by Johnston et al. (1994). The process is illustrated on Figure 3.5. With this approach, a prior distribution for maximum magnitude is specified based on regional knowledge. The prior distribution is then updated with a likelihood function for various maximum-magnitude values that is based on the catalogue of earthquakes that have occurred in the seismic source. The resulting posterior distribution is then discretised for use in a logic tree format.

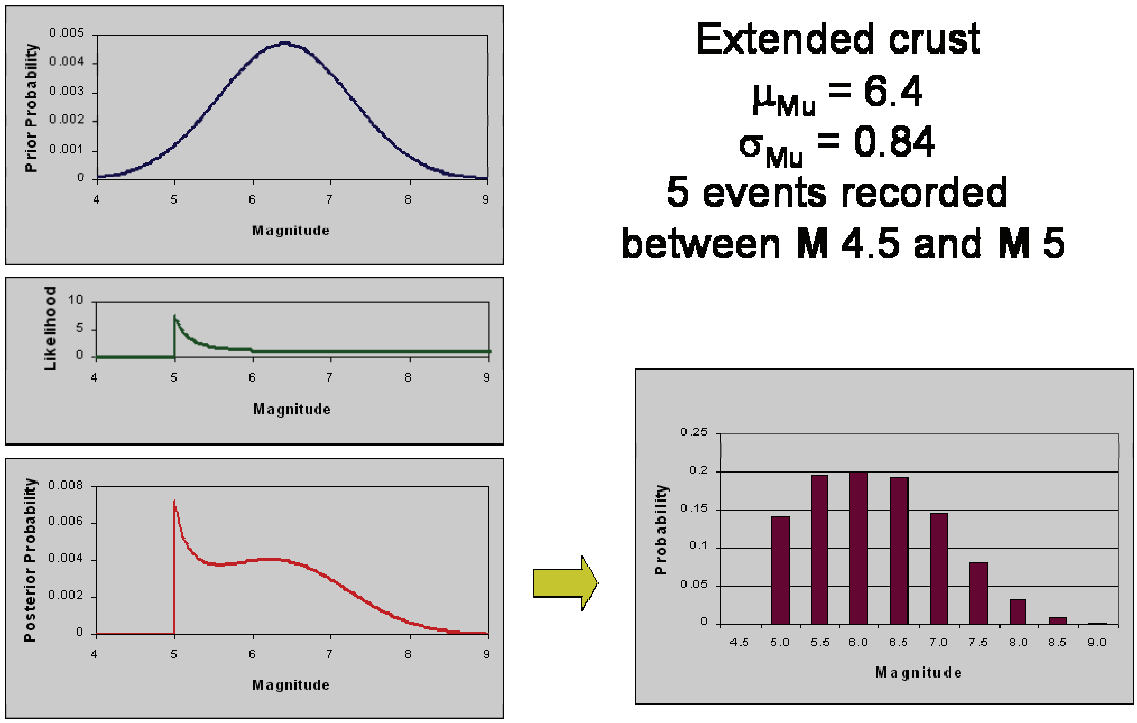

Figure 3.5: Illustration of the Bayesian Approach for Assessment of Maximum Magnitude

The likelihood function for maximum magnitude is derived from the form of the magnitude distribution used. The likelihood function is based on the premise that the maximum possible earthquake must be equal to or larger than the maximum size that has already been observed. For the truncated exponential distribution used in this study, the likelihood function for the upper-limit magnitude, m^u, is:

$$L[m^u] = \begin{cases} 0 & \text{for } m^u < m_{\max}^{observed} \\ \left[1 - \exp\left\{-b\ln(10)(m^u - m_0)\right\}\right]^{-N} & \text{for } m^u \geq m_{\max}^{observed} \end{cases} \quad (3.3)$$

where b is the Gutenberg-Richter b-value and N is the number of recorded earthquakes with magnitudes larger than a minimum value m_0, and $m_{\max}^{observed}$ is the largest recorded earthquake. Figure 3.5 shows an example of this likelihood function. The function has a small peak near

the maximum observed and then is very flat, indicating that the likelihood is nearly the same for a large range of values of m^u.

Johnston et al. (1994) developed prior distributions for maximum magnitude from a study of large earthquakes in stable continental regions (SCR). The study led to the development of a worldwide database of large SCR earthquakes. The SCR crust was subdivided into domains on the basis of crustal characteristics (e.g., age, type of crust, stress state, and tectonic history). By pooling like domains, the investigators were able to obtain sufficient numbers of earthquakes within each "super" domain such that estimates of the maximum magnitude for each domain type could be made. From these data, Johnston et al. (1994) developed two types of general prior distributions for m^u. Their first approach is based on a simple division of the SCR into extended and non-extended crust. The statistics of the values of m^u for the super (pooled) domains in each group were used to define a normal distribution for m^u. Their second approach was to develop a regression model relating m^u to the characteristics of the super domains. However, the regression model did not provide much predictive improvement over the simple statistics. Therefore, only the prior distributions based on the categories of extended crust and non-extended crust were used to develop maximum magnitude distributions for this study.

An additional approach was used in this study to assess maximum magnitudes for the local sources. The maximum dimensions of possible fault ruptures were combined with an empirical relationship relating fault rupture dimensions to earthquake magnitude. Mohajer (1995) provided estimates of rupture length for features in the region, and these were used to derive a distribution for maximum magnitude that is used for the local sources.

3.4.2 Earthquake Occurrence Rates

The frequency of occurrence of earthquakes associated with a source was computed from the statistics of the earthquake catalogue for the source. For source zones, the standard truncated exponential magnitude distribution was used to define the relative frequency of various sizes of earthquakes. This occurrence model contains three parameters: (1) the annual rate for earthquakes above a specified minimum, $N(m_0)$; (2) the Gutenberg-Richter b-value and (3) the maximum magnitude. The parameters $N(m_0)$ and b are estimated from the earthquake counts in the seismic source zone using the maximum likelihood formulation developed by Weichert (1980). In this approach, the input data are the period of complete catalogue reporting and the number of earthquakes for a range of magnitude intervals. As discussed in Section 2.3.4, the catalogue completeness assessment for the study region assessed the probability of detection of earthquakes as a function of time. EPRI (1988) extended the Weichert (1980) approach to incorporate partial catalogue reporting. The process used is to count all of the earthquakes within the usable portion of the catalogue and then define an equivalent period of completeness, T_E, as:

$$T_E(m) = \sum_i T_i \times P_i^D(m) \qquad (3.4)$$

where T_i is the length of the i^{th} time interval and $P_i^D(m)$ is the probability of detection of earthquakes in magnitude interval m in the i^{th} time interval.

EPRI (1988) also extended the Weichert (1980) formulation to include a prior distribution for the b-value. This is useful to stabilise the assessment in regions with limited data.

Once the values of $N(m_0)$ and b are obtained, a range of possible $N(m_0)$ – b pairs are defined based on the uncertainty estimates for the two parameters. The modified Weichert (1980) likelihood function is then used to compute the relative likelihood that the observed catalogue of earthquakes was produced by these $N(m_0)$ – b pairs. These relative likelihoods are then normalised to produce a discrete joint distribution for $N(m_0)$ and b that accounts for the correlation between the two parameters. The process is repeated for each assessed maximum magnitude for the source to include the effect of m^u on the joint $N(m_0)$ – b distribution. Figure 3.6 shows an example of the distribution of earthquake occurrence computed for a source zone. The observed rate of earthquakes for various magnitude intervals and the uncertainty in these values are shown by the solid points and vertical error bars. The discrete set of earthquake occurrence models is shown on the left-hand plot (a), and the resulting distribution for earthquake occurrence rates is shown on the right-hand plot (b).

The zoneless approach (Section 3.2.3) uses a somewhat different approach. Based on the statistics of seismicity across the entire region, 25 bootstrap samples of cell-by-cell seismicity parameters for each are drawn, in essence, 25 maps of a-values and b-values. These 25 sets of parameters are used to characterise the uncertainty in seismicity rates for the entire region. The difference between the two approaches is that in the methodology applied to the zoneless approach, the b-value is allowed to vary within the source, while in the methodology defined in Figure 3.6, the b-value is assumed to be the same throughout the source.

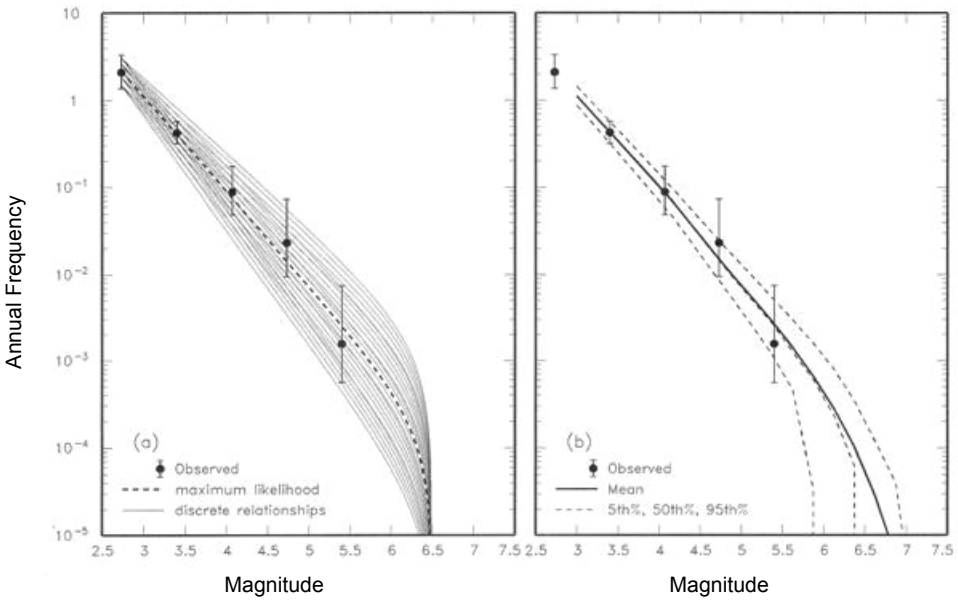

Notes: (a) Discrete occurrence model for a M_{max} of 6.5; (b) Resulting uncertainty distribution for earthquake occurrence frequency, including uncertainty in M_{max}.

Figure 3.6: Uncertainty Assessment for Earthquake Occurrence Frequencies

3.4.3 Seismicity Parameters for Regional Sources

Figure 3.7 shows the logic tree for the geologic/tectonic regions regional source zones defined on Plates 1 through 24. As discussed in Section 2.5.4, two alternative catalogue

completeness models were developed that reflect differences in the weight assigned to the magnitude interval 3.3 ≤ **M*** < 3.9 in fitting the truncated exponential recurrence model to the seismicity data: Model A assigns a weight of 0.1 to this magnitude interval, and Model B assigns a weight of 0.01 (essentially ignoring the data in this interval). These models are given equal weight in fitting the seismicity parameters, as they both produce similar fits to the observed occurrence rates for the larger magnitudes of primary interest in assessing the hazard.

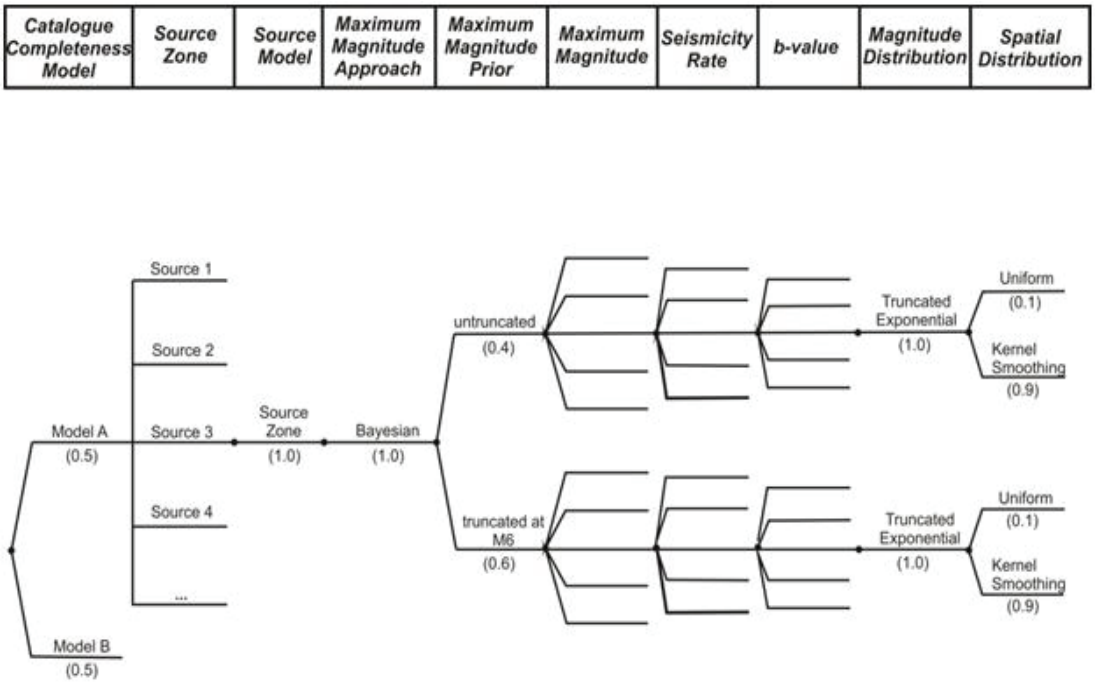

Figure 3.7: Logic Tree for Geology-Based Source Zone Seismicity Parameters

Following this global branch, seismicity parameter assessments are made for each regional source zone. The regional sources are all modeled as source zones: the truncated exponential recurrence model is used to represent the size distribution of earthquakes, and the ruptures of future earthquakes are assumed to have a random orientation.

The Bayesian methodology (Johnston et al. 1994) is used to estimate maximum magnitude, resulting in a distribution for maximum magnitudes such as the one shown on Figure 3.5. Two alternatives for a prior distribution are used. The first is the prior developed by Johnston et al. (1994) based on crustal category, either mean M_{max} **M** 6.3, σ_{Mmax} 0.5 for non-extended crust, or mean M_{max} **M** 6.4, σ_{Mmax} 0.84 for extended crust. The second is the same prior with the lower tail truncated at magnitude **M** 6. The lower tails of the Johnston et al. (1994) prior distributions extend down to $-\infty$. A review of the literature, however, indicates that applying small maximum magnitudes to regional-scale sources does not reflect the current scientific interpretation of the earthquake potential in central and eastern North America. This truncated prior is slightly favoured (0.6) over the untruncated prior. The likelihood function used to update the priors is defined based on the largest observed earthquake in each source zone. Table 3.5 lists the resulting maximum-magnitude distributions.

Table 3.5: Maximum Magnitude Distributions

Source[1]	Prior[2]	Weight on Maximum Magnitude Value:													
		5	5.25	5.5	5.75	6	6.25	6.5	6.75	7	7.25	7.5	7.75	8	8.25
GMH	NE-U		0.034	0.069	0.120	0.170	0.194	0.176	0.125	0.070	0.031	0.011			
	NE-T					0.219	0.250	0.226	0.161	0.090	0.040	0.014			
NGR	NE-U	0.011	0.028	0.063	0.115	0.168	0.195	0.178	0.128	0.072	0.032	0.011			
	NE-T					0.215	0.249	0.227	0.163	0.092	0.040	0.014			
CC-E	NE-U		0.082	0.102	0.136	0.166	0.175	0.151	0.105	0.058	0.025				
	NE-T					0.241	0.254	0.219	0.152	0.084	0.037	0.013			
CC-W	NE-U		0.082	0.102	0.136	0.166	0.175	0.151	0.105	0.058	0.025				
	NE-T					0.241	0.254	0.219	0.152	0.084	0.037	0.013			
CCGR-E	NE-U		0.264	0.149	0.130	0.128	0.119	0.096	0.064	0.035	0.015				
	NE-T					0.277	0.258	0.208	0.139	0.075	0.032	0.011			
CCGR-C	NE-U		0.246	0.147	0.132	0.132	0.124	0.100	0.067	0.036	0.016				
	NE-T					0.274	0.257	0.209	0.140	0.076	0.033	0.011			
CCGR-WA	NE-U		0.182	0.136	0.137	0.146	0.141	0.117	0.079	0.043	0.019				
	NE-T					0.264	0.256	0.212	0.144	0.078	0.034	0.012			
CCGR-WB	NE-U		0.181	0.136	0.137	0.146	0.142	0.117	0.079	0.043	0.019				
	NE-T					0.264	0.256	0.212	0.144	0.078	0.034	0.012			
SGR-EE	NE-U	0.019	0.060	0.088	0.129	0.166	0.180	0.158	0.111	0.062	0.027				
	NE-T					0.233	0.252	0.222	0.156	0.086	0.038	0.013			
SGR-CE	NE-U	0.019	0.060	0.088	0.129	0.166	0.180	0.158	0.111	0.062	0.027				
	NE-T					0.233	0.252	0.222	0.156	0.086	0.038	0.013			
SGR-WAE	NE-U	0.011	0.045	0.078	0.125	0.170	0.189	0.168	0.119	0.067	0.029				
	NE-T					0.226	0.251	0.224	0.159	0.089	0.039	0.013			
SGR-WBE	NE-U	0.011	0.045	0.078	0.125	0.170	0.189	0.168	0.119	0.067	0.029				
	NE-T					0.226	0.251	0.224	0.159	0.089	0.039	0.013			
SGR-EW	NE-U	0.019	0.060	0.088	0.129	0.166	0.180	0.158	0.111	0.062	0.027				
	NE-T					0.233	0.252	0.222	0.156	0.086	0.038	0.013			
SGR-CW	NE-U	0.019	0.060	0.088	0.129	0.166	0.180	0.158	0.111	0.062	0.027				
	NE-T					0.233	0.252	0.222	0.156	0.086	0.038	0.013			
SGR-WAW	NE-U	0.011	0.045	0.078	0.125	0.170	0.189	0.168	0.119	0.067	0.029				
	NE-T					0.226	0.251	0.224	0.159	0.089	0.039	0.013			
SGR-WBW	NE-U	0.011	0.045	0.078	0.125	0.170	0.189	0.168	0.119	0.067	0.029				
	NE-T					0.226	0.251	0.224	0.159	0.089	0.039	0.013			

Table 3.5: Maximum Magnitude Distributions

Source[1]	Prior[2]	Weight on Maximum Magnitude Value:													
		5	5.25	5.5	5.75	6	6.25	6.5	6.75	7	7.25	7.5	7.75	8	8.25
NAZ	E-U				0.149	0.183	0.155	0.135	0.115	0.093	0.070	0.049	0.032	0.019	
	E-T					0.213	0.180	0.157	0.134	0.108	0.082	0.057	0.037	0.022	0.011
ECC	E-U						0.064	0.242	0.206	0.167	0.126	0.088	0.057	0.033	0.018
	E-T						0.064	0.242	0.206	0.167	0.126	0.088	0.057	0.033	0.018
SLR	E-U										0.195	0.385	0.227	0.128	0.065
	E-T										0.195	0.385	0.227	0.128	0.065
IRM-E	E-U	0.150	0.128	0.097	0.092	0.092	0.092	0.087	0.078	0.065	0.049	0.035	0.022	0.013	
	E-T					0.170	0.170	0.161	0.144	0.120	0.091	0.064	0.042	0.025	0.013
IRM-C	E-U	0.150	0.128	0.097	0.092	0.092	0.092	0.087	0.078	0.065	0.049	0.035	0.022	0.013	
	E-T					0.170	0.170	0.161	0.144	0.120	0.091	0.064	0.042	0.025	0.013
IRM-WA	E-U	0.235	0.153	0.096	0.082	0.078	0.076	0.071	0.063	0.052	0.039	0.028	0.018	0.011	
	E-T					0.177	0.172	0.161	0.142	0.118	0.090	0.063	0.041	0.024	0.013
IRM-WB	E-U	0.235	0.153	0.096	0.082	0.078	0.076	0.071	0.063	0.052	0.039	0.028	0.018	0.011	
	E-T					0.177	0.172	0.161	0.142	0.118	0.090	0.063	0.041	0.024	0.013
SLIRM-E	E-U										0.194	0.385	0.227	0.128	0.066
	E-T										0.194	0.385	0.227	0.128	0.066
SLIRM-C	E-U										0.194	0.384	0.227	0.128	0.066
	E-T										0.194	0.384	0.227	0.128	0.066
SLIRMWA	E-U										0.194	0.384	0.227	0.128	0.066
	E-T										0.194	0.384	0.227	0.128	0.066
SLIRMWB	E-U										0.194	0.384	0.227	0.128	0.066
	E-T										0.194	0.384	0.227	0.128	0.066
OBGHI	NE-U		0.024	0.059	0.113	0.170	0.200	0.184	0.132	0.075	0.033	0.011			
	NE-T					0.211	0.248	0.228	0.164	0.093	0.041	0.014			
GSC-M	E-U						0.076	0.266	0.206	0.159	0.117	0.080	0.051	0.030	0.016
	E-T						0.076	0.266	0.206	0.159	0.117	0.080	0.051	0.030	0.016
GSC-SL	E-U									0.100	0.243	0.319	0.184	0.102	0.052
	E-T									0.100	0.243	0.319	0.184	0.102	0.052
GSC-Background	NE-U		0.040	0.074	0.123	0.170	0.191	0.171	0.122	0.068	0.030	0.010			
	NE-T					0.223	0.251	0.225	0.160	0.089	0.039	0.014			
Zoneless	E-U									0.102	0.242	0.316	0.183	0.103	0.053
	E-T									0.102	0.242	0.316	0.183	0.103	0.053

Table 3.5: Maximum Magnitude Distributions

Source[1]	Prior[2]	Weight on Maximum Magnitude Value:													
		5	**5.25**	**5.5**	**5.75**	**6**	**6.25**	**6.5**	**6.75**	**7**	**7.25**	**7.5**	**7.75**	**8**	**8.25**
Local Sources as Zones	NE-U		0.024	0.059	0.113	0.170	0.200	0.184	0.132	0.075	0.033	0.011			
	NE-T					0.211	0.248	0.228	0.164	0.093	0.041	0.014			
Local Sources as Faults	Not Used	Magnitude		6.7	7.0	7.2	7.3	7.5							
		Weight		0.2	0.2	0.1	0.3	0.2							

Notes:
1. Source designations are indicated on Plates 1 through 26.
2. NE-U: Non-extended, untruncated; NE-T: Non-extended, truncated at **M** 6; E-U: Extended, untruncated; E-T: Extended, truncated at **M** 6.

The approach illustrated on Figure 3.6 is used to define the distributions of seismicity parameters for the zone, and a truncated exponential magnitude distribution is used. The joint distribution of seismicity parameters is defined by 25 pairs of a-values and b-values.

Two alternative spatial density models for the variation in a-value are used: a uniform spatial density and a kernel density estimate. The kernel density estimate is strongly preferred (0.9) to the uniform model (0.1) because most of the zones exhibit evidence of clustering of the seismicity. A Gaussian kernel was used to model the spatial distribution. Selection of the kernel-size parameter h controls the balance between accurately portraying the areas of high seismicity without introducing areas of unrealistically low seismicity in areas of sparse seismicity. The need to balance these two objectives arises in part from the use of a fixed kernel size in all parts of the region. Stock and Smith (2002) recommend that an improved approach is to use adaptive kernel smoothing (Silverman 1986), in which the kernel size is adjusted throughout the study region, decreasing in size in areas of higher data (earthquake) density and increasing in size in areas of lower data density. The starting value was selected by computing the optimum kernel size from the data (Silverman 1986). These values ranged from 12 to 65 km for earthquakes larger than **M*** 3.3.

Figure 3.8 shows the logic tree for the seismicity-based source zones shown on Plate 25. There are two differences between the logic tree and the model for the geology-based source zones. The first is that the likelihood distribution for updating the maximum-magnitude prior distribution is based on the largest observed earthquakes in groups of seismic sources, rather than in each individual source. Grouping was used because the area of the majority of the individual sources is much smaller than the geologic domains used by Johnston et al. (1994) to create the prior distributions. The groupings were based on the location of the sources: St. Lawrence rift system sources, St. Lawrence margin sources, southern Ontario background region, and the southeastern Canada background region. These maximum magnitude distributions are listed in Table 3.5. The second difference is that a uniform spatial density is the only model used for these sources. The sources were defined in part on the basis of differences in seismicity rate, and use of a uniform spatial distribution maintains that distinction.

Figure 3.9 shows the logic tree for the zoneless approach. The region is assumed to have the characteristics of a single source zone, and the Bayesian approach is used to assess the maximum magnitude. Seismicity parameters are estimated globally for all cells of one degree

longitude and latitude. Twenty-five sets of cell-by-cell a-values and b-values are simulated from the statistics of the regional fit to the data.

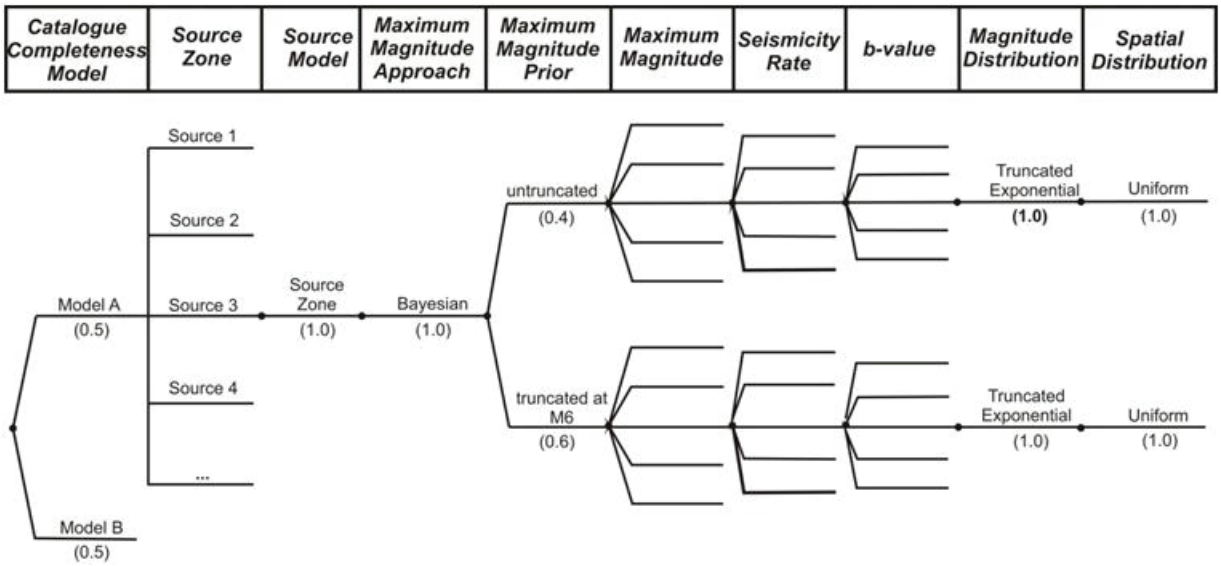

Figure 3.8: Logic Tree for Seismicity-Based Source Zone Seismicity Parameters

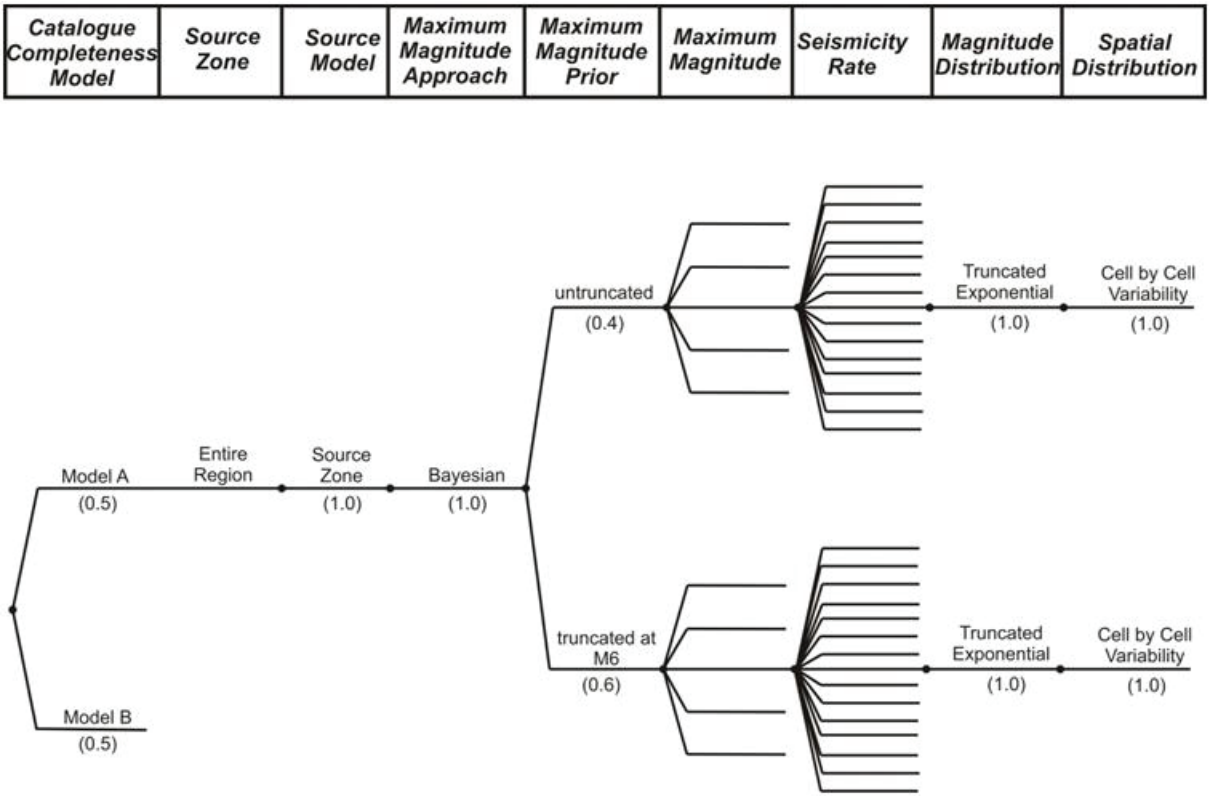

Figure 3.9: Logic Tree for Zoneless Approach Seismicity Parameters

3.4.4 Seismicity Parameters for Local Sources

Figure 3.10 shows the logic tree that is used to characterise the seismicity parameter assessments for the local sources (Plates 27 and 28). The logic tree again begins with the global choice of catalogue completeness models. The individual local sources are then characterized.

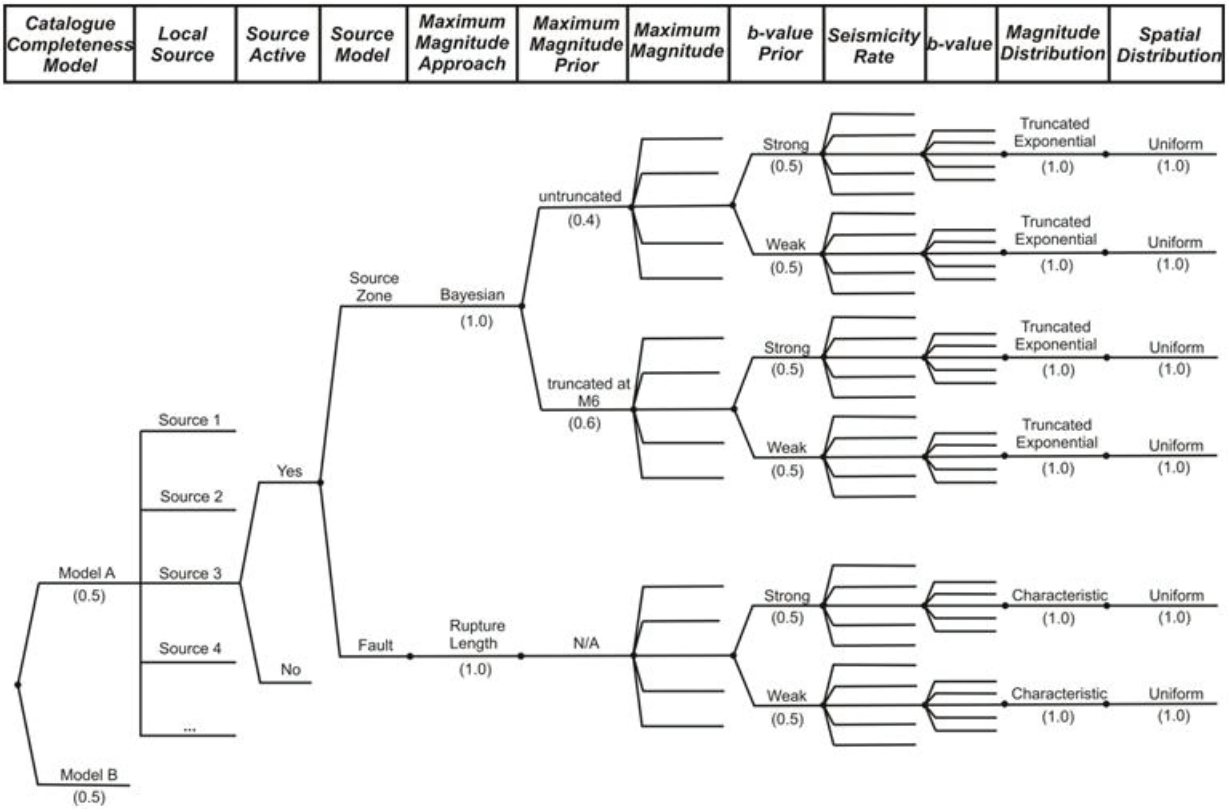

Figure 3.10: Logic Tree for Local Source Seismicity Parameters

The first assessment for a local source is whether or not it is active. These assessments are described above in Section 3.3. The next assessment is whether to consider it a concentrator of seismicity, and thus have the characteristics of a zone, or whether to consider it a through-going fault. The weight assigned to the concentrator (zone) model versus the through-going fault model is dependent on the local source's being considered. The GBLZ and the Mississauga seismic zone appear to have no single fault-like feature, and the zone model is strongly favoured (0.95) over that of the through-going fault model (0.05). At the other end of the spectrum, the Clarendon-Linden fault system has been identified as a fault system, and the through-going fault model is favoured (0.8) for this local source over the zone model (0.2). The Grenville Front zone, the Niagara-Pickering linear zone, the Hamilton-Presqu'ile fault, and the Wilson–Port Hope lineament do not display clear evidence of behaviour as through-going faults in the present tectonic regime, and the zone model is favoured (0.8) over the fault model (0.2) for these sources.

If the local source is considered a zone, then the Bayesian approach for maximum magnitude applied to the regional zone in which the local source lies is used to define the maximum magnitude distribution. The likelihood function used to update the maximum magnitude distribution is based on the largest observed earthquake in the southern Ontario background source region shown on Plate 25. The maximum magnitude distribution is listed in Table 3.5. The seismicity parameters are determined using the approach illustrated on Figure 3.6, and the truncated exponential magnitude distribution is used. If the local source is considered a through-going fault, then rupture dimensions are used to assess the maximum magnitude. The values derived from the assessments of rupture length given by Mohajer (1995) are listed in Table 3.5. The seismicity rate parameters are assessed in the same way as when the source is considered a zone, except that the characteristic magnitude distribution is assumed to apply. This distribution is shown on Figure 3.11.

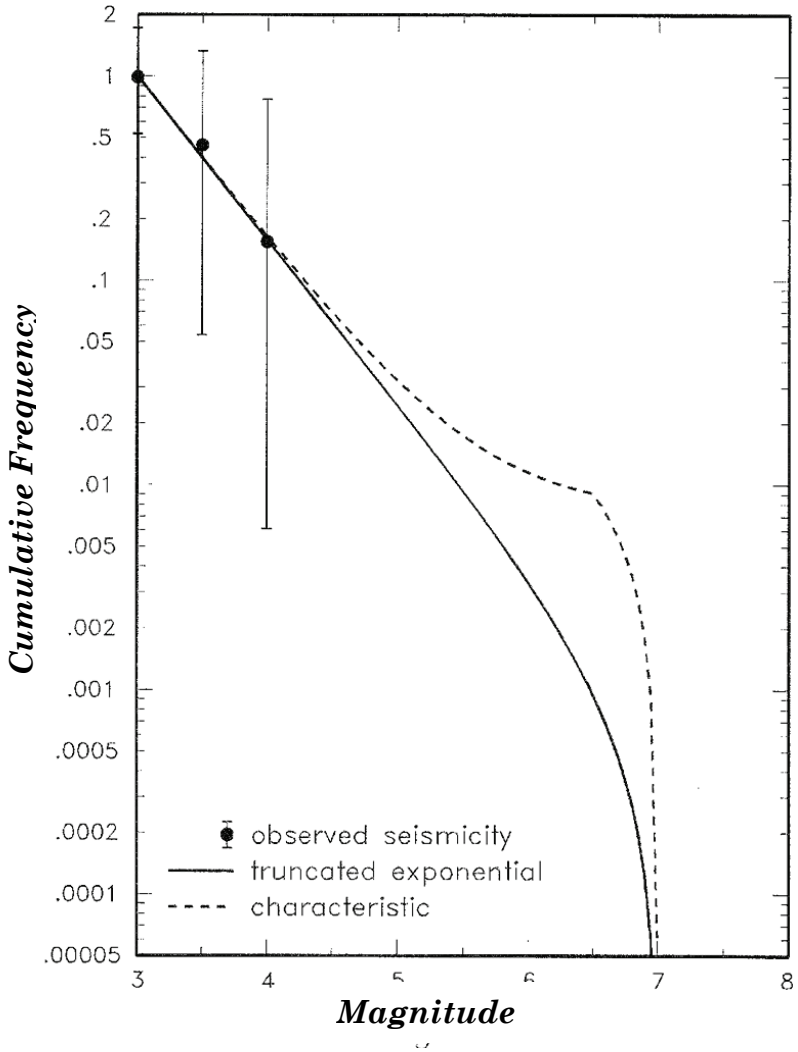

Figure 3.11: Magnitude Distribution Models Fit to Observed Seismicity

The seismicity data associated with any single local source is unlikely to provide a tight constraint on the b-value. Therefore, a prior value is set equal to the value for the region source zone and a penalised maximum likelihood technique is used to fit the data (EPRI 1988). Two options are considered for the penalty (weight) assigned to the prior. A strong prior produces a b-value very similar to the regional value with a similar degree of uncertainty. A weak prior allows greater variation from the regional b-value and results in greater uncertainty in the b-value for the local source. These two options are given equal weight in the hazard model. The spatial distribution of seismicity is assumed to be uniform along the length of the local source.

The assessment of earthquake occurrence rates is based on the observed rate of earthquakes obtained from the earthquake catalogue. Following the approach used in Geomatrix (1997a, b), the number of earthquakes assigned to each local source is obtained by collecting events that have occurred within 25 km of the source. To avoid double counting of earthquakes in the assessments of regional and local sources, the events assigned to the local sources were removed from the catalogue used for calculating the seismicity parameters for the regional sources. Specifically, the probability that an earthquake is assigned to a local source, assuming that it occurs within 25 km of the source, is set equal to the probability that the source is seismogenic. One minus this probability is then the probability that the earthquake should be counted in the statistics for the regional sources.

3.4.5 Depth Distribution of Earthquakes

The ground motion models used to assess the seismic hazard (see Section 4) use two measures of source-to-site distance: surface distance and rupture distance. For the rupture distance measure, the depth of earthquake ruptures is needed. Dineva et al. (2004) and Ma and Atkinson (2006) provide data on the focal depths of earthquakes in the region. Ma and Atkinson (2006) divided the data into events occurring north and south of latitude 45º N, with the northern data set showing somewhat deeper depths. The depth distribution data from Dineva et al. (2004) are very similar to the southern data set of Ma and Atkinson (2006), as shown on the left-hand plot of Figure 3.12. The right-hand plot of Figure 3.12 shows the smoothed depth distributions developed from the published data. These distributions represent the aleatory variability of the focal depth of future earthquakes. Rupture areas are assumed to be centered on the focal depth for the purpose of computing rupture distance.

3.4.6 Comparison of Observed and Predicted Seismicity Rates

Figure 3.13, Figure 3.14, Figure 3.15 and Figure 3.16 compare the observed and predicted seismicity rates within 100, 200, 300 and 500 km of the Bruce nuclear site, respectively. At all distances, the seismic hazard model provides a reasonably good representation of the observed seismicity rates. The uncertainty in the predicted rates is highest in the vicinity of the site where the observed rate of earthquakes is low. The larger uncertainty is due to the limited data sample, as few earthquakes have been recorded within 100 and 200 km of the site.

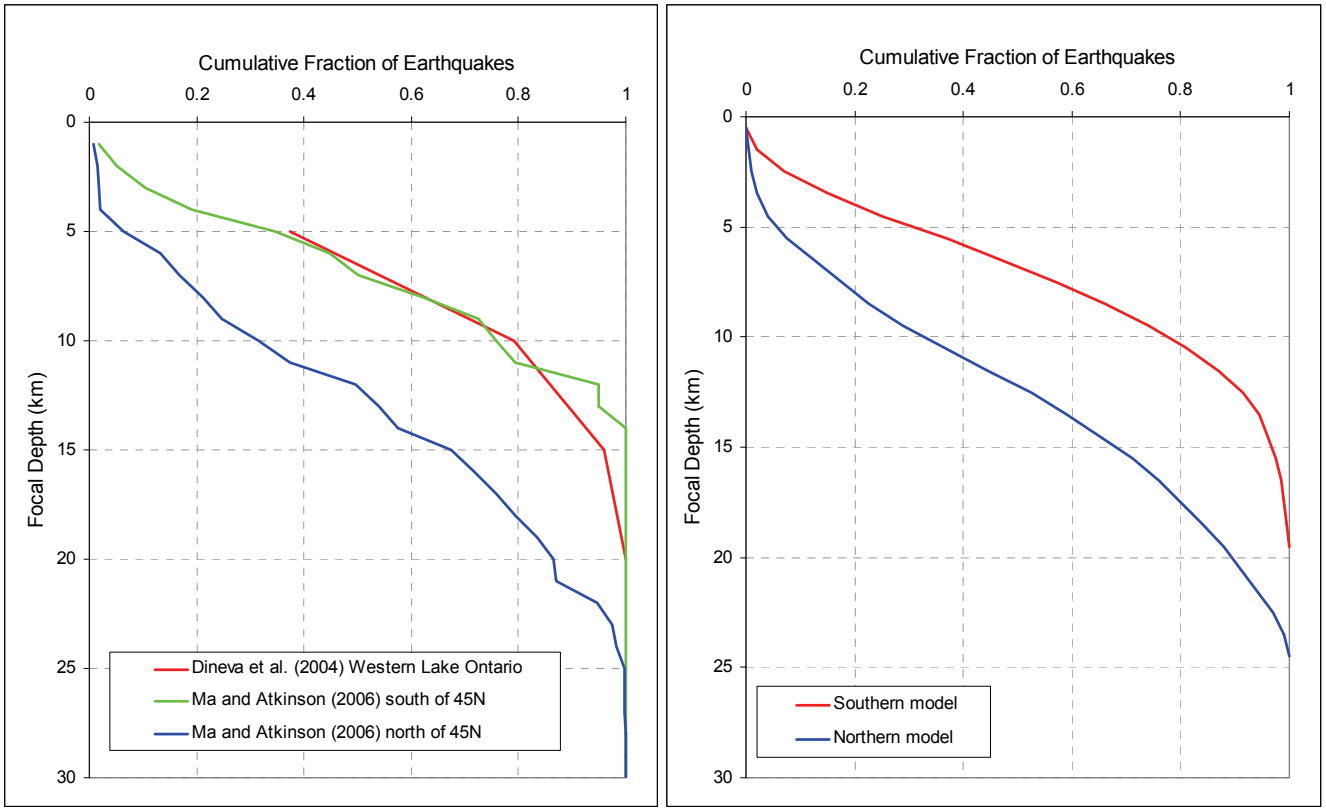

Notes: Left side shows distributions taken from Ma and Atkinson (2006). Right side shows smoothed distributions used in the PSHA model.

Figure 3.12: Focal Depth Distributions Used in the PSHA Model

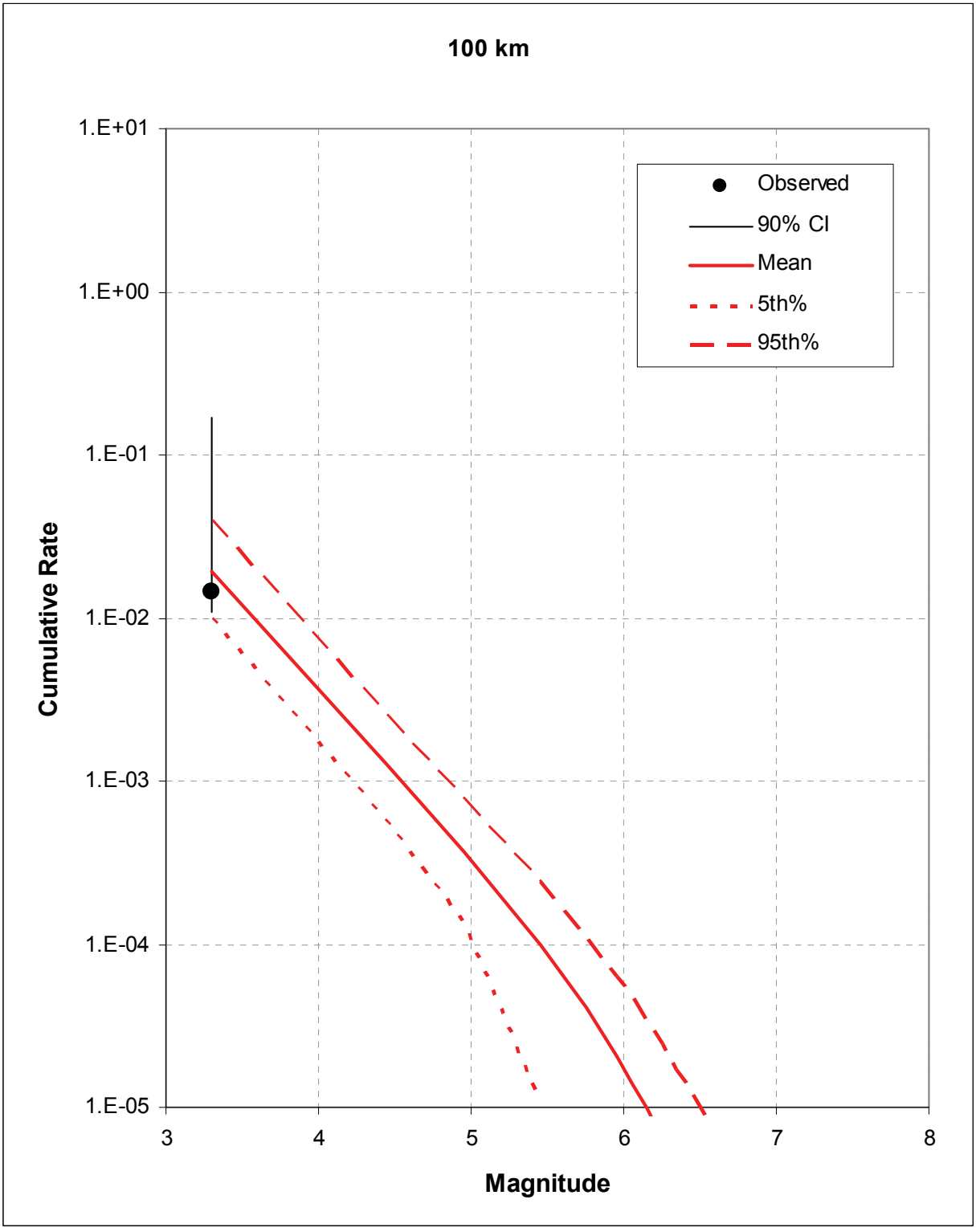

Figure 3.13: Comparison of Observed and Predicted Seismicity Rates within 100 km of the Bruce Nuclear Site

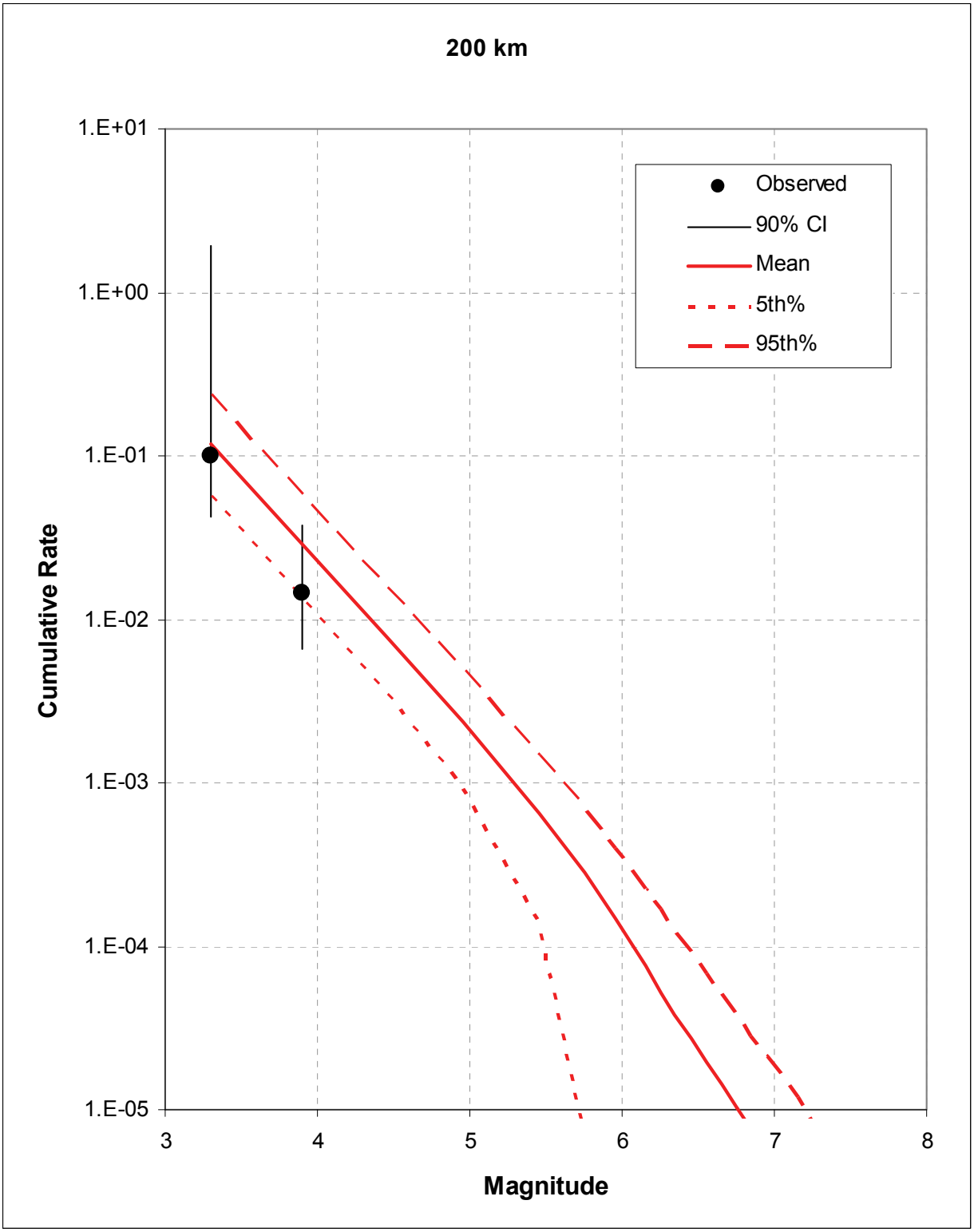

Figure 3.14: Comparison of Observed and Predicted Seismicity Rates within 200 km of the Bruce Nuclear Site

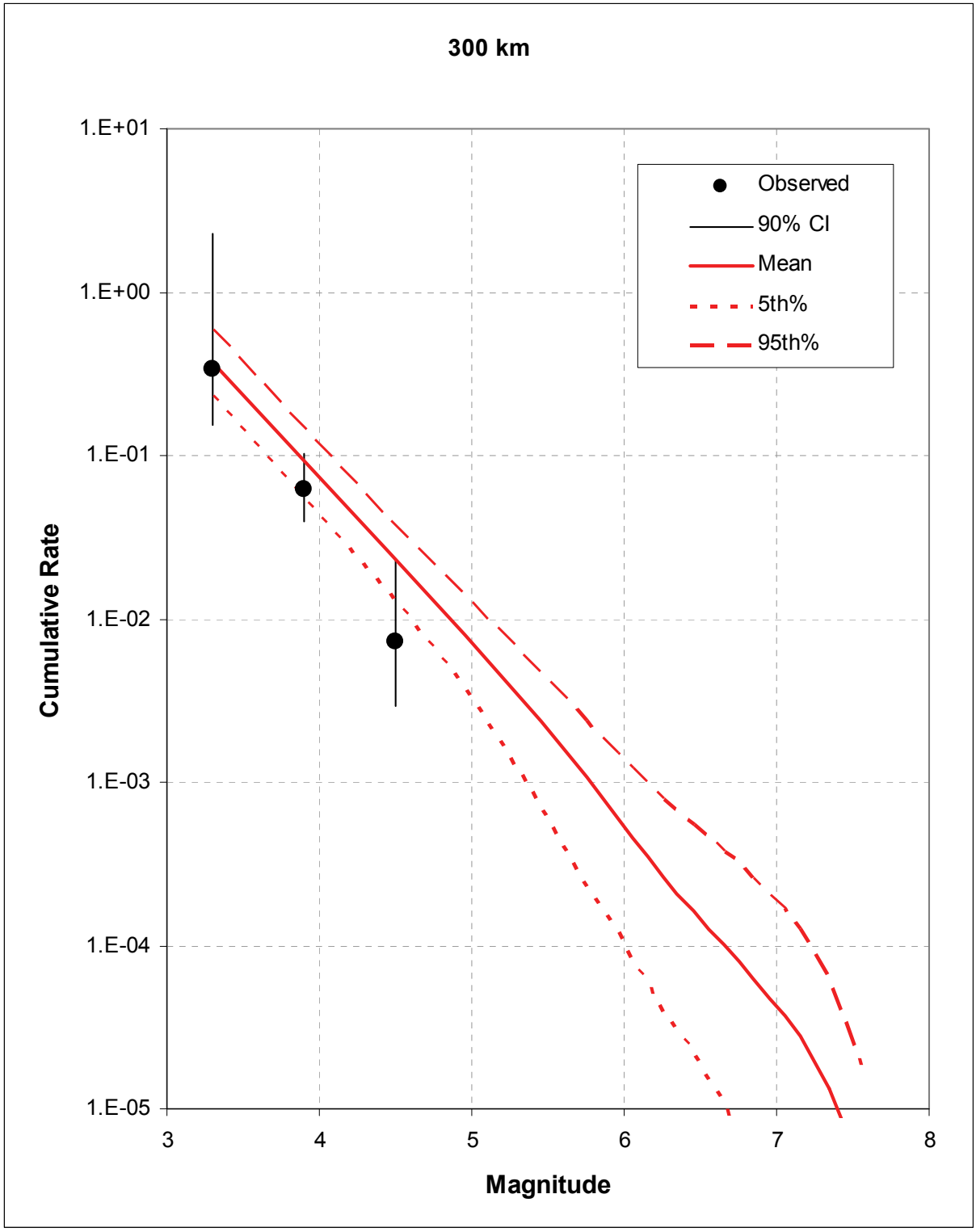

Figure 3.15: Comparison of Observed and Predicted Seismicity Rates within 300 km of the Bruce Nuclear Site

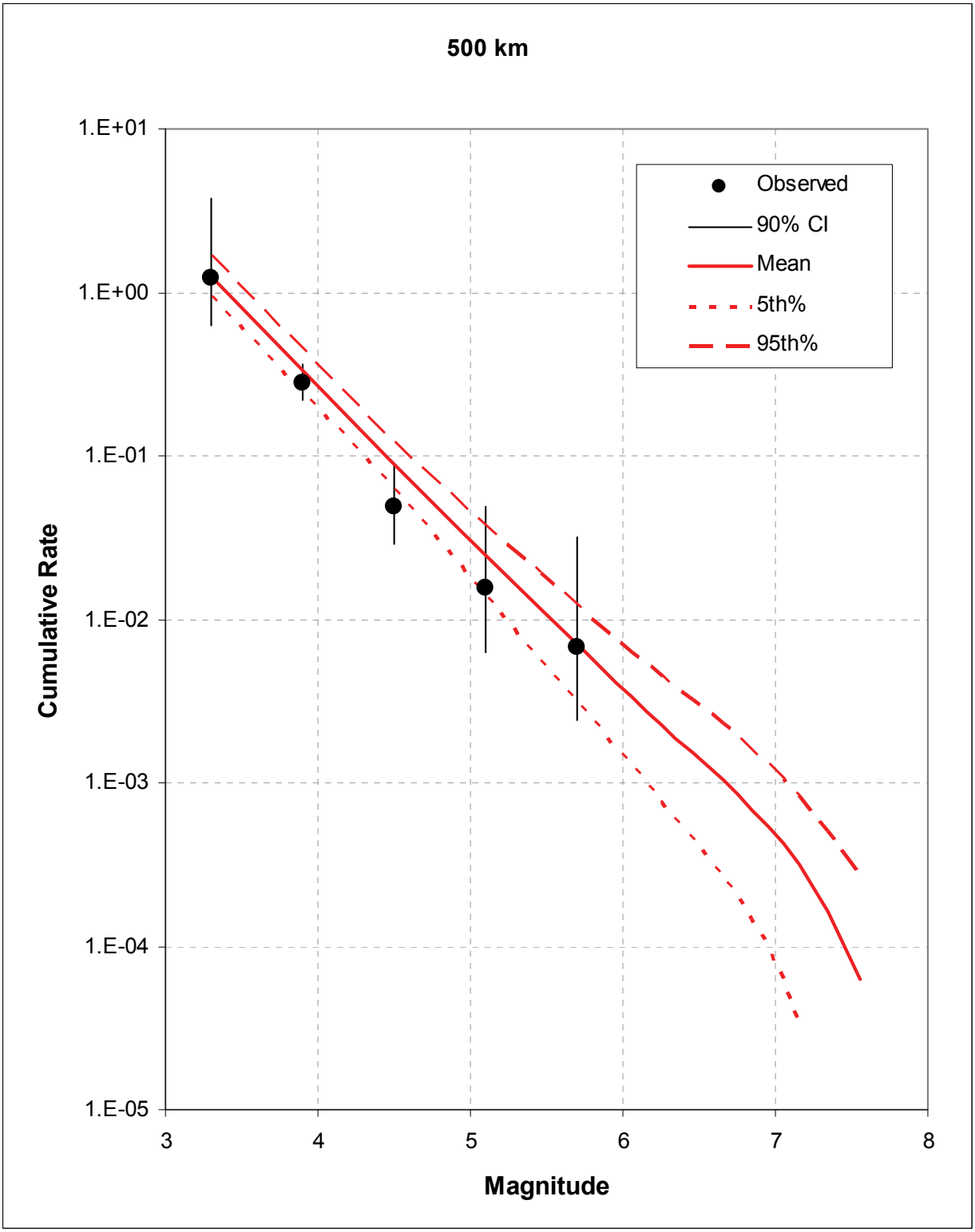

Figure 3.16: Comparison of Observed and Predicted Seismicity Rates within 500 km of the Bruce Nuclear Site

4. GROUND MOTION PREDICTION EQUATIONS FOR CENTRAL AND EASTERN NORTH AMERICA

Completion of the probabilistic seismic hazard model for the Bruce nuclear site requires specification of earthquake ground motions. In most PSHA applications, earthquake ground motions are specified in terms of ground motion prediction equations (GMPEs). There are two necessary components of a GMPE. The first is a relationship for the median amplitude (mean log amplitude) of peak ground motions as a function of earthquake magnitude, source-to-site distance, and spectral frequency of interest, as well as other explanatory variables that may be appropriate. The second and equally important component is a relationship for the aleatory variability (random variation) of peak ground motions about the median amplitude.

In areas of active tectonic and high seismicity rates, GMPEs are often based on analyses of recorded strong ground motion. In central and eastern North America (CENA), however, recorded strong-motion data is very limited. As a result, the available ground-motion models are primarily based on theoretical/numerical modelling approaches that have been calibrated using comparisons with recorded data from more active regions, in addition to the relatively sparse CENA data. Section 4.1 discusses the selection of an appropriate set of such models for the analysis of the seismic hazard at the Bruce nuclear site. These models are developed to represent surface motions on generic CENA hard rock sites. Completion of the site hazard assessment requires specification of the motions at depth in the Bruce nuclear site-specific geology. This specification is discussed in Section 5.3. Specification of the aleatory variability in the peak ground motions is discussed in Section 4.2. As with the seismic source model, there is uncertainty in specification of the appropriate GMPEs. The representation of that uncertainty in the seismic hazard model is discussed in Section 4.3.

4.1 Selection of Models for Median Ground Motions

During the past two decades, a substantial amount of research effort has been focused on developing strong ground-motion models for the stable continental regions of CENA. Because of the limited strong-motion database, these models have been developed from analysis of seismographic network data (e.g., Atkinson and Mereu 1992) and the use of numerical ground-motion models (e.g., Boore and Atkinson 1987, Atkinson and Boore 1995, 2006, EPRI 1993). More recently, Campbell (2003) has developed a hybrid ground-motion model that used numerical modelling and network data to transfer empirical ground-motion models developed in active tectonic regimes to conditions in the central and eastern United States (CEUS).

In 2004, EPRI performed an evaluation of the ground motion models available at that time in order to characterise ground motion modelling for application to safety studies for nuclear power plants. EPRI's approach was to group the available models into clusters defined by the general approach used for the model development. EPRI (2004) then developed a representative model for each cluster, as well as a characterization of the epistemic uncertainty in the ground motion models for each cluster.

The conceptual approach used by EPRI in 2004 is followed in this study using the most recent versions of the ground motion models representative of the EPRI clusters. The Atkinson and Boore (2006) model is an update of the previous model (Atkinson and Boore 1995) that was used in the EPRI (2004) study. This updated model uses additional constraints on wave propagation from the analysis of empirical data, and uses the stochastic finite-fault numerical modelling approach in place of the point-source stochastic

simulation technique. The Atkinson and Boore (2006) model includes a characterization of epistemic uncertainty in the median predictions.

The Silva et al. (2003) model is also an update of one of the models used in the EPRI (2004) study. This model is a point-source, stochastic model that represents an update of the model and modelling approach followed by EPRI in 1993 and Toro et al. in 1997. The single-corner variable-stress-drop set of models from Silva et al. (2003) was selected for this study because these models provide better calibration with empirical models. The Silva et al. (2003) model also includes a characterization of epistemic uncertainty in the median predictions.

The third model selected was the Campbell (2003) hybrid model described above. Campbell (2003) also developed a characterization of epistemic uncertainty in the median prediction models.

The fourth type of model (Somerville et al. 2001) used in the EPRI (2004) study was one based on full numerical modelling of the source and path. The Somerville et al. (2001) model was somewhat limited in its application, however, because it did not include earthquakes in the magnitude range of **M** 5 to 6, and these events often have a large contribution to the hazard at sites in CENA. The Atkinson and Boore (2006) model incorporated finite-fault modelling techniques used by Somerville et al. (2001), thus providing representation of this modelling approach in the ground motion set.

A new model developed by Atkinson (2008) was included. This model is based on comparing the strong motion data for CENA earthquakes with the predictions provided by a well-constrained empirical model for active tectonic regions, in this case the Next Generation Attenuation (NGA) model of Boore and Atkinson (2008). An algebraic relationship is fitted to the residuals from this comparison, providing an adjustment factor from active tectonic regions to CENA. The approach is somewhat analogous to the hybrid model, except that the adjustment from western North America (WNA) to CENA is based primarily on CENA recordings rather than numerical modelling.

The four ground-motion models are compared on Figure 4.1 and Figure 4.2 in terms of the attenuation of peak ground acceleration and 1 Hz spectral acceleration, respectively. Figure 4.3 compares the GMPEs in terms of the predicted response spectra for **M** 5 and **M** 7 earthquakes. The four models compare reasonably well, although the Atkinson (2008) reference empirical model tends to predict lower motions at longer spectral periods.

4.2 Selection of Model for Aleatory Variability

Specification of the aleatory variability about the median ground-motion predictions for the modelling-based GMPEs had typically been based on the results of parametric variability in the parameters. EPRI (1993) and Toro et al. (1997) developed a model for aleatory variability based on representation of the parametric uncertainty in ground-motion modelling predictions combined with an added component from model misfit in calibration studies. The resulting values of epistemic uncertainty were somewhat larger than typical values found for empirical ground-motion data in WNA. Silva et al. (2003) applied the same approach in developing their GMPEs, with similar results.

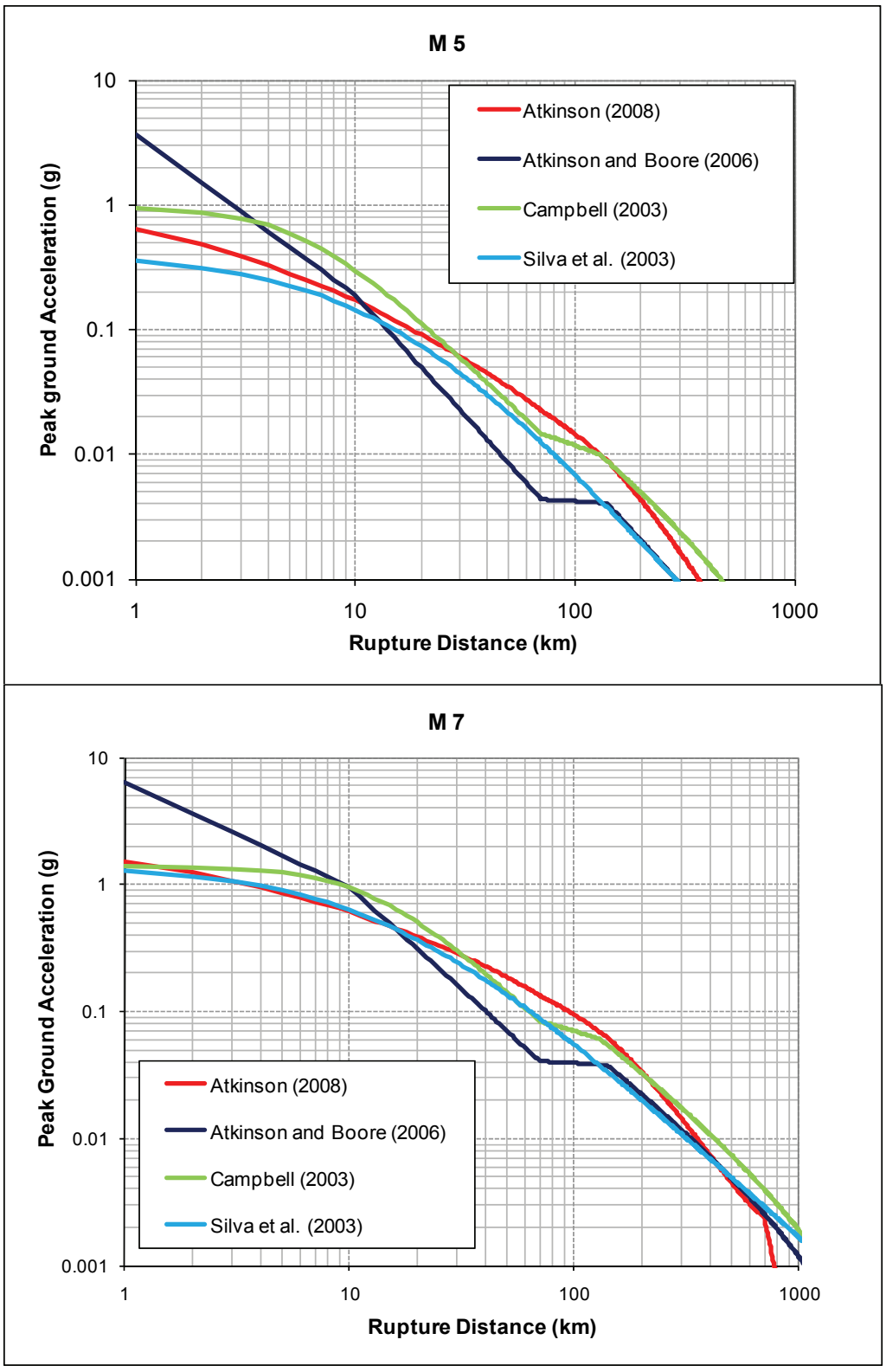

Figure 4.1: Comparison of Median Peak Ground Acceleration Estimates from the Selected GMPEs as a Function of Magnitude and Distance

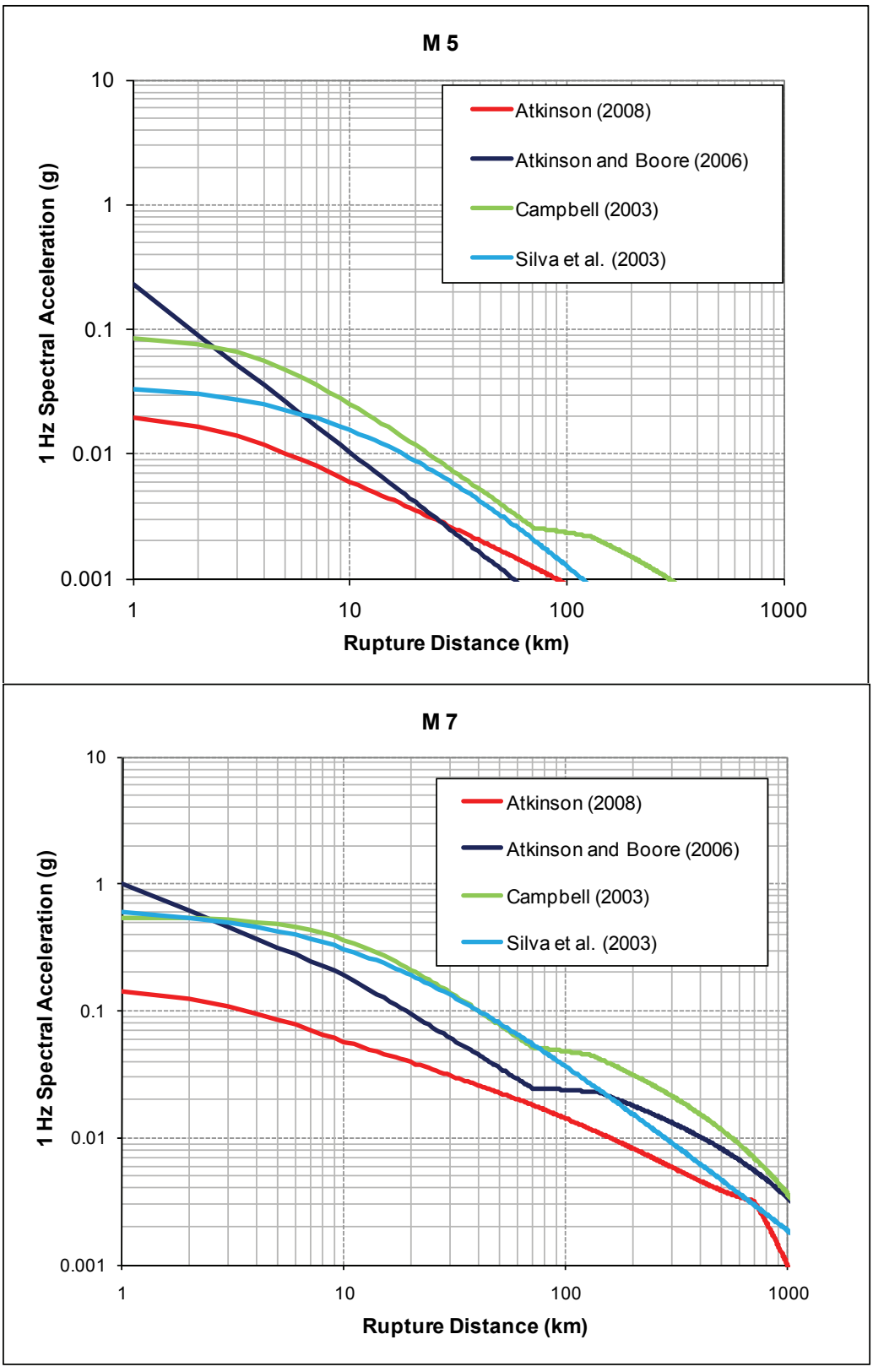

Figure 4.2: Comparison of Median 1 Hz Spectral Ground Acceleration Estimates from the Selected GMPEs as a Function of Magnitude and Distance

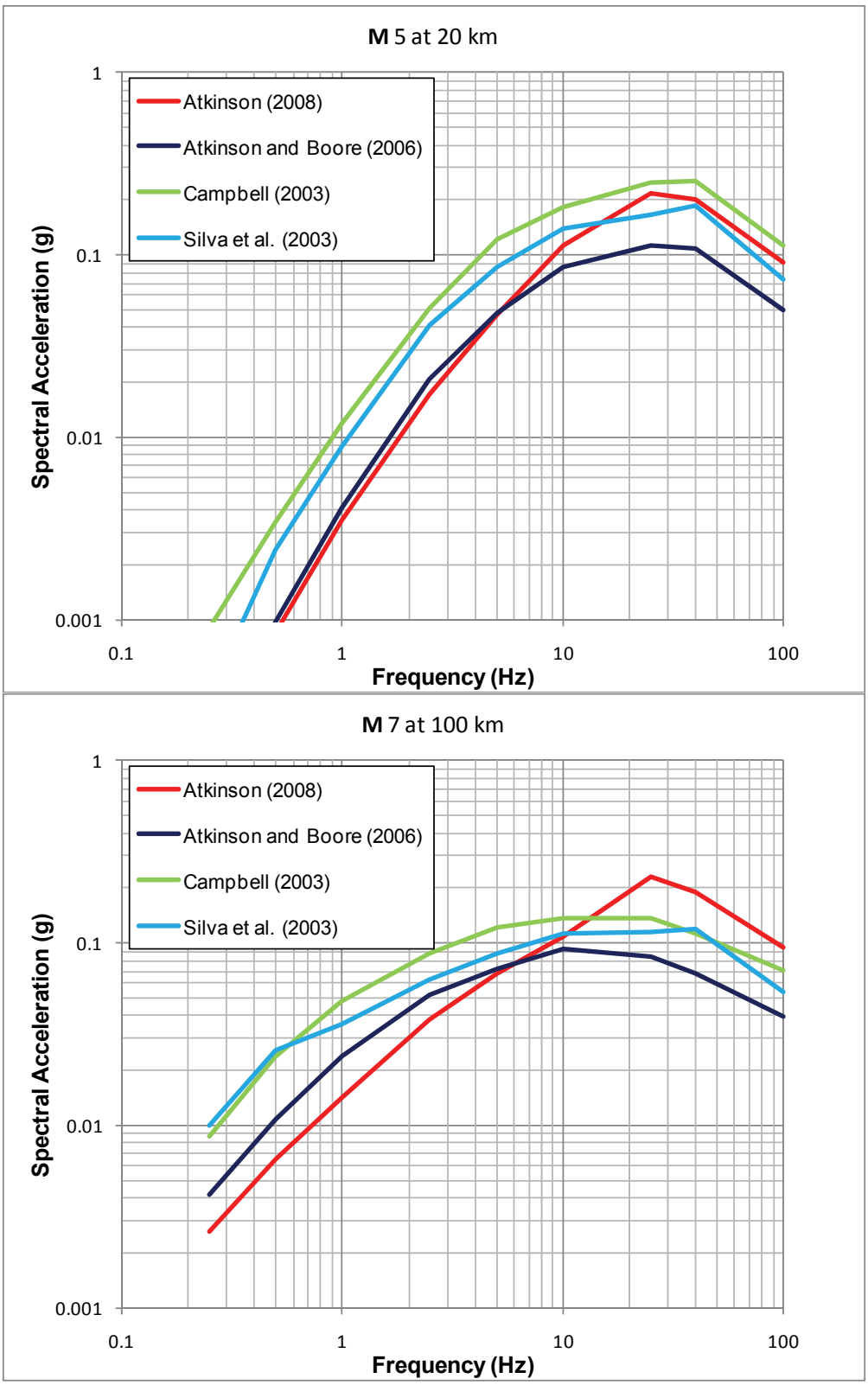

Figure 4.3: Comparison of Median 5 Percent Damped Response Spectral Amplitudes Predicted by the Selected GMPEs

More recently, EPRI (2006) performed an extensive analysis of the basis for assessing the proper aleatory variability (sigma) to assign to CENA ground-motion models. The study concluded that empirically based estimates from active tectonic regions are appropriate for CENA ground motions with some minor adjustments. That approach has been followed in assigning aleatory variability models for this study. Table 4.1 lists the average of the aleatory variability values for the five recently published NGA empirical models developed for active tectonic regions (Abrahamson and Silva 2008, Boore and Atkinson 2008, Campbell and Bozorgnia 2008, Chiou and Youngs 2008, Idriss 2008). Values are listed for **M** 5 and **M** 7 earthquakes as three of the relationships include magnitude-dependent aleatory variability. Following the approach used in EPRI (2006), these values are adjusted for application to CENA by slightly increasing the earthquake-to-earthquake variability and increasing the high-frequency (>10 Hz) values to account for the increased high-frequency content of CENA ground motions.

Table 4.1: Aleatory Variability for NGA Models and the Selected Values for CENA

Spectral Period (sec)	Average of NGA		Adjusted for CENA	
	M 5	M 7	M 5	M 7
0.01 (PGA*)	0.65	0.55	0.67	0.57
0.025	0.66	0.56	0.73	0.62
0.04	0.68	0.57	0.73	0.62
0.1	0.71	0.60	0.73	0.62
0.2	0.71	0.61	0.72	0.62
0.4	0.70	0.62	0.72	0.63
1.0	0.71	0.66	0.73	0.67
2.0	0.73	0.69	0.75	0.70
4.0	0.74	0.71	0.76	0.72

Note: * peak ground acceleration.

4.3 Representation of Epistemic Uncertainty

Figure 4.4 shows the logic tree structure used to characterise epistemic uncertainty in the specification of CENA ground motions in the Bruce PSHA. The Atkinson and Boore (2006), Campbell (2003), and Silva et al. (2003) models are given equal weight (0.3 each). Previous versions of two of these models were given roughly comparable weights to the Campbell (2003) hybrid model in the EPRI (2004) study. Equal weights are considered a reasonable approximation to the EPRI (2004) results. The Atkinson (2008) referenced empirical model is given lower weight (0.1) in part because of its newness and lack of experience in its application. The Atkinson (2008) model is also specified at only a limited number of spectral periods, requiring significant interpolation of coefficients in order to apply it to the analysis. The model was included in the PSHA following the intent of its developer to use it to more fully represent the epistemic uncertainty in modelling CENA ground motions.

The Atkinson and Boore (2006), Campbell (2003), and Silva et al. (2003) models all include characterization of epistemic uncertainty in the median motions. We have used the three-point discrete distribution developed by Keefer and Bodily (1983) to represent that uncertainty with three alternatives: a median model with a weight of 0.63, and 5th and 95th percentile models with weights of 0.185 each. The Atkinson (2008) model contains two estimates of the median adjustment from WNA to CENA, and these two estimates are given equal weight in the ground motion modelling.

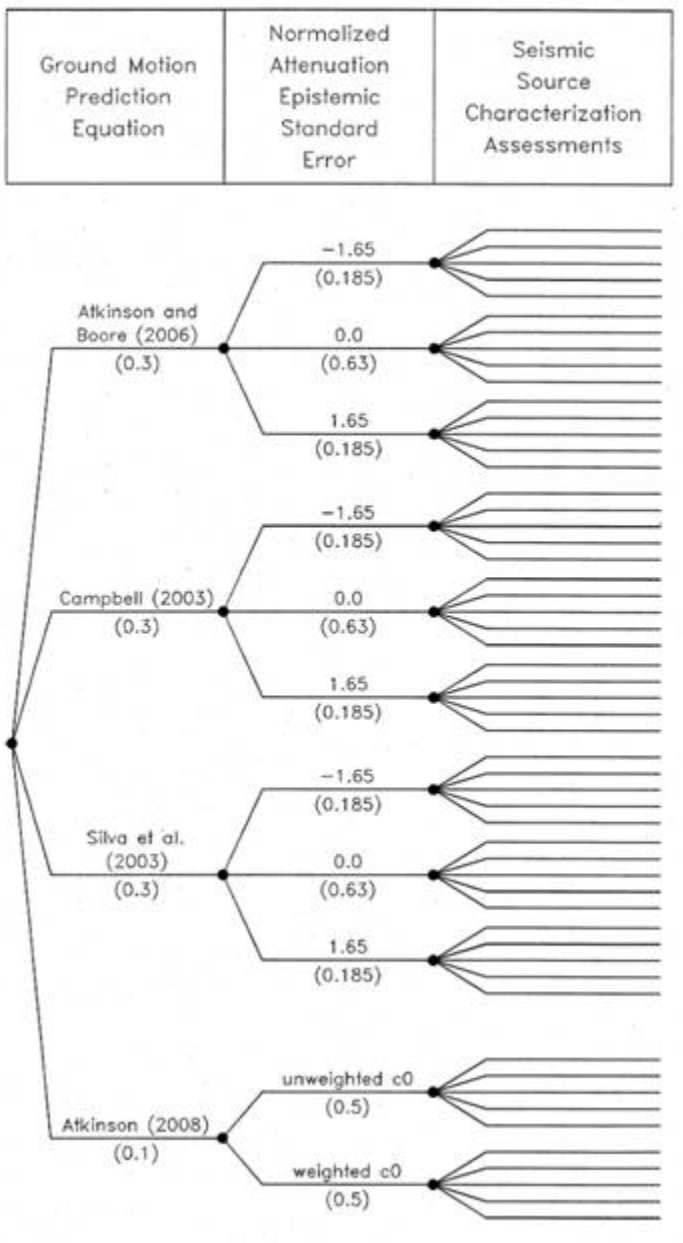

Figure 4.4: Logic Tree for CENA GMPEs Used in the Bruce Nuclear Site PSHA

Figure 4.5 shows the epistemic uncertainties in median ground motions that result from implementing the logic tree shown on Figure 4.4. The epistemic uncertainty, σ_μ, is defined as the standard deviation (natural log units) of the weighted median ground-motion predictions as a function of magnitude and distance for two spectral periods. As a comparison, Peterson et al. (2008) used values of σ_μ in the range of 0.15 to 0.25 (90 percent confidence interval ranges of 0.25 to 0.4 natural log units, respectively) to characterise the epistemic uncertainty in GMPEs for WNA. The much larger values for CENA reflect the fact that there is very limited empirical strong-motion data available to constrain CENA ground motions.

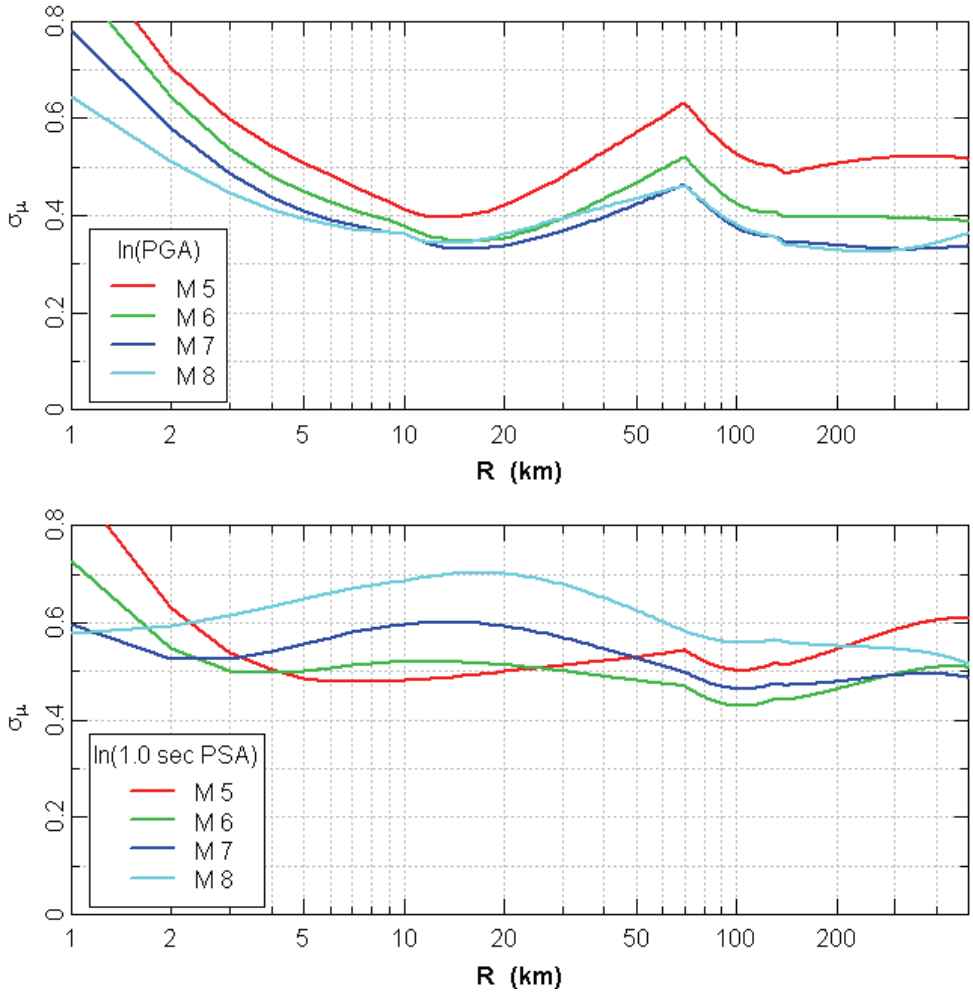

Figure 4.5: Epistemic Uncertainty in Median Ground Motions Resulting from the Uncertainty Model for the CENA GMPEs Shown on Figure 4.3

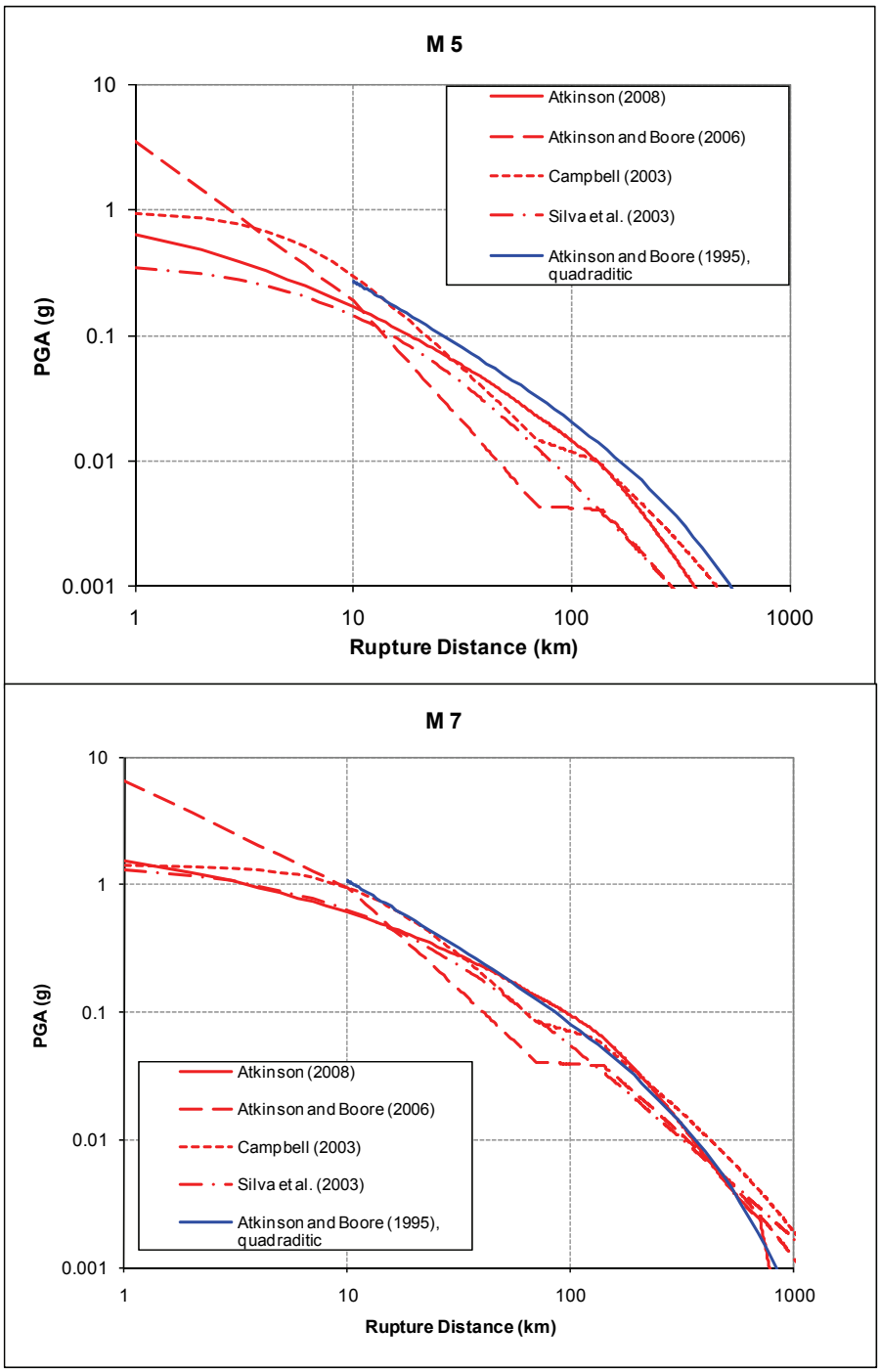

Notes: Comparison is between peak ground accelerations predicted by quadratic model of Atkinson and Boore (1995) and those predicted by the ground motion models used in this study.

Figure 4.6: Comparison of Median Peak Ground Accelerations

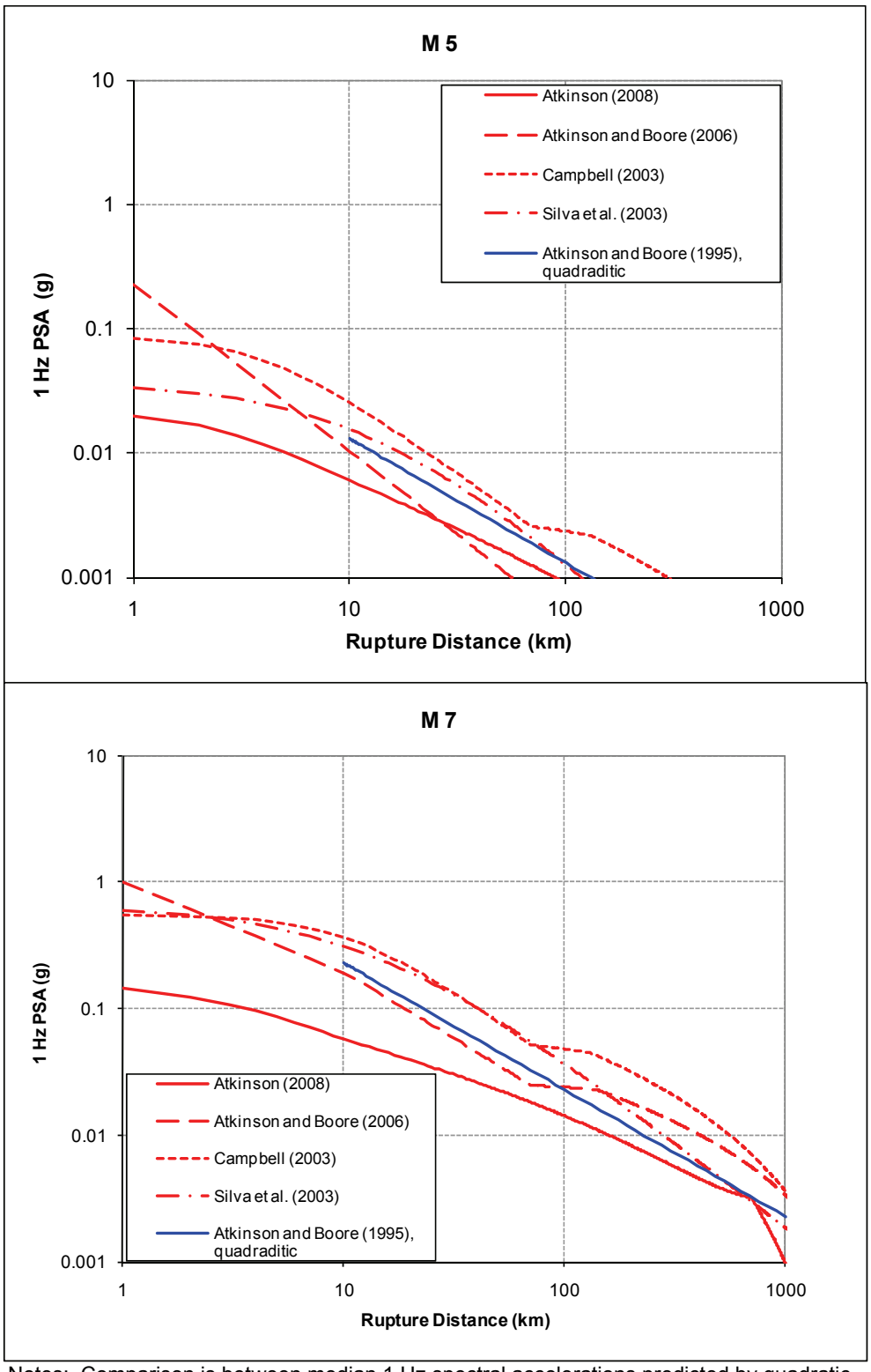

Notes: Comparison is between median 1 Hz spectral accelerations predicted by quadratic model of Atkinson and Boore (1995) and those predicted by the ground motion models used in this study.

Figure 4.7: Comparison of Median 1 Hz Spectral Accelerations

4.4 Comparison with Ground Motion Modesl Used for NBCC

Adams and Halchuk (2003) and Halchuk and Adams (2008) develop seismic hazard values for Canada for use in the National Building Code of Canada (NBCC). These hazard values were computed using models based on the quadratic form GMPE published by Atkinson and Boore (2005). Figure 4.6 and 4-7 compare the ground motions predicted by the quadratic GMPE of Atkinson and Boore (1995) to those predicted by the GMPEs selected for use in this study. For PGA, the Atkinson and Boore (1995) quadratic GMPE predicts somewhat higher ground motions than the average of the models used in this study. For 1 Hz spectral acceleration, the Atkinson and Boore (1995) quadratic GMPE predicts somewhat lower ground motions than the average of the models used in this study. The Atkinson and Boore (1995) GMPE has been updated by the Atkinson and Boore (2006) GMPE used in this study. The updated Atkinson and Boore model predicts lower ground motions that the earlier 1995 model. Based on its more recent publication date, the Atkinson and Boore (2006) GMPE is considered an update of the Atkinson and Boore (1995) GMPE, and thus more representative of the current knowledge for ground motion prediction in ENA.

5. PROBABILISTIC SEISMIC HAZARD ANALYSIS AND DESIGN GROUND MOTIONS

The development of design ground motions for the Bruce nuclear site was accomplished in a two-stage process. The first stage involved performing a PSHA using the seismic sources described in Section 3.0 and the ground motion models described in Section 4.0. The second stage involved developing site-specific hazard results using the dynamic properties of the Bruce nuclear site. The following sections describe the approaches used to perform the two analyses, the results of the PSHA for the reference site conditions, and the development of the site-specific design ground motions.

5.1 PSHA Analysis Approach

5.1.1 Analysis for Reference Site Conditions

The mathematical formulation used in most PSHAs assumes that the occurrence of damaging earthquakes can be represented as a Poisson process. Under this assumption, the probability that a ground motion parameter, Z, will exceed a specified value, z, in time period t is given by:

$$P(Z > z \mid t) = 1 - e^{-\nu(z)\cdot t} \le \nu(z)\cdot t \tag{5.1}$$

where $\nu(z)$ is the average frequency during time period t at which the level of ground motion parameter Z exceeds value z at the site from all earthquakes on all sources in the region. Equation 5.1 is valid provided that $\nu(z)$ is the appropriate average value for time period t. In this study, the hazard results are reported in terms of the frequency of exceedance $\nu(z)$.

The frequency of exceedance, $\nu(z)$, is a function of the frequency of earthquake occurrence, the randomness of size and location of future earthquakes, and the randomness in the level of ground motion that future earthquakes may produce at the site. It is computed by the expression:

$$\nu(z) = \sum_n \alpha_n(m^0) \int_{m^0}^{m^u} f(m) \left[\int_0^\infty f(r \mid m) \cdot P(Z > z \mid m, r) \cdot dr \right] \cdot dm \tag{5.2}$$

where $\alpha_n(m^0)$ is the frequency of earthquakes on source n above a minimum magnitude of engineering significance, m^0; f(m) is the probability density of earthquake size between m^0 and a maximum earthquake the source can produce, m^u; $f(r \mid m)$ is the probability density function for distance to an earthquake of magnitude m occurring on source n; and $P(Z>z \mid m,r)$ is the probability that, given an earthquake of magnitude m at distance r from the site, the peak ground motion will exceed level z. The frequency of earthquake occurrence, $\alpha_n(m^0)$, and the size distribution of earthquakes, f(m), were determined by the earthquake recurrence relationships developed in Section 3.0. The distribution for the distance between the earthquake rupture and the site was determined by the geometry of the seismic sources defined in Chapter 3. The conditional probability of exceedance, $P(Z>z \mid m,r)$, was determined using the ground motion prediction equations described in Section 4.0. The attenuation relationships defined the level of ground motion in terms of a lognormal distribution. Based on the studies presented in EPRI (2006), the ground motion distributions were not truncated in the PSHA calculation.

The seismic hazard model for the site region developed in Sections 3 and 4 treats all of the parameters of Equation (5.2) as uncertain and specifies discrete probability functions for each one. The result is a large number of alternative parameter sets, each with a finite probability that it represents the "correct" parameter set. The computation of $\nu|(z)$ is made for a particular parameter set, and the result is assigned the probability associated with that parameter set. The process is repeated over all parameter sets, producing a discrete probability density for the frequency of exceedance, $\nu(z)$. The probability density for $\nu(z)$ is then used to compute the mean or expected hazard and various percentiles of the distribution that define the uncertainty in the hazard given the uncertainty in the input parameters.

The computational scheme used to compute the hazard involves replacing the integrals of Equation (5.2) with summations over 0.1 unit magnitude and small distance intervals (e.g., 1 km for distances less than 100 km). The distance density function, $f|(r|m)$, was computed numerically over each source region (assuming either a uniform density or a spatially varying density computed using a Gaussian kernel density estimator), assuming that each earthquake has a finite rupture length dependent on magnitude and that the orientation of the rupture is random. The local sources were modelled as a set of parallel line sources with a width of 10 km to address the uncertainty in the location of the actual source. The probability function $P|(Z|>z|m,r)$ was computed assuming that peak ground motions are lognormally distributed about the specified attenuation relationships.

The generic hard-rock hazard was computed using a fixed lower-bound magnitude (m^0 in Equation 5.2) of **M** 5.0. This magnitude is generally considered to be the lowest magnitude that has the potential to cause damage to well-engineered structures. The distance density functions were computed consistent with the distance measure used in the attenuation relationships. Earthquake rupture orientations were assumed to be random in the areal source zones and aligned parallel to the long dimension of the local sources.

Distributions for the annual frequency of exceeding various levels of spectral acceleration (PSA) were computed for nine spectral frequencies: PGA (set at 100 Hz), 40 Hz, 25 Hz, 10 Hz, 5 Hz, 2.5 Hz, 1 Hz, 0.5 Hz and 0.25 Hz. At each ground motion level, the complete set of results forms a discrete distribution for frequency of exceedance, $\nu(z)$. The computed distributions were used to obtain the mean frequency of exceeding various levels of peak ground motion (mean hazard curve) as well as hazard curves representing various percentiles of the distributions. The logic trees represent a best judgment as to the uncertainty in defining the input parameters, and thus the computed distributions represent the implied confidence in the output, the estimated hazard.

5.1.2 Site-Specific Hazard for Horizontal Motions

Site-specific seismic hazard results for the Bruce site were obtained using what is called Approach 3 in McGuire et al. (2001, 2002). The approach is also described in Bazzurro and Cornell (2004). In this approach, the hazard at the various repository horizons is computed by integrating the hazard curve for the reference site condition with the probability distribution for the transfer function that defines the ground motion at a specific repository horizon relative to those on a reference site condition. For the Bruce nuclear site study, the reference site condition is central and eastern North America (CENA) hard rock with a surface shear-wave velocity of 2.83 km/sec (EPRI 1993, 2004). The Bruce nuclear site-specific amplification relative to this reference site is characterised by a suite of frequency-dependent amplification factors that can account for any nonlinearity in response. Approach 3 involves approximations to the hazard integration using suites of transfer functions, which result in

complete hazard curves at the repository horizons for specific ground-motion parameters (e.g., PGA) at a range of frequencies.

The basis for Approach 3 is a modification of Equation 5.2 to incorporate the additional integration over a probabilistic amplification into the hazard integral:

$$\nu(z) = \sum_n \alpha_n(m^0) \int_0^{\infty} \int_{m^0}^{m^u} P\left(AF > \frac{z}{x} \middle| m, r, x \right) f(m) \left[\int_0^{\infty} f(r|m) \cdot f(x|m,r) \cdot dr \right] dm dx \quad (5.3)$$

In Equation 5-3, x is the ground motion level on the reference site and z is the ground motion level at the site horizon of interest. Parameter AF is the probabilistic amplification factor that transfers amplitude X on the reference site to amplitude Z on the site of interest, AF = Z/X. In theory, it is a function of the amplitude and relative frequency content of the ground motions, and thus would depend upon m, r and x.

Equation 5-3 represents full incorporation of all the variables into a single integration such that one does not actually compute the hazard curve, $\nu(x)$, for the reference site condition. In practice, Approach 3 implements Equation 5.3 in steps. The hazard is computed for the reference site condition. This provides information on the range of m, r and x of importance for defining the relative amplification AF. The probabilistic AF is then combined with the reference site hazard results $\nu(x)$ to produce the site-specific hazard $\nu(z)$. As such, Equation 5.3 is rewritten as:

$$\nu(z) = \int_0^{\infty} \int_{m^0}^{m^u} \int_0^{\infty} P\left(AF > \frac{z}{x} \middle| m, r, x \right) f(m, r|x) f(x) dm \cdot dr \cdot dx \quad (5.4)$$

where f(x) is the absolute value of the derivative of the hazard curve for the reference site, and $f(m,r \mid x)$ is the joint distribution of m and r for events contributing to the reference site hazard at level x obtained from deaggregation of the hazard curve.

Equation 5.3 can be simplified, depending on how sensitive AF is to changes in m, r and x. McGuire et al. (2001) indicate that the effect of variations in r for given values of m and x is usually insignificant, which is to be expected as x and r are highly correlated for a given value of m. This leads to the form implemented in this study:

$$\nu(z) = \int_0^{\infty} \int_{m^0}^{m^u} P\left(AF > \frac{z}{x} \middle| m, x \right) f(m|x) f(x) dm \cdot dx \quad (5.5)$$

In the actual computation, Equation 5.5 is implemented in discretised form as (e.g., Bazzurro and Cornell 2004):

$$\nu(z) = \sum_{x_j} \sum_{m_k} P\left(AF > \frac{z}{x_j} \middle| m_k, x_j \right) p(m_k|x_j) p(x_j) \quad (5.6)$$

In Equation 5.6, $p(x_j)$ is obtained by differencing the hazard curve [$p(x_j) = \nu(x-\Delta x) - \nu(x+\Delta x)$], and $p(m_k \mid x_j)$ is the discrete magnitude deaggregation of the hazard at ground motion level x_j. Depending on the variation of AF with m and the range of magnitudes contributing to the

hazard, $p(m_k \mid x_j)$ may be specified at a few discrete magnitude values. Assuming that AF is lognormally distributed, given m_k and x_j, leads to the expression:

$$P\left(AF > \frac{z}{x_j} \middle| m_k, x_j \right) = 1 - \Phi \left(\frac{\ln\left[\frac{z}{x_j}\right] - \overline{\ln[AF(m_k, x_j)}}{\sigma_{\ln[AF]}(m_k, x_j)} \right) \tag{5.7}$$

where $\overline{\ln[AF(m_k, x_j)}$ and $\sigma_{\ln[AF]}(m_k,x_j)$ are the conditional mean and standard deviation of the natural log of AF at the values m_k and x_j. These are computed by developing probabilistic representations of the site properties; generating one suite of randomised profiles that represent the randomness of the reference site and another suite of profiles that represent the randomness of the site of interest; computing the response of both suites to an appropriate set of values of m_k and x_j; and then computing the statistics of the relative response. Epistemic uncertainty in the characterization of the site properties is incorporated by developing alternative sets of parameters with their associated weights, computing the resulting site-specific hazard for each set, and then computing the weighted mean in the same way that uncertainty in characterising the seismic source models and reference-site ground-motion models is treated.

5.1.3 Application to Vertical Site-Specific Hazard

Typically, the vertical uniform hazard response spectrum (UHRS) is developed by a deterministic application of V/H ratios applied to the horizontal UHRS. Since V/H ratios vary with both magnitude and distance for sites with nonlinear response and with distance for linear sites (e.g., hard rock; Silva 1997, McGuire et al. 2001), it is essential to capture these dependencies, identified through modal deaggregations, in developing the vertical UHRS. For the deterministic approach, conservative estimates of appropriate V/H ratios must be used to ensure achievement of the same hazard levels and target performance goals as the horizontal UHRS. Additionally, V/H ratios reflect epistemic variability, as is evidenced by western North America (WNA) empirical soft rock and deep firm soil V/H ratios (Abrahamson and Shedlock 1997), further pointing out the necessity of conservatism in a deterministic approach to developing vertical UHRS. Incorporation of epistemic variability in a deterministic framework is not unambiguous, as one cannot simply average over suites of motions or transfer functions that reflect epistemic variability. This process will not generally achieve desired hazard levels, and reliance on conservatism in V/H ratios remains the most reliable option. These considerations, along with a desire for easy implementation as a function of expected horizontal PGA, led to the purposeful incorporation of conservatism in the development of the CENA hard-rock V/H ratios (McGuire et al. 2001).

To accurately achieve desired hazard levels as well as performance goals, a fully probabilistic approach was used, directly paralleling that for the horizontal hazard. Implementation of the full integration Approach 3 (Section 5.1.2) for vertical hazard simply substitutes V/H ratios for horizontal amplification factors. In this case, the distribution of V/H ratios is integrated with the horizontal site-specific hazard curves (presumably developed using Approach 3). As with the horizontal case, Approach 3 then admits the proper and unambiguous incorporation of both aleatory variability and epistemic uncertainty in V/H ratios, achieving desired hazard levels. Again, in parallel with the development of the horizontal hazard, modal deaggregations are

used, but as previously stated, in addition to magnitude, source distance is required as V/H ratios depend on both magnitude and distance for soil or soft-rock site conditions.

5.2 Results of the PSHA for Reference Site Conditions

Figure 5.1, Figure 5.2 and Figure 5.3 show the hazard results for PGA (100 Hz PSA), 10 Hz and 1 Hz spectral acceleration (PSA), respectively. The ground motion measures span the frequency range of primary interest. The plots on Figure 5.1 through Figure 5.3 show the mean hazard curves defining the mean frequency of exceeding specified ground-motion levels over all of the sources of uncertainty defined in Sections 3 and 4. The range in the results is shown by curves defining the 5th, 16th, 50th (median), 84th and 95th percentiles of the distributions for frequency of exceedance computed from the logic tree. These percentile hazard curves define confidence intervals for the hazard resulting from uncertainties in specifying the inputs to the analysis. The results shown are typical of seismic hazard estimates in CENA in that there is a wide confidence band reflecting the large uncertainties in most of the input parameters. The results are also typical in that the distribution for frequency of exceedance is skewed such that the mean hazard lies above the central point (median) of the distribution, and the amount of skewness increases with increasing peak ground-motion level.

5.2.1 Contributions to Mean Hazard

Figure 5.4, Figure 5.5 and Figure 5.6 show the total mean hazard curves from Figure 5.1, Figure 5.2 and Figure 5.3, respectively, together with the mean hazard curves for the regional and local sources. These results indicate that the regional sources are the dominant contributors to the hazard at all ground motion levels. The relative contribution of the local sources increases somewhat for 1 Hz hazard because of the potential of these features to have fault-like behaviour, with relatively more frequent large-magnitude earthquakes. This effect can be seen on Figure 5.7, Figure 5.8 and Figure 5.9, which show the hazard from the individual local sources. Of the local sources, the Clarendon-Linden fault has among the highest contributions, even though it is the most distant. This high contribution is a result of the relatively larger probability that it is active (0.4) and has a high weight on fault-like behaviour. This effect is illustrated in Section 5.2.2.

Another way of examining the contributions to the hazard is to deaggregate the results to show the relative contributions from earthquakes in individual magnitude and distance increments. Deaggregation of the hazard is displayed on Figure 5.10, Figure 5.11 and Figure 5.12 for PGA, 10 Hz PSA and 1 Hz PSA motions, respectively. Shown are histograms of the relative contributions of earthquakes in 1/2 magnitude intervals and a range of distance intervals to the hazard at ground motions with annual exceedance frequencies of 10^{-2}, 10^{-4} and 10^{-6}. At an exceedance frequency of 10^{-2}, the major contribution is from distant earthquakes. Larger-magnitude events dominate the 1 Hz hazard (Figure 5.12a), reflecting the fact that larger earthquakes produce relatively greater low-frequency motion than smaller earthquakes (see Figure 4.1, Figure 4.2 and Figure 4.3). As the exceedance frequency decreases, the hazard contributions shift to earthquakes at closer distances, reflecting the fact that earthquake ground motions increase as the source-to-site distance decreases. This effect is strongest for the PGA and 10 Hz hazard. The majority of earthquakes contributing to the 1 Hz hazard at an exceedance frequency of 10^{-6} remain large-magnitude distant events because of their potential to induce larger motions and their much higher occurrence frequency compared to similar events in the vicinity of the Bruce nuclear site. At an annual exceedance frequency

(AEF) of 10^{-6}, the contributions to the PGA and 10 Hz hazard are dominated by earthquakes within 15 km of the site, including events occurring at depth in the immediate site vicinity.

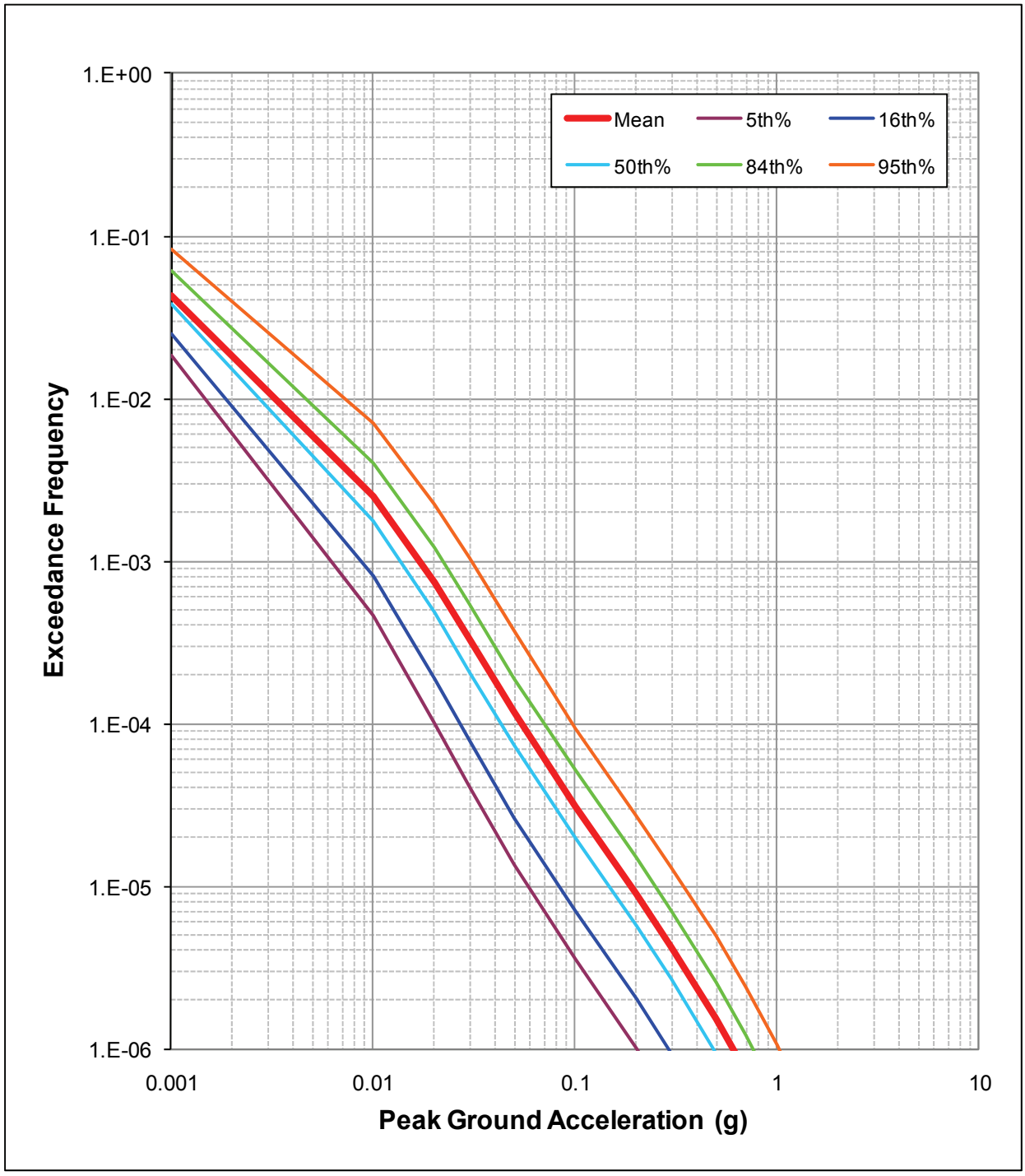

Figure 5.1: Mean and Fractile Hazard Results for Peak Ground Acceleration and Reference Rock Conditions

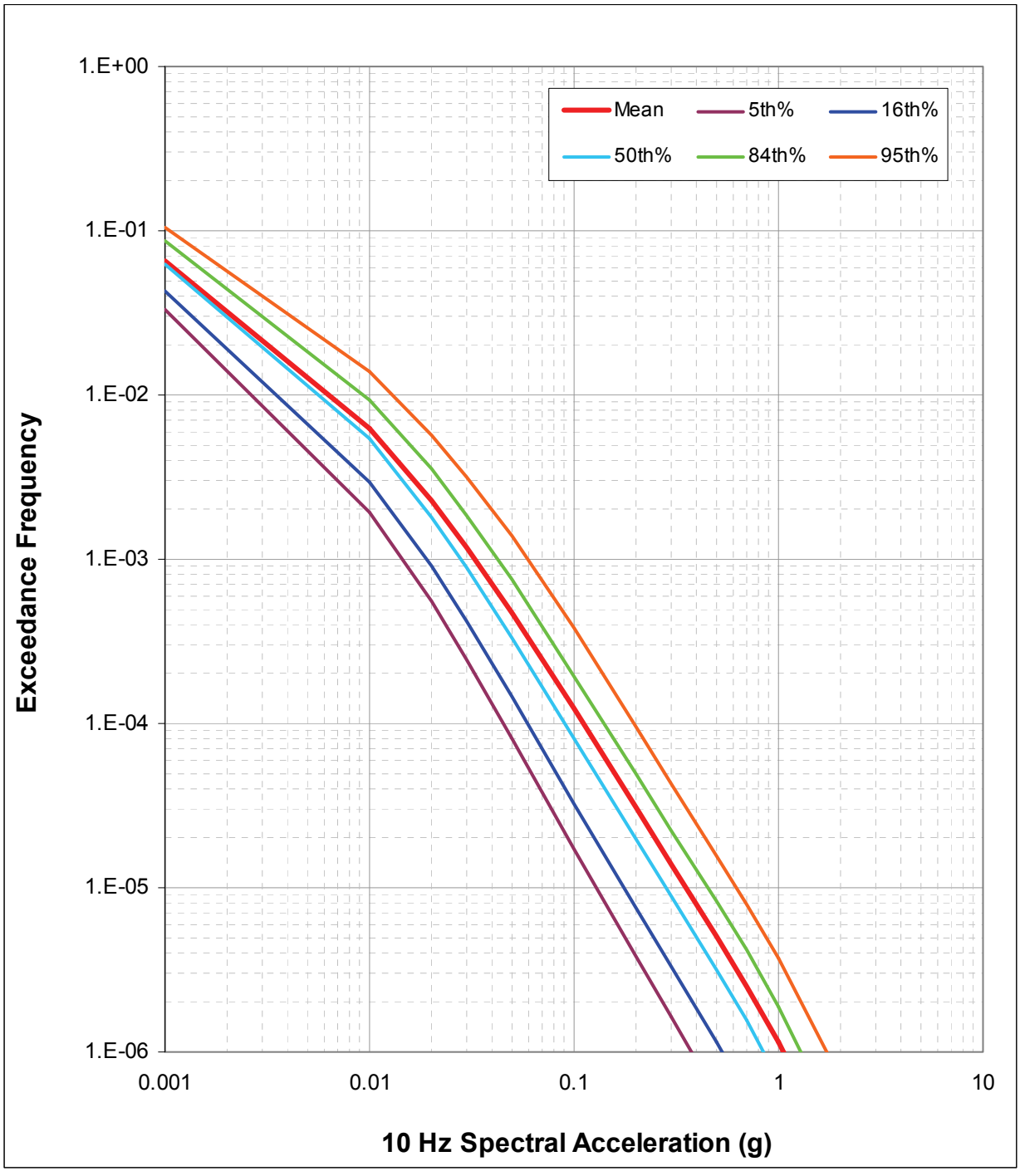

Figure 5.2: Mean and Fractile Hazard Results for 10 Hz Spectral Acceleration and Reference Rock Conditions

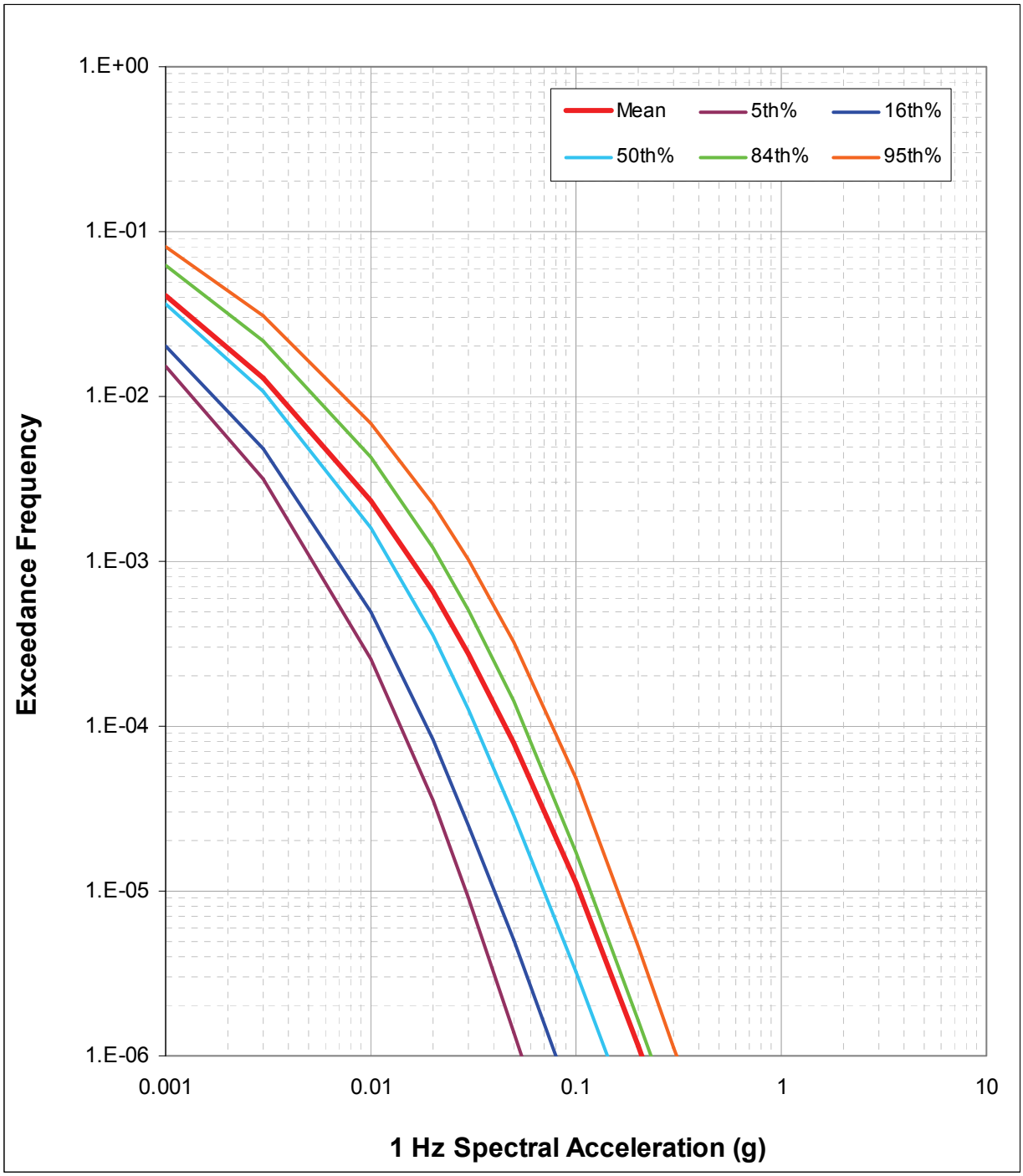

Figure 5.3: Mean and Fractile Hazard Results for 1 Hz Spectral Acceleration and Reference Rock Conditions

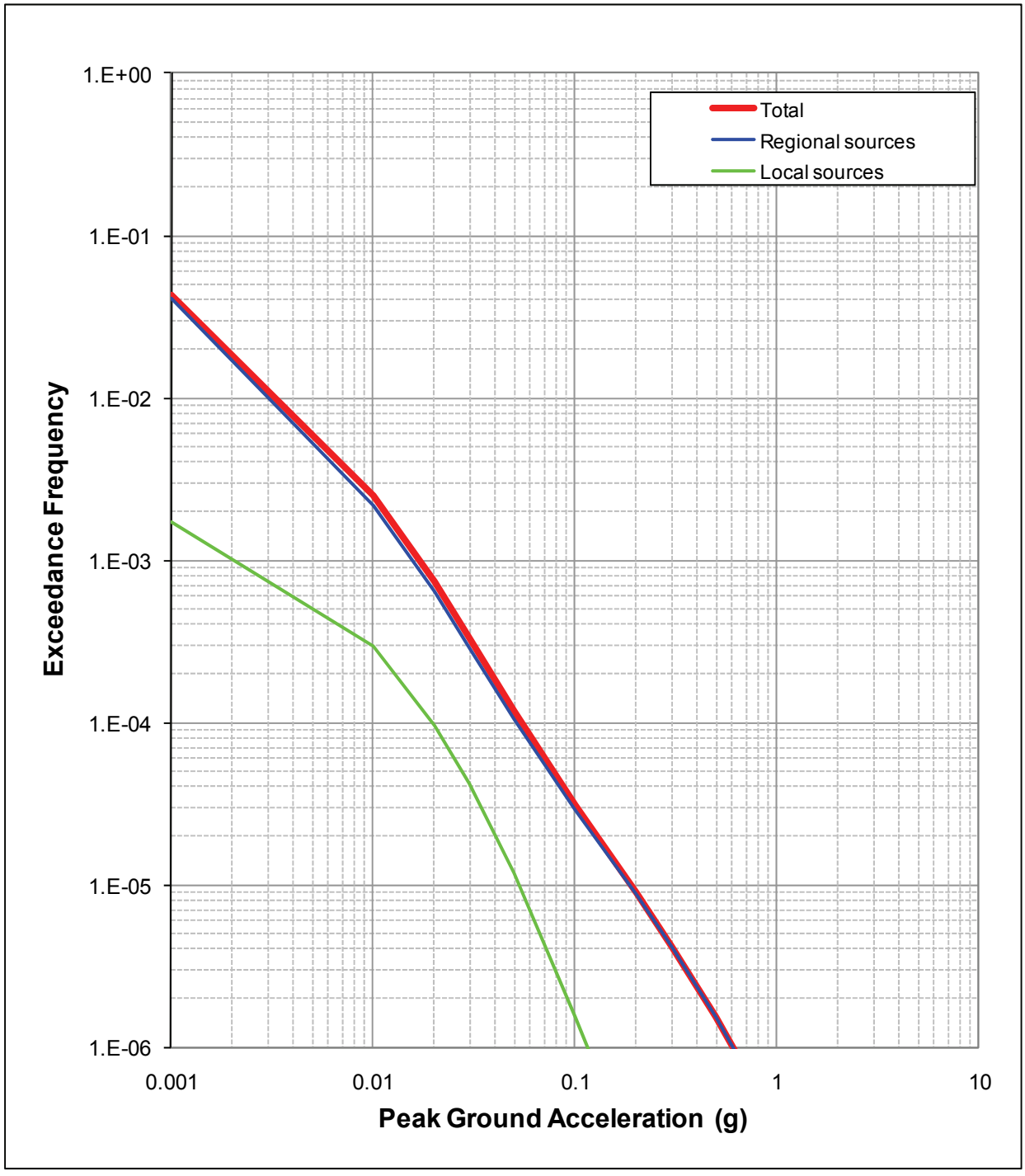

Figure 5.4: Contribution of Regional and Local Sources to Total Mean Hazard for Peak Ground Acceleration

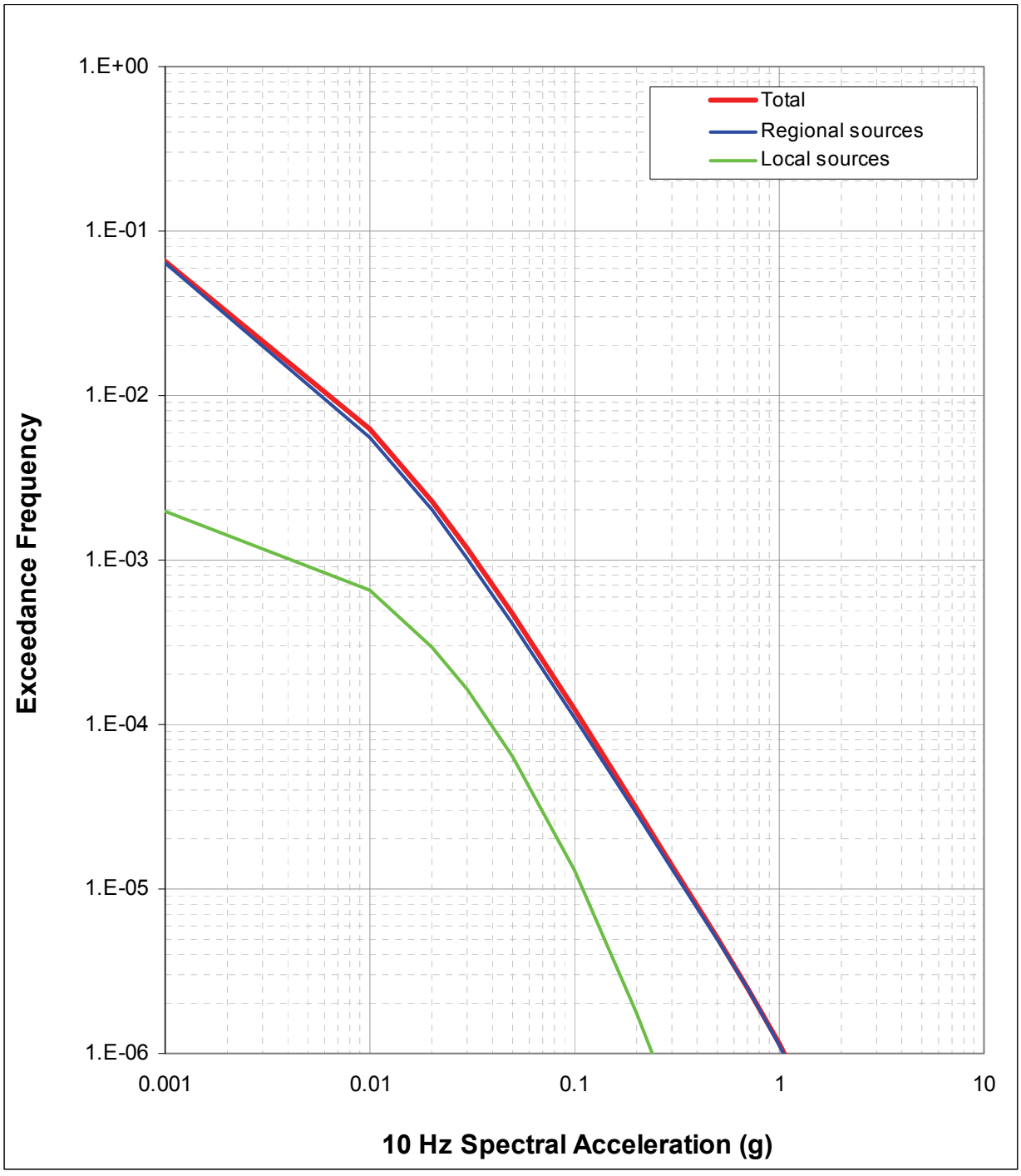

Figure 5.5: Contribution of Regional and Local Sources to Total Mean Hazard for 10 Hz Spectral Acceleration

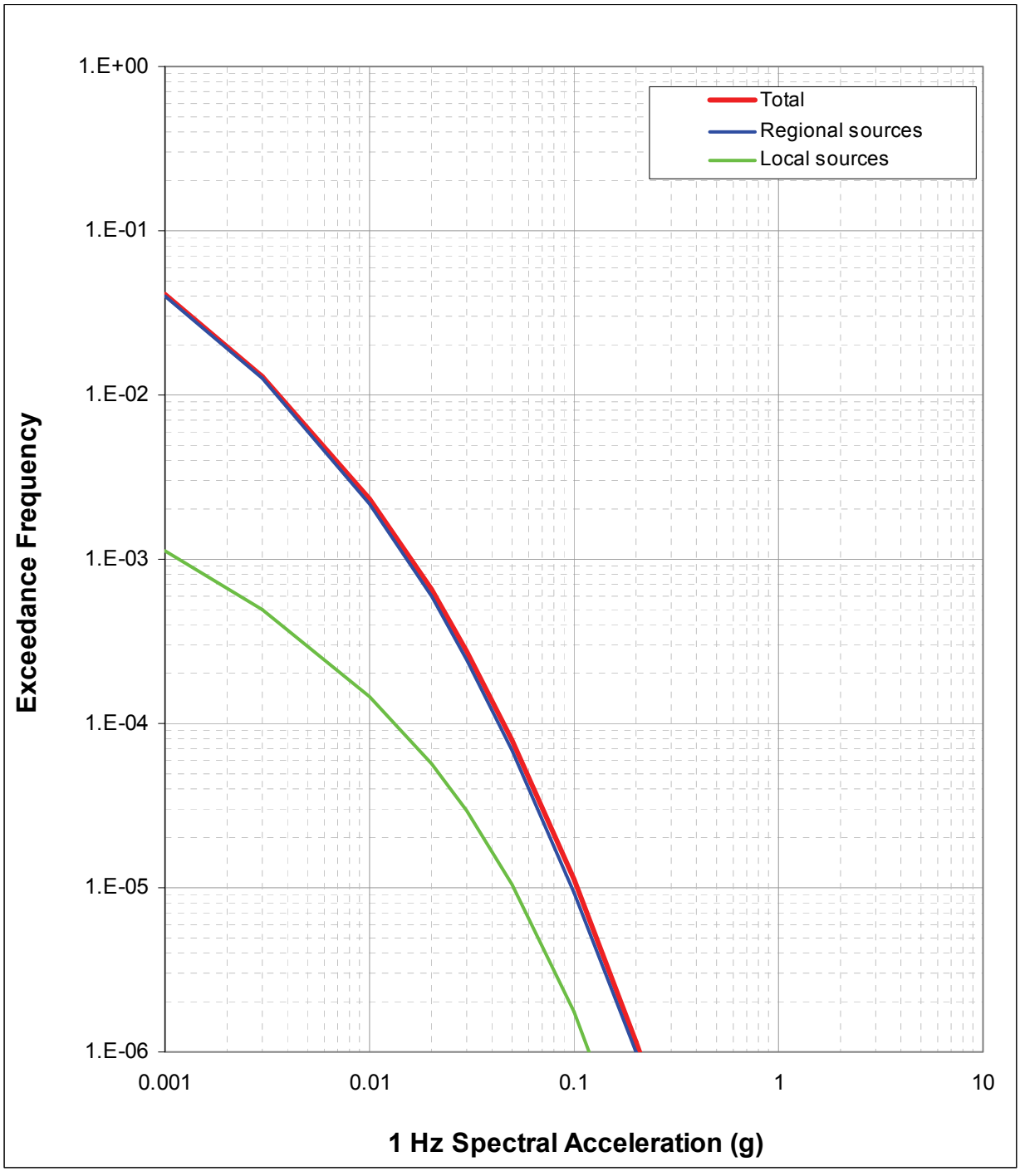

Figure 5.6: Contribution of Regional and Local Sources to Total Mean Hazard for 1 Hz Spectral Acceleration

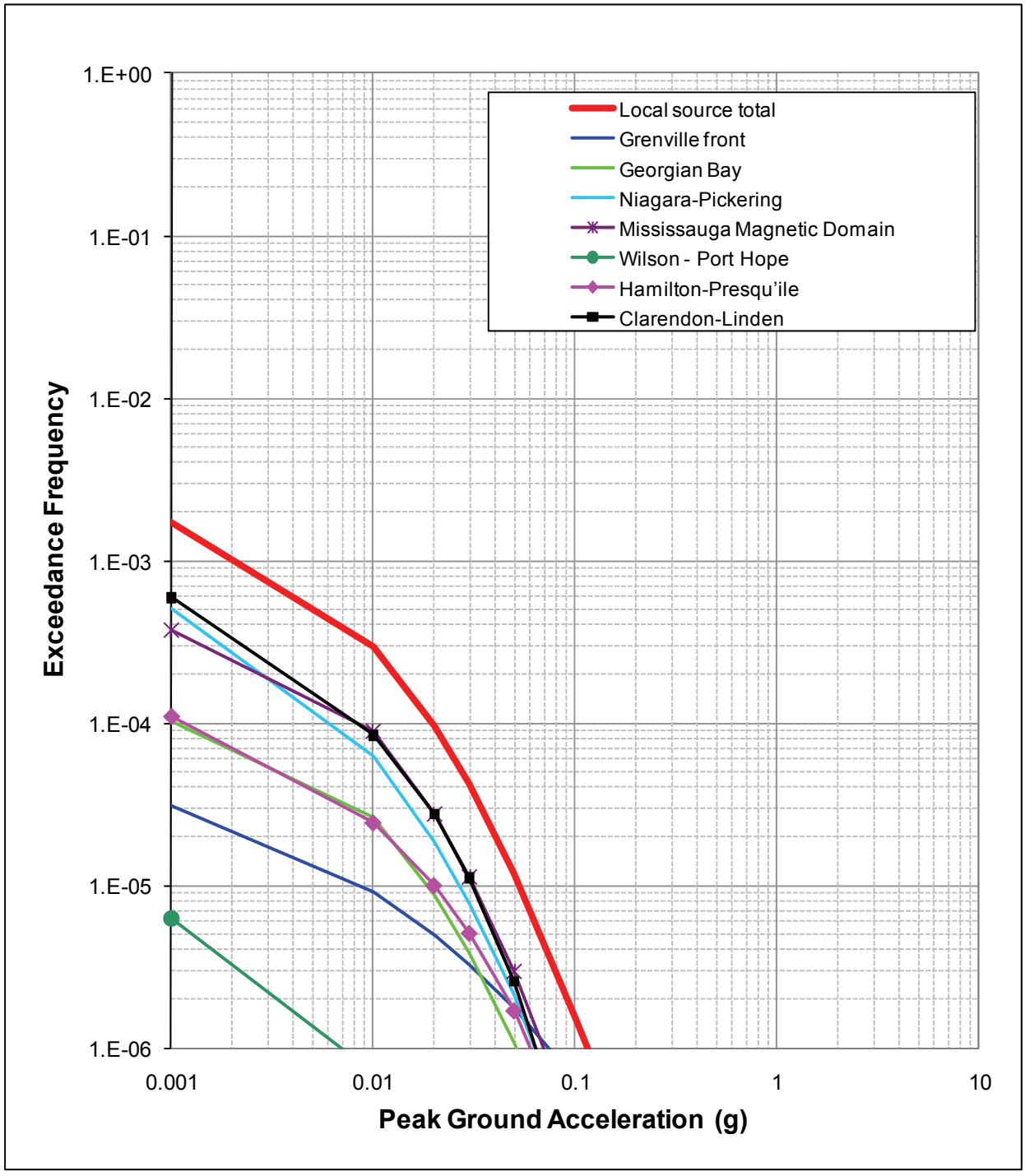

Figure 5.7: Contribution of Individual Local Sources to Total Mean Hazard from Local Sources for Peak Ground Acceleration

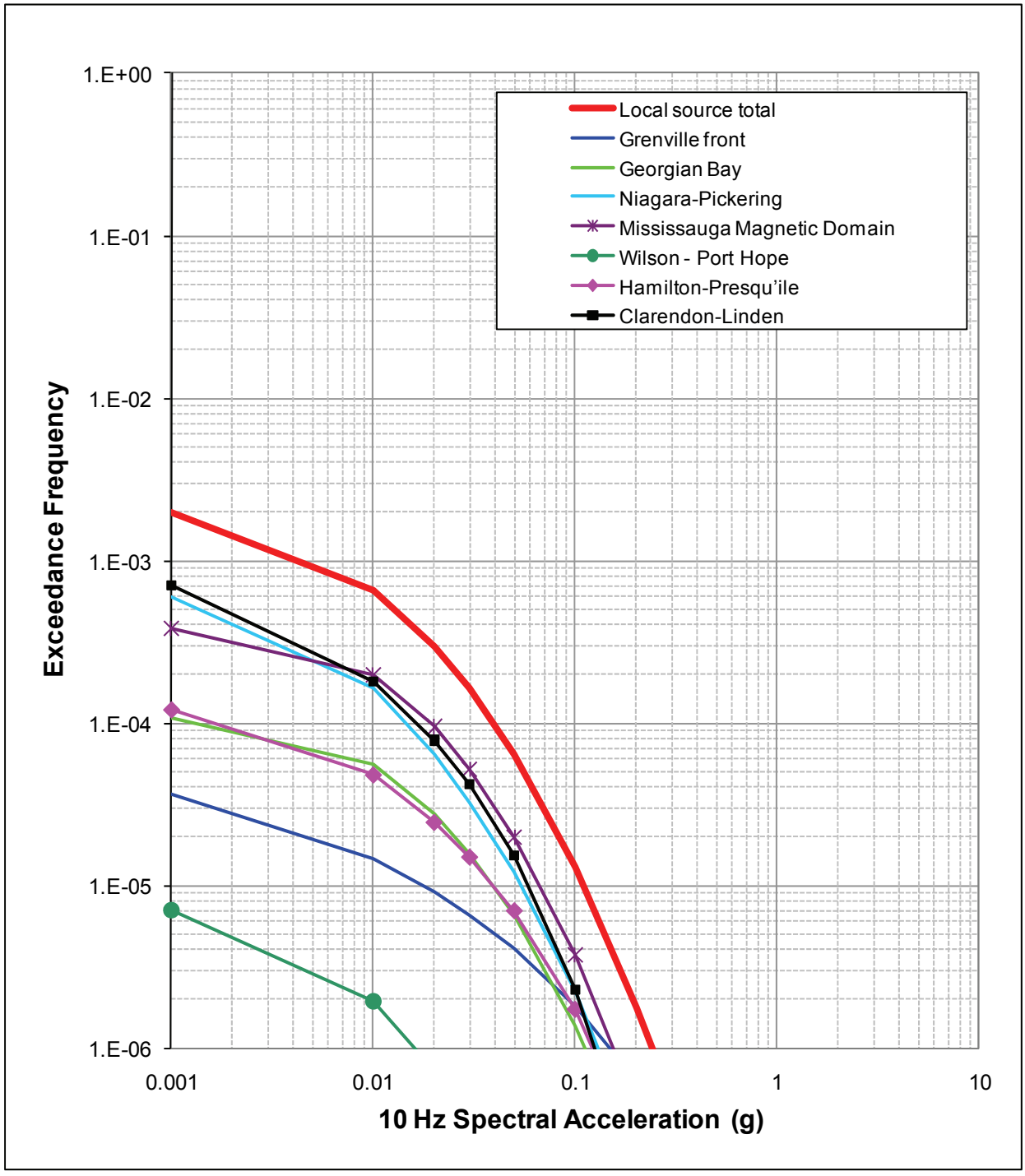

Figure 5.8: Contribution of Individual Local Sources to Total Mean Hazard from Local Sources for 10 Hz Spectral Acceleration

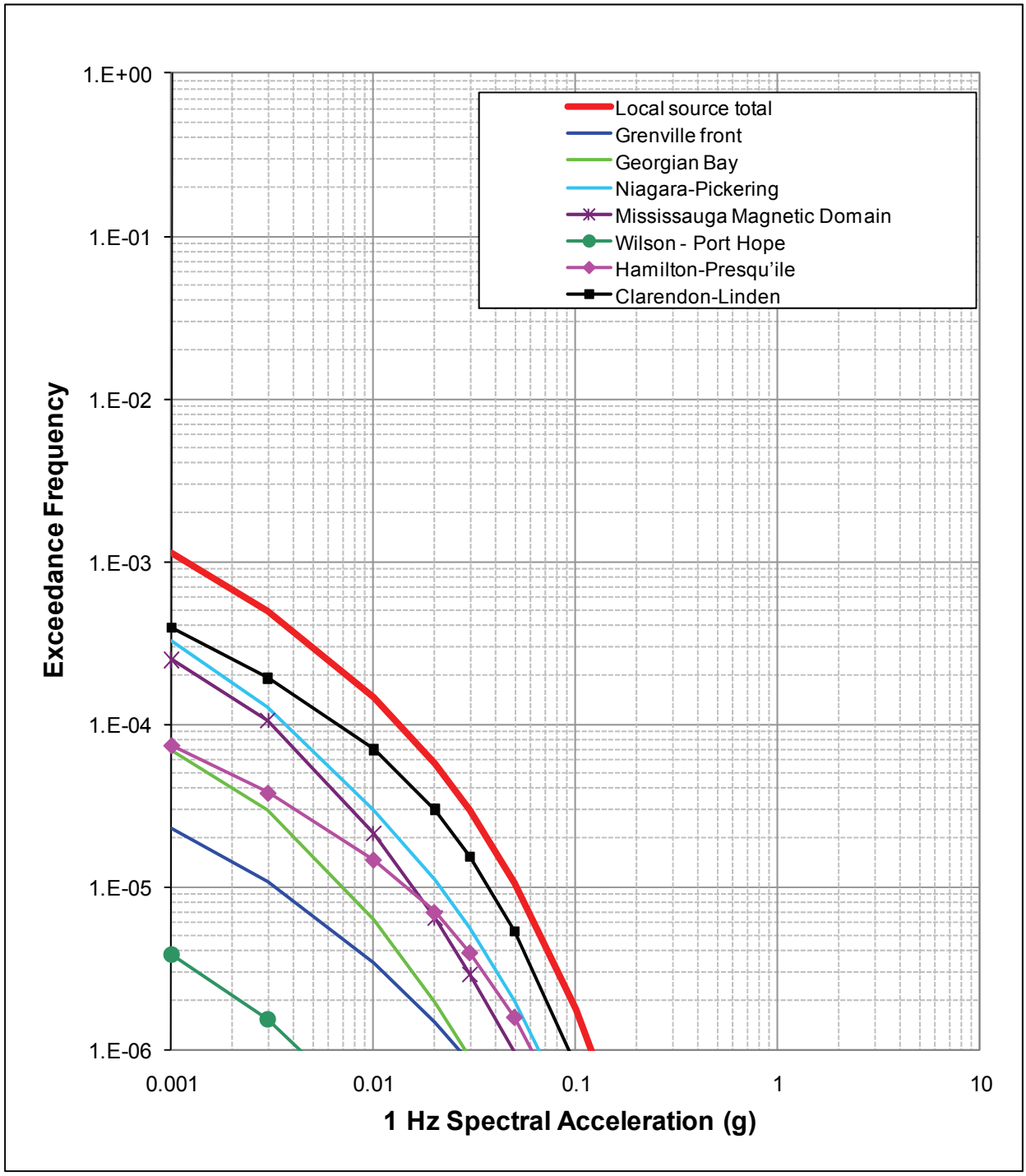

Figure 5.9: Contribution of Individual Local Sources to Total Mean Hazard from Local Sources for 1 Hz Spectral Acceleration

5.2.2 Contributions to Uncertainty

The fractile hazard results shown on Figure 5.1, Figure 5.2 and Figure 5.3 represent the variation in hazard over all of the alternative model parameters defined by the seismic hazard model characterization. The contribution of individual assessments to the uncertainty in the hazard can be displayed by selecting a node of the logic tree and computing the mean hazard, giving each branch in succession a weight of unity, and all of the other branches at that node a weight of zero.

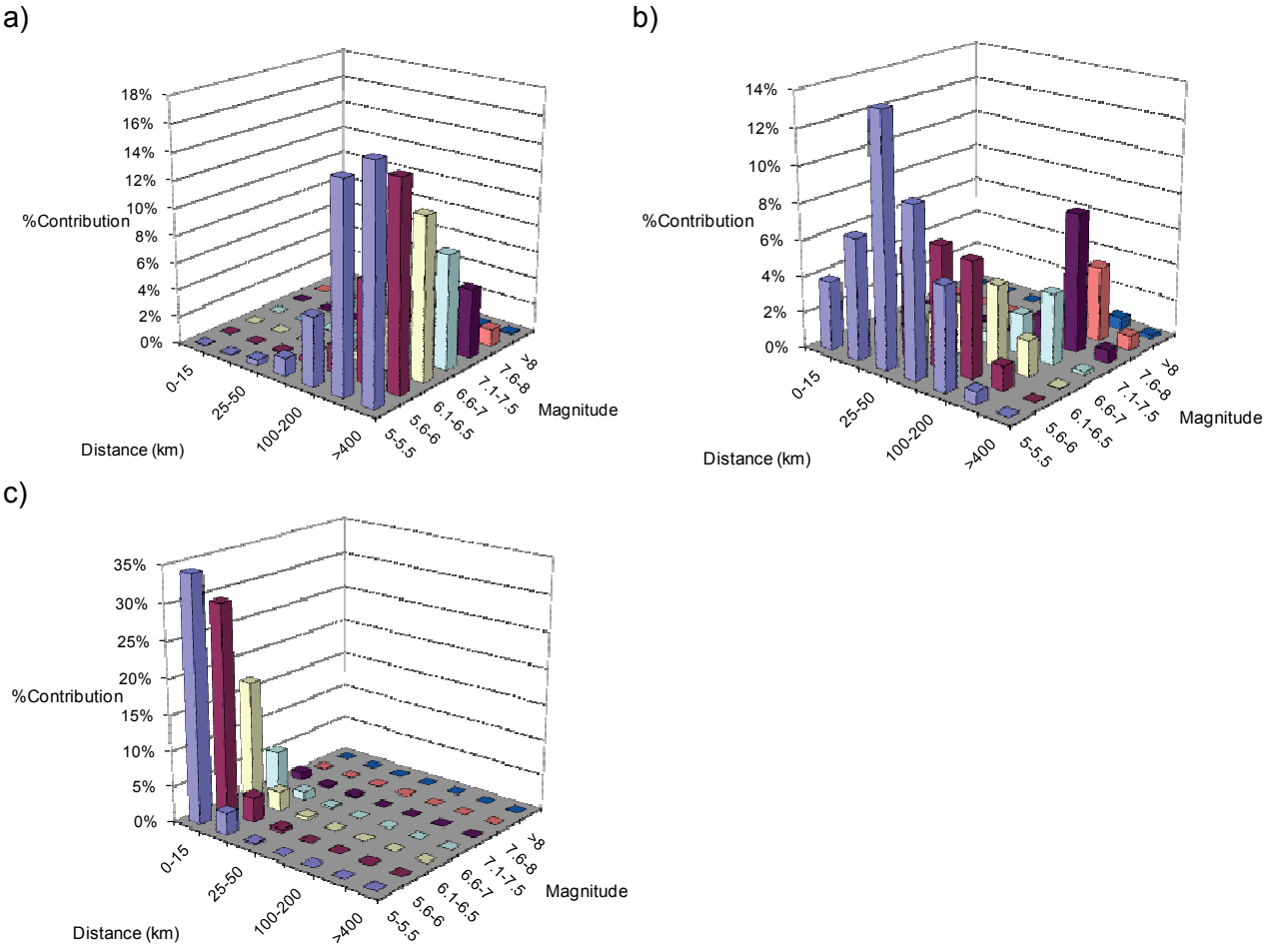

Notes: (a) Deaggregation of the 10^{-2} peak ground acceleration hazard; (b) Deaggregation of the 10^{-4} peak ground acceleration hazard; (c) Deaggregation of the 10^{-6} peak ground acceleration hazard.

Figure 5.10: Deaggregation of Peak Ground Acceleration Hazard

5.2.2.1 Ground Motion Model

The uncertainty in ground motion modelling was characterised by specifying four alternative ground motion prediction equations (GMPEs). Figure 5.13, Figure 5.14 and Figure 5.15

compare the hazard from all sources computed, assuming that each of the four GMPEs is the "correct" model. All four GMPEs produce similar PGA and 10 Hz hazard results. The spread among the results for the four GMPEs is larger for 1 Hz hazard and contributes a large part of the hazard uncertainty. The Atkinson (2008) GMPE produces lower hazard than the other models, consistent with its lower estimate of 1 Hz PSA. The Campbell (2003) hybrid model produces the highest hazard estimates.

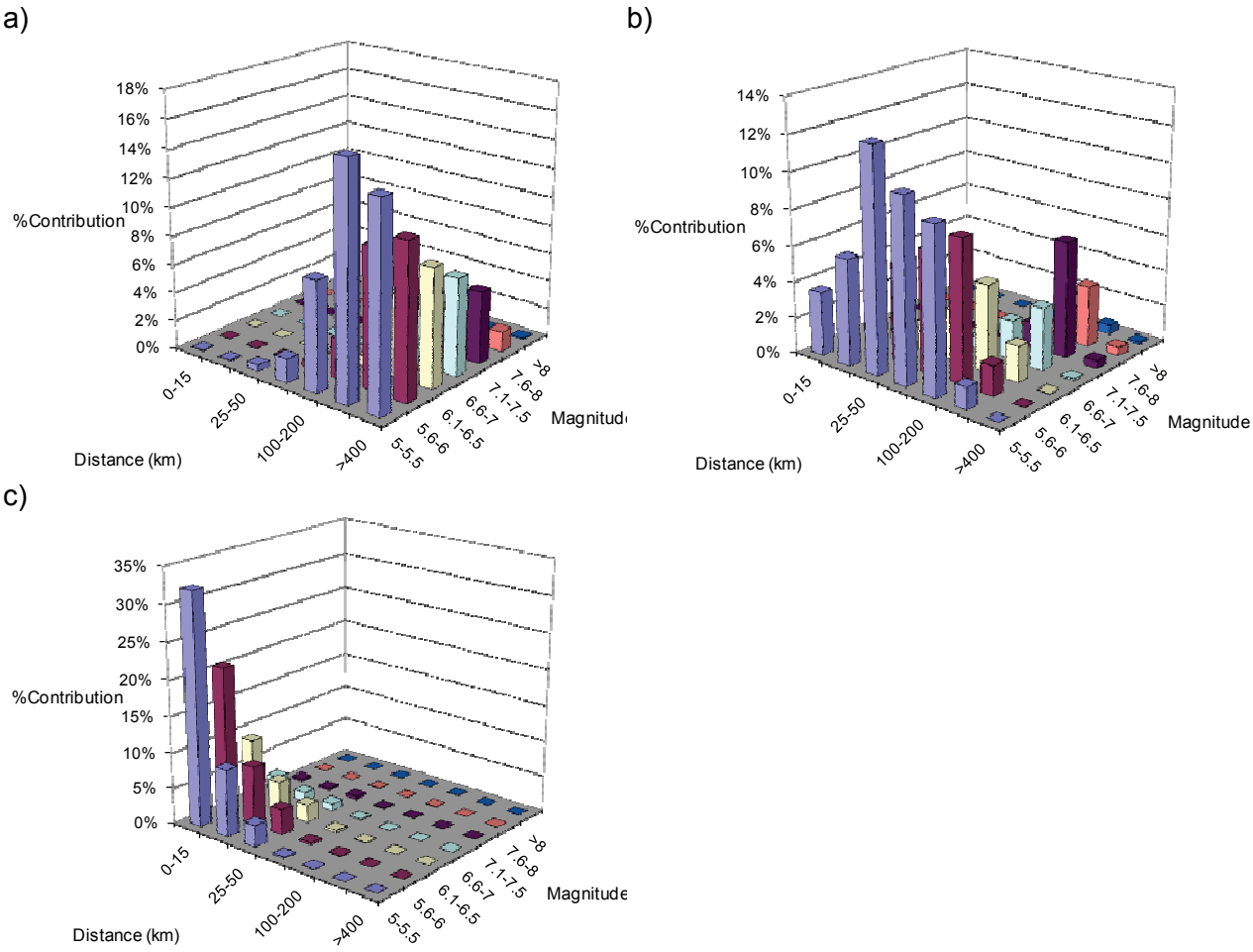

Notes: (a) Deaggregation of the 10^{-2} 10 Hz spectral acceleration hazard; (b) Deaggregation of the 10^{-4} 10 Hz spectral acceleration hazard; (c) Deaggregation of the 10^{-6} 10 Hz spectral acceleration hazard.

Figure 5.11: Deaggregation of the 10 Hz Spectral Acceleration Hazard

Figure 5.16, Figure 5.17 and Figure 5.18 show the contributions of the epistemic uncertainty in the median GMPE to the uncertainty in the hard-rock hazard. For PGA and 10 Hz hazard, the contribution of uncertainty in the median for each of the GMPEs to the overall uncertainty is larger than the contribution from the variability among four GMPEs. For 1 Hz hazard, the reverse is the case.

5.2.2.2 Regional Source Models

Figure 5.19, Figure 5.20 and Figure 5.21 show the effect of the three alternative regional source models on the hazard from regional sources. The hazard results for the seismotectonic branch are shown for the case where kernel smoothing is used and for the case where a uniform spatial distribution is assumed within each source zone. The highest hazard is obtained using a uniform spatial distribution within each seismotectonic source zone. This results from averaging the higher seismicity rates that occur at large distances from the site with the low local rate. The GSC H-Model produces the next highest hazard. This model also uses uniform seismicity rates, but areas of higher seismicity are defined as separate source zones such that the seismicity in the site vicinity represents the average rate over only the lower seismicity areas in southeast Canada. The zoneless approach produces the lowest hazard because it defines a local rate and b-value representing the conditions in the site vicinity, where there are few earthquakes to define the seismicity parameters. The effect of the alternative models for distributed seismicity is larger for PGA and 10 Hz hazard than for 1 Hz hazard because the hazard for these ground motion measures is controlled by the local seismicity.

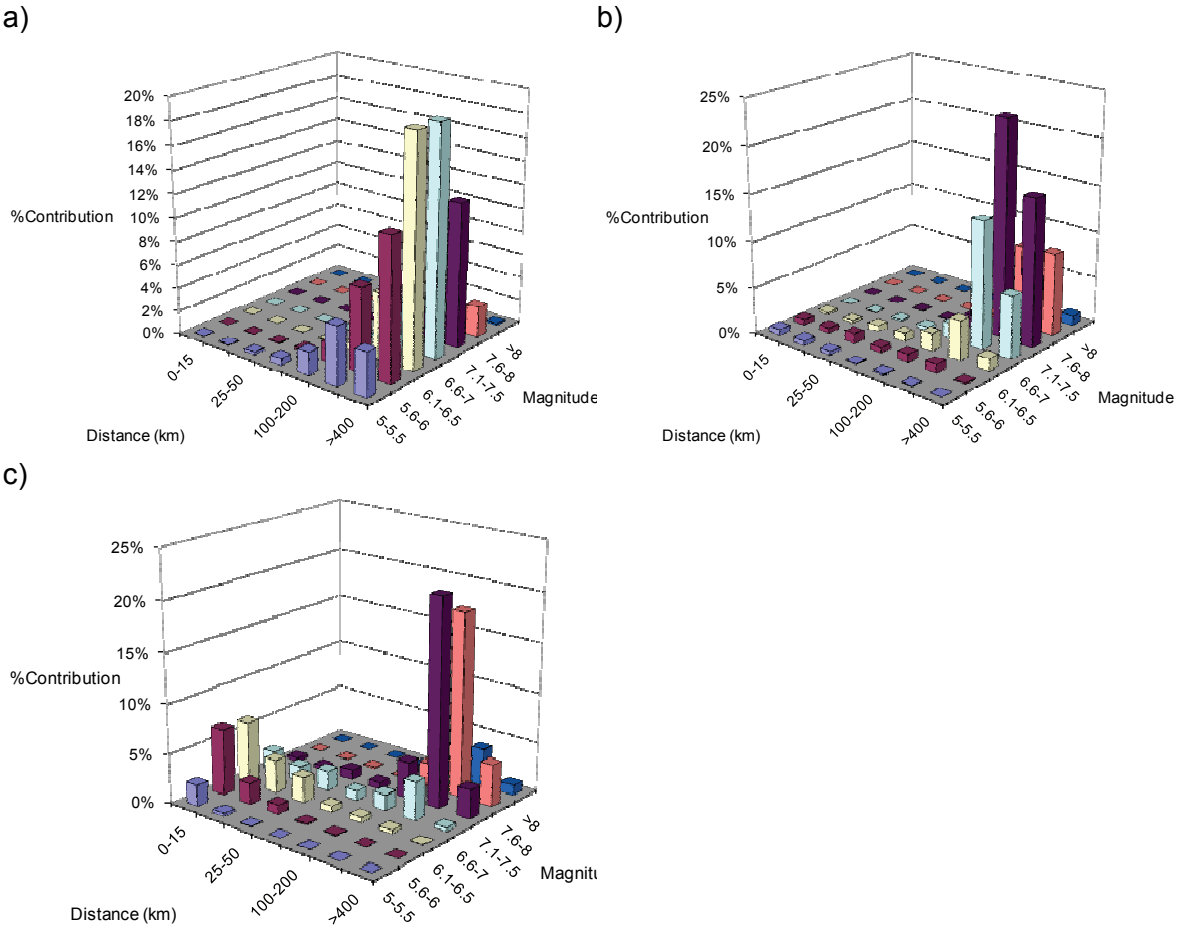

Notes: (a) Deaggregation of the 10^{-2} 1 Hz spectral acceleration hazard; (b) Deaggregation of the 10^{-4} 1 Hz spectral acceleration hazard; (c) Deaggregation of the 10^{-6} 1 Hz spectral acceleration hazard.

Figure 5.12: Deaggregation of the 1 Hz Spectral Acceleration Hazard

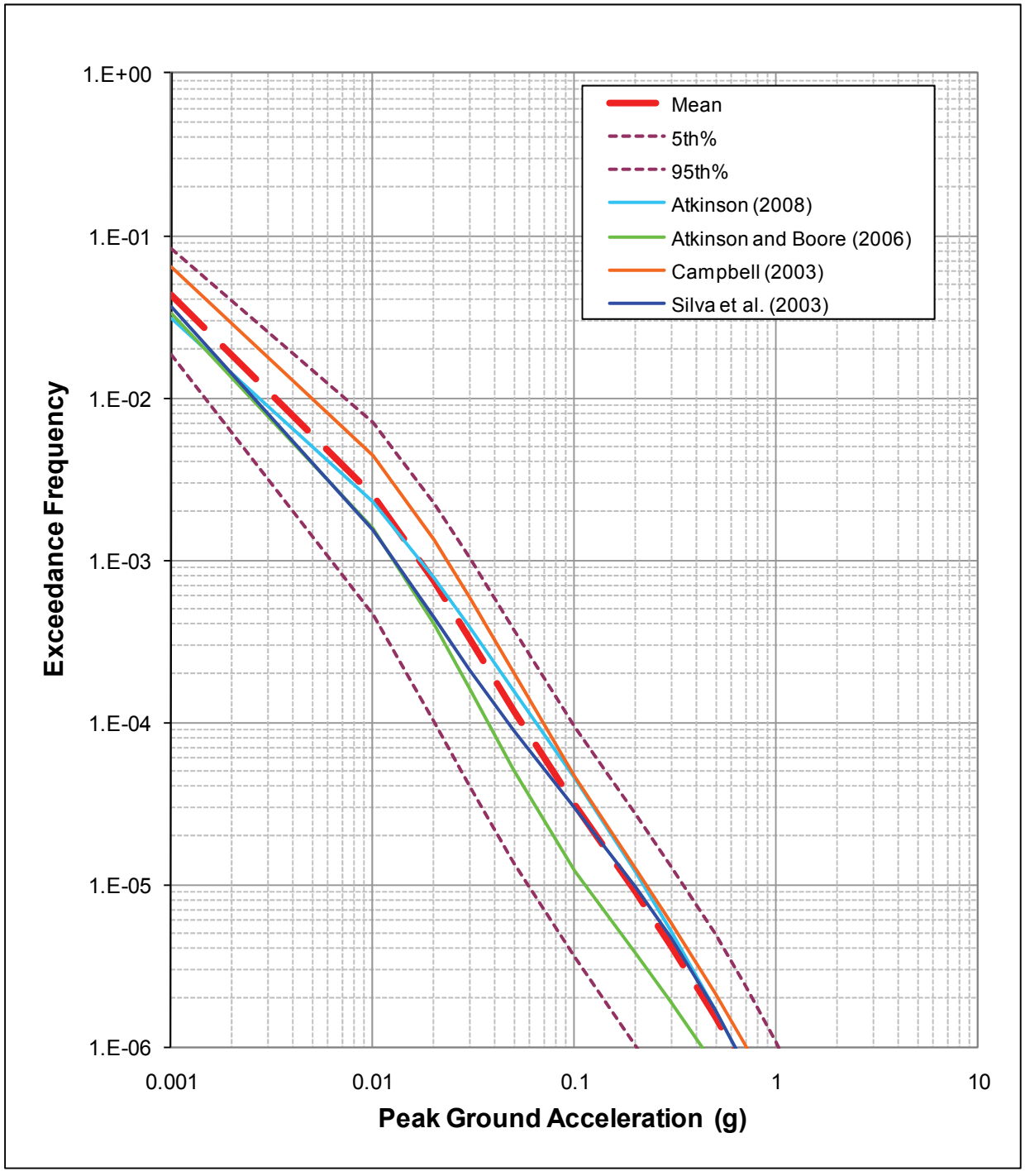

Figure 5.13: Contribution of Alternative Ground-Motion Prediction Equations to the Uncertainty in Peak Ground Acceleration Hazard

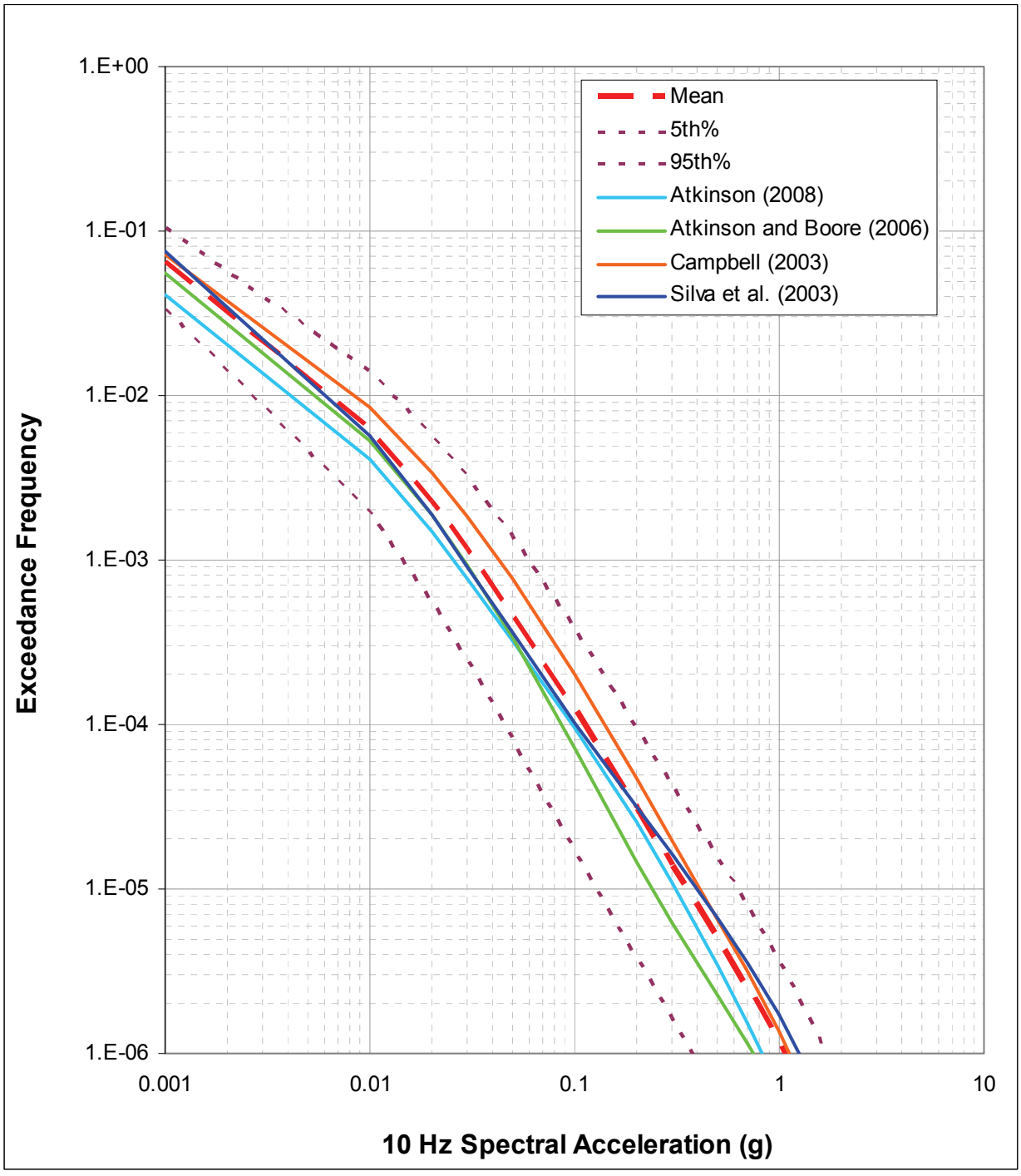

Figure 5.14: Contribution of Alternative Ground-Motion Prediction Equations to the Uncertainty in 10 Hz Spectral Acceleration Hazard

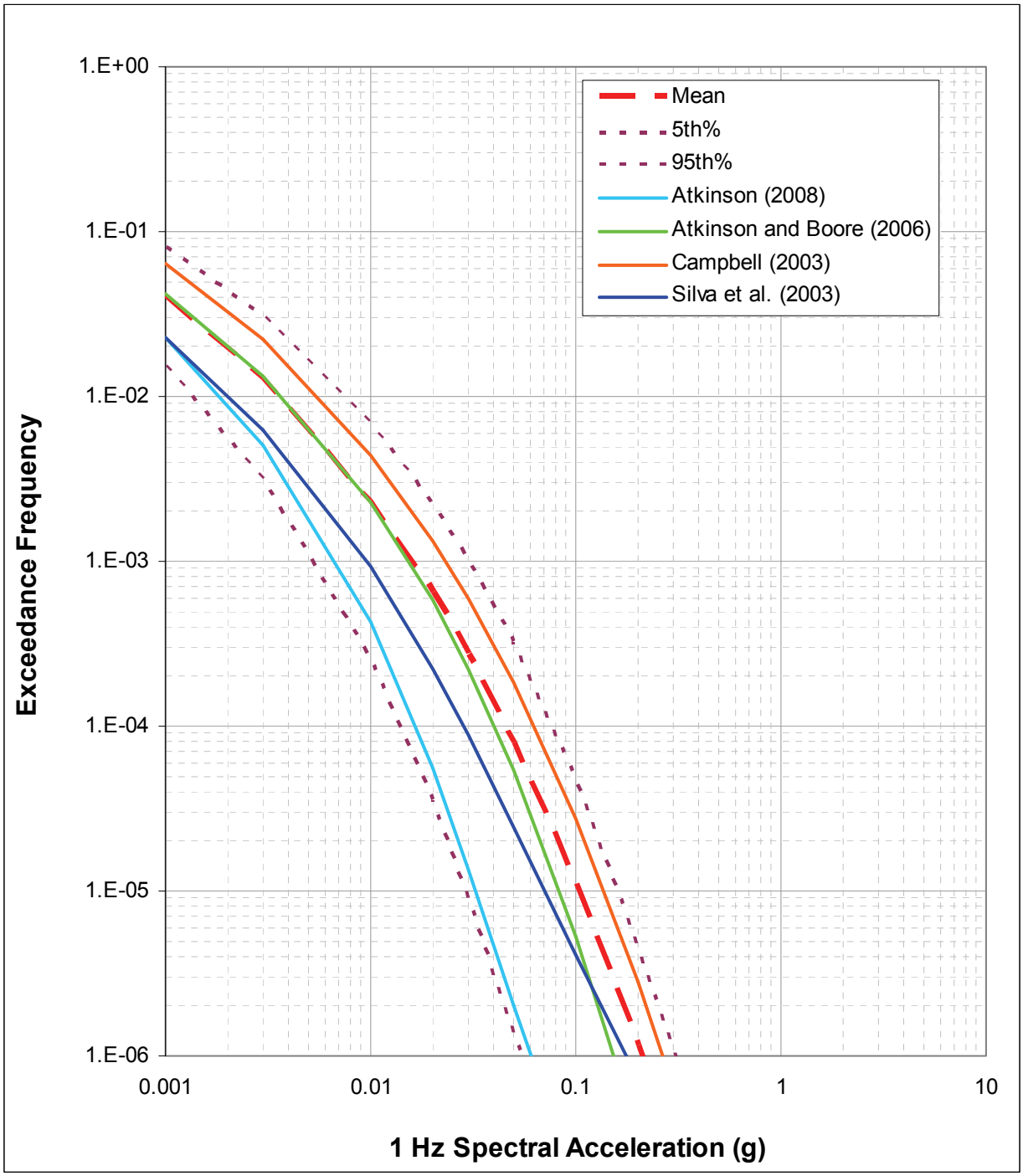

Figure 5.15: Contribution of Alternative Ground-Motion Prediction Equations to the Uncertainty in 1 Hz Spectral Acceleration Hazard

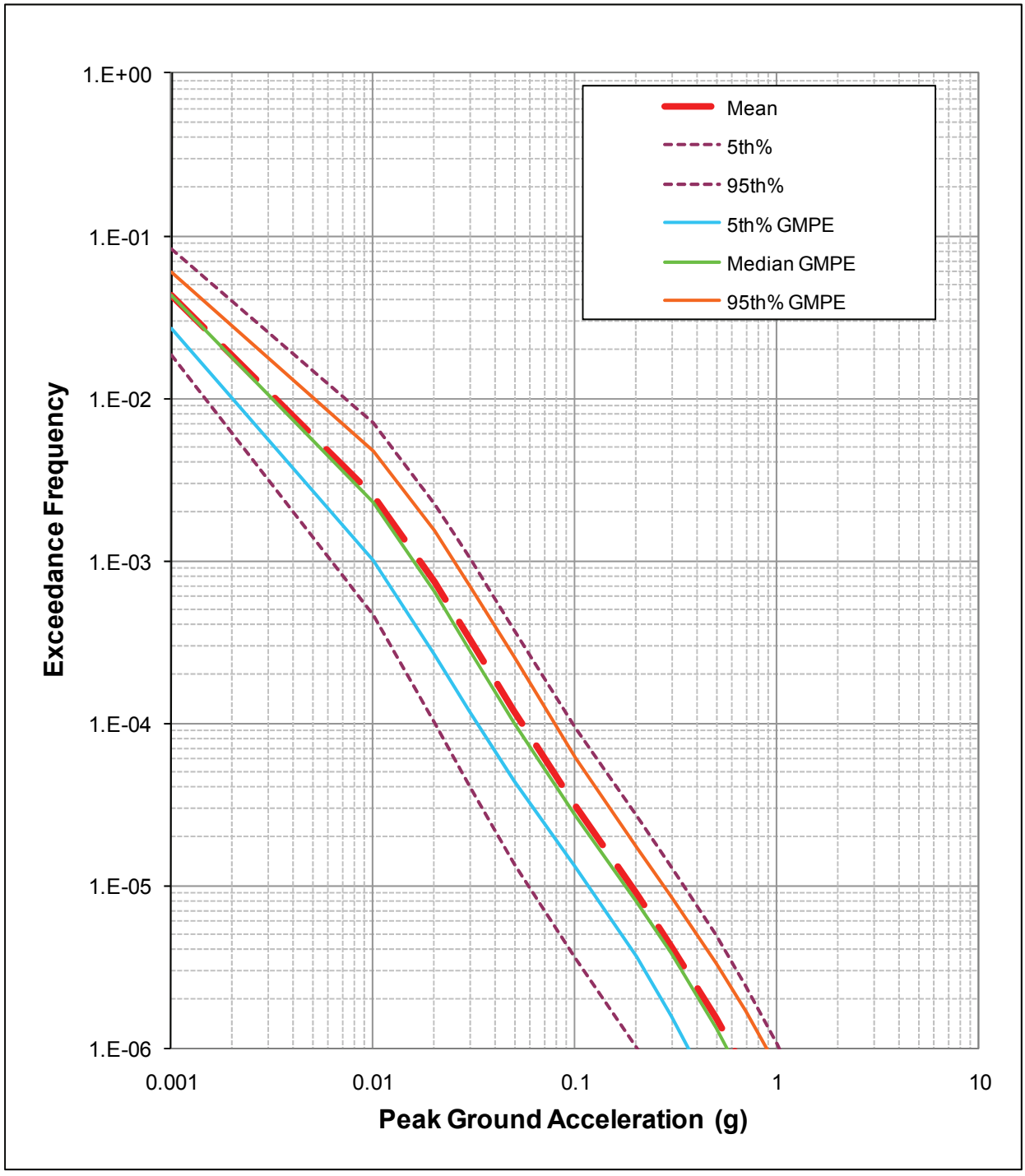

Figure 5.16: Contribution of Uncertainty in the Median Ground-Motion Prediction Equations to the Uncertainty in Peak Ground Acceleration Hazard

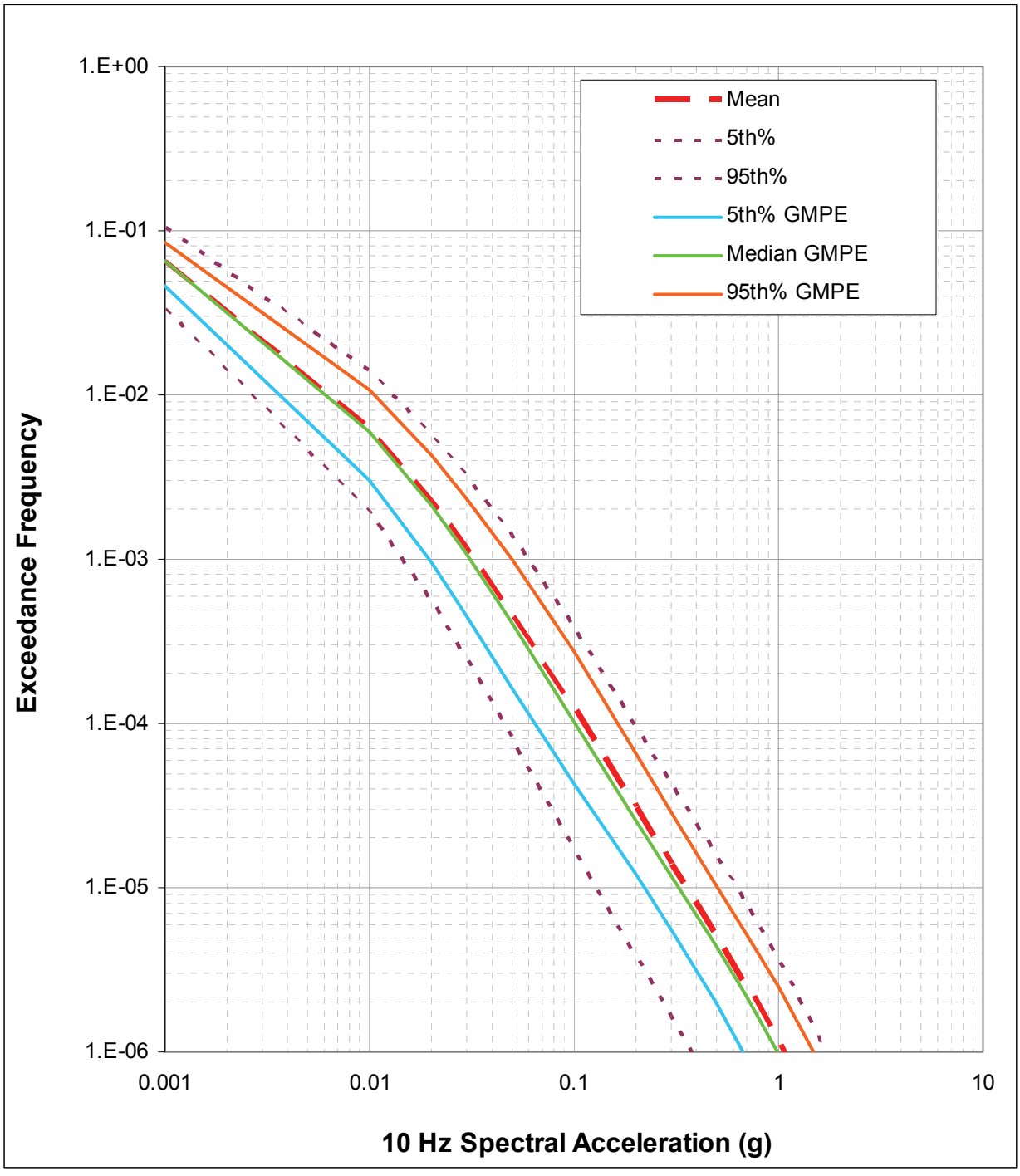

Figure 5.17: Contribution of Uncertainty in the Median Ground-Motion Prediction Equations to the Uncertainty in 10 Hz Spectral Acceleration Hazard

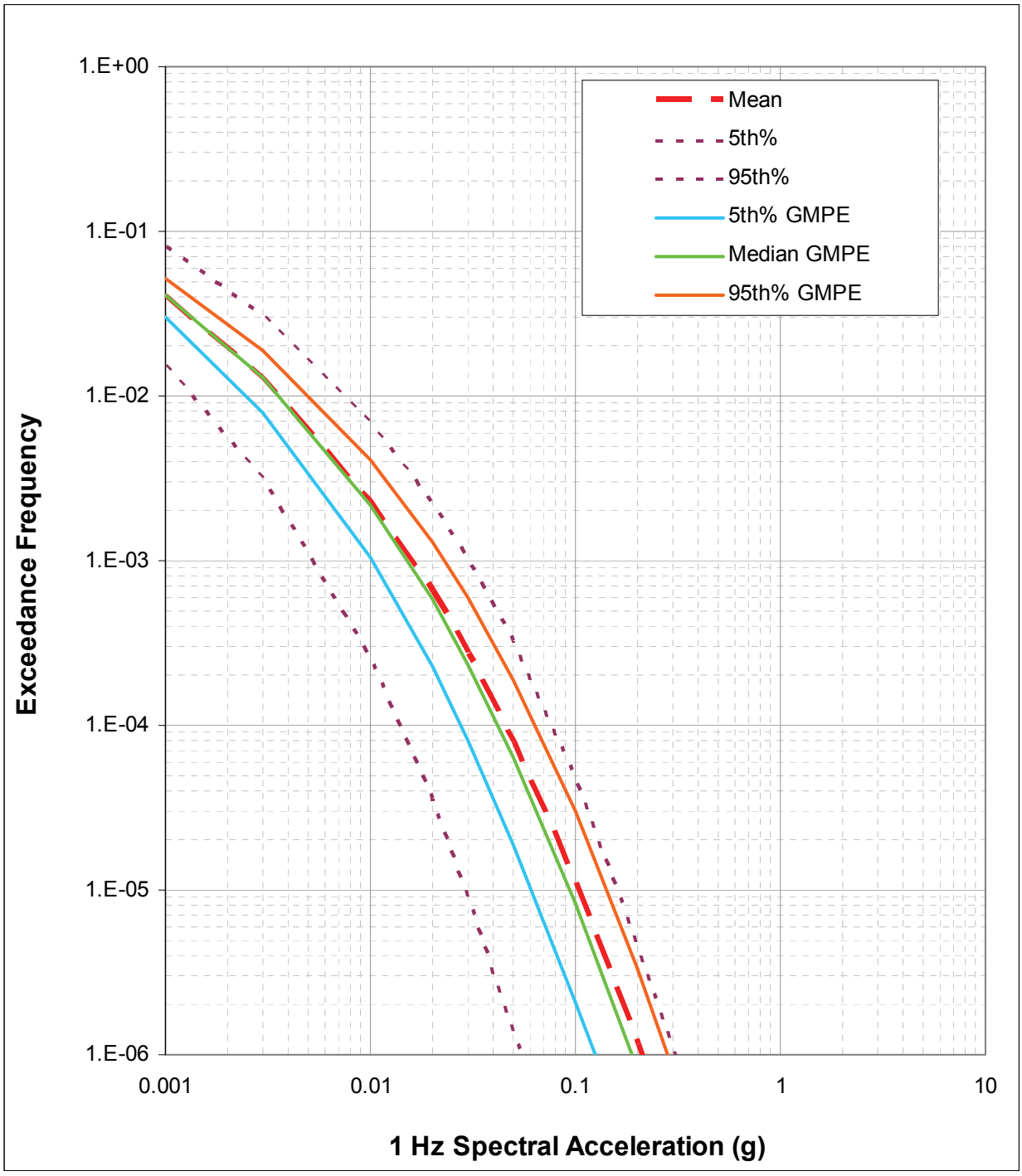

Figure 5.18: Contribution of Uncertainty in the Median Ground-Motion Prediction Equations to the Uncertainty in 1 Hz Spectral Acceleration Hazard

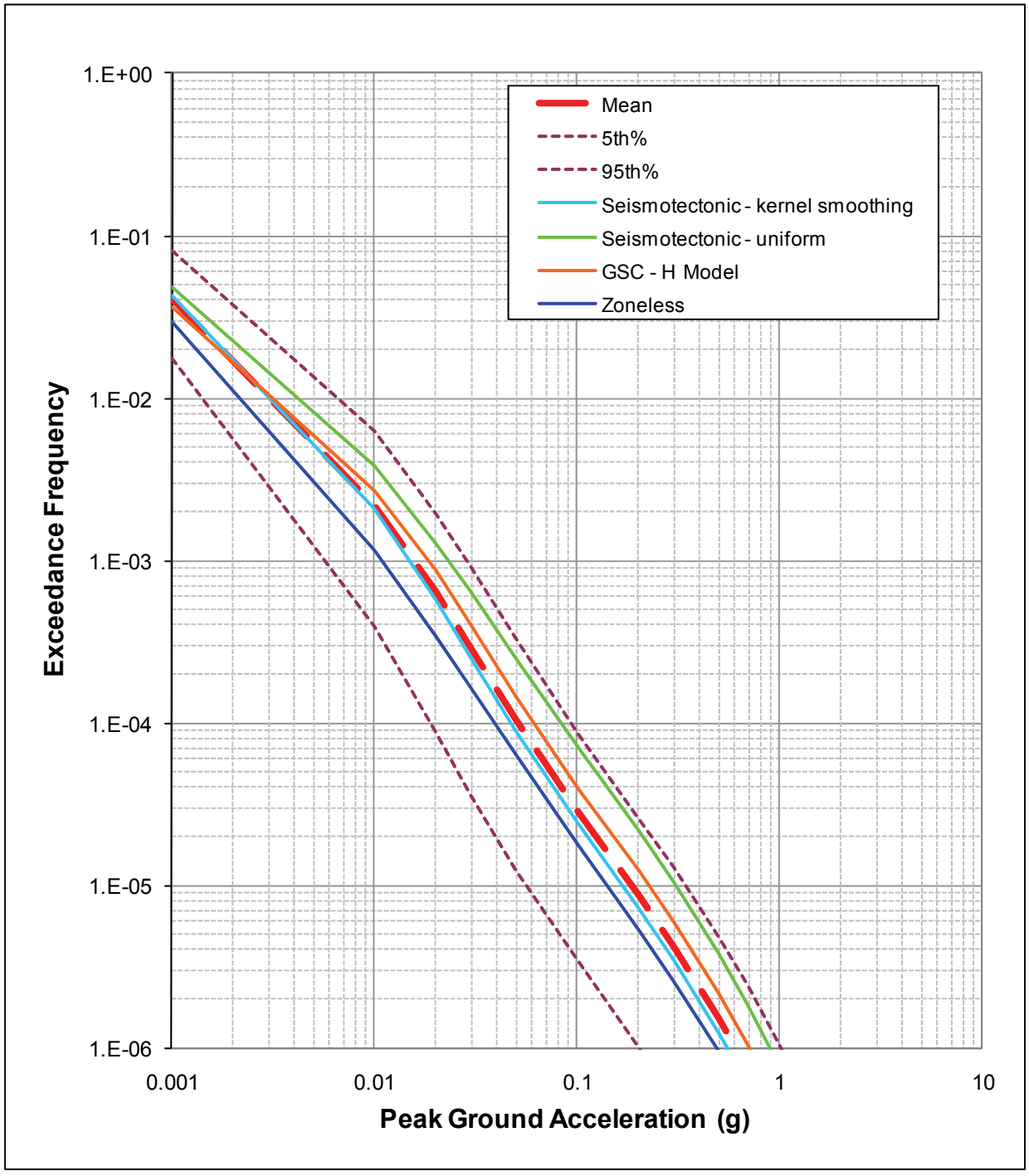

Figure 5.19: Contribution of Alternative Characterizations of Distributed Seismicity to Uncertainty in Hazard from Regional Seismic Sources for Peak Ground Acceleration

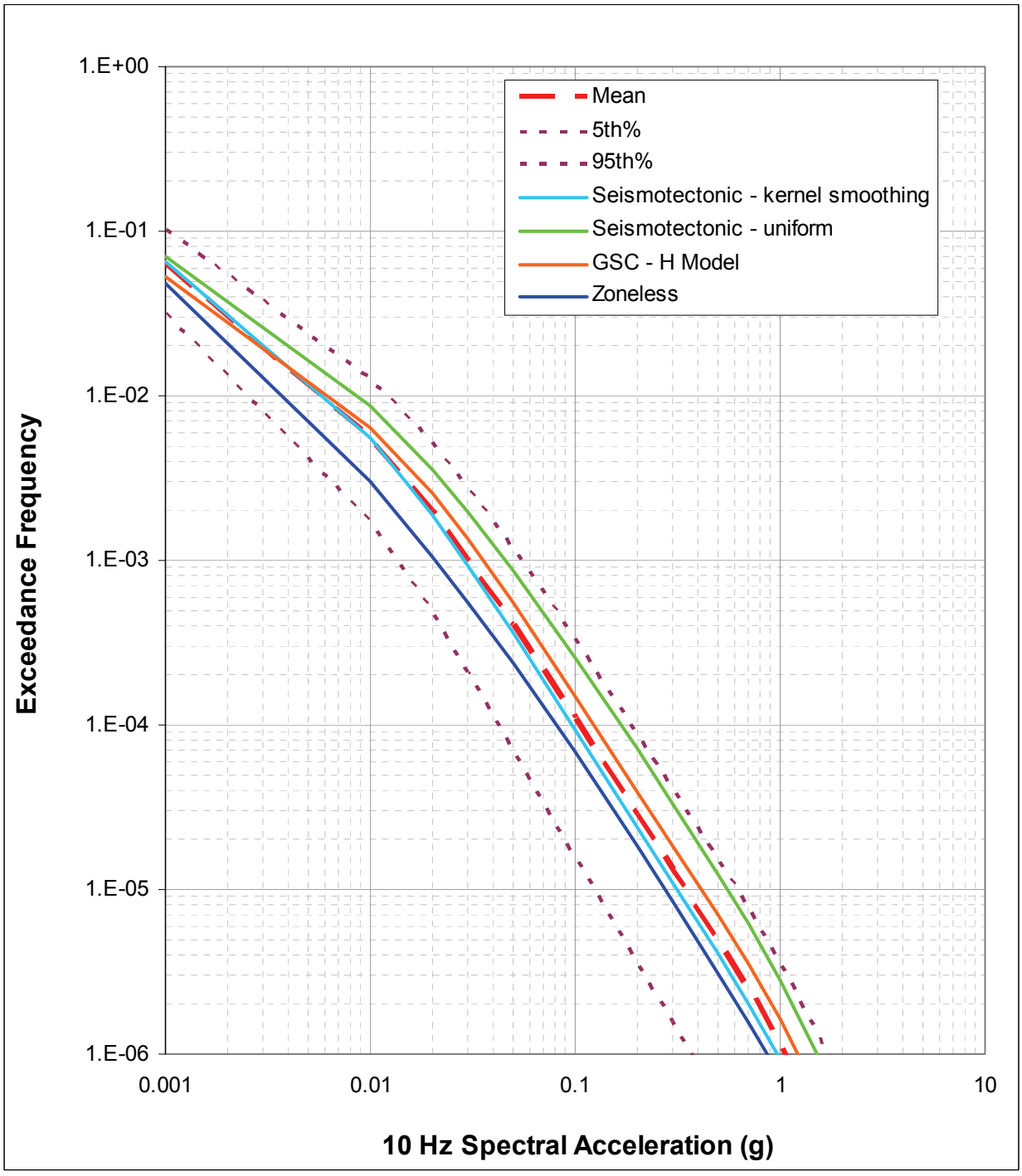

Figure 5.20: Contribution of Alternative Characterizations of Distributed Seismicity to Uncertainty in Hazard from Regional Seismic Sources for 10 Hz Spectral Acceleration

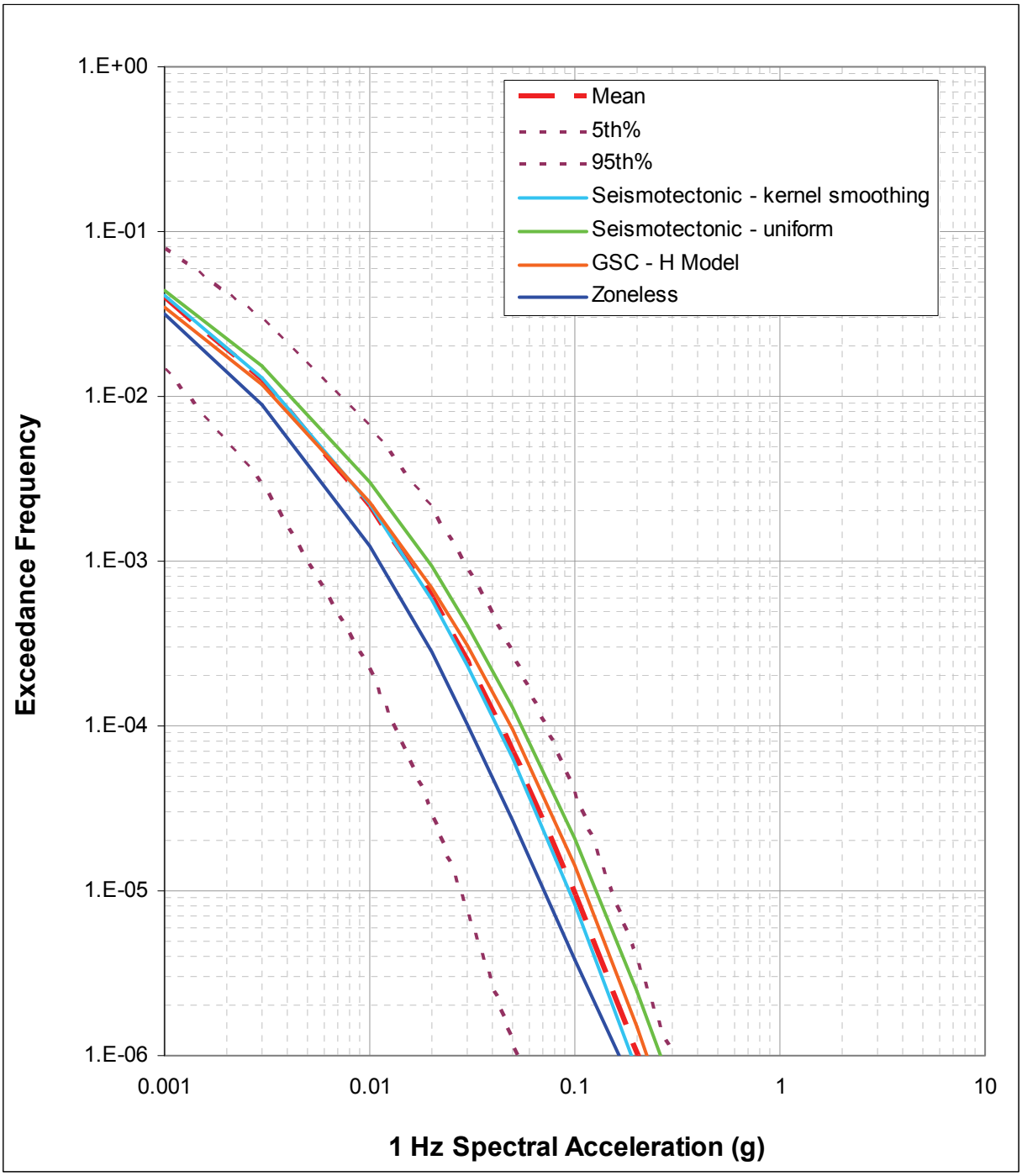

Figure 5.21: Contribution of Alternative Characterizations of Distributed Seismicity to Uncertainty in Hazard from Regional Seismic Sources for 1 Hz Spectral Acceleration

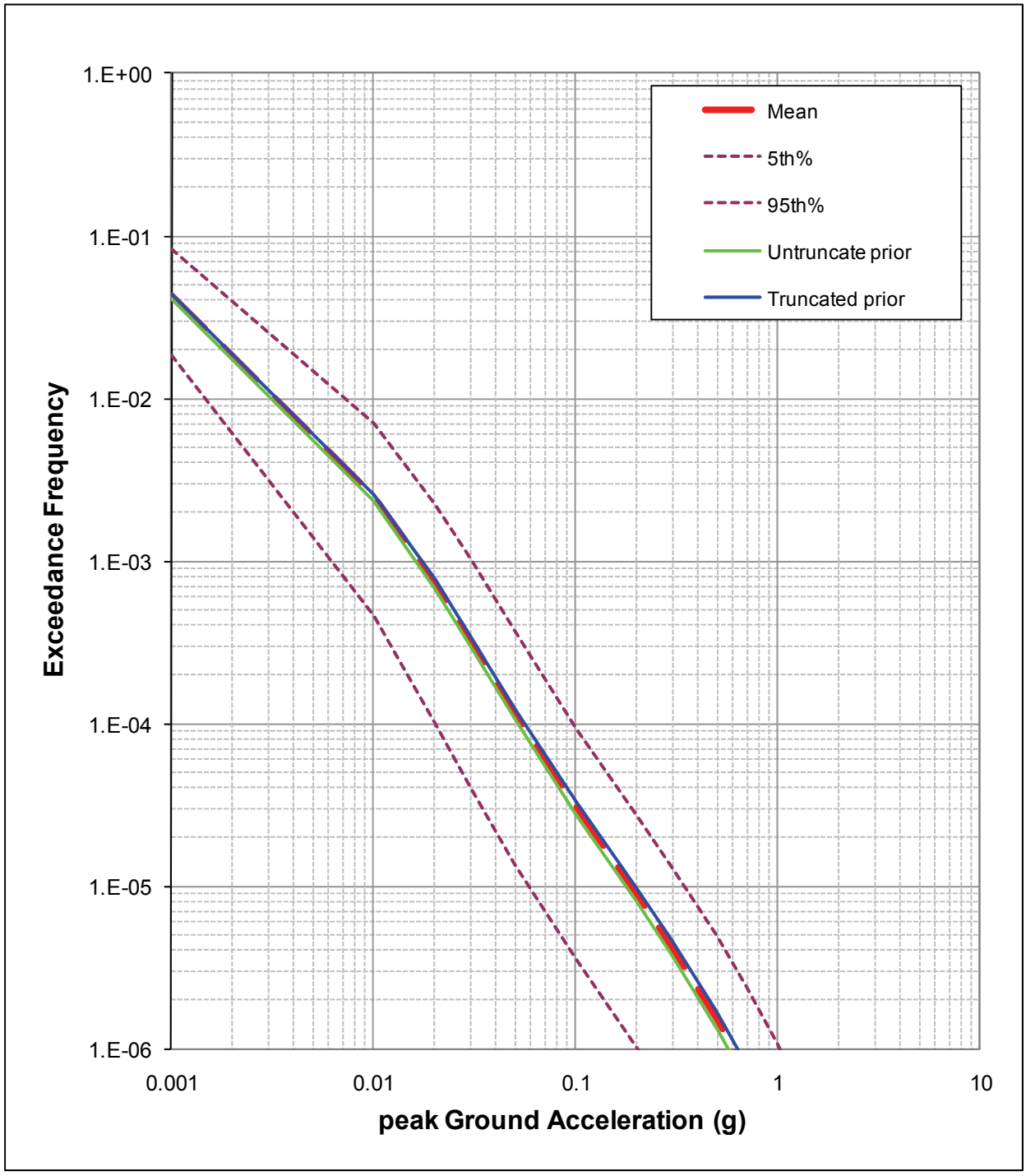

Figure 5.22: Effect of Alternative Prior Distributions for Maximum Magnitude on Total Hazard for Peak Ground Acceleration

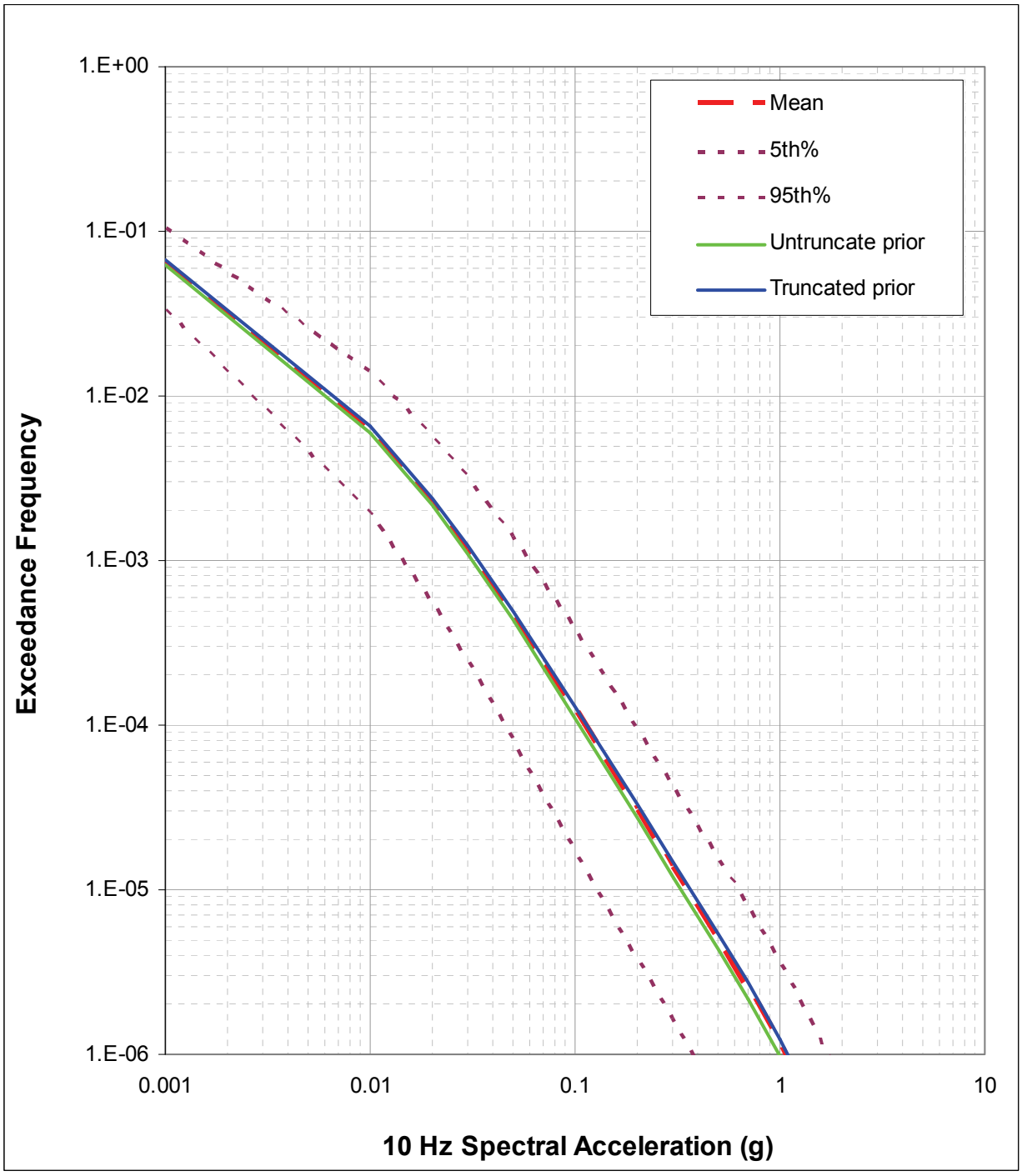

Figure 5.23: Effect of Alternative Prior Distributions for Maximum Magnitude on Total Hazard for 10 Hz Spectral Acceleration

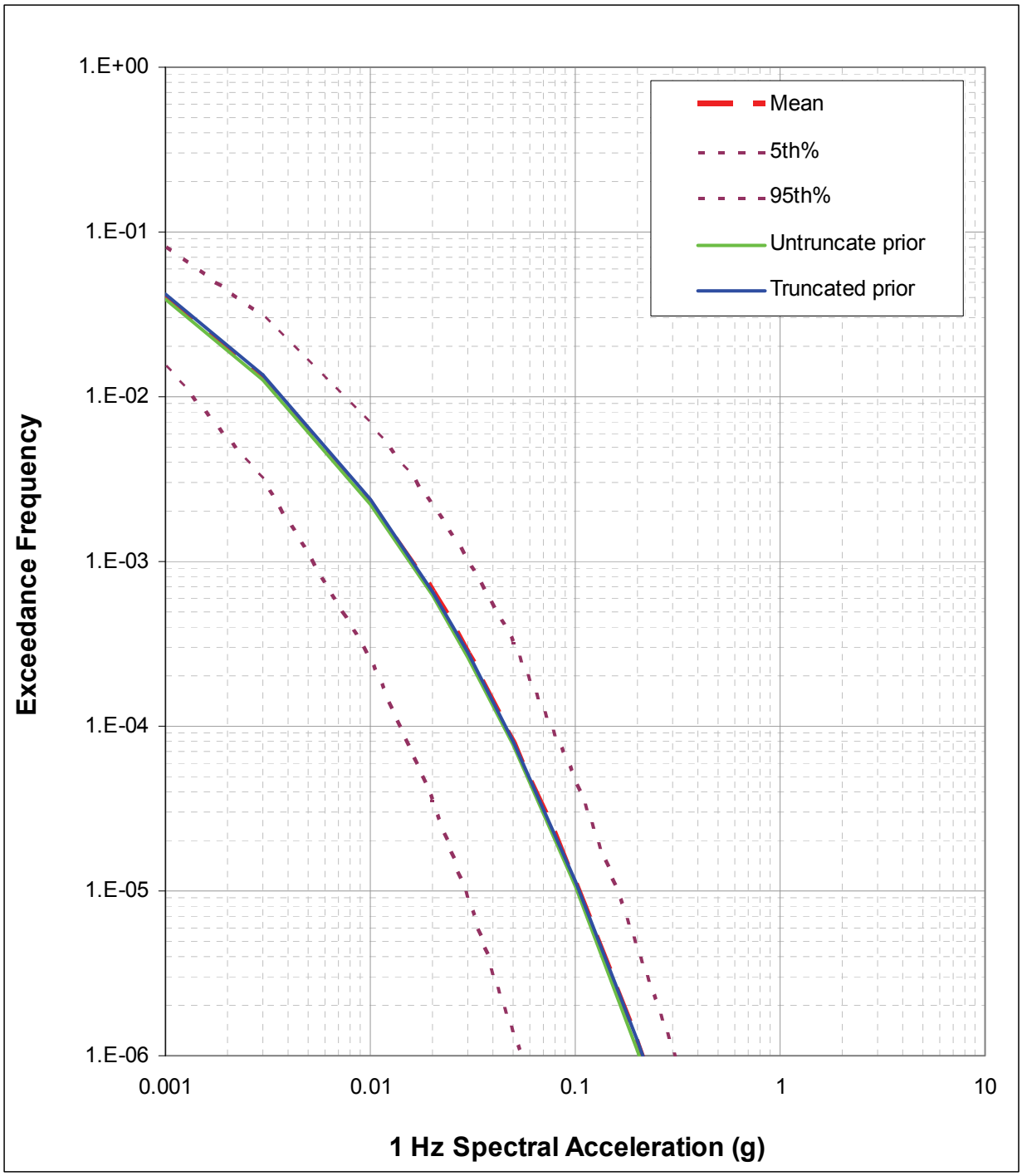

Figure 5.24: Effect of Alternative Prior Distributions for Maximum Magnitude on Total Hazard for 1 Hz Spectral Acceleration

5.2.2.3 Maximum Magnitude Prior

Figure 5.22, Figure 5.23 and Figure 5.24 show the impact of the alternative prior distributions used to develop maximum magnitude distributions on the computed total hazard. Two

alternatives are used, an untruncated prior and a prior that is truncated in the lower tail to limit the maximum magnitudes to **M** 6 and larger. There is little difference in the hazard computed from these two models.

5.2.2.4 Local Source Model

The largest source of uncertainty related to the local sources is the question of whether an individual local source is seismogenic. The hazard results for the individual sources shown on Figure 5.7, Figure 5.8 and Figure 5.9 are weighted mean hazard curves. The mean frequency of exceedance at any ground motion level is directly proportional to the probability the source is seismogenic. Thus changing the probability that an individual source is seismogenic would produce a corresponding change in the mean hazard from the source. The effect of an increase in the probability of activity would be partially offset by the fact that the earthquakes spatially associated with the source would no longer be used to estimate the seismicity rate in the surrounding regional seismic sources.

Two alternatives were considered for modelling the characteristics of the local sources. One approach was to consider that the local sources act as concentrations of seismicity in the regional zones and thus have the attributes of the host regional zone. Under this assumption, the magnitude distribution was assumed to conform to a truncated exponential distribution appropriate for regions, and the maximum magnitude distribution was assumed to be the same as that of the regional zone in which the source lies.

The other approach was to assume that the local sources act truly as individual faults with unique individual attributes. Under the fault-like assumption, the magnitude distribution was assumed to conform to the “characteristic” magnitude model (Youngs and Coppersmith 1985), and the maximum magnitude distribution was estimated from postulated maximum rupture dimensions. Consideration of fault-like behaviour resulted in larger maximum magnitudes and a much higher predicted frequency of large events. As a result, the alternative modelling assumptions for the local sources have a major impact on the hazard from these sources, as illustrated on Figure 5.25, Figure 5.26 and Figure 5.27. The 5th percentile hazard from local sources does not appear on these plots because the combined probability that none of them are active is greater than 5 percent.

5.2.2.5 Summary of Contributions to Uncertainty

Figure 5.28, Figure 5.29 and Figure 5.30 present the contributions to the uncertainty in the computed hazard resulting from the uncertainties in the various components of the PSHA model. Each plot shows the percentage of the total variance in the computed frequency of exceedance contributed by the uncertainty in each of the model components. These results, which are presented for 10^{-2}, 10^{-4} and 10^{-6} annual frequencies of exceedance, indicate that uncertainty in the ground motion models is the largest contributor to uncertainty in the computed hazard. The aspects of seismic source characterization that have the largest contribution to uncertainty in the hazard are the alternative spatial distribution models used for the seismotectonic sources and uncertainty in the maximum magnitude and b-value.

5.2.2.6 Hard Rock UHRS

The mean hazard results for the nine spectral frequencies were interpolated to obtain pgs at annual exceedance frequencies (AEFs) from 10^{-2} to 10^{-8}. The resulting values form UHRS representing ground motions on an outcrop of generic hard rock. Figure 5.31 shows the resulting UHRS and the spectral accelerations are listed in Table 5.1. The shape of the 10^{-2}

AEF spectrum is indicative of the large contribution of distant sources to the hazard at all spectral frequencies. As the exceedance frequency decreases, the UHRS become more peaked, reflecting increasing contribution of nearby smaller earthquakes to the hazard.

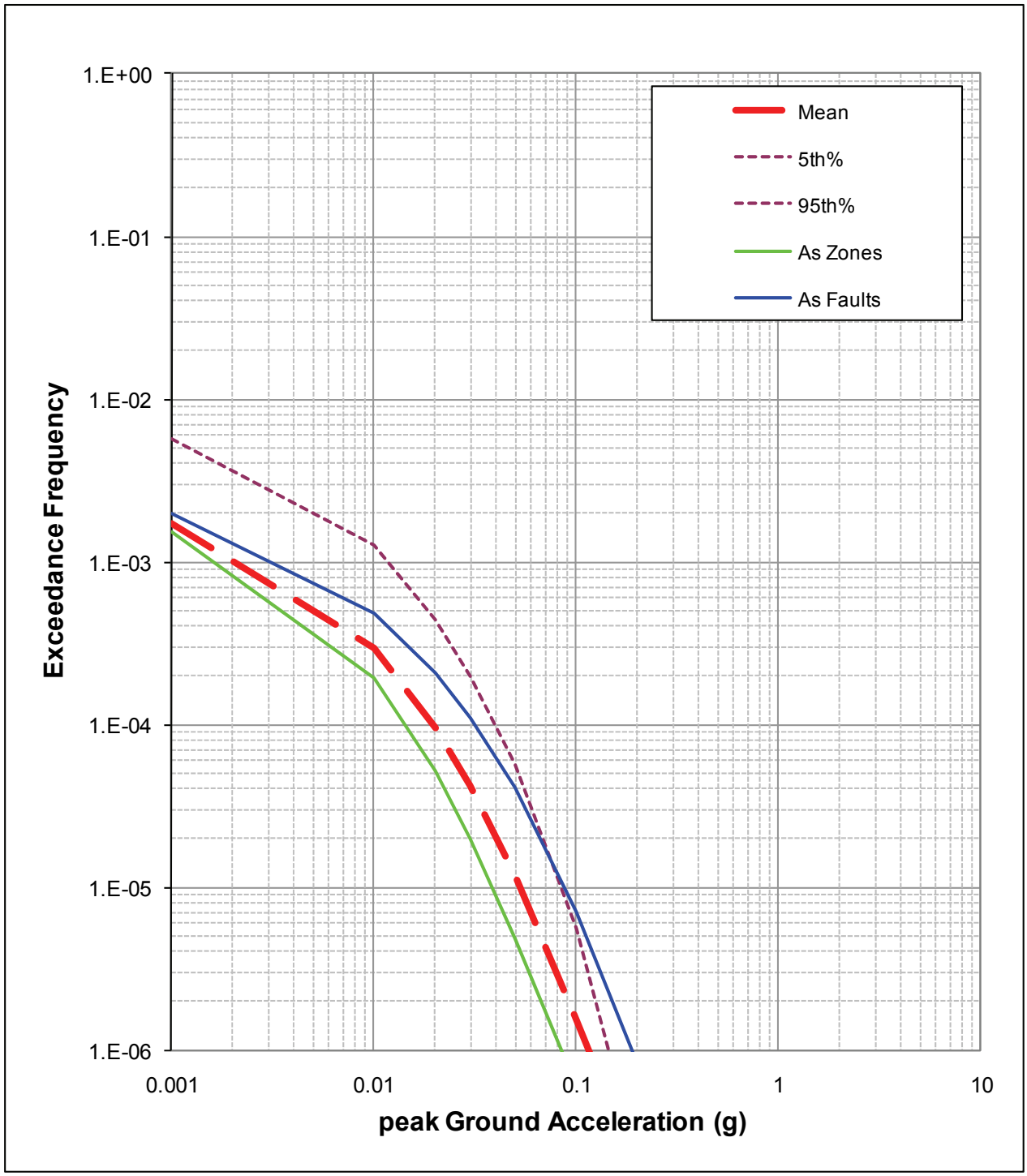

Figure 5.25: Effect of Characterization of Local Sources as Either Zones or Faults on the Peak Ground Acceleration Hazard from Local Sources

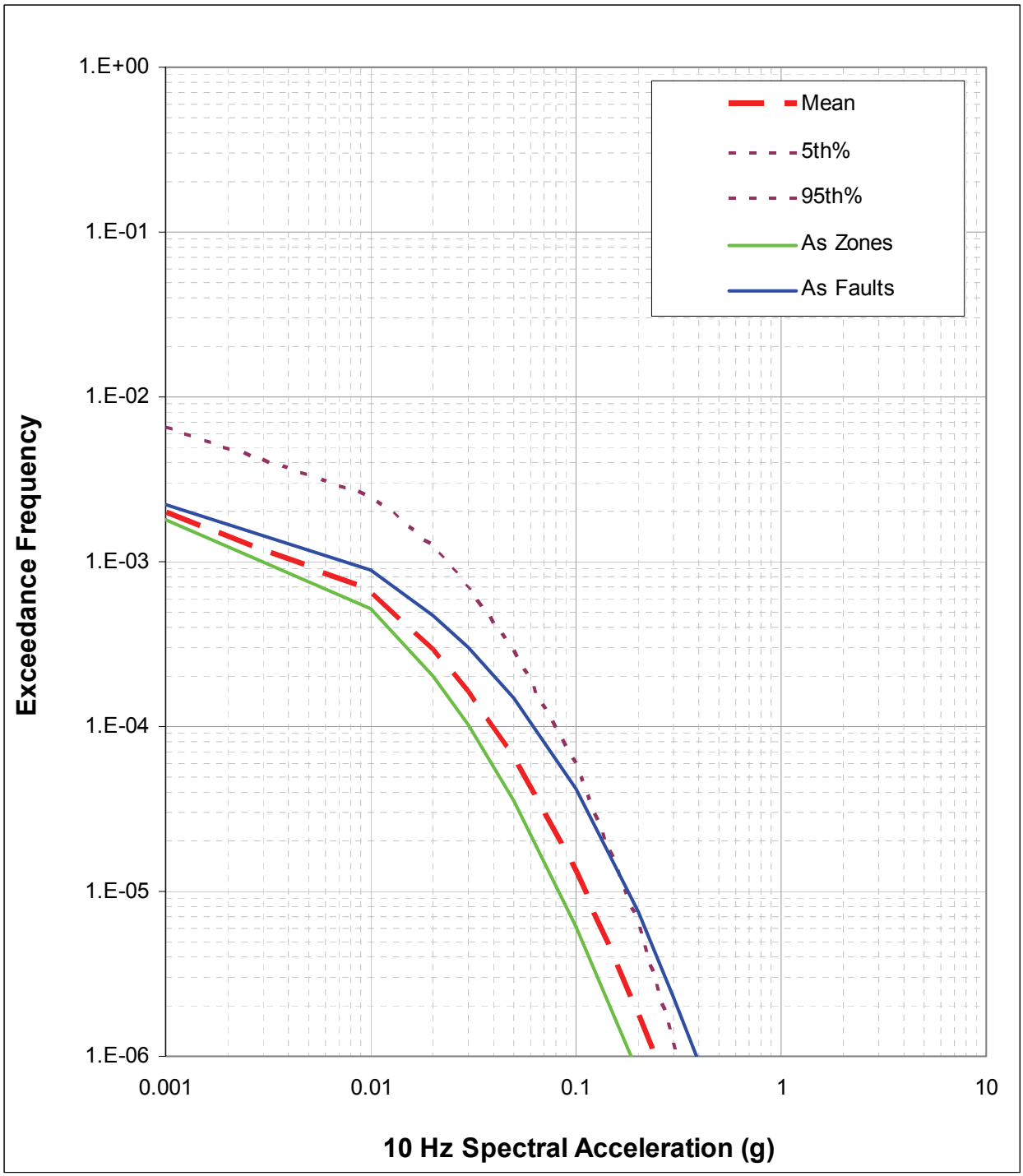

Figure 5.26: Effect of Characterization of Local Sources as Either zones or Faults on the 10 Hz Spectral Acceleration Hazard from Local Sources

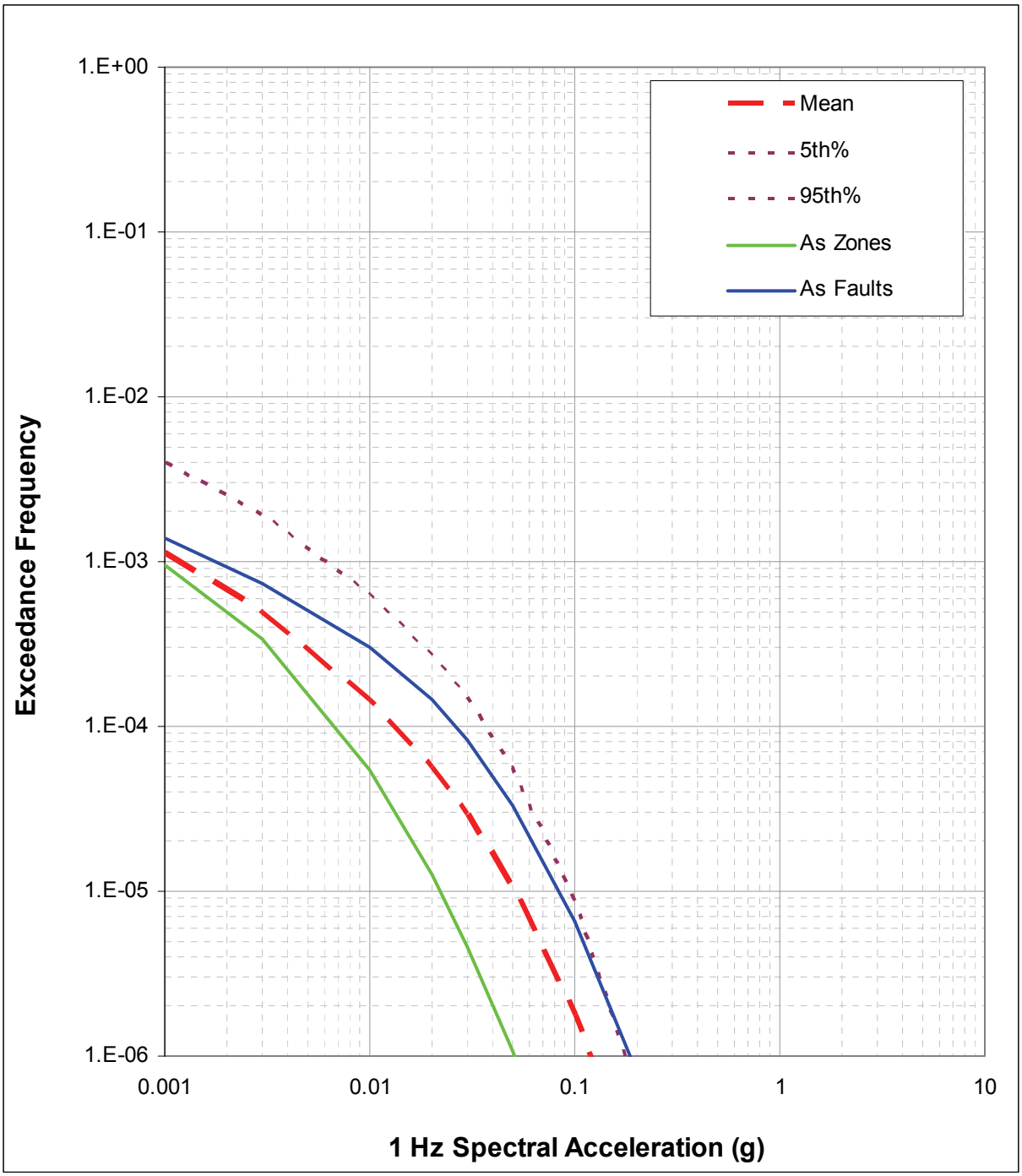

Figure 5.27: Effect of Characterization of Local Sources as Either Zones or Faults on the 1 Hz Spectral Acceleration Hazard from Local Sources

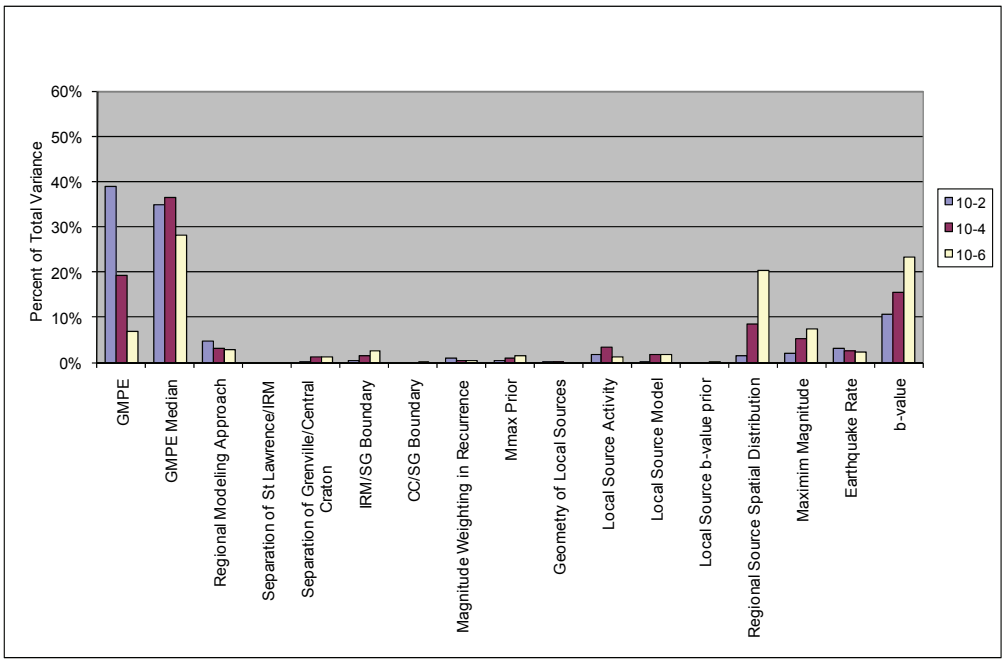

Note: Analysis is done for exceedance frequencies of 10^{-2}, 10^{-4}, and 10^{-6}.

Figure 5.28: Contributions of Uncertainty in Model Inputs to Total Variance in Peak Ground Acceleration Hazard

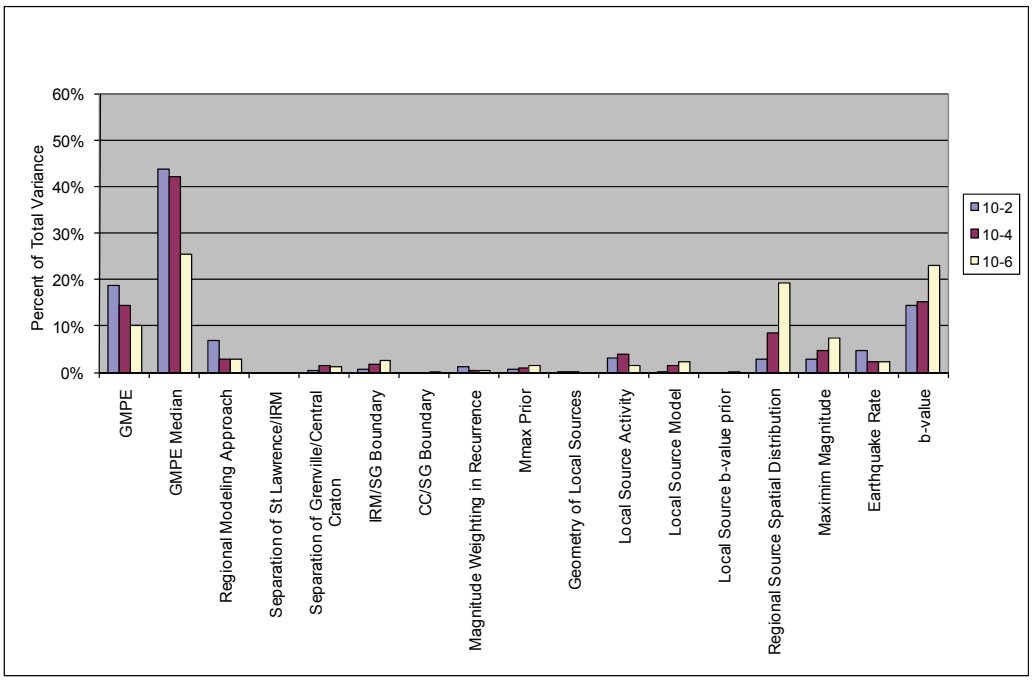

Note: Analysis is done for exceedance frequencies of 10^{-2}, 10^{-4}, and 10^{-6}.

Figure 5.29: Contributions of Uncertainty in Model Inputs to Total Variance in 10 Hz Spectral Acceleration Hazard

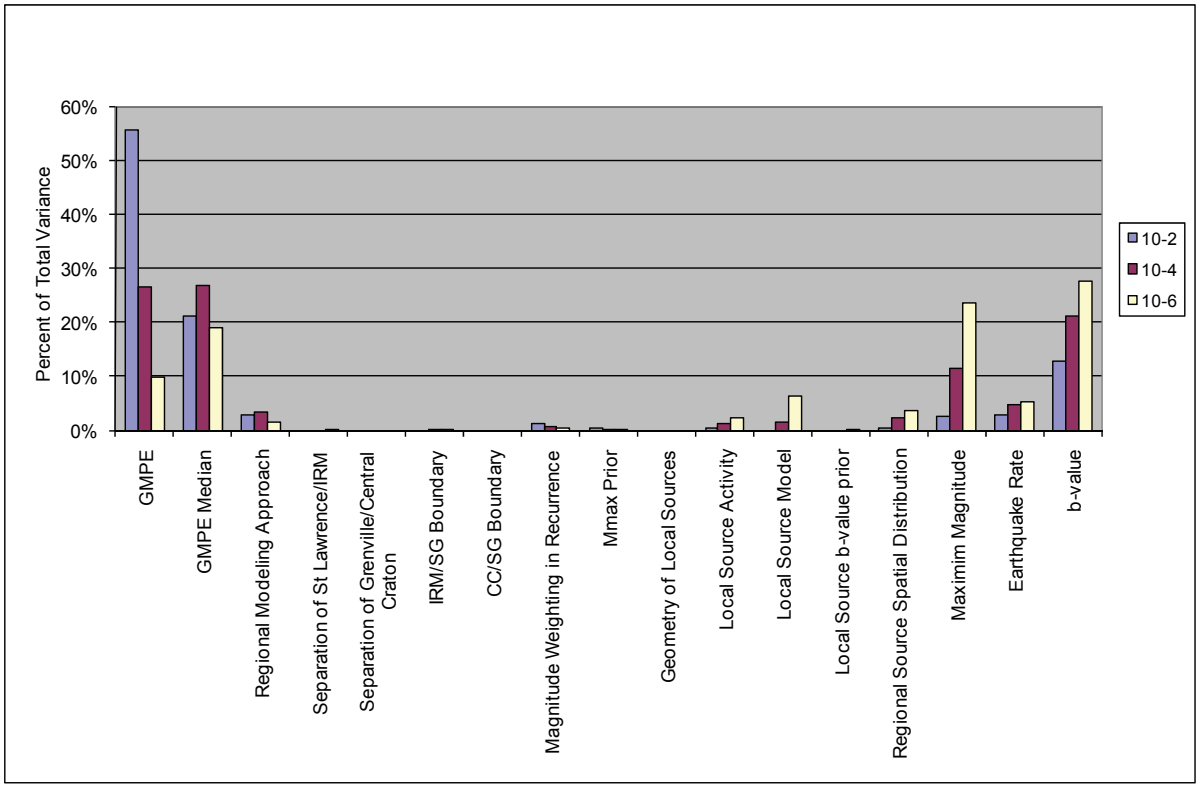

Note: Analysis is done for exceedance frequencies of 10^{-2}, 10^{-4}, and 10^{-6}.

Figure 5.30: Contributions of Uncertainty in Model Inputs to Total Variance in 1 Hz Spectral Acceleration Hazard

5.2.2.7 Comparison with National Building Code of Canada Seismic Hazard Values

The UHRS for the reference hard rock site conditions for an annual exceedance frequency of $4x10^{-4}$ (return period of 2,500 years) is compared with the hazard values reported for the National Building Code of Canada (Halchuk and Adams 2008) on Figure 5.32. The values reported in (Halchuk and Adams 2008) are for site conditions C. These values were adjusted to hard rock conditions using the amplification factors listed in Table 2 of Adams and Halchuk (2003). The NBCC seismic hazard values are based on PSHA calculations performed using the quadratic ground motion model published in Atkinson and Boore (1995). As shown on Figure 4.6 and Figure 4.7, the Atkinson and Boore (1995) quadratic ground motion model predicts generally higher ground motions at high frequencies than the more recent models used in this study. To examine this effect, the seismic hazard values for the Bruce nuclear site were recomputed using the Atkinson and Boore (1995) quadratic ground motion model. The resulting $4x10^{-4}$ annual exceedance frequency UHRS is shown on Figure 5.32. The computed values are close to those reported for the NBCC. Thus, the differences in hazard results between the two studies are attributed primarily to differences in the ground motion models. The ground motion models used in this

study represent more recent updates of the models used to develop the 2005 NBCC hazard maps.

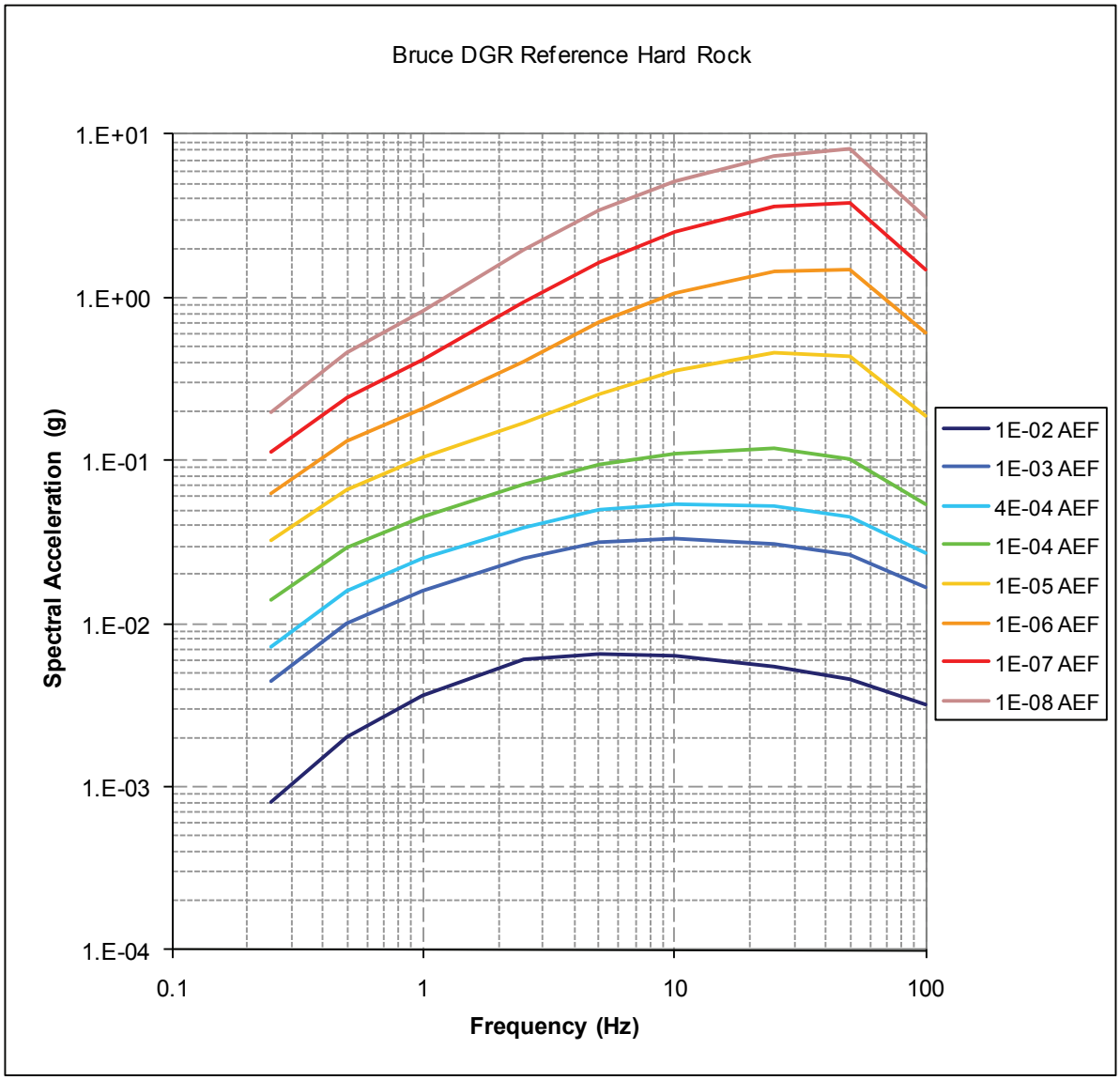

Figure 5.31: Uniform Hazard Response Spectra for Horizontal Motions on Reference Hard-Rock Site Conditions (5% damping)

5.3 Site-Specific PSHA and Development of Design Ground Motions

5.3.1 Characterization of the Bruce Nuclear Site and Reference Sites

The development of the site-specific hazard requires performing site response analyses using the dynamic properties of the Bruce nuclear site and the reference site. The required data are

the shear- and compressional-wave velocities as well as the strain-dependent modulus and hysteretic damping relationships for the subsurface materials.

5.3.1.1 Site-Specific Profiles

The Bruce nuclear site profile consists of a shallow, stiff Pleistocene soil layer of varying thickness overlying firm to hard sedimentary rock composed largely of dolomites, shales and limestones. The sedimentary rock column extends to a depth of approximately 860 m, where it is underlain by Precambrian granitic gneiss basement (Sterling 2010), as illustrated on Figure 5.33. The proposed repository horizon is located at a depth of approximately 680 m (Figure 5.33), with the site having a lateral extent of approximately 1 to 2 km.

Table 5.1: Uniform Hazard Response Spectra for Bruce Nuclear Site

Spectral Frequency (Hz)	Spectral Acceleration (g) for AEF of:							
	1.E-02	1.E-03	4.E-04	1.E-04	1.E-05	1.E-06	1.E-07	1.E-08
100	0.0032	0.0167	0.0272	0.0544	0.1869	0.6058	1.4710	3.0673
50	0.0046	0.0262	0.0456	0.1031	0.4352	1.4928	3.8344	8.1048
25	0.0054	0.0307	0.0531	0.1185	0.4548	1.4414	3.5721	7.3914
10	0.0063	0.0330	0.0545	0.1107	0.3532	1.0550	2.5385	5.2015
5	0.0066	0.0314	0.0501	0.0940	0.2557	0.7023	1.6560	3.3966
2.5	0.0060	0.0251	0.0391	0.0706	0.1709	0.4018	0.9284	1.9378
1	0.0036	0.0158	0.0251	0.0454	0.1034	0.2090	0.4100	0.8148
0.5	0.0020	0.0101	0.0160	0.0296	0.0660	0.1309	0.2450	0.4592
0.25	0.0008	0.0044	0.0073	0.0139	0.0322	0.0626	0.1133	0.1967

Note: Analysis is for reference hard rock conditions (5% damping).

As part of the site characterization, boreholes were drilled and compressional- and shear-wave velocities measured at five locations, DGR-1 through 4 and US-3, as shown on Figure 5.33. At boreholes DGR-1 through 4, velocities were determined by suspension log (Pehme and Melaney 2010), while at the shallow US-3 borehole, the downhole method was used. In the first step, to develop base-case profiles, the suspension log profiles were smoothed and plotted with the shallow downhole profile as shown on Figure 5.34 for both shear and compressional waves. The comparison of the smoothed suspension log profiles revealed little lateral variability as well as general consistency with the shallow downhole profiles. In the second step, to develop the base-case shear- and compressional-wave profiles, the smoothed profiles were averaged with equal weights, as illustrated on Figure 5.35. The very high shear-wave velocity approaching 4,500 m/sec at a depth near 50 m seen in the downhole profile (Figure 5.34) was considered a very local feature and averaged with the shallowest suspension log profile (Figure 5.34). Finally, the base-case profiles shown on Figure 5.35 were developed as a sequence of constant velocity layers to capture the significant changes in velocity with depth while maintaining the travel times of the average profiles (Figure 5.35). As an additional constraint in developing the layered profiles, Poisson

ratios of the base-case profiles were examined for general consistency with those of the smoothed profiles. The base-case shear- and compressional-wave velocities are listed in Table 5.2 along with the layer thicknesses.

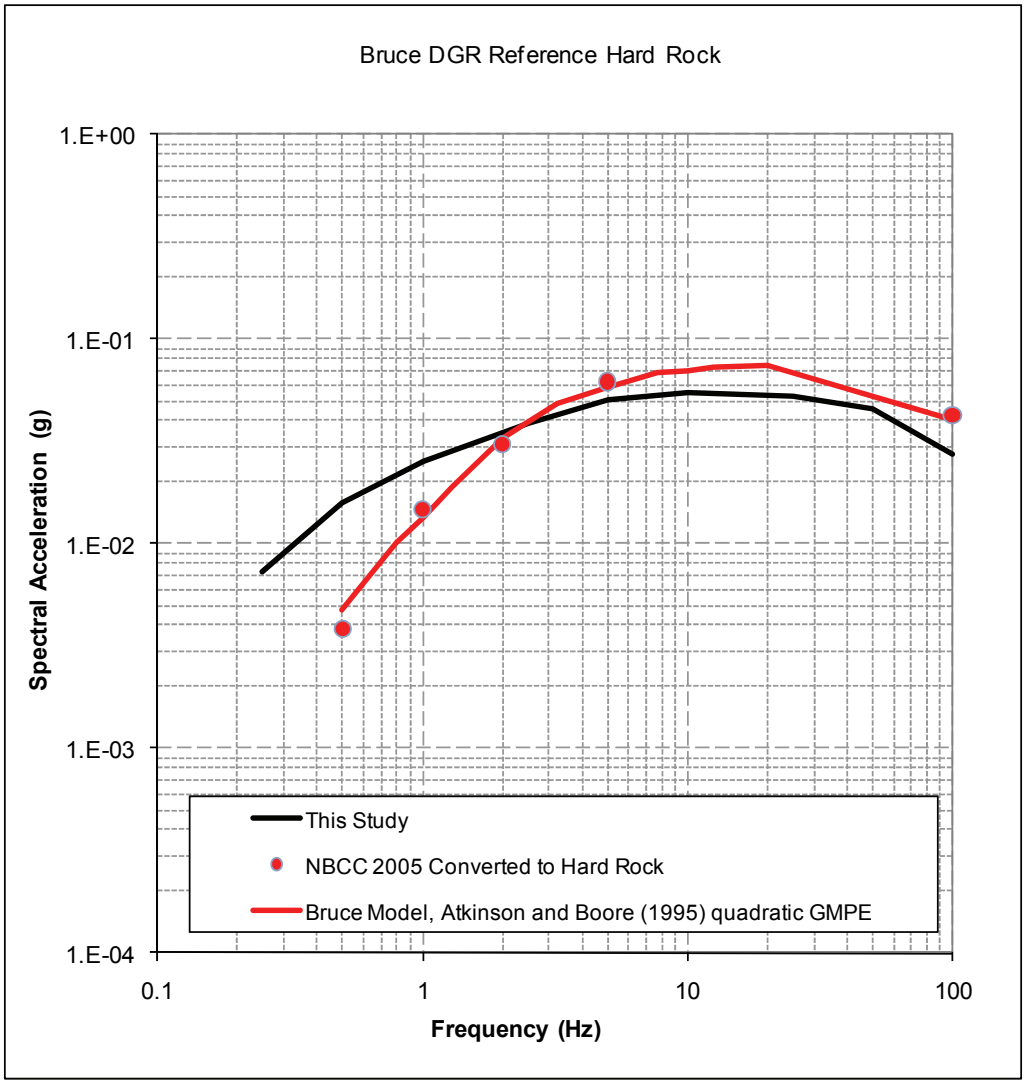

Note: Also shown are values from the National Building Code of Canada (NBSS 2005) converted to hard-rock site conditions (5% damping).

Figure 5.32: Comparison of UHRS for $4x10^{-4}$ Annual Exceedance Frequency Computed in This Study

Lateral Variability

To accommodate the potential impacts of changes in thickness of the very shallow soils and firm rock across the repository on both the surface, and at-depth, design motions, three base-case profiles were developed. In developing the three profiles, location US-3 on the cross section illustrated on Figure 5.33 was taken to reflect an average thickness of shallow

materials over the area of the repository that has the largest accumulation of soils and firm rock conditions. The Pleistocene soils and shallow firm rock materials were taken as layers one and two for shear waves and layers one to three for compressional waves in the downhole and base-case profiles shown on Figure 5.34 and Figure 5.35 (Table 5.2). The full profile as listed in Table 5.2 was designated profile 1 (P1), while the thinning of the shallow materials was modelled by removing the stiff soils and firm rock layers in two steps. In the first step, the Pleistocene soil, considered to be reflected in the top two layers of the shear-wave profile with velocities of 590 m/sec over a depth of 15 m (Table 5.2), was removed to form an alternative base-case profile (P2) with firm rock outcropping. The third base-case profile (P3) consisted of removal of the next layer of firm rock with a shear-wave velocity of 1,860 m/sec (Table 5.2).

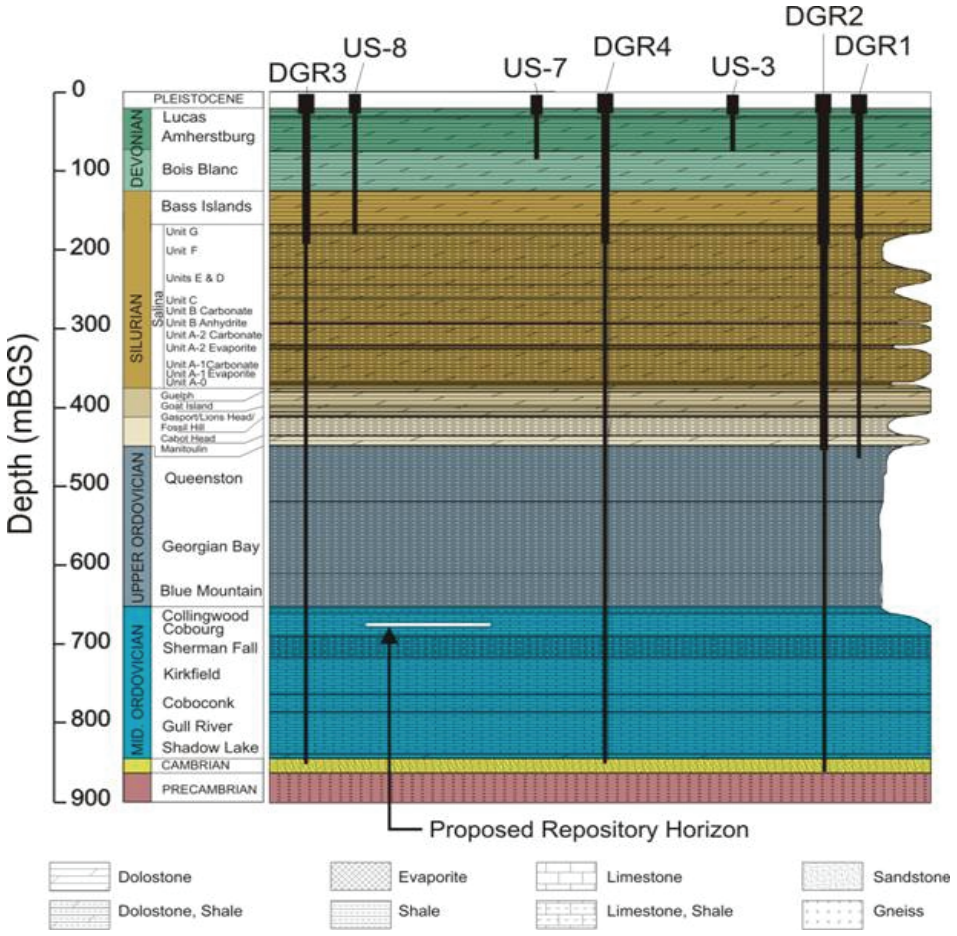

Notes: DGR-1, -2, -3, and -4, and US-3, -7, and -8 boreholes are projected onto a schematic cross-section to show depths of penetration of suspension logging into the Paleozoic stratigraphy beneath the Bruce nuclear site. The figure is modified from INTERA (2011). Proposed repository depth at 680 m is also indicated.

Figure 5.33: Subsurface Stratigraphy at the Bruce Nuclear Site

To properly accommodate the deterministic variation of shallow materials across the repository (Figure 5.33), site specific hazard curves and corresponding UHRS were developed for each profile (P1, P2 and P3). Final design motions that are appropriate for any location across the repository should then reflect an envelope of hazard developed for each profile. Alternatively,

to reduce conservatism for cases were large differences exist reflecting the effects of using profiles 1, 2 and 3, the repository may be microzoned. Such a process necessitates location-specific determination of the presence or absence of the shallow materials.

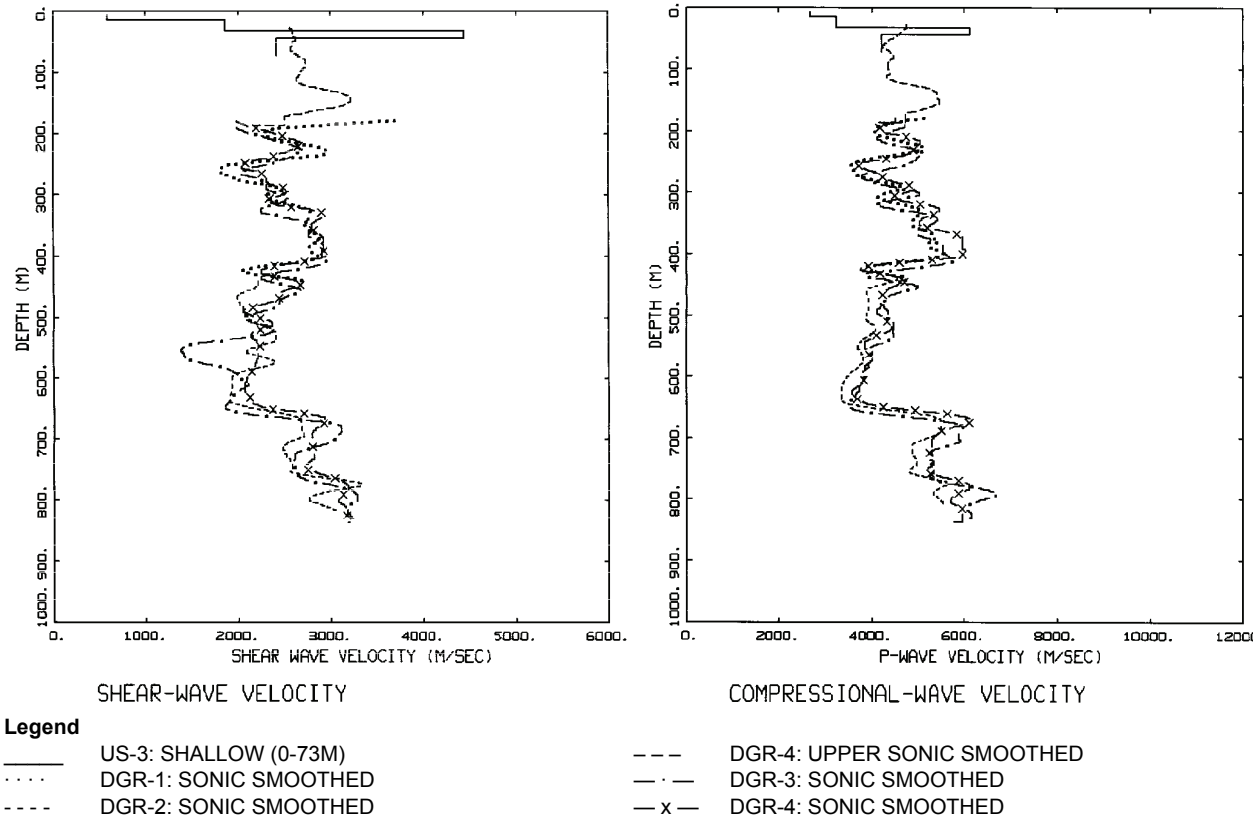

Figure 5.34: Smoothed Velocity Profiles for DGR-1, -2, -3, and -4 Along with Downhole Profile US-3: Shear Waves Followed by Compressional Waves

Reference Site

The reference site conditions of the suite of GMPEs (Section 4.0) used in the PSHA (Section 5.2) reflect hard-rock basement material in CENA. The hard-rock reference site has been quantified with a generic crustal model appropriate for CENA and is listed in Table 5.2 (EPRI 1993). The shear-wave velocity at the surface of the crustal model is 2.83 km/sec, as was taken to reflect conditions at a depth of about 750 m in the site-specific profile (Figure 5.35).

5.3.1.2 Nonlinear Dynamic Material Properties

To accommodate the possible nonlinear dynamic response of the shallow materials at the site, equivalent-linear analyses were used for the horizontal site response in the top three layers of the shear-wave velocity profile (Table 5.2). At shear-wave velocities of 590 m/sec, reflecting very stiff soil or soft rock and 1,860 m/sec reflecting firm rock, some degree of nonlinearity may be expected at high loading levels (low AEF). The remaining profile was considered to be sufficiently stiff to permit linear analyses.

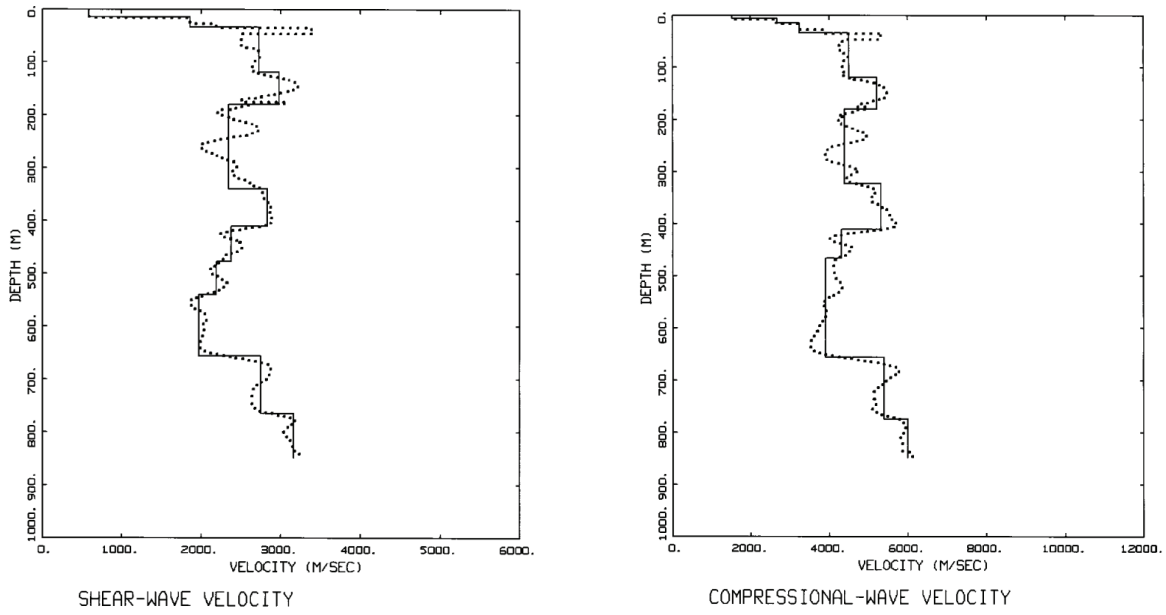

Legend

_____ BASE-CASE PROFILE

. . . . AVERAGE PROFILE BASED ON US-3; DGR-1,4

Note: Average velocity profiles are based on smoothed suspension log profiles and downhole profiles shown in Figure 5.34.

Figure 5.35: Average Velocity Profiles Based Along with the Base-Case Profiles Used in the Analyses: Shear Waves Followed by Compressional Waves

For the equivalent-linear analyses, generic soil shear modulus reduction (G/ G_{max}) and hysteretic damping curves were used (EPRI 1993). These curves were intended to capture potential nonlinearity in the shallow soils as well as in soft and firm rock. The EPRI curves have been validated by modelling recorded motions at soil and rock sites in western North America (Silva et al. 1996). The EPRI (1993) G/G_{max} and hysteretic damping curves are shown on Figure 5.36. To capture epistemic variability (uncertainty in mean or base-case curves) in nonlinear dynamic material properties, two sets of curves were used. The first set was the original EPRI (1993) suite as shown on Figure 5.36. To consider the possibility that the shallow materials may behave more linearly, a subset of the EPRI (1993) curves, developed by modelling recorded motions at firm cohesionless soil sites (Silva et al. 1996), was also used for each profile. The second set, termed Peninsular Range curves, uses the EPRI (1993) 51- to 120-foot (15.5 to 36.6 m) curves for 0 to 50 feet (0 to 6.1 m) and the 501- to 1,000-foot (152.7 to 304.8 m) curves for deeper materials.

Table 5.2: Velocity Profiles

Base-Case		
Thickness (m)	**V_S (m/sec)**	**V_P (m/sec)**
6.0	590	1,515
9.0	590	2,667
18.0	1,860	3,232
85.0	2,725	4,500
62.0	2,980	5,200
143.0	2,345	4,390
17.0	2,345	5,320
70.0	2,830	5,310
56.0	2,375	4,300
10.5	2,375	3,910
63.5	2,195	3,910
115.0	2,750	3,910
102.0	2,750	5,400
18.0	3,160	5,400
73.0	3,160	6,000
Reference Site		
1,000	2,830	4,900
11,000	3,520	6,100
28,000	3,750	6,500
	4,620	8,000

5.3.2 Development of Transfer Functions

Transfer functions include spectral ratios (5 percent damping) of horizontal site-specific motions to hard-rock (reference site) motions (amplification factors), as well as vertical-to-horizontal ratios (5 percent damping) computed for each profile for a suite of expected (reference site) peak accelerations (0.01 to 1.50 g; Table 5.3). For each base-case profile (P1, P2 and P3, Section 5.3.1.1.1), amplification factors relative to the reference site were developed for surface motions corresponding to layer 1, as well as to layers 3 and 4 at the surface. To develop site-specific hazard, for the repository and eight selected reference horizon levels (listed in Table 5.5), in-layer (total motion) amplification factors were also computed. Because the in-layer motions contain all the upgoing and downgoing wavefields at depth (total motions), the horizon and repository amplification factors were also developed for each base-case profile. Due to the proximity of Horizon 8 to Horizon 7 and considering Horizon 8 is located in the same velocity material as Horizon 7, amplification factors were

developed for Horizons 1 through 7, and the repository elevation at Horizon 8 would have very similar amplification to that of Horizon 7.

To approximate nonlinear soil response, for horizontal motions, a random vibration theory-based equivalent-linear approach was used (EPRI 1993, Silva et al. 1996). The approach has been validated by modelling strong ground motions recorded at over 500 sites and 19 earthquakes for a wide range in site conditions and loading levels (up to 1 g) (EPRI 1993, Silva et al. 1996). Comparisons with fully nonlinear codes for loading levels up to 1 g showed that the equivalent-linear approach adequately captured both high- and low-frequency soil response in terms of 5 percent damped response spectra. The validations revealed that the equivalent-linear approach significantly underestimated durations (time domain) of high-frequency motions at high loading levels compared to both fully nonlinear analysis and recorded motions. However, for 5 percent damped response spectra, the equivalent-linear approach performed as well as fully nonlinear codes and was somewhat conservative near the fundamental column resonance (EPRI 1993). For vertical motions, site-specific V/H ratios were developed using the point-source model to compute both horizontal (normally incident, horizontally polarised shear [SH]) waves and vertical (inclined-incident compression and vertically polarised shear [P-SV]) waves (Silva 1976, Silva 1997, EPRI 1993).

Table 5.3: Point Source Magnitudes, Distances and Source Depths Used in Developing Amplification Factors

Peak Acceleration (g)	Distance (km)					Depth (km)				
	M 5	**M** 6 1c	**M** 6 2c	**M** 7 1c	**M** 7 2c	**M** 5	**M** 6 1c	**M** 6 2c	**M** 7 1c	**M** 7 2c
1.50	0.00	0.00	0.00	0.00	5.40	1.70	3.47	5.20	6.60	8.00
1.25	0.00	0.00	0.00	0.00	8.060	2.02	4.10	6.10	7.95	8.00
1.00	0.00	0.00	0.00	5.10	11.00	2.48	5.01	7.43	8.00	8.00
0.75	0.00	0.00	5.28	9.58	15.63	3.24	6.57	8.00	8.00	8.00
0.50	0.00	4.95	10.80	15.72	22.99	4.66	8.00	8.00	8.00	8.00
0.40	0.00	8.00	14.00	19.56	27.75	5.64	8.00	8.00	8.00	8.00
0.30	0.00	12.05	18.50	25.57	34.85	7.23	8.00	8.00	8.00	8.00
0.20	6.05	18.28	26.10	35.22	46.50	8.00	8.00	8.00	8.00	8.00
0.10	15.02	32.18	42.20	58.17	77.80	8.00	8.00	8.00	8.00	8.00
0.05	26.51	51.70	67.50	105.00	133.30	8.00	8.00	8.00	8.00	8.00
0.01	76.00	163.00	188.00	317.00	338.00	8.00	8.00	8.00	8.00	8.00

Notes:
1c = single-corner source model (Boore 1983, Silva et al. 1997)
2c = double-corner source model (Atkinson and Boore 1997)
$Q = 670\ f^{0.33}$
$\Delta\sigma$ (1c) = 110 bars
κ = 0.006 sec, hard rock

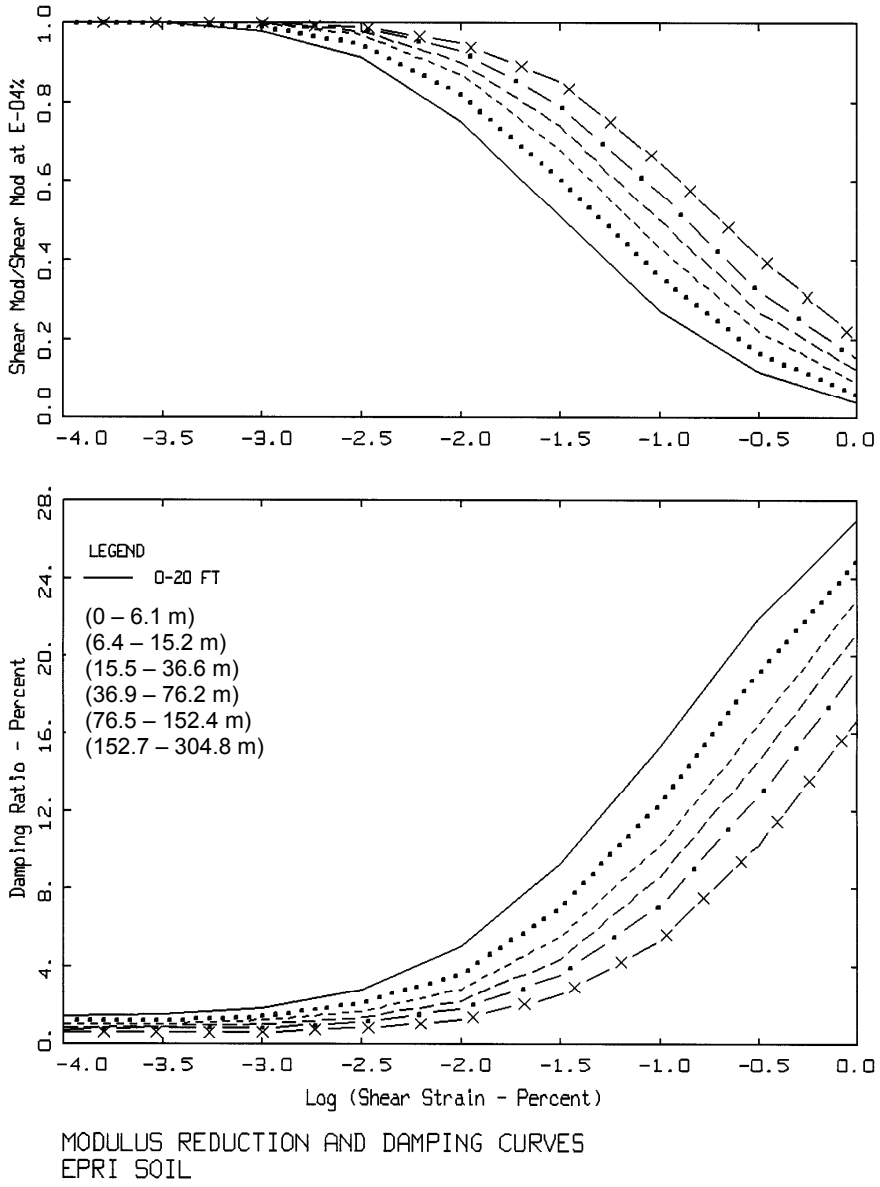

Notes: This figure illustrates the effects of depth dependent confining pressure. The Peninsular Range curves reflect a subset of the EPRI curves and apply the 51- to 120-foot (15.5 to 36.6 m) EPRI curves over the depth range of 0 to 50 feet (0 to 15.2 m) and the 501- to 1,000-foot (15.5 to 36.6 m) curves beyond.

Figure 5.36: Generic G/G_{max} and Hysteretic Damping Curves for Cohesionless Soils

In the implementation of Approach 3 to develop vertical hazard curves, empirical as well as site-specific V/H ratios were used along with two sets of G/G_{max} and hysteretic damping curves. The resulting epistemic uncertainty was properly accommodated in the vertical mean UHRS, reflecting a weighted average over multiple vertical hazard curves computed for each model. The vertical UHRS then maintain the desired hazard levels, consistent with the horizontal UHRS.

5.3.2.1 Site Aleatory Variability

To accommodate random fluctuations in velocity, depth to basement, G/G_{max} and hysteretic damping values across a site, multiple realisations (30) were developed for dynamic material properties. The profile randomisation scheme for shear-wave velocity is based on an analysis of variance of over 500 measured shear-wave velocity profiles and varies in both velocity and layer thickness (EPRI 1993, Silva et al. 1996). The model includes a velocity distribution at depth coupled with a velocity correlation with depth. The depth correlation is intended to eliminate unnatural velocity variations at a given depth that are independent of realisations above and below. The measured velocity data indicates an increase in correlation length (distance) with depth, with a corresponding decrease in the velocity coefficient of variation at a given depth. Profiles vary less as depth increases and, on average, become more uniform.

To accommodate random fluctuations in compression-wave velocity when modelling vertical motions (Section 5.3.2.4), Poisson ratios were held constant at the base-case values and random compression-wave velocities were then generated based on shear-wave velocity realisations and base-case Poisson ratios. In reality, Poisson ratio will vary as well but is likely correlated with shear-wave velocity. As a result, varying Poisson ratio when properly correlated with shear-wave velocity will likely not result in a greater variation in compression-wave velocity than assumed here. Additionally, variation in compression-wave velocity has a much less significant effect on motions than does the shear-wave velocity, as the wavelengths typically are two to five times greater. A correlated shear- and compression-wave profile randomisation scheme is desirable but not yet available.

To capture random fluctuations in modulus reduction and hysteretic damping curves, values were randomised assuming a lognormal distribution consistent with shear-wave velocity and material damping (EPRI 1993). Based on random variations in laboratory dynamic testing for soils of the same type or classification (EPRI 1993), a σ_{ln} of 0.15 and 0.3 is used for G/G_{max} and hysteretic damping, respectively. These standard deviations are taken at a cyclic shear strain of 0.03 percent, where the G/G_{max} curves typically show significant reduction. Suites of curves were generated by sampling the distribution, applying the random perturbation to the base-case (initial) curve at 0.03 percent shear strain, and preserving the shape of the base-case curve to generate an entire random curve. Bounds are placed at $\pm 2\ \sigma$ over the entire strain range to prevent nonphysical excursions.

Shear-wave damping is separately (independently) randomised following the same procedure. The randomisation code can accommodate coupling or correlation of any degree (-1 to 1) between modulus reduction and hysteric damping, which is expected to occur between mean or base-case curves reflecting curves of different types of material. However, for random fluctuations within the same type of material, the correlation is likely to be low, that is, a randomly linear curve is not necessarily associated with a randomly low damping. Additionally, because modulus reduction is far more significant than material damping in site response (Silva 1992), the issue is not significant.

5.3.2.2 Point-Source Model Parameters

The omega-square point-source model (Boore 1983, Atkinson 1993, Silva et al. 1996) was used to generate the hard-rock reference site as well as site-specific motions (profiles P1, P2 and P3; Section 5.3.1.1) for a range in expected reference-site PGA values (0.01 to 1.50 g; Table 5.3).

To accommodate potential effects of control motion spectral shape (magnitude) on nonlinear site response, amplification factors were computed for **M** 5.0, 6.0 and 7.0 based on the magnitude deaggregations (Section 5.2.1). Additionally, because large **M** (**M** ≥ 5.5) CENA source processes may be significantly different from those of WNA in spectral shape, typified by an intermediate-frequency spectral sag or two corner frequencies (Atkinson 1993), transfer functions were computed for this source model as well (Table 5.3). The hard-rock crustal model used to generate vertical and horizontal component reference-site motions is listed on Table 5.2, with the remaining point-source parameters (stress drop, $\Delta\sigma$; Q; and kappa) listed on Table 5.3.

To include the effects of the change in magnitude contributions to the reference site hazard with both structural and exceedance frequency, indicated in the magnitude deaggregations (Section 5.2.1), weights were assigned to the respective amplification factors according to Table 5.4. The weighting over magnitude accommodates potential effects of control motion spectral shape, due to magnitude, on the nonlinear response of the shallow soil and rock layers on the amplification factors. Because the amplification factors vary slowly with magnitude, with a maximum change of about 30 percent for a unit change in **M** (McGuire et al. 2001), only an approximate accommodation of the change in amplification due to a change in magnitude with hard-rock hazard level is required.

5.3.2.3 Horizontal Amplification Factors

As an example of the horizontal amplification factors, Figure 5.38 shows median and ±1 σ estimates computed at the surface of Profile 1 (Section 5.3.1.1.1) with **M** 6.0 control motions (single-corner source model; Table 5.3) using the EPRI (1993) G/G_{max} and hysteretic damping curves (Section 5.3.1.2). Peak ground accelerations reflect expected hard-rock (reference site; Table 5.2) values ranging from 0.01 g to 1.50 g (Table 5.3). The amplification of the shallow, stiff profile (Figure 5.35 and Table 5.2) is apparent in the high-frequency amplification (≥3 Hz), with values at peak acceleration (100 Hz) of about 2. Figure 5.38 clearly shows the effects of nonlinearity, with high-frequency factors decreasing with increasing loading levels. For example, at 1.5 g and 40 Hz, the median factors decrease to about 1. Such a large deamplification may represent a shortcoming of the equivalent-linear approach that reflects a frequency-independent softening. However, careful validations with recorded motions at high loading levels (EPRI 1993, Silva et al. 1996) showed no indication of equivalent-linear inadequacy in modelling overall levels of response spectra of recorded motions, particularly at high frequency. While these local particular soils were not sampled in the validations, the overall adequacy of the equivalent-linear approach has been validated for deamplification to levels as low as 0.5, which was set as a lower bound in all analyses.

Figure 5.39 shows the amplification factors computed for the repository location at a depth of 680 m (Figure 5.37). These motions were computed as total or in-layer motions which then include all upgoing and downgoing wavefields at the repository elevation. Relative to hard-rock outcropping, the in-layer motions show deamplification at frequencies above about 0.2 Hz due to some cancellation of upgoing and downgoing wavefields. Due to the randomisation process, these spectral holes or nulls (Silva et al. 1986) are smoothed over frequency.

Table 5.4: Amplification Factor Magnitudes and Relative Weights

Annual Exceedance Frequency	**M** 5.0	**M** 6.0 (1c)*	**M** 6.0 (2c)*	**M** 7.0 (1c)*	**M** 7.0 (2c)*
PGA 100.00 Hz					
1.00E-02	0.63600	0.13845	0.13845	0.04355	0.04355
1.00E-03	0.51790	0.13710	0.13710	0.10395	0.10395
1.00E-04	0.64010	0.09740	0.09740	0.08255	0.08255
1.00E-05	0.80470	0.08085	0.08085	0.01680	0.01680
1.00E-06	0.77800	0.10455	0.10455	0.00645	0.00645
1.00E-07	0.70890	0.13625	0.13625	0.00930	0.00930
PGA 50.00 Hz					
1.00E-02	0.65420	0.12895	0.12895	0.04395	0.04395
1.00E-03	0.59990	0.11935	0.11935	0.08070	0.08070
1.00E-04	0.75360	0.08010	0.08010	0.04310	0.04310
1.00E-05	0.84110	0.07215	0.07215	0.00730	0.00730
1.00E-06	0.80510	0.09215	0.09215	0.00530	0.00530
1.00E-07	0.73470	0.12470	0.12470	0.00795	0.00795
PGA 25.00 Hz					
1.00E-02	0.65660	0.12680	0.12680	0.04490	0.04490
1.00E-03	0.61580	0.11340	0.11340	0.07870	0.07870
1.00E-04	0.74800	0.08285	0.08285	0.04315	0.04315
1.00E-05	0.82890	0.07695	0.07695	0.00860	0.00860
1.00E-06	0.79660	0.09595	0.09595	0.00575	0.00575
1.00E-07	0.72570	0.12865	0.12865	0.00850	0.00850
PGA 10.00 Hz					
1.00E-02	0.64640	0.12975	0.12975	0.04705	0.04705
1.00E-03	0.57050	0.12650	0.12650	0.08825	0.08825
1.00E-04	0.67440	0.09515	0.09515	0.06765	0.06765
1.00E-05	0.79050	0.08505	0.08505	0.01970	0.01970
1.00E-06	0.77270	0.10580	0.10580	0.00785	0.00785
1.00E-07	0.69590	0.14140	0.14140	0.01065	0.01065
PGA 5.00 Hz					
1.00E-02	0.61850	0.14080	0.14080	0.04995	0.04995
1.00E-03	0.47500	0.15605	0.15605	0.10645	0.10645

Table 5.4: Amplification Factor Magnitudes and Relative Weights

Annual Exceedance Frequency	**M** 5.0	**M** 6.0 (1c)*	**M** 6.0 (2c)*	**M** 7.0 (1c)*	**M** 7.0 (2c)*
1.00E-04	0.51310	0.12740	0.12740	0.11605	0.11605
1.00E-05	0.65800	0.10745	0.10745	0.06355	0.06355
1.00E-06	0.71040	0.12705	0.12705	0.01775	0.01775
1.00E-07	0.63990	0.16405	0.16405	0.01600	0.01600
PGA 2.50 Hz					
1.00E-02	0.50570	0.18275	0.18275	0.06440	0.06440
1.00E-03	0.30210	0.20225	0.20225	0.14670	0.14670
1.00E-04	0.27140	0.16925	0.16925	0.19505	0.19505
1.00E-05	0.36610	0.13690	0.13690	0.18005	0.18005
1.00E-06	0.50570	0.15380	0.15380	0.09335	0.09335
1.00E-07	0.48050	0.22085	0.22085	0.03890	0.03890
PGA 1.00 Hz					
1.00E-02	0.32980	0.24635	0.24635	0.08875	0.08875
1.00E-03	0.12070	0.23030	0.23030	0.20935	0.20935
1.00E-04	0.06850	0.16185	0.16185	0.30390	0.30390
1.00E-05	0.08240	0.11740	0.11740	0.34140	0.34140
1.00E-06	0.12570	0.13205	0.13205	0.30510	0.30510
1.00E-07	0.15180	0.20595	0.20595	0.21815	0.21815
PGA 0.50 Hz					
1.00E-02	0.25650	0.26665	0.26665	0.10510	0.10510
1.00E-03	0.04250	0.20205	0.20205	0.27670	0.27670
1.00E-04	0.02060	0.11860	0.11860	0.37110	0.37110
1.00E-05	0.02230	0.08715	0.08715	0.40170	0.40170
1.00E-06	0.03020	0.08405	0.08405	0.40085	0.40085
1.00E-07	0.04070	0.14075	0.14075	0.33890	0.33890
PGA 0.25 Hz					
1.00E-02	0.20730	0.27980	0.27980	0.11655	0.11655
1.00E-03	0.02660	0.19510	0.19510	0.29160	0.29160
1.00E-04	0.00550	0.08025	0.08025	0.41700	0.41700
1.00E-05	0.00460	0.03570	0.03570	0.46200	0.46200
1.00E-06	0.00500	0.03210	0.03210	0.46540	0.46540

Table 5.4: Amplification Factor Magnitudes and Relative Weights

Annual Exceedance Frequency	**M** 5.0	**M** 6.0 (1c)*	**M** 6.0 (2c)*	**M** 7.0 (1c)*	**M** 7.0 (2c)*
1.00E-07	0.00600	0.04980	0.04980	0.44720	0.44720

5.3.2.4 Development of V/H Ratios

In the following sections, the development of site-specific ratios and the motivation for inclusion of empirical V/H ratios is presented.

Empirical V/H Ratios

Empirical V/H ratios for soft rock in WNA were included in the development of vertical surface motions in addition to site-specific point-source simulations. The use of WNA empirical V/H ratios implicitly assumes similarity in shear- and compression-wave profiles and nonlinear dynamic material properties between site conditions in WNA and the Bruce nuclear site. Whereas this may not be the case for the average WNA rock site profile (Silva 1996), the range in site conditions sampled by the WNA empirical generic rock relations likely accommodates site-specific conditions, at least for the shallow, stiff soil/soft rock (profile P1) and firm rock materials (profile P2) (Section 5.3.1.1.1). For profile P1, equal weight was given to the vertical hazard developed with the empirical V/H ratios and the hazard developed with the site-specific V/H ratios. The firm-rock outcropping profile (P2), with a shallow stiffness of 1,860 m/sec (Table 5.2) and only 18 m overlying hard rock, was considered to be less well represented within the WNA empirical GMPEs and was given a reduced weight of 0.2, with the remaining 0.8 given to the site-specific vertical hazard.

The WNA soft-rock empirical GMPEs that specify both horizontal and vertical motions are those of Abrahamson and Silva (1997), Campbell and Bozorgnia (2003) and Sadigh et al. (1993), and all three were used with equal relative weights (Table 5.7) to develop vertical V/H ratios. As an example, the entire suite of empirical V/H ratios in terms of magnitudes and distances is shown on Figure 5.40 for all three GMPEs. As Figure 5.40 illustrates, V/H ratios depend on both magnitude and distance, generally increasing with increasing magnitude and decreasing distance (Silva 1997, Campbell and Bozorgnia 2003).

Site-Specific V/H Ratios

To develop site-specific vertical motions, inclined-incident P-SV waves were modelled from the source to the site using the plane-wave propagators of Silva (1976) and EPRI (1993), assuming a shear-wave point-source spectrum (Boore 1983, 2003). The point-source model was used to accommodate the effects of source distance and source depth on V/H ratios. For consistency, both the horizontal and vertical motions were modelled using the same source and path parameters and suite of distances (Table 5.3). The horizontal motions were modelled as vertically propagating shear waves. For the vertical motions, the angles of incidence were computed by two-point ray tracing through the crust and site-specific profile. To model site response, the near-surface V_P and V_S profiles (Section 5.3.1.1; Figure 5.34) were merged with reference-site crustal structure (Table 5.2), the incident P-SV wavefield was propagated to the surface assuming a linear analysis, and the vertical motions were computed.

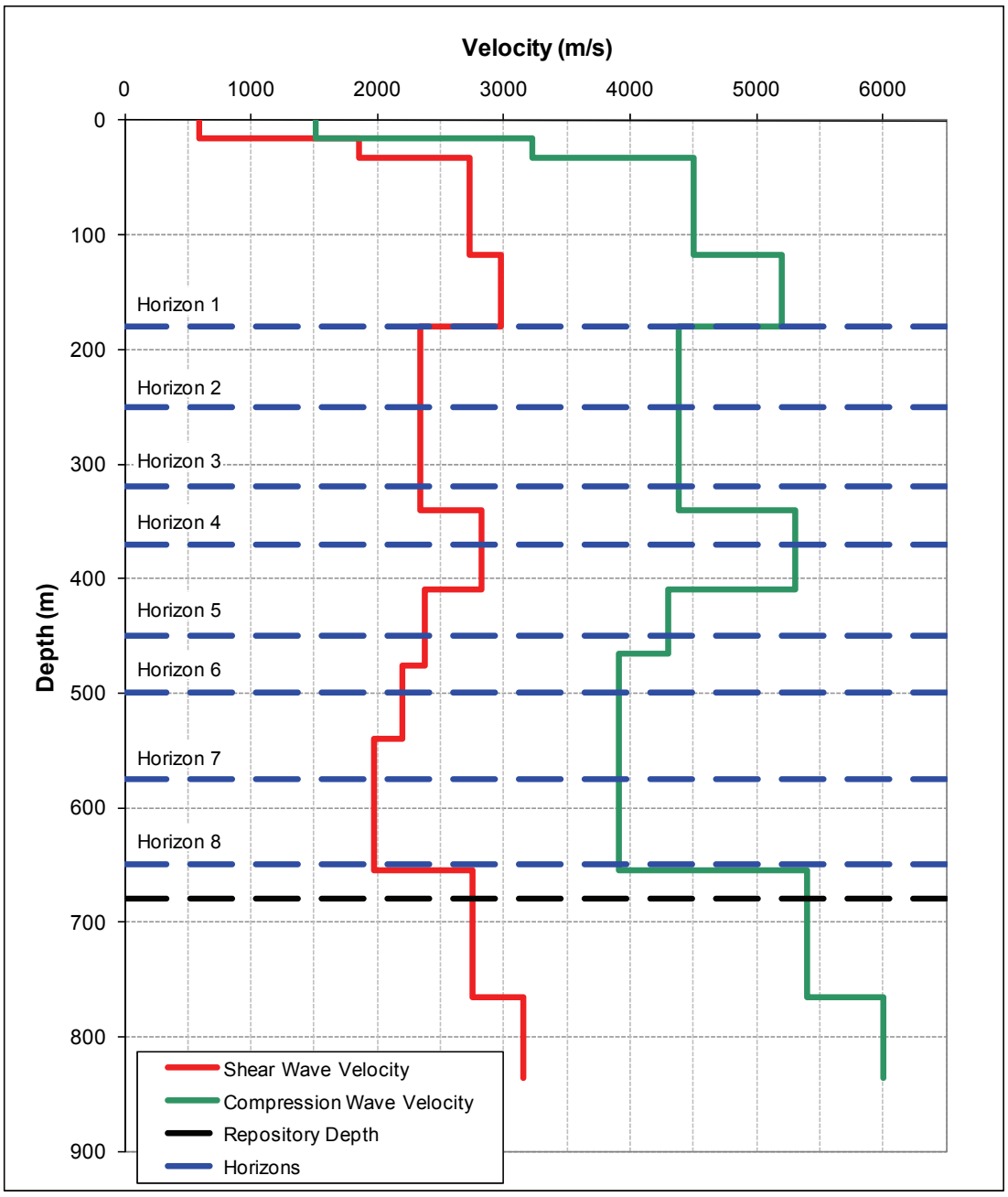

Figure 5.37: Base-Case Shear- and Compressional-Wave Profiles Along with Locations of the Eight Reference Horizons and Repository Horizon

In the implementation of the equivalent-linear approach to estimate V/H response spectral ratios, the horizontal component analyses are performed for vertically propagating shear waves. To compute the vertical motions, a linear analysis is performed for inclined-incident P-SV waves using low-strain V_P and V_S derived from the base-case profiles. The P-wave damping is assumed to be equal to the low-strain S-wave damping (Johnson and Silva 1981, EPRI 1993), and the horizontal-component and vertical-component analyses are assumed to be independent.

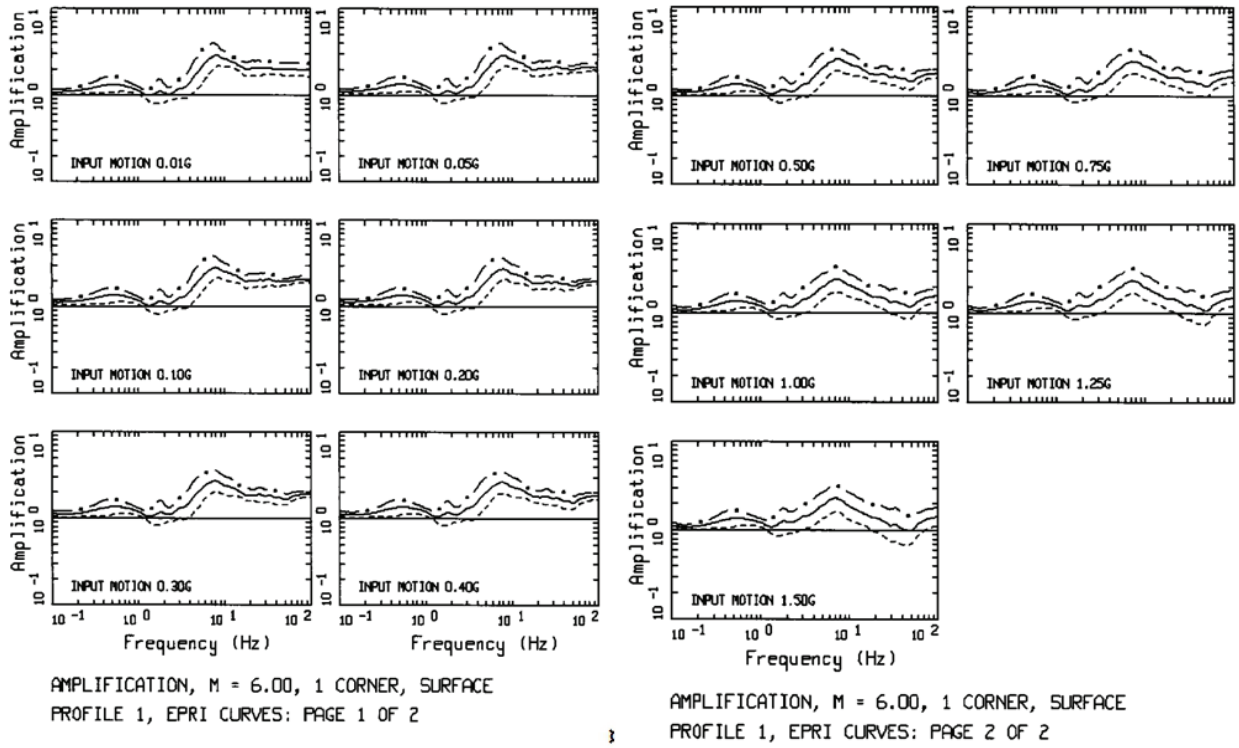

Notes: Analysis is relative to the reference site condition of hard-rock outcrop with a shear-wave velocity of 2.83 km/sec. Figure is from EPRI (1993, 2004): M 6.0, single-corner source model, profile 1 (Section 5.3.1.1), and EPRI (1993) G/G_{max} and hysteretic damping curves.

Figure 5.38: Example of Horizontal Amplification at the Surface

The approximations of linear analysis for the vertical component and uncoupled vertical and horizontal components have been validated in two ways. Fully nonlinear modelling using a 3-D soil model shows that the assumption of largely independent horizontal and vertical motions for loading levels up to about 0.5 g (soil surface, horizontal component) for moderately stiff profiles is appropriate (EPRI 1993). Additionally, validation exercises with recorded motions have been conducted at over 50 sites that recorded the 1989 **M** 6.9 Loma Prieta and 1992 **M** 6.7 Northridge earthquakes (EPRI 1993). These validations show that the overall bias and variability is acceptably low for engineering applications but is larger than that for horizontal motions. The vertical model does not perform as well as the model for horizontal motions (EPRI 1993, Silva 1997). An indirect validation was also performed by comparing V/H ratios from WNA empirical GMPEs with model predictions over a wide range in loading conditions (Silva 1997). The results showed a favourable comparison, with the model exceeding the empirical V/H ratios at high frequency, particularly at high loading levels. In the V/H comparisons with empirical relations, the model also shows a small underprediction at low frequency (≤1 Hz) and at large distance (≥20 km).

For the vertical analyses, a hard-rock kappa value of 0.003 sec, half that of the horizontal, was used. This factor of 50 percent is based on observations of kappa at strong-motion sites (Anderson and Hough 1984), validation exercises (EPRI 1993), and the observation that the peak in the vertical spectral acceleration (5 percent damped) for WNA rock and soil sites is generally near 10 to 12 Hz, compared to the horizontal motion peak that occurs at about 5 Hz, conditional on **M** 6.5 at a distance of about 10 to 30 km (Abrahamson and Silva 1997, Campbell 1997, Campbell and Bozorgnia 2003). This difference of about 2 in peak frequency is directly attributable to differences in kappa of about 2. Similar trends are seen in CEUS

hard-rock spectra with the vertical component peaking at higher frequencies than the horizontal component.

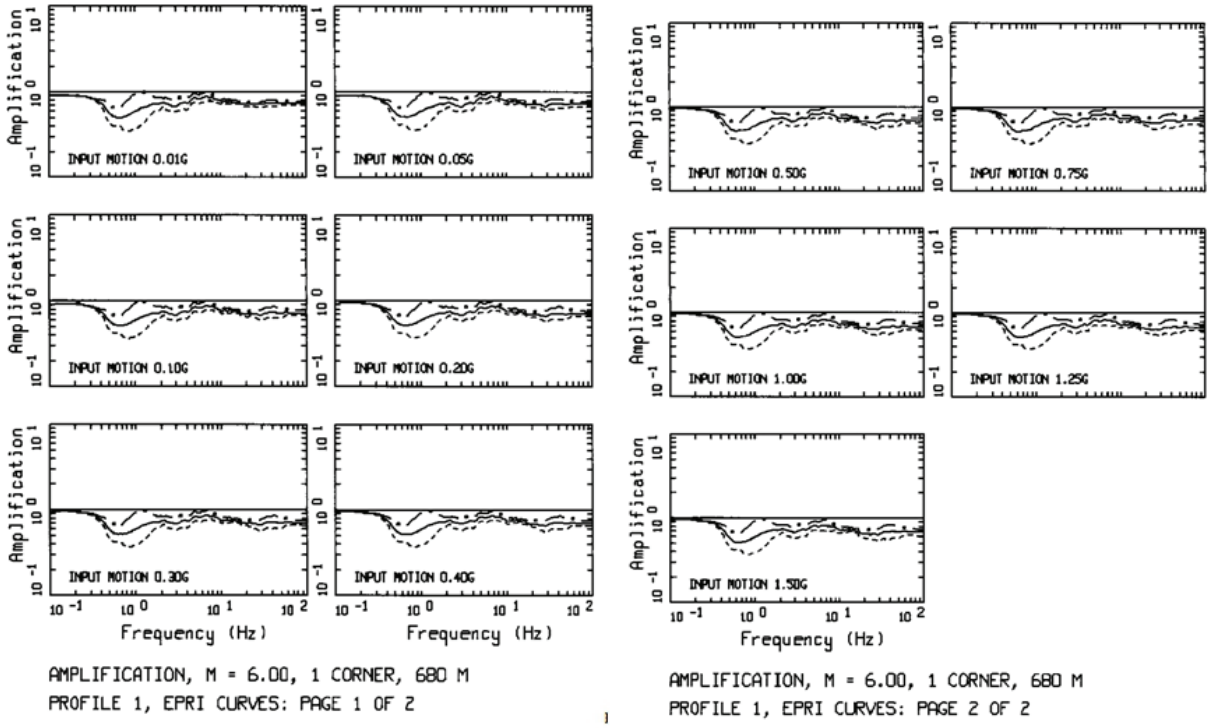

Notes: Analysis is relative to the reference site condition of hard-rock outcrop with a shear-wave velocity of 2.83 km/sec. Figure is from EPRI (1993, 2004): M 6.0, single-corner source model, profile 1 (Section 5.3.1.1.1), and EPRI (1993) G/G_{max} and hysteretic damping curves.

Figure 5.39: Example of Horizontal Amplification at the Repository Horizon (680 m within layer or total motion)

In computing the vertical motions, multiple G/G_{max} and hysteretic damping curves were not run for the verticals as the analysis was linear, using the lowest small-strain damping between the Peninsular Range and EPRI (1993) curves (Section 5.3.1.2). However V/H ratios do reflect multiple base-case modulus reduction and hysteretic damping curves in the denominator, or horizontal motions. As such, the epistemic variability (uncertainty) in V/H ratios due to the uncertainty in nonlinear dynamic material properties in the horizontal analyses was accommodated through two sets of V/H ratios reflecting EPRI (1993) and Peninsular Range (Silva et al. 1996) G/G_{max} and hysteretic damping curves. Additionally, differences in horizontal site response due to differences in source processes (spectral shape) between single- and double-corner source models (as control motions) also reflect epistemic variability and are accommodated with V/H ratios computed using both source models.

As an example of the site-specific V/H ratios, Figure 5.41 shows median estimates of the complete suite of site-specific V/H ratios developed for profile 1 (Section 5.3.1.1) at the surface and the repository (680 m; Figure 5.37 and Table 5.5) using the EPRI (1993) G/G_{max} and hysteretic damping curves. The magnitudes and distances were selected to accommodate the contributing source deaggregations (Section 5.2.1) and are discussed in in this section.

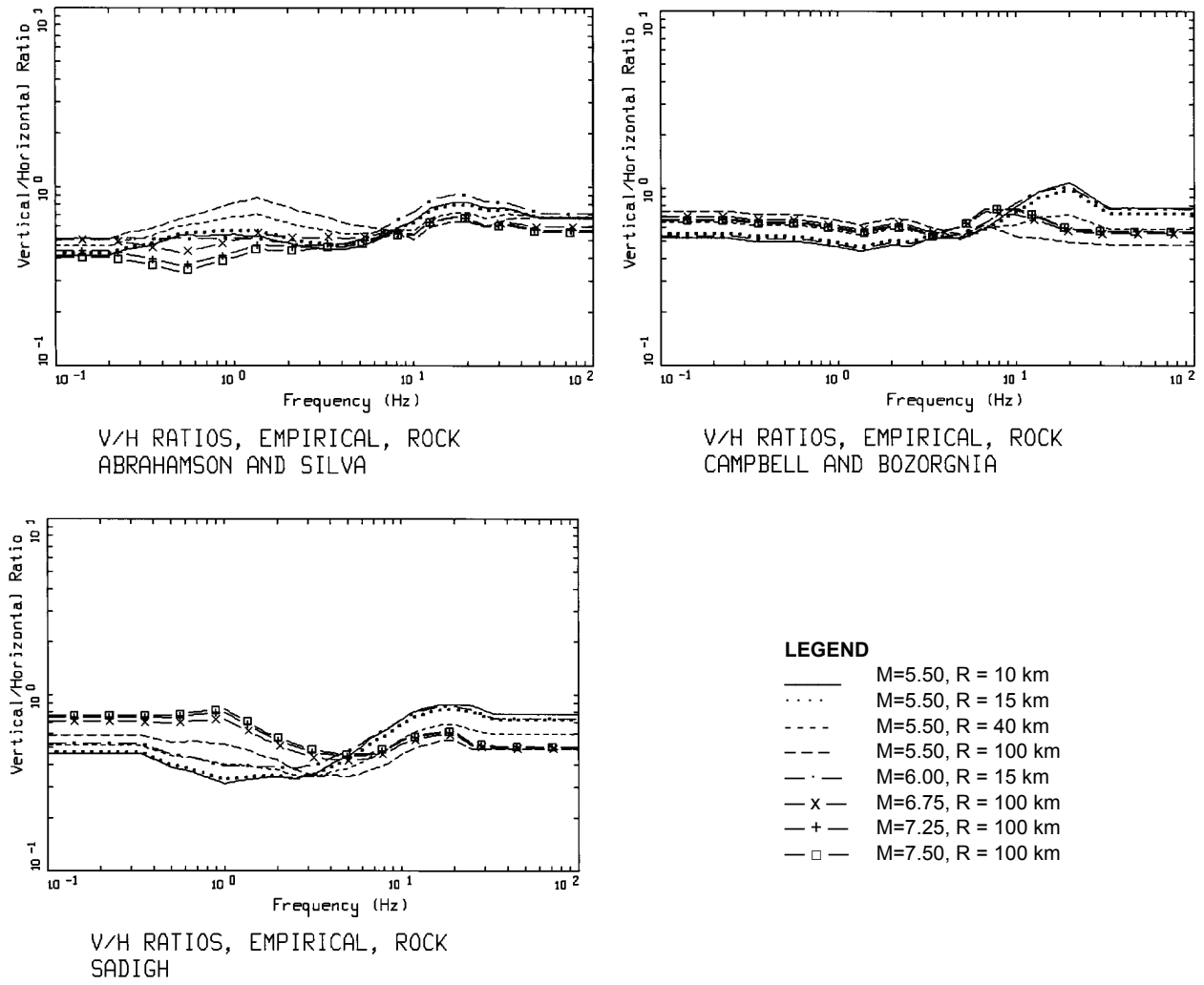

Note: Data are from Abrahamson and Silva (1997), Campbell and Bozorgnia (2003) and Sadigh (1997).

Figure 5.40: Suite of Empirical Rock V/H ratios Used in Developing the Surface Hazard for Profiles 1 and 2 (Section 5.3.1.1)

As previously discussed, the model predictions of V/H ratios at low frequency may be slightly unconservative and at high frequency they may be conservative. Additionally, empirical V/H ratios of Fourier amplitude spectra based on CENA recordings at hard-rock sites for small magnitudes and at very large distances have median values near about 0.8 and vary slowly with frequency (Gupta and McLaughlin 1987, Atkinson 1993). To accommodate potential model deficiencies as well as the large uncertainty in hard- and firm-rock V/H ratios for CENA, a minimum value of 0.7 was adopted, the average of the empirical CENA and site-specific V/H ratios at large distance (>20 km).

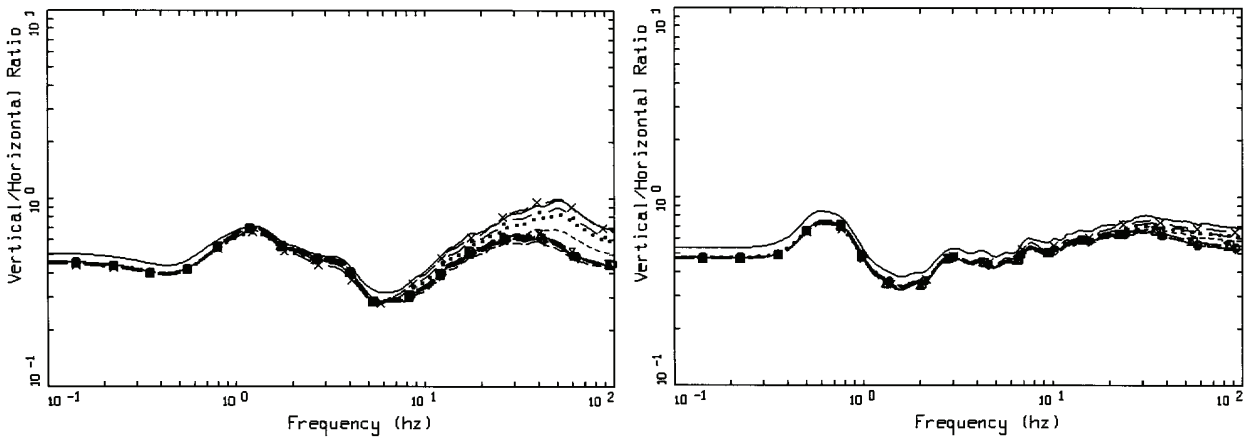

LEGEND

_____	M=5.50, R = 10 km	— + —	M=6.75, R = 100 km, 1-CORNER
· · · ·	M=5.50, R = 15 km	— □ —	M=6.75, R = 100 km, 2-CORNER
- - - -	M=5.50, R = 40 km	— ○ —	M=7.25, R = 100 km, 1-CORNER
– – –	M=5.50, R = 100 km	— Δ —	M=7.25, R = 100 km, 2-CORNER
— · —	M=6.00, R = 15 km, 1-CORNER	— ◊ —	M=7.50, R = 100 km, 1-CORNER
— x —	M=6.75, R = 100 km, 2-CORNER	— X —	M=7.50, R = 100 km, 2-CORNER

Notes: Profile 1 (Section 5.3.1.1.1), and EPRI (1993) G/G_{max} and hysteretic damping curves; surface followed by repository horizon at a depth of 680 m).

Figure 5.41: Example Suite of Site-Specific V/H Ratios at the Magnitudes and Distances Used in the Development of the Vertical Hazard

Aleatory Variability in the Site-Specific V/H Ratios

In addition to the epistemic variability accommodated through the use of multiple models for V/H ratios (two sets of G/G_{max} and hysteretic damping curves, single- and double-corner source models, and empirical versus site-specific V/H ratios), aleatory variability due to randomness of dynamic material properties varying vertically and laterally across the site should be accommodated as well. However, in developing the vertical hazard, since site-specific aleatory variability has been incorporated in developing the horizontal site-specific hazard curves, it is advisable to constrain the sigma of the site-specific V/H ratios to values less than about 0.15 to 0.20 (σ_{ln}). This range is to accommodate the observation of slightly larger variability about median attenuation relations in the vertical component compared to the horizontal component (Abrahamson and Silva 1997).

Implementation of V/H Ratios In Developing Vertical Hazard

Based on the changes in contributing sources across exceedance and structural frequency, the dependencies of the V/H ratios on magnitude and distance were accommodated with relative weights based on the deaggregations (Section 5.2.1). Because the empirical and site-specific V/H ratios change slowly with magnitude and distance (Figure 5.40 and Figure 5.41), only a smooth approximation to the hazard deaggregation is necessary. To adequately capture the change in magnitude and distance with AEF, only a few magnitudes and distances were required and reflected in the weights listed in Table 5.6.

Table 5.5: Horizon Locations

Horizon	Depth (m)
1	180
2	250
3	320
4	370
5	450
6	500
7	575
8	650
Repository	680

Table 5.6: V/H Ratio Magnitudes, Source Distances, and Relative Weights

Frequency (Hz)	AEF	Mag	Dist	Wt
100 (PGA)	10-2	5.50	100	1.00
	10-3	5.50	100	0.60
		7.25	100	0.40
	10-4	5.50	40	0.70
		7.25	100	0.30
	10-5	5.50	15	1.00
	10-6	5.50	15	1.00
	10-7	5.50	10	1.00
50	10-2	5.50	100	1.00
	10-3	5.50	100	0.70
		7.25	100	0.30
	10-4	5.50	40	0.90
		7.25	100	0.10
	10-5	5.50	15	1.00
	10-6	5.50	15	1.00
	10-7	5.50	10	1.00
25	10-2	5.50	100	1.00
	10-3	5.50	100	0.60
		7.25	100	0.40
	10-4	5.50	40	0.90
		7.25	100	0.10

Table 5.6: V/H Ratio Magnitudes, Source Distances, and Relative Weights

Frequency (Hz)	AEF	Mag	Dist	Wt
	10-5	5.50	15	1.00
	10-6	5.50	15	1.00
	10-7	5.50	10	1.00
10	10-2	5.50	100	1.00
	10-3	5.50	100	0.55
		7.25	100	0.45
	10-4	5.50	40	0.80
		7.25	100	0.20
	10-5	5.50	15	1.00
	10-6	5.50	15	1.00
	10-7	5.50	10	1.00
5	10-2	5.50	100	1.00
	10-3	5.50	100	0.50
		7.25	100	0.50
	10-4	5.50	40	0.50
		7.25	100	0.50
	10-5	5.50	15	0.75
		7.25	100	0.25
	10-6	5.50	15	1.00
	10-7	5.50	10	1.00
2.5	10-2	7.25	100	1.00
	10-3	7.25	100	1.00
	10-4	5.50	40	0.25
		7.25	100	0.75
	10-5	5.50	15	0.50
		7.25	100	0.50
	10-6	5.50	15	0.85
		7.25	100	0.15
	10-7	6.00	15	1.00
1	10-2	6.75	100	1.00
	10-3	7.25	100	1.00
	10-4	7.25	100	1.00
	10-5	7.25	100	1.00
	10-6	6.00	15	0.25
		7.50	100	0.75

Table 5.6: V/H Ratio Magnitudes, Source Distances, and Relative Weights

Frequency (Hz)	AEF	Mag	Dist	Wt
	10-7	6.00	15	0.60
		7.50	100	0.40
0.5	10-2	6.75	100	1.00
	10-3	7.25	100	1.00
	10-4	7.25	100	1.00
	10-5	7.25	100	1.00
	10-6	7.50	100	1.00
	10-7	6.00	15	0.40
		7.50	100	0.60
0.25	10-2	6.75	100	1.00
	10-3	7.50	100	1.00
	10-4	7.50	100	1.00
	10-5	7.50	100	1.00
	10-6	7.50	100	1.00
	10-7	6.00	15	0.10
		7.50	100	0.90

As discussed previously, epistemic variability in nonlinear dynamic material properties for the horizontal motions was addressed by computing V/H ratios for both EPRI (1993) as well as Peninsular Range (Silva et al. 1996) G/G_{max} and hysteretic damping curves. In addition, V/H ratios were computed for both single- and double-corner source models as well as both empirical and site-specific V/H ratios. Equal weights were applied to the vertical hazard computed using the EPRI (1993) and Peninsular Range curves as well as single- versus double-corner source models. For profiles 1 and 2 (Section 5.3.1.1.1), which included the shallow stiff soil/soft rock and firm rock materials, equal weight was given to the empirical rock and site-specific V/H ratios. For profile 3, with those softer near-surface layers removed, the site-specific V/H ratios were given a weight of 0.8, with 0.2 for the empirical WNA soft-rock V/H ratios. The relative weights are listed in Table 5.7.

It is important to note that the weights regarding V/H ratios were not applied to the ratios themselves. This approach would neglect the epistemic variability due to uncertainty in the correct mean V/H ratios. Rather, for each case, full vertical hazard curves were developed and weights applied over exceedance frequency to develop appropriate estimates of mean vertical hazard with AEF consistent with that of the horizontal.

Table 5.7: Weights for Amplification Factors and V/H Ratios

Source Model		
Single-Corner (1c)		0.5
Double-Corner (2c)		0.5
Modulus Reduction and Hysteretic Damping Curves		
EPRI (1993)		0.5
Peninsular Range		0.5
V/H Ratios		
	Empirical	Site-Specific
Profile 1 (P1)	0.5	0.5
Profile 2 (P2)	0.5	0.5
Profile 3 (P3)	0.2	0.8
Horizon 1 to 7	0.0	1.0
Repository (680 m)	0.0	1.0

5.3.3 Site-Specific Horizontal and Vertical UHRS

5.3.3.1 Within Repository UHRS

Site-specific horizontal and vertical URHS were developed at the repository horizon and at the elevations of Horizons 1 through 7 (Table 5.5). At each location three horizontal and vertical UHRS were developed corresponding to profiles P1, P2 and P3 (Section 5.3.1.1.1) and AEF values of $4x10^{-4}$, 10^{-5}, and 10^{-6}. As discussed above in Section 5.3.1.1.1, the intent of the three profiles was to capture the potential effects of lateral variability in site surface conditions on the site-specific ground motions. Figure 5.42 and Figure 5.43 show the resulting 10^{-5} AEF UHRS for the repository elevation and Horizon 1 elevation, respectively. As indicated on the figures, the differences in the surface conditions (Profiles P1, P2 and P3) have minimal effect on the ground motions at depth within the elevation range of interest to repository design. Therefore, a single UHRS is developed for each AEF and repository elevation by enveloping the results obtained for the three profiles. These UHRS are then smoothed to remove dips in the spectra caused by wavefield cancellations in the idealised one-dimensional site profile, as shown on Figure 5.42 and Figure 5.43. The smoothed envelope UHRS are shown on Figure 5.44 through Figure 5.49 and are listed in Table 5.8, Table 5.9, and Table 5.10.

5.3.4 Development of Design Time Histories

Three component spectrally matched design time histories were developed for UHRS at AEF 10^{-5} and 10^{-6} for selected elevations within the repository and shaft system. The matching criteria followed those specified in the U.S. NRC Regulatory Guide 1.208 (USNRC 2007). To maintain hazard levels defined by the UHRS at high frequency, the matching criteria were extended from 0.2 – 25.0 Hz to 0.2 – 50.0 Hz.

Design time histories were developed for the repository horizon as well as the reference horizon levels. Due to the similarity in the UHRS at several horizon elevations (see Figure

5.46 through Figure 5.49), the seven UHRS were combined into four distinct UHRS: Horizon 1, envelope of Horizons 2 and 3, envelope of Horizons 4 and 5, and envelope of Horizons 6 and 7. Including the repository horizon, there are a total of five distinct sets of three-component spectrally matched time histories corresponding to AEF 10^{-5} and 10^{-6}.

The spectral matching approach adjusts the Fourier amplitude spectrum of an input (basis) time history such that its response spectrum matches that of a target (Silva and Lee 1987). The resulting time history has its phase spectrum largely unaltered, preserving the nonstationarity of the basis time history as well as relative phasing between components, both of which may be important for structural analyses.

5.3.4.1 Surface UHRS

Site-specific horizontal and vertical UHRS were developed for the surface for an AEF of 4×10^{-4} (return period of 2,500 years). These spectra are shown on Figure 5.50 and Figure 5.51 and are listed in Table 5.12. These spectra represent surface motions for three site conditions. The results for profile P1 represent surface motions on top of the Pleistocene soils. The results for profile P2 represent surface motions at the top of the firm rock with the Pleistocene soils removed (average depth below present grade of 15 m). The results for profile P3 represent surface motions at the top of the hard sedimentary rock at an average depth below the present grade of 33 m. These three conditions are provided to allow evaluation of the surface facilities using a range of possible site conditions. The results for profile P1 are considerably higher than for profiles P2 and P3, reflecting the amplification effects of the lower-velocity Pleistocene sediments.

5.3.4.2 Target Spectra

The magnitude-distance deaggregations of the 10^{-6} AEF hazard shown on Figure 5.10c, Figure 5.11c and Figure 5.12c indicate that the earthquakes that provide a majority of the hazard are different at high and low frequencies. Thus it would be unrealistic to expect a single earthquake recording to represent the entire UHRS. Instead, scenario earthquake spectra were developed to represent the earthquakes that are the dominate contributors to the hazard at various spectral frequency ranges. The selected scenarios are listed below.

The GMPEs selected for the PSHA (Section 4) were used to compute spectra for the scenario earthquakes. The scenario spectra were developed as the average of the motions predicted by the models of Atkinson and Boore (2006), Campbell (2003) and Silva et al. (2003). The model developed by Atkinson (2008) was not used because of the limited number of spectral frequencies provided. The number of standard deviations above the median motions for each scenario was selected such that the resulting spectrum provided a close match to the UHRS over the spectral frequency range of interest. Figure 5.52 and Figure 5.53 show the resulting scenario spectra compared to the UHRS for AEF values of 10^{-5} and 10^{-6}, respectively. The reference rock scenario spectra were then scaled by the transfer functions developed in Section 5.3.2 to produce target spectra for each repository elevation.

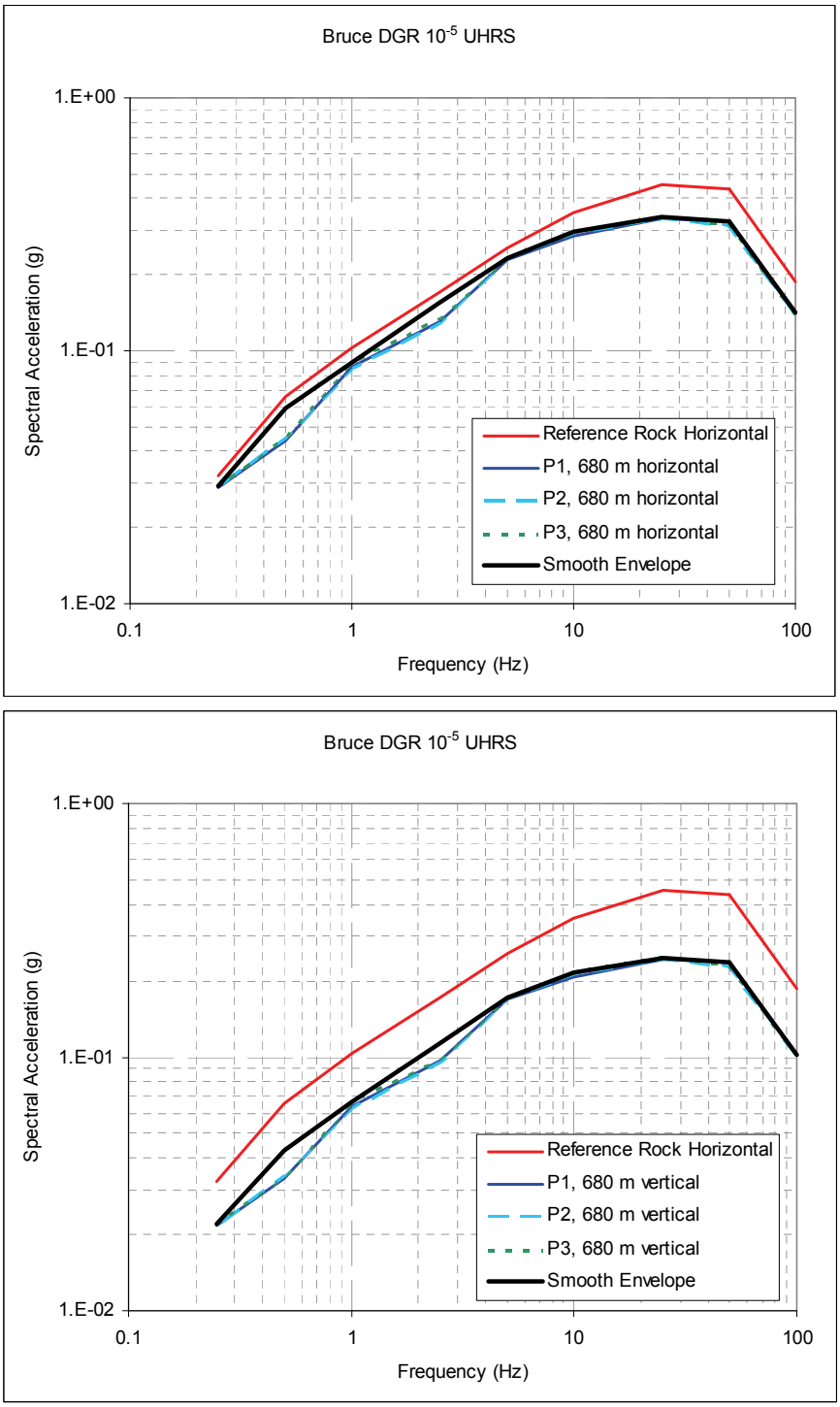

Figure 5.42: Comparison of the Horizontal Component Mean UHRS at the 680 m Repository Elevation with the Reference Rock UHS for Profiles 1, 2 and 3, and Smooth Envelope UHRS for AEF 10^{-5}

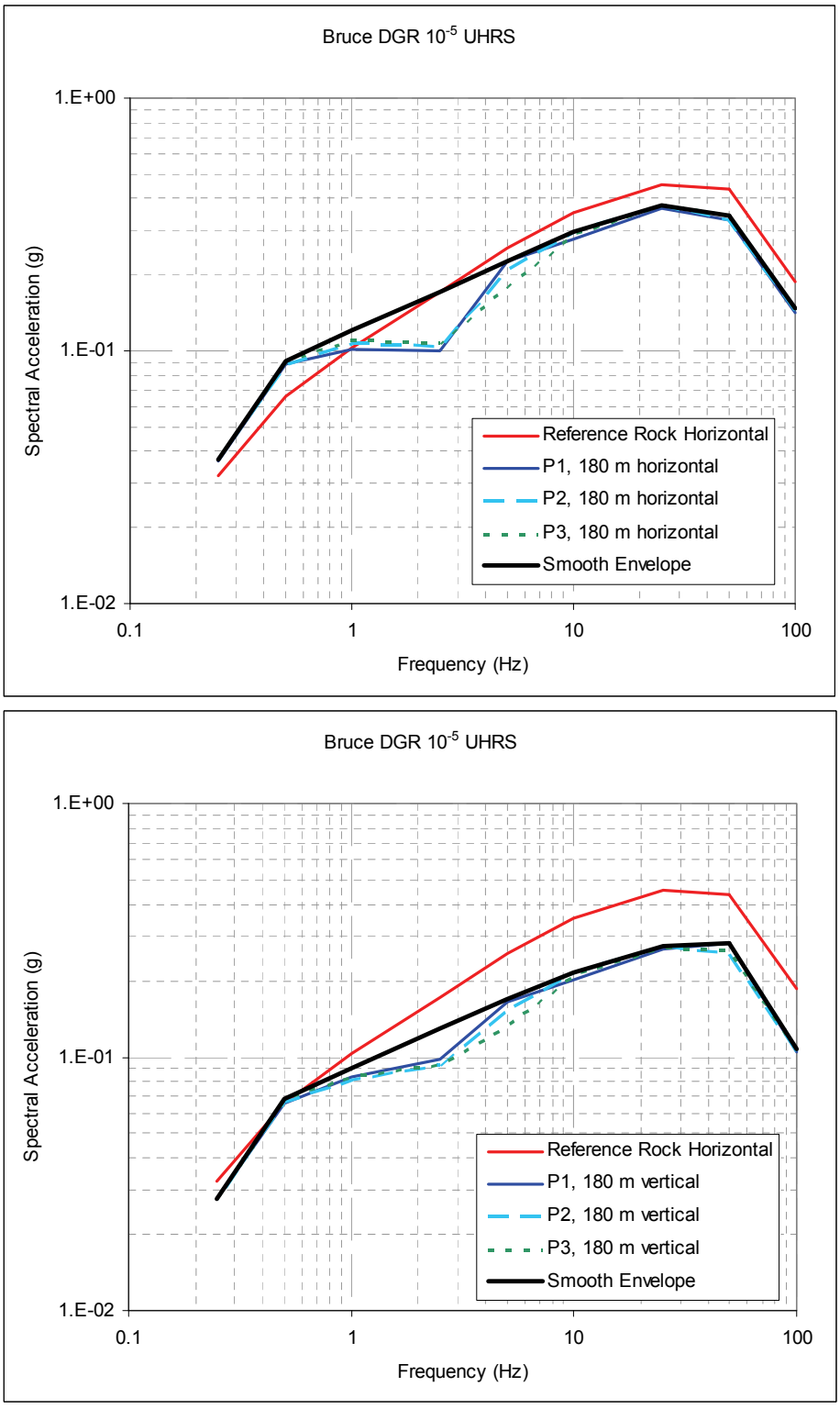

Figure 5.43: Comparison of the Horizontal Component Mean UHRS at the 180 m Horizon 1 Elevation with the Reference Rock UHS for Profiles 1, 2 and 3, and Smooth Envelope UHRS for AEF 10^{-5}

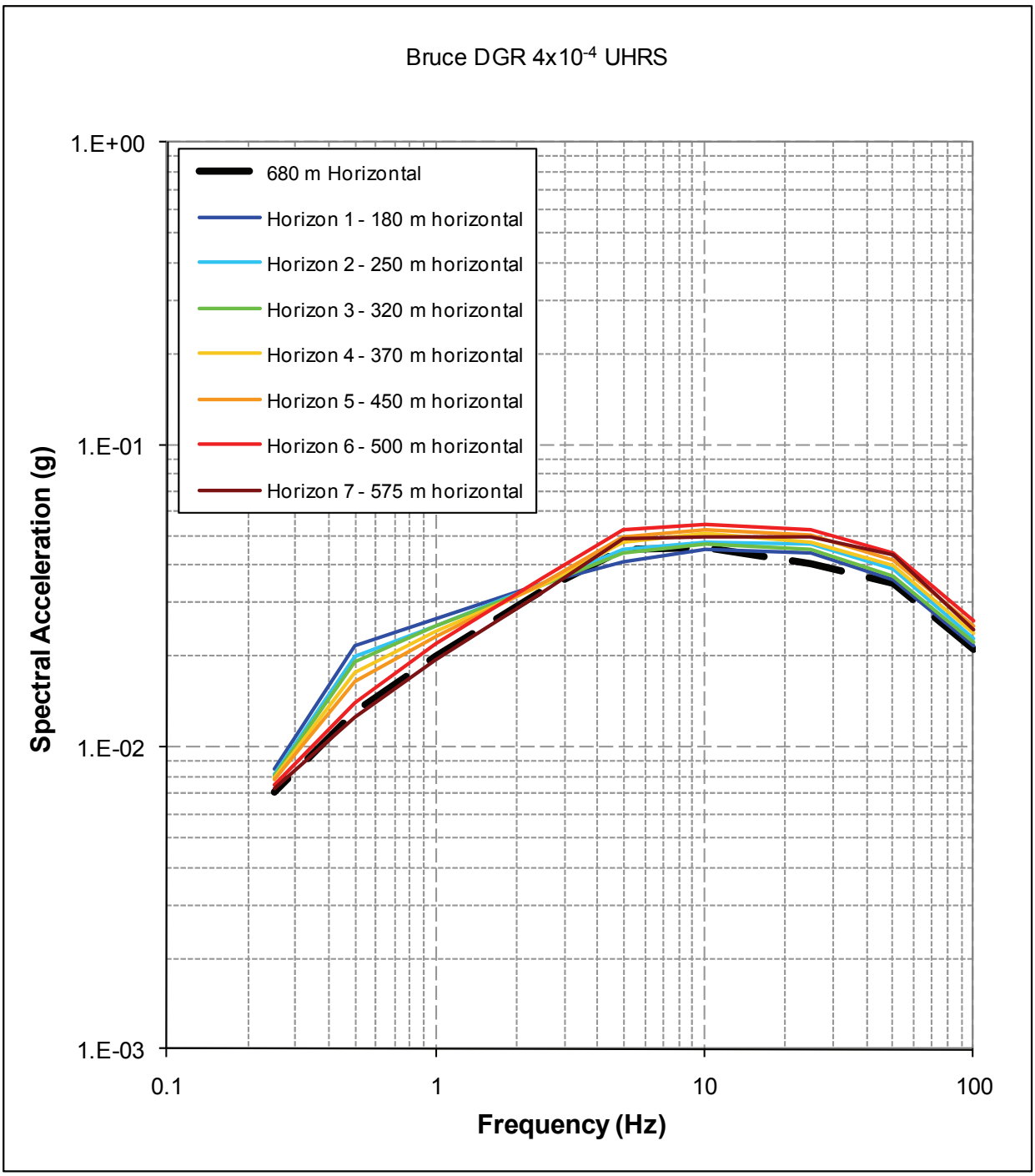

Figure 5.44: At Depth $4x10^{-4}$ AEF UHRS for Horizontal Motions

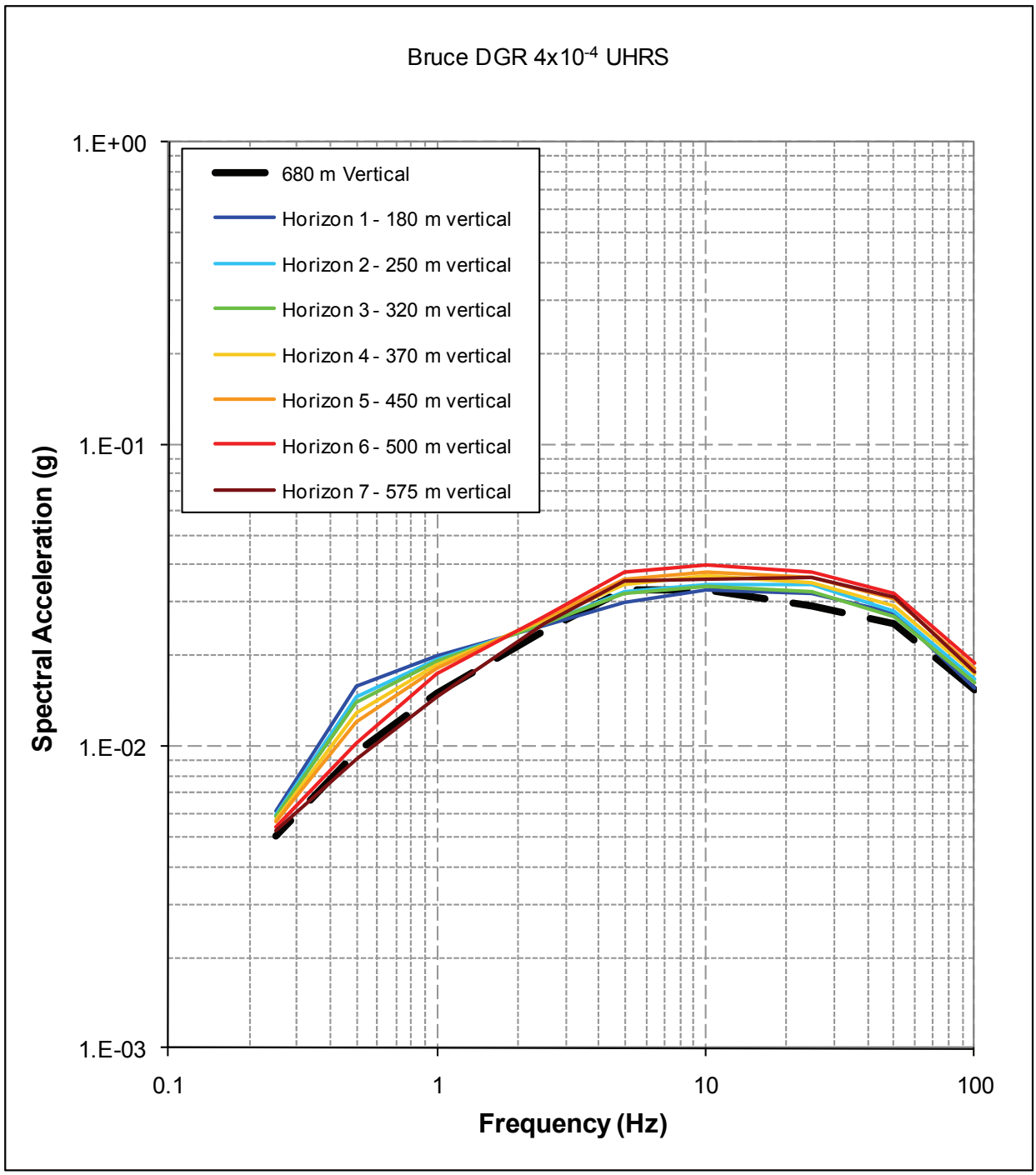

Figure 5.45: At Depth $4x10^{-4}$ AEF UHRS for Vertical Motions

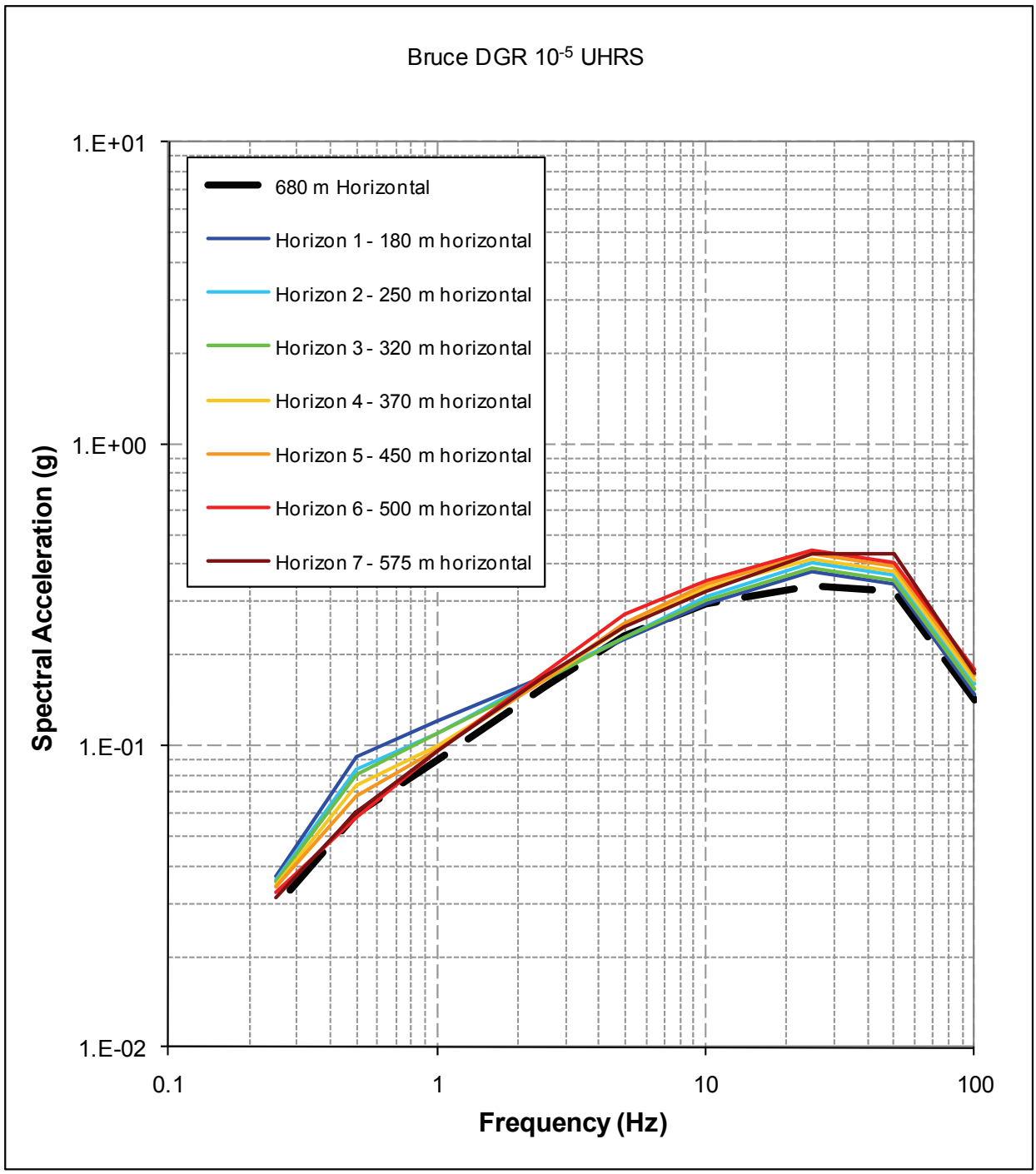

Figure 5.46: At Depth 10^{-5} AEF UHRS for Horizontal Motions

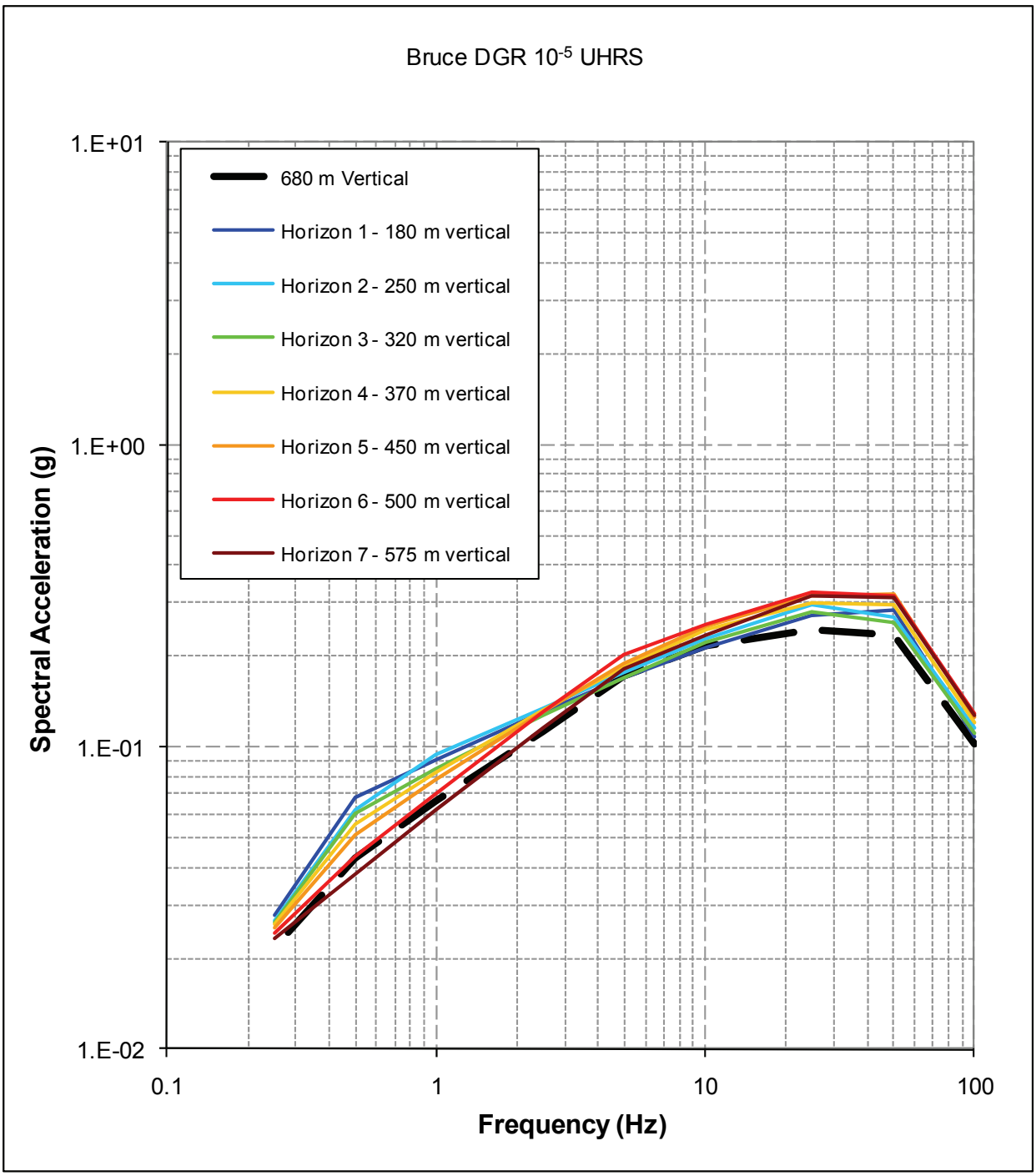

Figure 5.47: At Depth 10^{-5} AEF UHRS for Vertical Motions

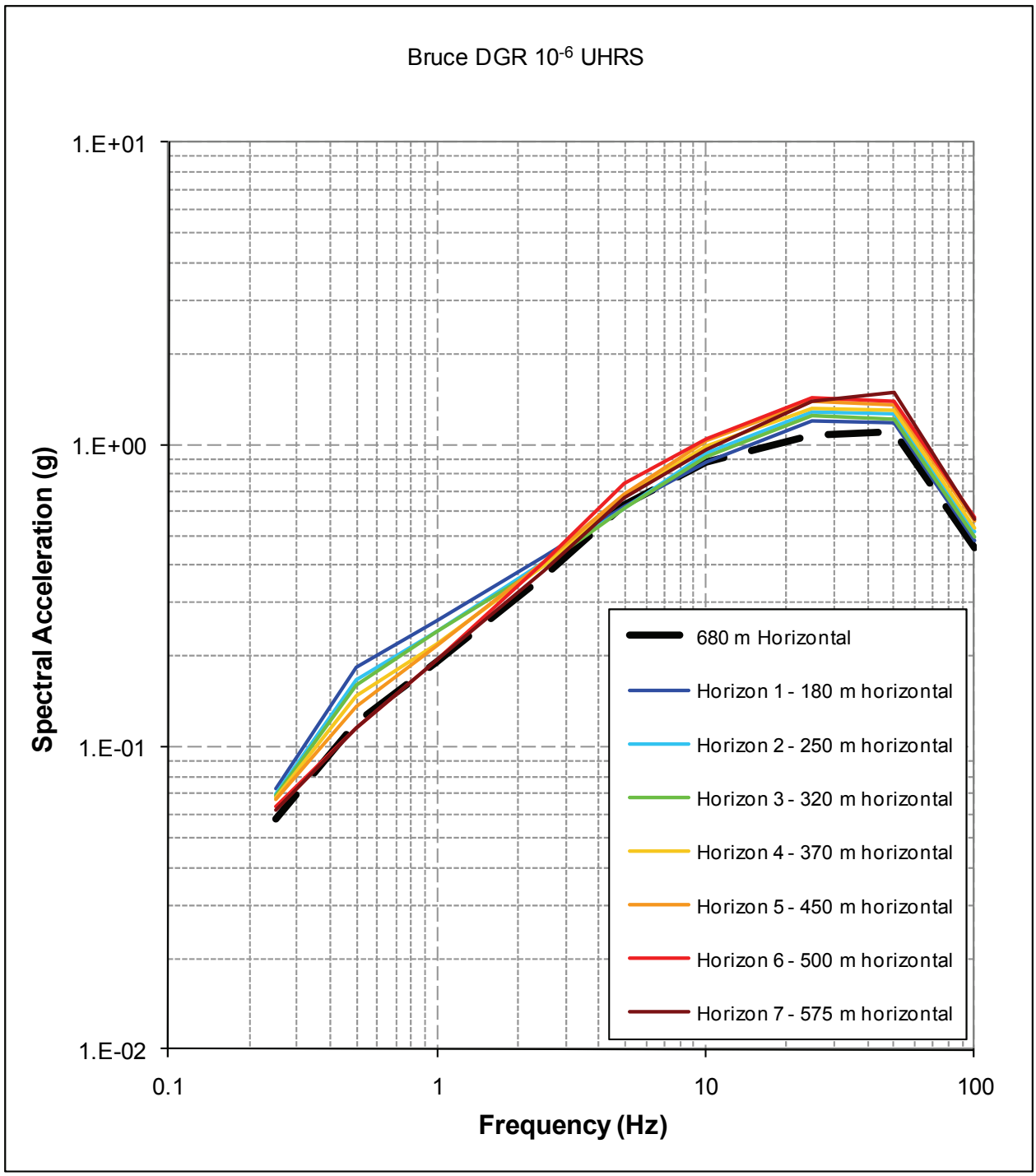

Figure 5.48: At Depth 10^{-6} AEF UHRS for Horizontal Motions

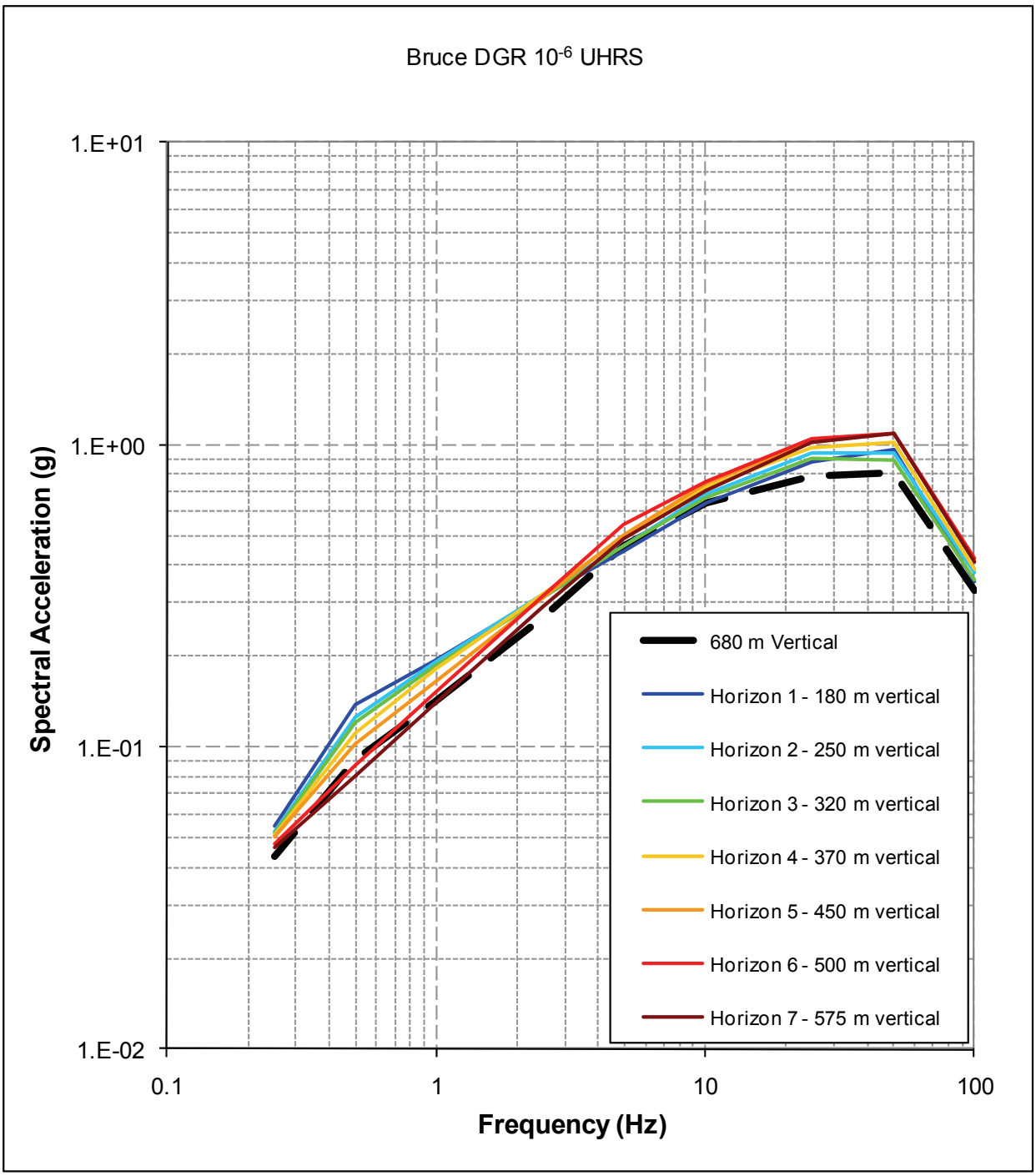

Figure 5.49: At Depth 10^{-6} AEF UHRS for Vertical Motions

Table 5.8: At Depth UHRS for $4x10^{-4}$ AEF (5 percent damping)

Spectral Period (sec)	Spectral Acceleration (g) for Location:							
	Horizon 1	Horizon 2	Horizon 3	Horizon 4	Horizon 5	Horizon 6	Horizon 7	Repository
Horizontal								
0.01	0.0215	0.0230	0.0223	0.0239	0.0250	0.0260	0.0244	0.0211
0.02	0.0359	0.0385	0.0368	0.0396	0.0413	0.0436	0.0433	0.0350
0.04	0.0439	0.0471	0.0448	0.0478	0.0503	0.0523	0.0497	0.0402
0.1	0.0452	0.0476	0.0469	0.0509	0.0524	0.0546	0.0494	0.0454
0.2	0.0412	0.0447	0.0439	0.0476	0.0494	0.0523	0.0486	0.0453
0.4	0.0350	0.0350	0.0345	0.0344	0.0346	0.0360	0.0325	0.0330
1	0.0265	0.0250	0.0250	0.0240	0.0230	0.0220	0.0195	0.0199
2	0.0217	0.0198	0.0191	0.0177	0.0164	0.0140	0.0125	0.0130
4	0.0084	0.0081	0.0081	0.0079	0.0078	0.0074	0.0073	0.0071
Vertical								
0.01	0.0156	0.0167	0.0162	0.0174	0.0182	0.0189	0.0177	0.0153
0.02	0.0276	0.0279	0.0267	0.0291	0.0308	0.0320	0.0314	0.0254
0.04	0.0319	0.0341	0.0325	0.0347	0.0364	0.0379	0.0360	0.0292
0.1	0.0328	0.0345	0.0340	0.0369	0.0380	0.0396	0.0358	0.0329
0.2	0.0299	0.0325	0.0319	0.0345	0.0358	0.0380	0.0352	0.0329
0.4	0.0250	0.0253	0.0255	0.0260	0.0265	0.0270	0.0255	0.0240
1	0.0199	0.0195	0.0190	0.0185	0.0180	0.0175	0.0145	0.0150
2	0.0158	0.0145	0.0140	0.0130	0.0120	0.0102	0.0090	0.0095
4	0.0061	0.0059	0.0059	0.0057	0.0056	0.0054	0.0052	0.0051

Table 5.9: At Depth UHRS for 10^{-5} AEF (5 percent damping)

Spectral Period (sec)	Spectral Acceleration (g) for Location :							
	Horizon 1	Horizon 2	Horizon 3	Horizon 4	Horizon 5	Horizon 6	Horizon 7	Repository
Horizontal								
0.01	0.1484	0.1592	0.1528	0.1648	0.1724	0.1782	0.1739	0.1411
0.02	0.3444	0.3683	0.3512	0.3778	0.3938	0.4059	0.4302	0.3259
0.04	0.3765	0.4066	0.3879	0.4136	0.4343	0.4462	0.4335	0.3375

0.1	0.2939	0.3134	0.3054	0.3329	0.3441	0.3503	0.3228	0.2946
0.2	0.2259	0.2291	0.2277	0.2483	0.2553	0.2734	0.2474	0.2328
0.4	0.1700	0.1700	0.1644	0.1650	0.1650	0.1750	0.1700	0.1550
1	0.1200	0.1100	0.1100	0.1000	0.0975	0.0950	0.0950	0.0897
2	0.0916	0.0834	0.0800	0.0738	0.0683	0.0581	0.0600	0.0590
4	0.0370	0.0357	0.0353	0.0345	0.0339	0.0325	0.0312	0.0292
Vertical								
0.01	0.1078	0.1157	0.1111	0.1198	0.1254	0.1296	0.1263	0.1026
0.02	0.2827	0.2700	0.2565	0.2962	0.3185	0.3161	0.3111	0.2360
0.04	0.2728	0.2948	0.2812	0.2999	0.3151	0.3237	0.3144	0.2448
0.1	0.2145	0.2286	0.2228	0.2429	0.2511	0.2557	0.2354	0.2150
0.2	0.1700	0.1770	0.1700	0.1827	0.1878	0.2011	0.1821	0.1713
0.4	0.1300	0.1350	0.1270	0.1320	0.1300	0.1300	0.1150	0.1130
1	0.0910	0.0940	0.0850	0.0820	0.0780	0.0700	0.0616	0.0661
2	0.0682	0.0622	0.0599	0.0555	0.0512	0.0433	0.0380	0.0430
4	0.0276	0.0267	0.0264	0.0258	0.0253	0.0242	0.0233	0.0219

Table 5.10: At depth UHRS for 10^{-6} AEF (5 percent damping)

Spectral Period (sec)	Spectral Acceleration (g) for Location:							
	Horizon 1	Horizon 2	Horizon 3	Horizon 4	Horizon 5	Horizon 6	Horizon 7	Repository
Horizontal								
0.01	0.4824	0.5164	0.4956	0.5337	0.5580	0.5763	0.5660	0.4537
0.02	1.1885	1.2704	1.2089	1.3030	1.3585	1.3989	1.4904	1.1024
0.04	1.2037	1.2873	1.2409	1.3218	1.3871	1.4239	1.3865	1.0726
0.1	0.8712	0.9339	0.9083	0.9948	1.0290	1.0427	0.9606	0.8726
0.2	0.6200	0.6133	0.6176	0.6757	0.6830	0.7432	0.6690	0.6344
0.4	0.4250	0.4100	0.4000	0.4000	0.4100	0.4100	0.3850	0.3655
1	0.2600	0.2400	0.2400	0.2200	0.2150	0.1950	0.1950	0.1905
2	0.1827	0.1663	0.1599	0.1478	0.1363	0.1151	0.1150	0.1202
4	0.0725	0.0700	0.0693	0.0679	0.0667	0.0639	0.0616	0.0579
Vertical								
0.01	0.3508	0.3751	0.3596	0.3884	0.4069	0.4196	0.4118	0.3294

0.02	0.9643	0.9337	0.8899	1.0175	1.0972	1.0844	1.0864	0.8121
0.04	0.8818	0.9390	0.9049	0.9730	1.0155	1.0399	1.0120	0.7877
0.1	0.6373	0.6832	0.6647	0.7245	0.7495	0.7593	0.7014	0.6386
0.2	0.4450	0.4650	0.4600	0.4943	0.4996	0.5443	0.4893	0.4654
0.4	0.3150	0.3200	0.3100	0.3200	0.3100	0.3150	0.2900	0.2700
1	0.1950	0.1900	0.1850	0.1800	0.1650	0.1520	0.1400	0.1418
2	0.1384	0.1258	0.1208	0.1114	0.1026	0.0874	0.0800	0.0901
4	0.0547	0.0528	0.0522	0.0511	0.0502	0.0481	0.0465	0.0436

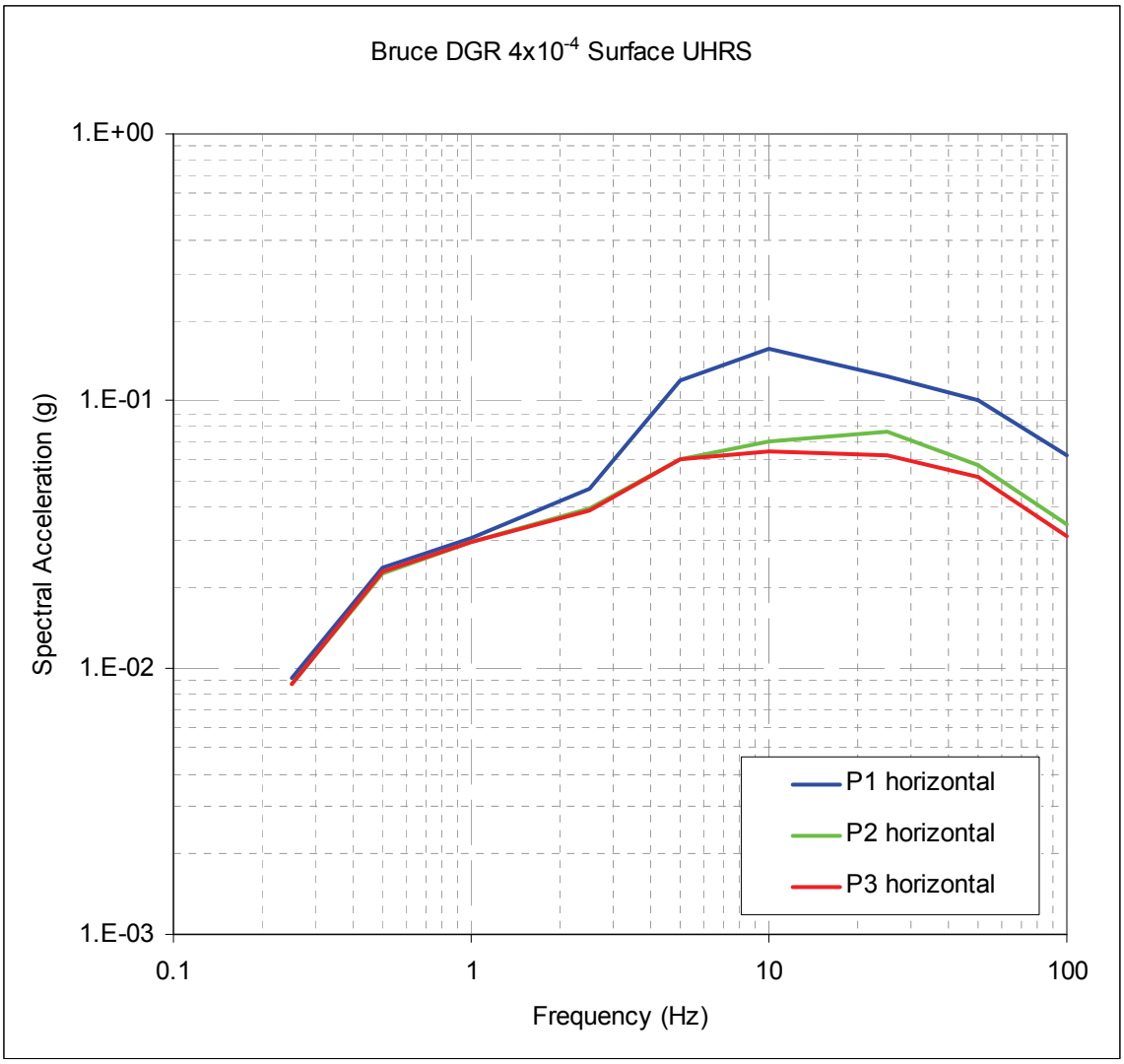

Figure 5.50: Surface 4×10^{-4} AEF Surface UHRS for Horizontal Motions

Table 5.11: Scenario Earthquakes for Time History Development

Annual Exceedance Frequency	Approximate Spectral Frequency Range (Hz)	Magnitude	Distance (km)
10^{-5}	5 to 100	5.5	20
	1 to 10	6.5	100
	0.1 to 2	7.4	300
10^{-6}	5 to 100	5.25	10
	1 to 10	6.25	25
	0.1 to 2	7.4	200

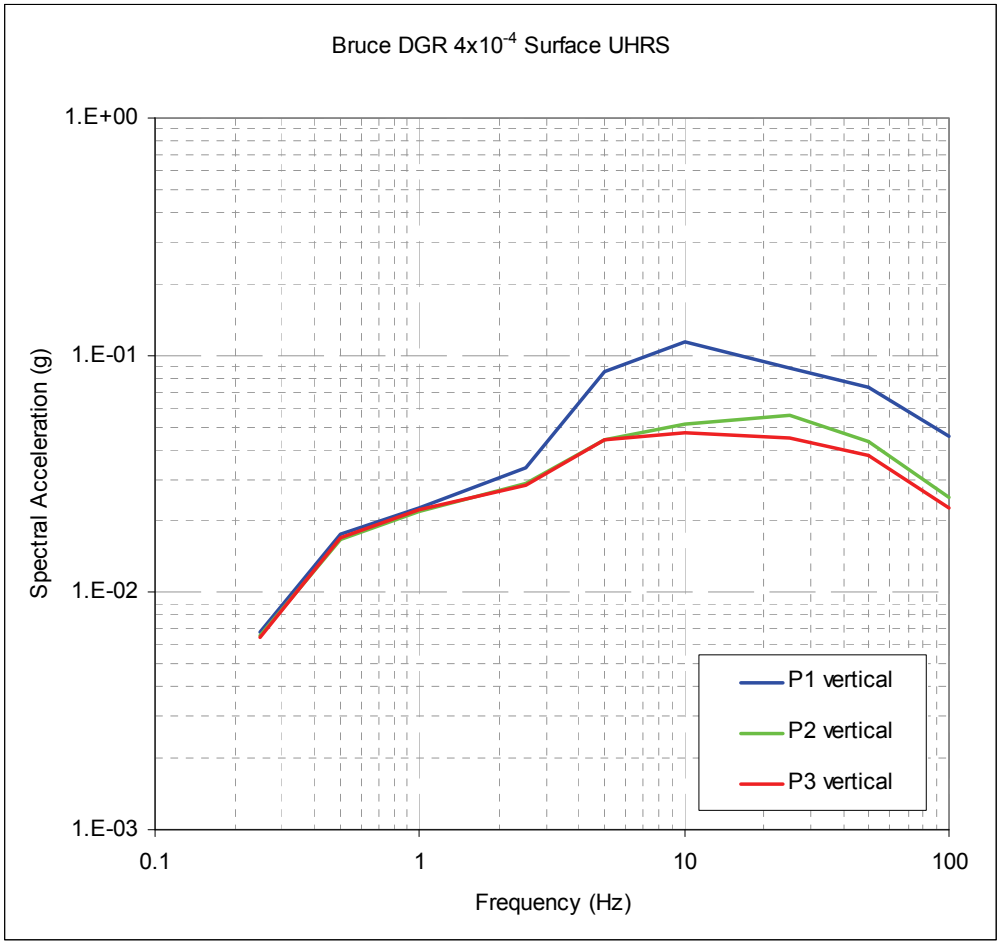

Figure 5.51: Surface 4×10^{-4} AEF Surface UHRS for Vertical Motions

5.3.4.3 Basis Time Histories

The basis time histories selected for the spectral matching to the three deterministic spectra include the 1994 Northridge earthquake, an **M** 5.3 aftershock as well as the **M** 6.7 main shock. For the largest deterministic magnitude, a rock site recording of the 1999 **M** 7.6 earthquake in Chi-Chi, Taiwan, was selected. Table 5.13 summarizes the basis earthquakes, site conditions, and distances.

Table 5.12: Surface UHRS for 4×10^{-4} AEF (5 percent damping)

Spectral Period (sec)	Spectral Acceleration (g) for Profile:		
	P 1	P 2	P 3
Horizontal			
0.01	0.0627	0.0346	0.0312
0.02	0.1013	0.0573	0.0518
0.04	0.1227	0.0769	0.0623
0.1	0.1566	0.0704	0.0643
0.2	0.1184	0.0603	0.0605
0.4	0.0465	0.0398	0.0390
1	0.0304	0.0294	0.0295
2	0.0238	0.0226	0.0230
4	0.0092	0.0087	0.0087
Vertical			
0.01	0.0457	0.0251	0.0227
0.02	0.0738	0.0435	0.0381
0.04	0.0889	0.0557	0.0452
0.1	0.1144	0.0513	0.0471
0.2	0.0859	0.0439	0.0440
0.4	0.0338	0.0288	0.0283
1	0.0229	0.0221	0.0222
2	0.0176	0.0167	0.0171
4	0.0069	0.0065	0.0065

5.3.4.4 Time Histories

The suite of 30 sets of three component design time histories are shown in Appendix A. For each spectral match the acceleration, velocity and displacement time histories are shown along with the target and spectra for the matched time histories (both linear and logarithmic

comparisons) and the ratio of the spectral ordinates for the matched time history to the target spectra.

Table 5.13: Basis Time Histories

Earthquake	Date	M	Site	D(km)	Site
Northridge aftershock	03/20/94	5.3	Temple and Hope	31.4	rock
Northridge	01/17/94	6.7	Rancho Cucamonga	80.0	rock
Chi-Chi	09/20/99	7.6	PNG	110.3	rock

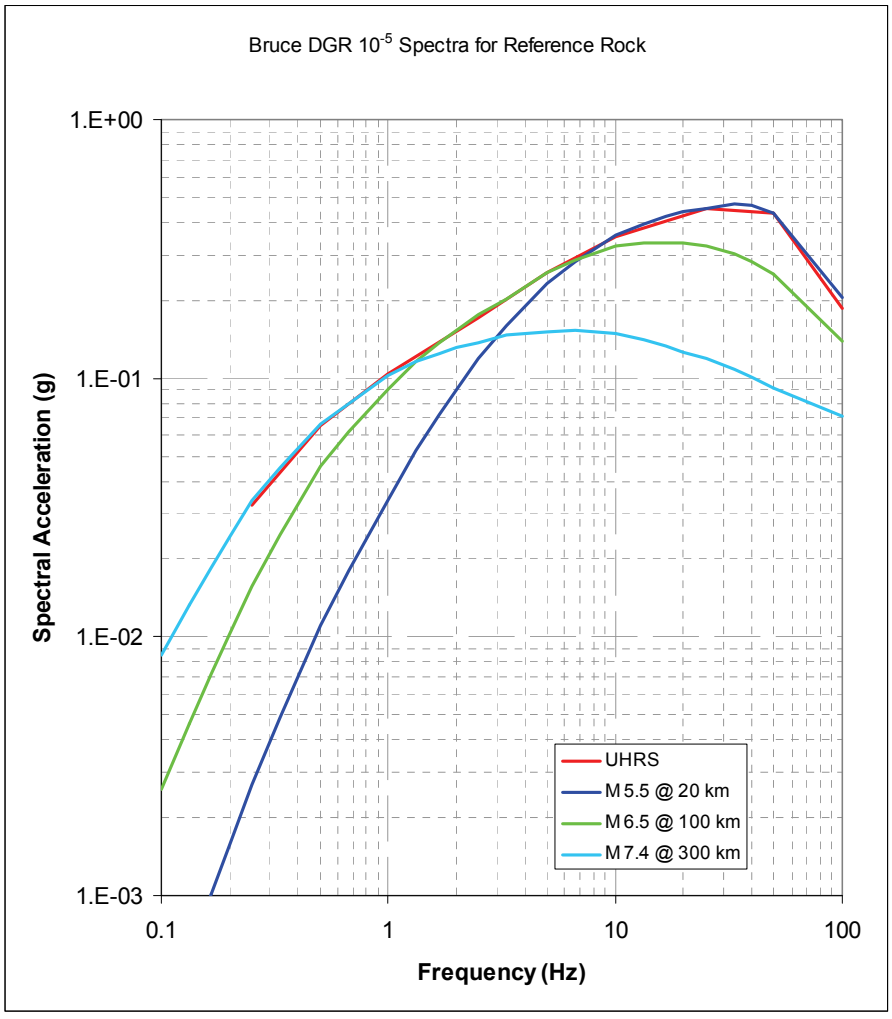

Figure 5.52: Scenario Earthquake Spectra for 10^{-5} AEF Horizontal Motions on Reference Hard Rock

The cross-correlations of the acceleration time histories are listed in Table 5.14. All are less than the minimum of 0.16 specified in Regulatory Guide 1.208 (U.S. NRC 2007).

Figure 5.54, Figure 5.55 and Figure 5.56 show how the response spectra for the three scenario time histories in aggregate provide a good match to the repository 10^{-5} AEF UHRS over the entire frequency range. Use of the three scenario time histories captures the ground motion levels corresponding to the target AEF with realistic motions that may be experienced in individual earthquakes. Figure 5.57, Figure 5.58, and Figure 5.59 show similar results for the 10^{-6} AEF time histories.

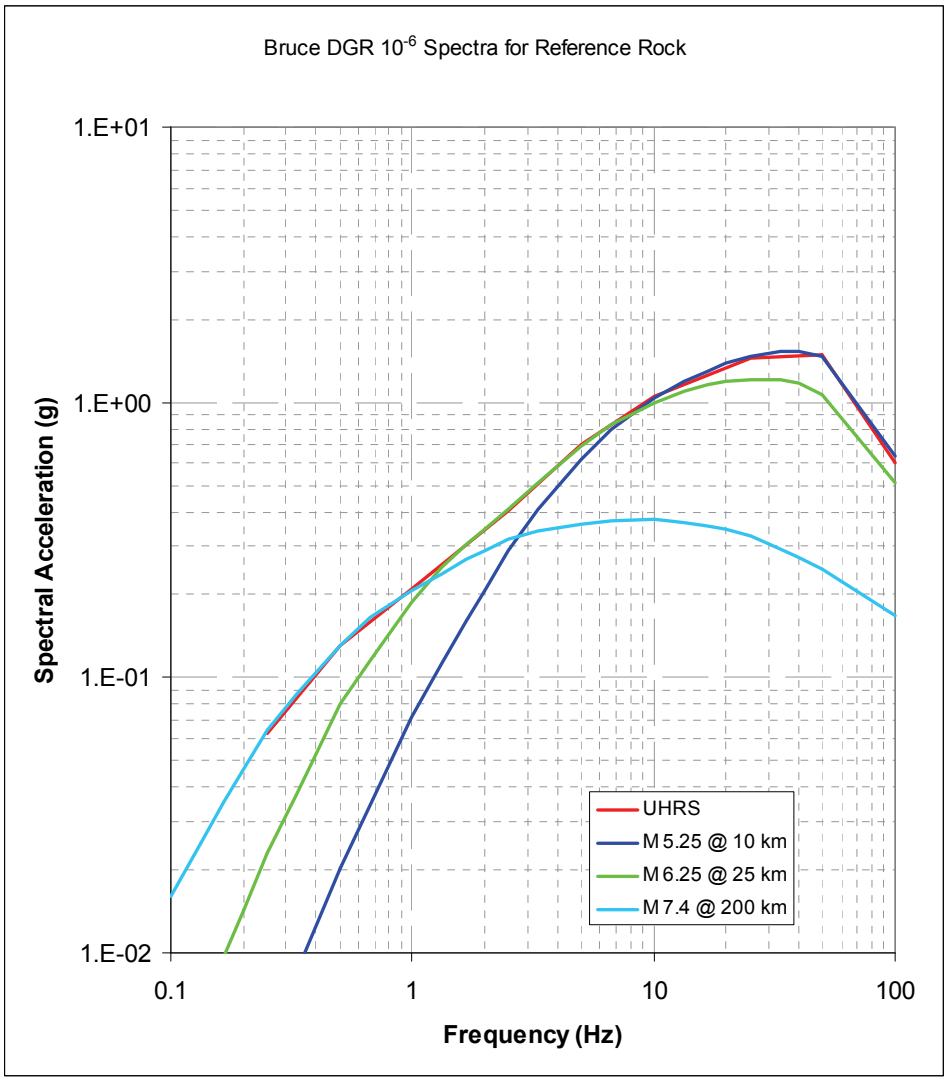

Figure 5.53: Scenario Earthquake Spectra for 10^{-6} AEF Horizontal Motions on Reference Hard Rock

Table 5.14: Cross-Correlations of Spectrally Matched Acceleration Time Histories

Time Histories for Location	Annual Exceedance Frequency	Scenario Magnitude	Cross-Correlation for Components:		
			H1 – H2	H1 – V	H2 – V
Horizon 1	10^{-5}	5.50	0.0354	-0.0376	0.0725
		6.50	0.0052	-0.0121	-0.0135
		7.40	0.0070	0.0643	-0.0457
	10^{-6}	5.25	0.0262	-0.0528	0.0760
		6.25	0.0134	-0.0368	-0.0080
		7.40	0.0135	0.0795	-0.0303
Horizons 2 and 3	10^{-5}	5.50	0.0335	-0.0368	0.0732
		6.50	0.0093	-0.0171	-0.0145
		7.40	0.0080	0.0725	-0.0336
	10^{-6}	6.25	0.0139	-0.0403	-0.0125
		5.25	0.0546	0.0554	0.0766
		7.40	0.0300	0.0826	-0.0227
Horizons 4 and 5	10^{-5}	5.50	0.0334	-0.0411	0.0742
		6.50	0.0052	-0.0206	-0.0255
		7.40	0.0248	0.0894	-0.0238
	10^{-6}	5.25	0.0266	-0.0518	0.0772
		6.25	0.0125	-0.0437	-0.0144
		7.40	0.0374	0.1017	-0.0098
Horizons 6 and 7	10^{-5}	5.50	0.0331	-0.0392	0.0727
		6.50	0.0018	-0.0233	-0.0267
		7.40	0.0333	0.1047	-0.0134
	10^{-6}	5.25	0.0277	-0.0529	0.0765
		6.25	0.0098	-0.0449	-0.0159
		7.40	0.0458	0.1120	-0.0017
Repository	10^{-5}	5.50	0.0379	-0.0265	0.0693
		6.50	-0.0028	-0.0168	-0.0261
		7.40	-0.0018	0.1061	-0.0182
	10^{-6}	5.25	0.0320	-0.0417	0.0737
		6.25	0.0088	-0.0413	0.0171
		7.40	0.0184	0.1021	-0.0095

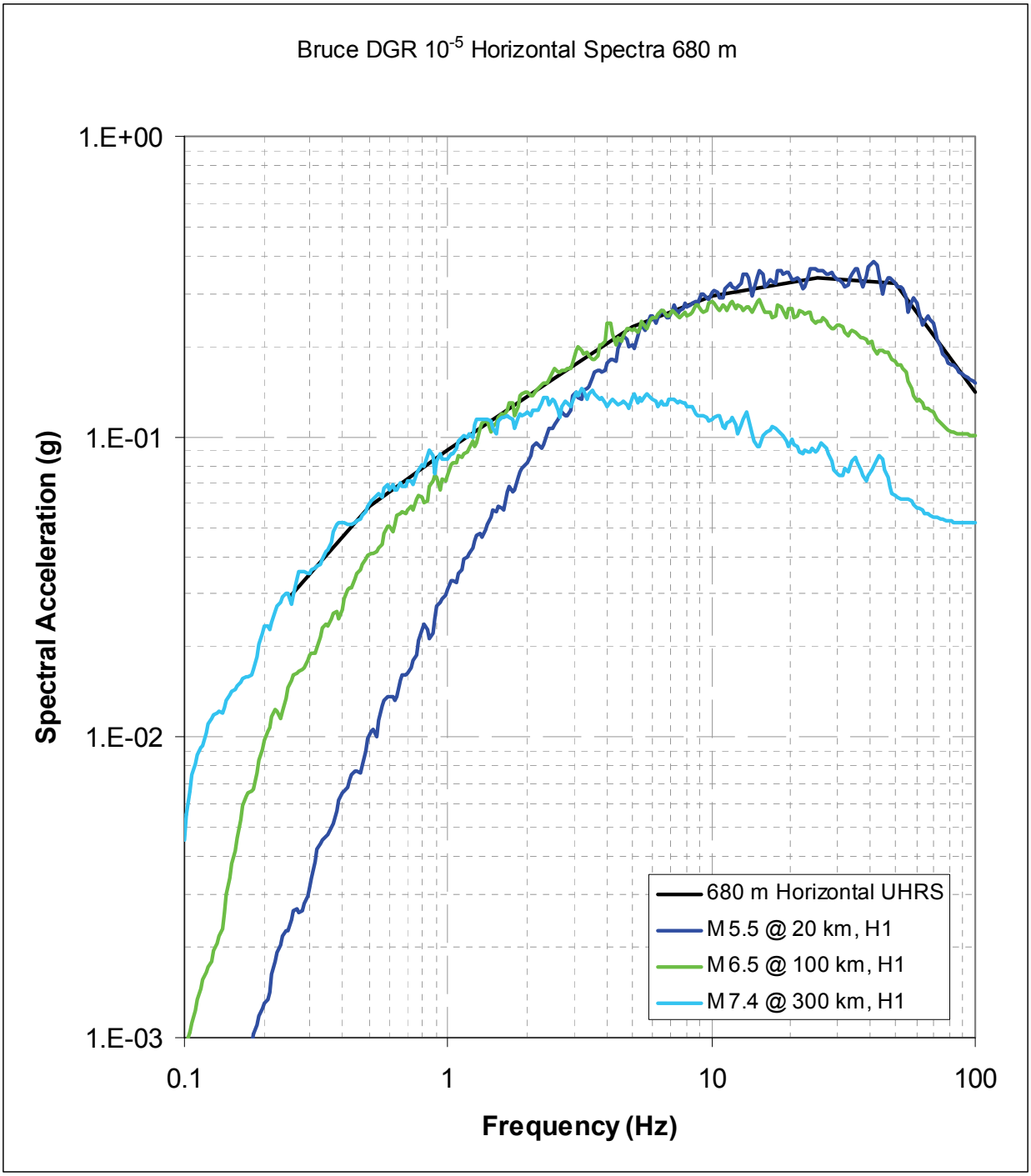

Figure 5.54: Comparison of Response Spectra for the H1 Component Scenario Time Histories with the 10^{-5} Horizontal UHRS for the Repository Elevation (680 m depth)

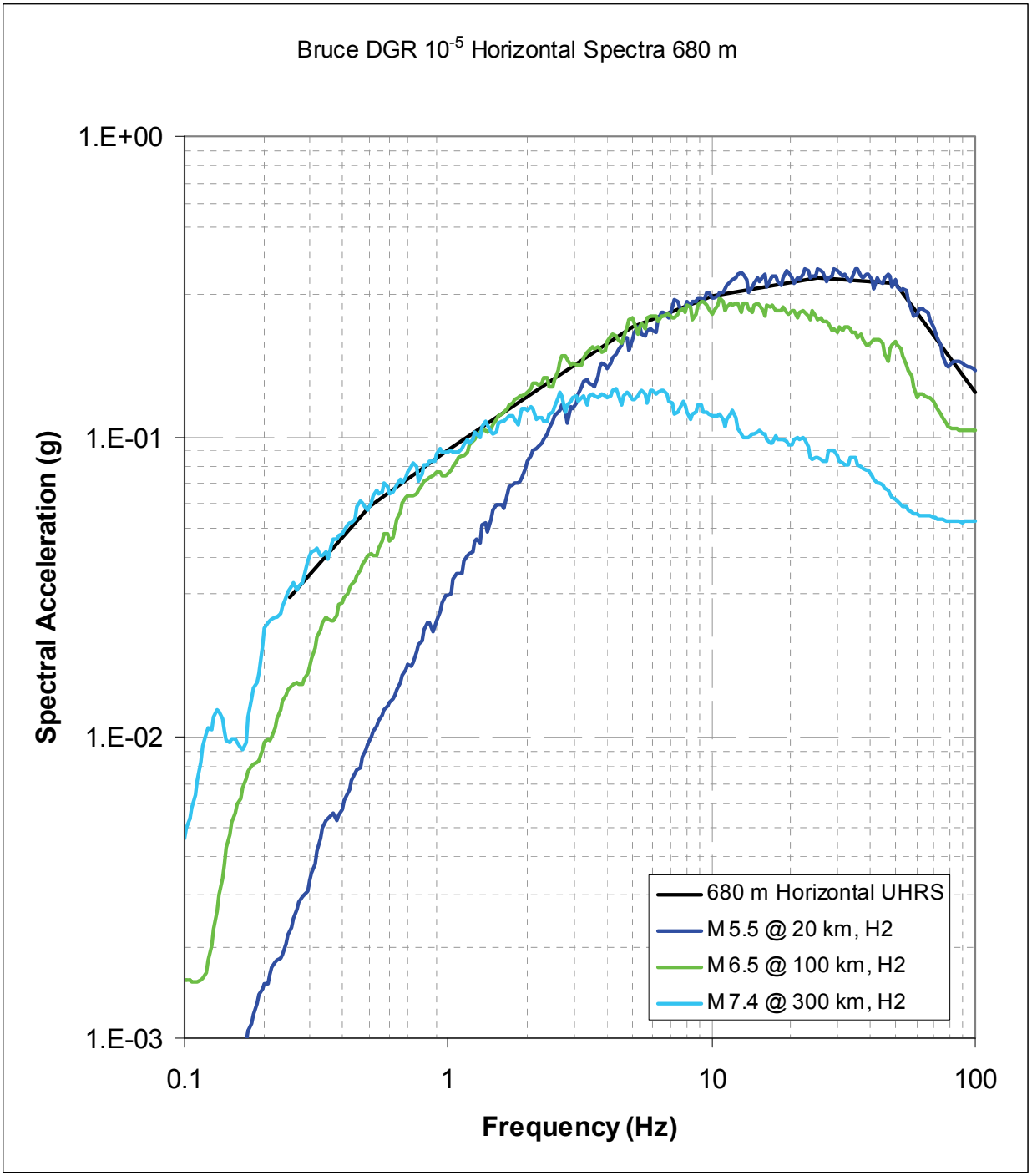

Figure 5.55: Comparison of Response Spectra for the H2 Component Scenario Time Histories with the 10^{-5} Horizontal UHRS for the Repository Elevation (680 m depth)

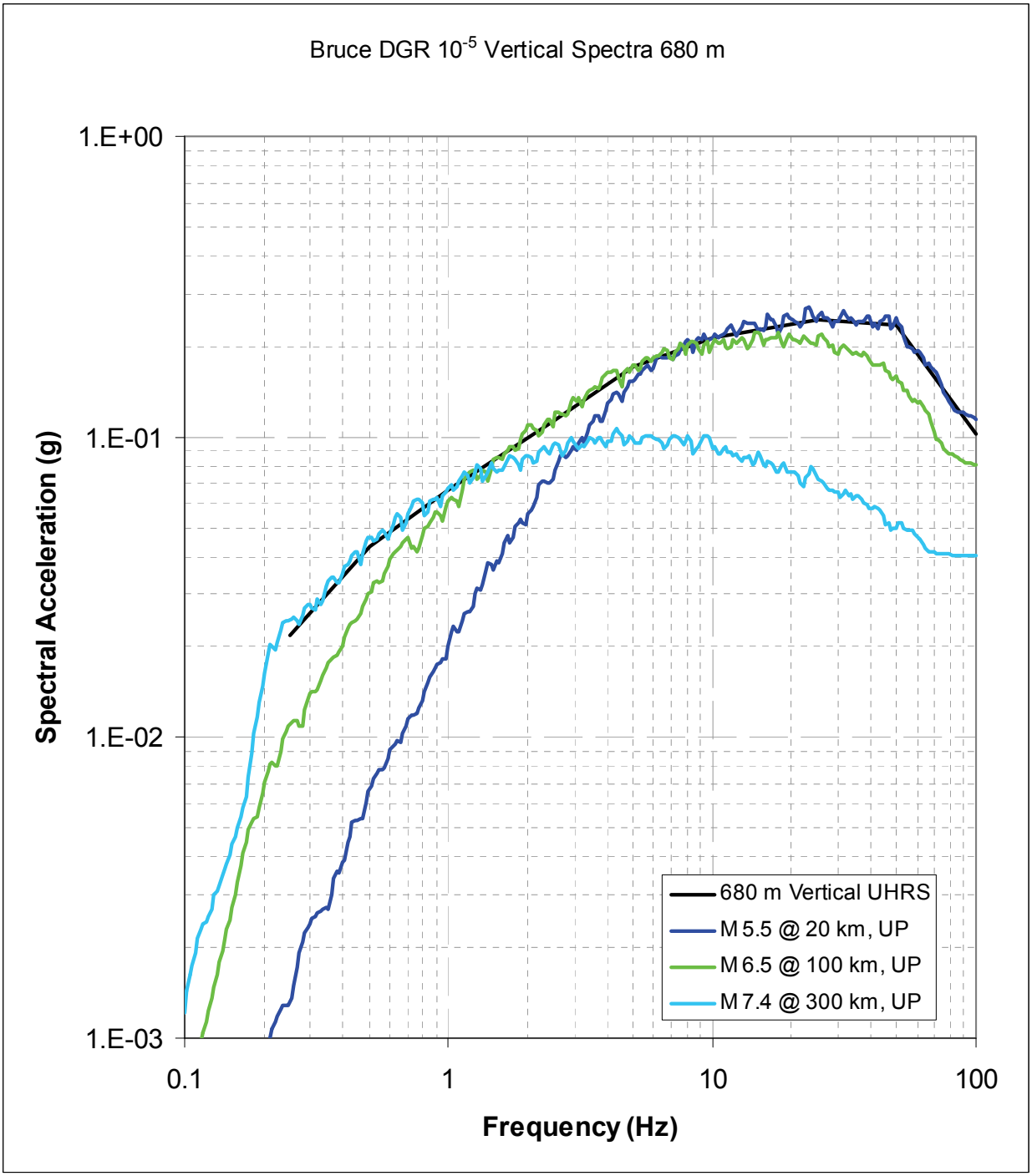

Figure 5.56: Comparison of Response Spectra for the V Component Scenario Time Histories with the 10^{-5} Vertical UHRS for the Repository Elevation (680 m depth)

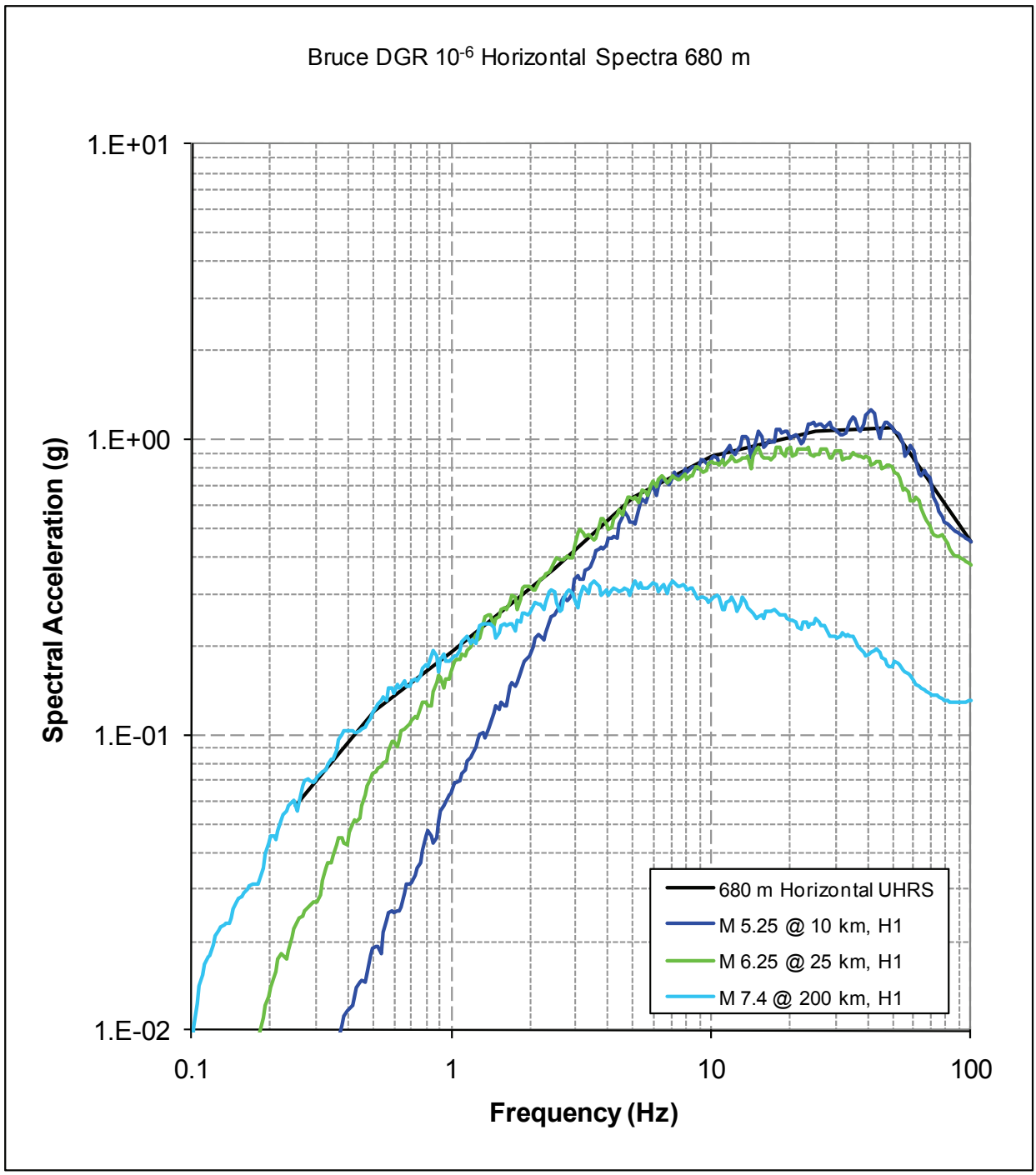

Figure 5.57: Comparison of Response Spectra for the H1 Component Scenario Time Histories with the 10^{-6} Horizontal UHRS for the Repository Elevation (680 m depth)

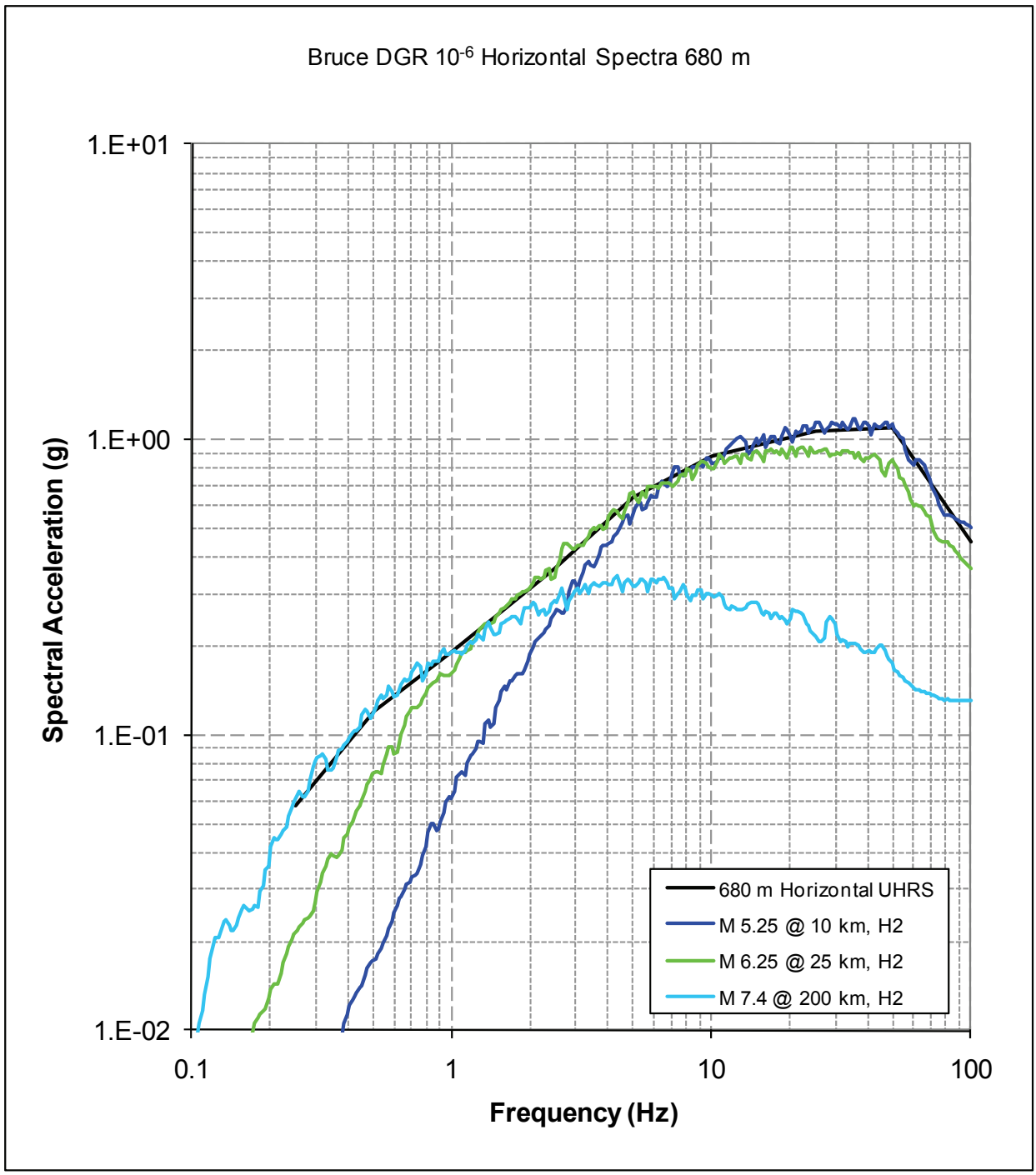

Figure 5.58: Comparison of Response Spectra for the H1 Component Scenario Time Histories with the 10^{-6} Horizontal UHRS for the Repository Elevation (680 m depth)

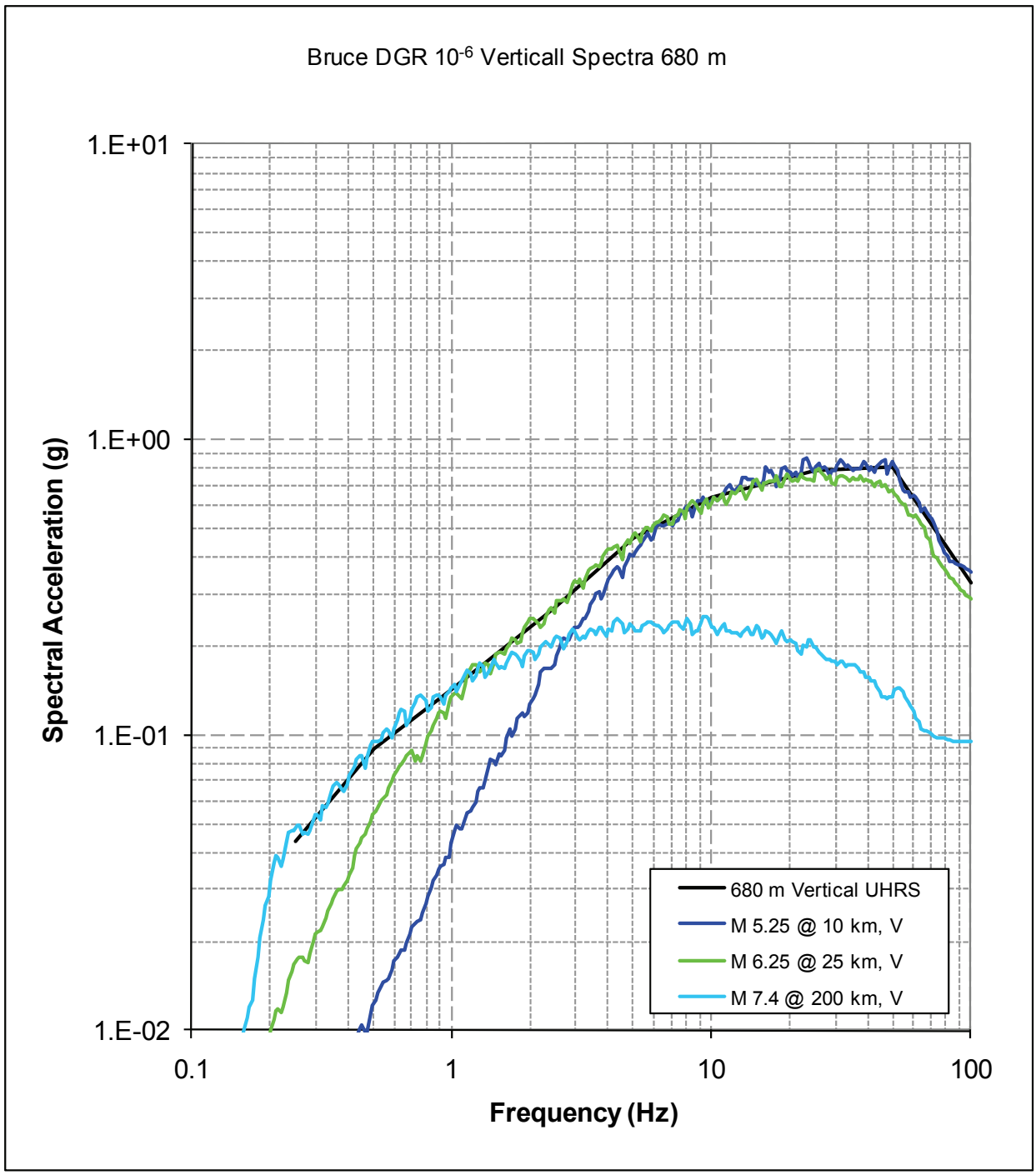

Figure 5.59: Comparison of Response Spectra for the V Component Scenario Time Histories with the 10^{-6} Vertical UHRS for the Repository Elevation (680 m depth)

6. CONCLUSIONS

This report develops design ground motions for the proposed Deep Geologic Repository (DGR) at the Bruce nuclear site in Ontario, Canada. The site is located in the stable continental region of eastern North America in a region of low, diffuse seismicity. Examination of the earthquake catalogue developed for the region indicates that only five earthquakes with estimated moment magnitudes greater than **M** 2 have occurred within 100 km of the site. The catalogue contains only 43 earthquakes with magnitudes greater than **M** 2 within 200 km of the site, the largest of these was the 1959/8/4 earthquake with an estimated moment magnitude of **M** 3.9 located 184 km from the site. Areas of higher seismicity in the region are located near the western end of Lake Ontario, approximately 175 km southeast of the site and in western Quebec, approximately 375 km northeast of the site.

The design ground motions for the DGR were developed in a two-stage process. The first stage involved performing a probabilistic seismic hazard assessment (PSHA) for the site for a reference site condition. The second stage involved translating the results of the PSHA to ground motions at appropriate horizons within the geologic profile at the Bruce nuclear site.

The PSHA was conducted for surface motions on a reference hard rock site condition that is representative of eastern North America. The main components of the PSHA are seismic source characterization and ground motion characterization. Seismic source characterization provides a probabilistic model for the rate of occurrence, spatial distribution, and size distribution of earthquakes within the region surrounding the site. Two types of seismic sources were included in the model. The primary sources are regional source zones used to model the occurrence of distributed seismicity throughout the region. In addition, specific geologic/geophysical features that have been proposed as possible active sources in the scientific literature were included as local seismic sources that may concentrate seismicity. These are located primarily in the vicinity of the western end of Lake Ontario. Ground motion characterization provides a probabilistic model for the level of ground shaking that earthquakes in the region may produce at the Bruce nuclear site. The PSHA conducted for the DGR explicitly incorporated uncertainties in the probabilistic models and model parameters that affect seismic hazard at the site. In particular, the probability that the local sources are indeed active was included in the PSHA model.

The results of the PSHA provided uniform hazard response spectra (UHRS) for annual exceedance frequencies (AEF) in the range of 10^{-2} to 10^{-8} (return periods of 100 to 10^{8} years). The regional source zones were found to be the dominant contributors to the hazard. The contribution of individual assessments to the uncertainty for various components in the seismic hazard computation was also examined. The results indicated that selection of the appropriate ground motion models is the largest contributor to the uncertainty in seismic hazard. Other significant sources of uncertainty are the regional seismotectonic source spatial distribution models, the maximum magnitude assessments, and the estimation of the b-value of the Gutenberg-Richter magnitude-frequency relationships. The results of the PSHA are generally consistent with values published in the 2005 National Building Code of Canada when corrected to a common site condition and accounting for the differences in the selected ground motion models used in the two studies.

The results of the PSHA indicate that the estimated ground motions at the surface on hard rock are expected to be less than 1.0g for annual exceedance frequencies of 10^{-5}, the reference case, and 10^{-6}, the extreme case. The following table summarizes the results of the PSHA.

Table 6.1: Summary of PSHA Results

Annual Exceedance Frequency (AEF)	Peak Ground Acceleration on Hard Rock (%g)
1/1000	1.7
1/2500*	2.7
1/100,000	18.7
1/1,000,000	60.6

Notes: * AEF used in 2005 NBCC

These relatively low levels of seismic hazard are consistent with the low level of seismicity in the site region. The estimated cumulative annual occurrence frequency for a M 5 **or** larger earthquake within 100 km of the Bruce nuclear site is 3x10-4, and for a M 6 **or** larger earthquake within 200 km of the site the value is 1x10-4.

The second stage of the process for development of design ground motions involved translating the reference hard rock PSHA results to appropriate horizons within the proposed repository system in a manner that preserves the probabilistic levels assigned to each UHRS. A probabilistic model for site response was developed utilizing measured dynamic properties of the site geologic units. This model was then used to develop UHRS at the repository level (depth 680 m) and at seven selected reference horizon levels between the surface and the repository. In addition UHRS were developed for the ground surface for three representative site conditions which reflect differences in the amount of surficial material that may be removed. These UHRS are provided for both horizontal and vertical motions. The resulting levels of ground motion are similar to those developed for the hard rock surface reflecting the generally high stiffness of the in-situ rock layers.

The final task was to develop design time histories for the repository and selected horizon levels. In order to represent the hazard with realistic earthquake motions, three scenario earthquakes were developed to represent the range of earthquakes contributing to the site hazard. Acceleration time histories were then spectrally matched to response spectra for these scenario earthquakes. The envelope of the response spectra for the three scenario earthquake time histories provides a good match to the repository and horizon UHRS.

7. REFERENCES

Abdel-Rahman, A.-F.M. and P.S. Kumarapeli. 1998. Geochemistry of mantle-related intermediate rocks from the Tibbit Hill volcanic suite, Quebec Appalachians. Mineralogical Magazine 62, 487-500.

Abrahamson, N.A. and K.M. Shedlock. 1997. Overview. In special issue on ground motion attenuation, Seismological Research Letters 68, 9-23.

Abrahamson, N.A. and W.J. Silva. 1997. Empirical response spectral attenuation relations for shallow crustal earthquakes. Seismological Research Letters 68, 94-127.

Abrahamson, N.A. and W.J. Silva. 2008. Summary of the Abrahamson and Silva NGA ground-motion relations. Earthquake Spectra 24, 67-97.

Adams, J. 1995. The Canadian Crustal Stress Database—A Compilation to 1994. Geological Survey of Canada, Open-File 3122.

Adams, J. and J.S. Bell. 1991. Crustal stresses in Canada. In Slemmons, D.B., E.R. Engdahl, M.D. Zoback and D.D. Blackwell (Eds.), Neotectonics of North America, Boulder, Colorado, Geological Society of America, Decade Map Volume 1, pp. 367-386.

Adams, J. and P. Basham. 1991. The seismicity and seismotectonics of eastern Canada. In Slemmons, D.B., E.R. Engdahl, M.D. Zoback and D.D. Blackwell (Eds.), Neotectonics of North America. Geological Society of America, Decade Map Volume 1.

Adams, J. and S. Halchuk. 2003. Fourth generation seismic hazard maps of Canada: values for over 650 Canadian localities intended for the 2005 National Building Code of Canada. Geological Survey of Canada, Open File 4459.

Adams, J., D.H. Weichert, S. Halchuk and P.W. Basham. 1996. Trial seismic hazard maps of Canada – 1995: final values for selected Canadian cities. Geological Survey of Canada, Open File 3283.

Adams, J., P.W. Basham and S. Halchuk. 1995. Northeastern North American earthquake potential—New challenges for seismic hazard mapping. Current Research 1995-D, Geological Survey of Canada, pp. 91-99.

AECOM and ITASCA CANADA. 2011. Regional Geology – Southern Ontario. AECOM Canada Ltd. and Itasca Consulting Canada, Inc. report for the Nuclear Waste Management Organization NWMO DGR-TR-2011-15 R000. Toronto, Ontario, Canada.

Amirbekian, R.V. and B.A. Bolt. 1998. Spectral comparison of vertical and horizontal seismic strong ground motions in alluvial basins. Earthquake Spectra 14, 573-595.

Anderson, J.G. and S.E. Hough. 1984. A model for the shape of the Fourier amplitude spectrum of acceleration at high frequencies. Bulletin of the Seismological Society of America 74, 1969-1993.

Anglin, F.M. 1984. Seismicity and faulting in the Charlevoix zone of the St. Lawrence valley. Bulletin of the Seismological Society of America 74, 595-603.

Armstrong, D.K. and T.R. Carter. 2006. An updated guide to the subsurface Paleozoic stratigraphy of southern Ontario. Ontario Geological Survey Open File Report 6191.

Atekwana, E.A. 1996. Precambrian basement beneath the central Midcontinent United States as interpreted from potential field data. In van der Pluijm, B.A. and P.A. Catacosinos (Eds.), Basement and Basins of Eastern North America, Geological Society of America Special Paper 308, 33-44.

Atkinson, G.M. 1993. Source spectra for earthquakes in eastern North America. Bulletin of the Seismological Society of America 83, 1778-1798.

Atkinson, G.M. 2004. Empirical attenuation of ground-motion spectral amplitudes in southeastern Canada and the northeastern United States. Bulletin of the Seismological Society of America 94, 1079-1095.

Atkinson, G.M. 2008. Ground motion prediction for eastern North America from a referenced empirical approach: implications for epistemic uncertainty. Bulletin of the Seismological Society of America 98, 1304-1318.

Atkinson, G.M. and D.M. Boore. 1995. New ground motion relations for eastern North America. Bulletin of the Seismological Society of America 85, 217-30.

Atkinson, G.M. and D.M. Boore. 2006. Earthquake ground-motion prediction equations for eastern North America. Bulletin of the Seismological Society of America 96, 2181-2205.

Atkinson, G.M. and R. Mereu. 1992. The shape of ground motion attenuation curves in southeastern Canada. Bulletin of the Seismological Society of America 82, 2014-2031.

Aylsworth, J.M., D.E. Lawrence and J. Guertin. 2000. Did two massive earthquakes in the Holocene induce widespread landsliding and near-surface deformation in part of the Ottawa Valley, Canada? Geology 28, 903-906.

Baranoski, M.T. 2002. Structure contour map on the Precambrian unconformity surface Ohio and related basement features. Ohio Geological Survey Map PG-23, Columbus, Ohio.

Baranoski, M.T., S.L. Dean, J.L. Wicks and V.M. Brown. 2009. Unconformity-bounded seismic reflection sequences define Grenville-age rift system and foreland basins beneath the Phanerozoic in Ohio. Geosphere 5, 140-151.

Barnett, P.J. 1992. Quaternary geology of Ontario. In Thurston, P.C., H.R. Williams, R.H. Sutcliffe and G.M. Stott (Eds.), Geology of Ontario. Ontario Geological Survey, Special Volume 4, Part 2, Chapter 21.

Bazzurro, P. and C.A. Cornell. 2004. Nonlinear soil-site effects in probabilistic seismic-hazard analysis. Bulletin of the Seismological Society of America 94, 2110-2123.

Behrendt, J.C., A.G. Green, W.F. Cannon, D.R. Hutchinson, M.W. Lee, B. Milkereit, W.F. Agena and C. Spencer. 1988. Crustal structure of the Midcontinent Rift System: results from GLIMPCE deep seismic reflection profiles. Geology 16, 81-85.

Benn, K., M. Warner, M. Ghassemi and J. Gilbert. 1994. Crustal structure and kinematic framework of the northwestern Pontiac subprovince, Quebec: an integrated structural and geophysical study. Canadian Journal of Earth Sciences 31, 271-281.

Bent, A.L. 1992. A re-examination of the 1925 Charlevoix, Quebec earthquake. Bulletin of the Seismological Society of America 82, 2097-2113.

Bent, A.L. 1996. Source parameters of the damaging Cornwall-Massena earthquake of 1944 from regional waveforms. Bulletin of the Seismological Society of America 86, 489-497,

Bent, A.L. 2010. Toward a moment magnitude catalog for earthquakes hazard assessment in eastern Canada (abs.). Seismological Research Letters 81, 354.

Beresnev, I.A, A.M. Nightengale and W.J. Silva. 2002. Properties of vertical ground motions. Bulletin of the Seismological Society of America 92, 3152-3164.

Bickford, M.E., W.R. Van Schmus and I. Zietz. 1986. Proterozoic history of the Midcontinent region of North America. Geology 14, 492-496.

Boatwright, J. 1994. Regional propagation characteristics and source parameters of earthquakes in northeastern North America. Bulletin of the Seismological Society of America 84, 1-15.

Bollinger, G.A. and R.L. Wheeler. 1983. The Giles County Seismic Zone. Science 219, 1063-1065.

Bollinger, G.A. and R.L. Wheeler. 1988. The Giles County, Virginia seismogenic zone – seismological results and geological interpretations. U.S. Geological Survey Professional Paper 1355.

Boore, D.M. 1983. Stochastic simulation of high-frequency ground motions based on seismological models of the radiated spectra. Bulletin of the Seismological Society of America 73, 1865-1894.

Boore, D.M. 2003. Simulation of ground motions using the stochastic method. Pure and Applied Geophysics 160, 635-676.

Boore, D.M. and G.M. Atkinson. 1987. Stochastic prediction of ground motion and spectral response parameters at hard-rock sites in eastern North America. Bulletin of the Seismological Society of America 77, 440-467.

Boore, D.M. and G.M. Atkinson. 2008. Ground-motion prediction equations for the average horizontal component of PGA, PGV, and 5%-damped PSA at spectral periods between 0.01 s and 10.0 s. Earthquake Spectra, v. 24, pp. 99-138.

Boyce, J.I. and W.A. Morris. 2002. Basement-controlled faulting of Paleozoic strata in southern Ontario, Canada: new evidence from geophysical lineament mapping. Tectonophysics 353, 151-171.

Brigham, R.J. 1971. Structural geology of southwestern Ontario and southeastern Michigan. Ontario Department of Mines and Northern Affairs, Petroleum Resource Section, Paper 71-2.

Brown, l., C. Ando, S. Klemperer, J. Oliver, S. Kaufman, B. Czuchra, T. Walsh and Y.W. Isachsen. 1983. Adirondack-Appalachian crustal structure: the COCORP Northeast Traverse. Geological Society of America Bulletin 94, 1173-1184.

Campbell, K.W. 1997. Empirical near-source attenuation relationships for horizontal and vertical components of peak ground acceleration, peak ground velocity, and pseudo-absolute acceleration response spectra. Bulletin of the Seismological Society of America 68, 154-176.

Campbell, K.W. 2003. Prediction of strong ground motion using the hybrid empirical method and its use in the development of ground-motion (attenuation) relations in eastern North America. Bulletin of the Seismological Society of America 93, 1012-1033.

Campbell, K.W. and Y. Bozorgnia. 2003. Updated near-source ground-motion (attenuation) relations for the horizontal and vertical components of peak ground acceleration and acceleration response spectra. Bulletin of the Seismological Society of America 93, 314-331.

Campbell, K.W. and Y. Bozorgnia. 2008. NGA ground motion model for the geometric mean horizontal component of PGA, PGV, PGD and 5% damped linear elastic response spectra for periods ranging from 0.01 to 10 s. Earthquake Spectra 24, 139-171.

Cannon, W.F. 1994. Closing of the midcontinent rift—A far-field effect of Grenvillian compression: Geology 22, 155-158.

Cannon, W.F., A.G. Green, D.R. Hutchinson, M. Lee, B. Milkereit, J.C. Behrendt, H.C. Halls, J.C. Green, A.B. Dickas, G.B. Morey, R. Sutcliffe and C. Spencer. 1989. The North American Midcontinent rift beneath Lake Superior from GLIMPCE seismic reflection profiling. Tectonics 8, 305-332.

Cannon, W.F., M.W. Lee, W.J. Hinze, K.J. Schulz and A.G. Green. 1991. Deep crustal structure of the Precambrian basement beneath northern Lake Michigan, midcontinent North America. Geology 19, 207-210.

Carr, S.D., R.M. Easton, R.A. Jamieson and N.G. Culshaw. 2000. Geologic transect across the Grenville orogen of Ontario and New York. Canadian Journal of Earth Sciences 37, 193-216.

Carter, T.R. and R.M. Easton. 1990. Extension of Grenville basement beneath southwestern Ontario: lithology and tectonic boundaries. In Subsurface geology of southwestern Ontario: a Core Workshop. Core Workshop 1990, Ontario Petroleum Institute, London, Ontario, 9-28.

Carter, T.R., R.A. Trevail and R.M. Easton. 1996. Basement controls on some hydrocarbon traps in southern Ontario, Canada. In van de Pluijm, B.A. and P.A. Catacosinos (Eds.), Basement and basins of eastern North America. Geological Society of America Special Paper 308, pp. 95-107.

Catacosinos, P.A., P.A. Daniels, Jr. and W.B. Harrison III. 1991. Structure, stratigraphy, and petroleum geology of the Michigan Basin. AAPG Memoir 51, Chapter 30, pp. 561-601.

Chiou, B.S.-J. and R.R. Youngs. 2008. An NGA model for the average horizontal component of peak ground motion and response spectra. Earthquake Spectra 24, 173-215.

Coppersmith, K.J. and R.R. Youngs. 1986. Capturing uncertainty in probabilistic seismic hazard assessment within intraplate tectonic environments. Proceedings of the Third U.S. National Conference on Earthquake Engineering 1, 301-312. Earthquake Engineering Research Institute.

Crone, A.J. and R.L. Wheeler. 2000. Data for Quaternary faults, liquefaction features and possible tectonic features in the central and eastern United States, east of the Rocky Mountain Front. U.S. Geological Survey Open-File Report 00-260.

Crough, S.T. 1981. Mesozoic hotspot epeirogeny in eastern North America. Geology 9, 2-6.

Culotta, R.C., T. Pratt and J. Oliver. 1990. A tale of two sutures: COCORP's deep seismic surveys of the Grenville Province in the eastern U.S. midcontinent. Geology 18, 646-649.

Cumming, J. and I.S. Al-Asam. 1999. Sediment characterization and porewater isotope chemistry of Quaternary deposits from the St. Clair delta, Ontario, Canada. Quaternary Research 51, 174-186.

Daniels, P.A., Jr. and R.D. Elmore. 1988. Upper Keweenawan rift-fill sequence, mid-continent rift system, Michigan. Michigan Basin Geological Society Field Trip Guidebook.

Dineva, S., D. Eaton and R. Mereu. 2004. Seismicity of the southern Great Lakes: revised earthquake hypocenters and possible tectonic controls. Bulletin of the Seismological Society of America 94, 1902-1918.

Doig, R. 1990. 2300 yr history of seismicity from silting events in Lake Tadoussac, Charlevoix, Quebec. Geology 18, 820-823.

Doig, R. 1991. Effects of strong seismic shaking in lake sediments, and earthquake recurrence interval, Témiscaming, Quebec. Canadian Journal of Earth Sciences 28, 1349-1352.

Doig, R. 1998. 3000-year paleoseismological record from the region of the 1988 Saguenay, Quebec, Earthquake. Bulletin of the Seismological Society of America 88, 1198-1203.

Du, W.-X., W.-Y. Kim and L.R. Sykes. 2003. Earthquake source parameters and state of stress for the northeastern United States and southeastern Canada from analysis of regional seismograms. Bulletin of the Seismological Society of America 93, 1633-1648.

DuBerger, R., D.W. Roy, M. Lamontagne, G. Woussen, R.G. North and R.J. Wetmiller. 1991. The Saguenay (Quebec) earthquake of November 25, 1988: seismologic data and geologic setting. Tectonophysics 186, 59-74.

Duncan, R.A. 1984. Age progressive volcanism in the New England Seamounts and the opening of the central Atlantic Ocean. Journal of Geophysical Research 89, 9980-9990.

Easton, R.M. 1992. The Grenville Province and the Proterozoic History of Central and Southern Ontario. In Thurston, P.C., H.R. Williams, R.H. Sutcliffe and G.M. Stott (Eds.), Geology of Ontario. Ontario Geological Survey, Special Volume 4, Part 2, Chapter 19.

Easton, R.M. and T.R. Carter. 1995. Geology of the Precambrian basement beneath the Paleozoic of southwestern Ontario. In Ojakangas, R.W., A.B. Dickas and J.C. Green (Eds.), Basement Tectonics 10, 221-264.

Eaton, D.W., S. Dineva and R. Mereu. 2006. Crustal thickness and VP/VS variations in the Grenville orogen (Ontario, Canada) from analysis of teleseismic receiver functions. Tectonophysics 420, 223-238.

Electric Power Research Institute (EPRI). 1988. Seismic Hazard Methodology for Central and Eastern United States, EPRI-NP 4726, 10 volumes.

Electric Power Research Institute (EPRI). 1993. Guidelines for Determining Design Basis Ground Motions. Electric Power Research Institute Report EPRI TR-102293.

Electric Power Research Institute (EPRI). 2004. CEUS Ground Motion Project Final Report. Technical Report 1009684, Palo Alto, California.

Electric Power Research Institute (EPRI). 2006. Program on Technology Innovation: Truncation of the Lognormal Distribution and Value of the Standard Deviation for Ground Motion Models in the Central and Eastern United States. Technical Report 1014381, Palo Alto, California.

Electric Power Research Institute and Seismic Owners Group (EPRI-SOG). 1988. Seismic Hazard Methodology for the Central and Eastern United States. Technical Report NP-4726-A. Electric Power Research Institute, Palo Alto, California, Vols. 1-10.

Eyles, N., J. Boyce and A.A. Mohajer. 1993. The bedrock surface of the western Lake Ontario region: evidence of reactivated basement structures? Geographie Physique et Quaternaire 473, 269-283.

Faill, R.T. 1997a. A geologic history of the north-central Appalachians, part 1: orogenesis from the Mesoproterozoic through the Taconic orogeny. American Journal of Science 297, 551-619.

Faill, R.T. 1997b. A geologic history of the north-central Appalachians, part 2: the Appalachian basin from the Silurian through the Carboniferous. American Journal of Science 297, 729-761.

Faill, R.T. 1998. A geologic history of the north-central Appalachians, part 3: the Alleghany orogeny. American Journal of Science 298, 131-179.

Fakundiny, R.H. and P.W. Pomeroy. 2002. Seismic-reflection profiles of the central part of the Clarendon-Linden fault system of western New York in relation to regional seismicity. Tectonophysics 353, 173-213.

Faure, S., A. Tremblay and J. Angelier. 1996a. Alleghenian paleostress reconstruction in the northern Appalachians: intraplate deformation between Laurentia and Gondwana. GSA Bulletin 108, 1467-1480.

Faure, S., A. Tremblay and J. Angelier. 1996b. State of intraplate stress and tectonism of northeastern America since Cretaceous times, with particular emphasis on the New England–Quebec igneous province. Tectonophysics 255, 111-134.

Faure, S., A. Tremblay and M. Malo. 2004. Reconstruction of Taconian and Acadian paleostress regimes in the Quebec and northern New Brunswick Appalachians. Canadian Journal of Earth Sciences 41, 619-634.

Faure, S., A. Tremblay, M. Malo and J. Angelier. 2006. Paleostress analysis of Atlantic crustal extension in the Quebec Appalachians. The Journal of Geology 114, 435-448.

Faust, T.H., K. Fujita, K.G. Mackey, L.J. Ruff and R.C. Ensign. 1997. The September 2, 1994 central Michigan earthquake. Seismological Research Letters 68, 460-464.

Filion, L., F. Quinty and C. Bégin. 1991. A chronology of landslide activity in the valley of Rivierre du Gouffre, Charlevoix, Quebec. Canadian Journal of Earth Sciences 28, 103-118.

Fletcher, J.B. and L.R. Sykes. 1977. Earthquakes related to hydraulic mining and natural seismicity in western New York state. Journal of Geophysical Research 82, 3767-3780.

Forsyth, D.A. 1981. Characteristics of the western Quebec seismic zone. Canadian Journal of Earth Sciences 18, 103-118.

Forsyth, D.A., B. Milkereit, A. Davidson, S. Hanmer, D.R. Hutchinson, W.J. Hinze and R.F. Mereu. 1994a. Seismic images of a tectonic subdivision of the Grenville orogen beneath Lakes Ontario and Erie. Canadian Journal of Earth Sciences 31, 229-242.

Forsyth, D.A., B. Milkereit, C.A. Zelt, D.J. White, R.M. Easton and D.R. Hutchinson. 1994b. Deep structure beneath Lake Ontario: crustal-scale Grenville subdivisions. Canadian Journal of Earth Sciences 31, 255-270.

Fujita, K. and N.H. Sleep. 1991. A re-examination of the seismicity of Michigan. Tectonophysics 186, 75-106.

Gardner, J.K. and L. Knopoff. 1974. Is the sequence of earthquakes in Southern California, with aftershocks removed, Poissonian? Bulletin of the Seismological Society of America 80, 757-783.

Gauthier, E.L. and K. Benn. 1996. Investigating a possible structural linkage between Lake Ontario and the St. Lawrence fault zone: geological and remote sensing studies. Geological Society of America Abstracts with Programs, Northeastern Section, 57.

Geomatrix Consultants, Inc. 1997a. Seismic Hazard in Southern Ontario, Final Report, Part 1: Seismic Source Models, Recurrence Models and Ground Motion Attenuation Models. Prepared for the Atomic Energy Control Board of Canada, March.

Geomatrix Consultants, Inc. 1997b. Seismic Hazard in Southern Ontario, Final Report, Part 2: Seismic Hazard Results and Sensitivity. Prepared for the Atomic Energy Control Board of Canada.

Grandjean, G., H. Wu, D. White, M. Mareschal and C. Hubert. 1995. Crustal velocity models for the Archean Abitibi Greenstone Belt from seismic refraction data. Canadian Journal of Earth Sciences 32, 149-166.

Green, A.G., B. Milkereit, A. Davidson, C. Spencer, D.R. Hutchinson, W.F. Cannon, M.W. Lee, W.F. Agena, J.C. Behrendt and W.J. Hinze. 1988. Crustal structure of the Grenville Front and adjacent terranes. Geology 16, 788-792.

Grier, M.E. 1995. Brittle faulting along the St. Lawrence Valley from Kingston to Cornwall. Atomic Energy Control Board Report, INFO-0578.

Gupta, I.N. and K.L. McLaughlin. 1987. Attenuation of ground motion in the Eastern United States. Bulletin of the Seismological Society of America 77, 366-383.

Gutenberg, B. and C.F. Richter. 1956. Earthquake magnitude; Intensity, energy and acceleration. Bulletin of the Seismological Society of America 46, 105-145.

Halchuk, S. 2009. Seismic Hazard Earthquake Epicentre File (SHEEF) used in the fourth generation seismic hazard maps of Canada. Geological Survey of Canada, Open File 6208.

Halchuk, S., and J. Adams. 2008. Fourth generation seismic hazard maps of Canada: Maps and Grid Values to be used with the 2005 National Building Code of Canada, Geological Survey of Canada, Open File Report 5813.

Hanmer, S. 1988. Ductile thrusting at mid-crustal level, southwestern Grenville Province. Canadian Journal of Earth Sciences 25, 1049-1059.

Harvard Global Centroid Moment Tensor (CMT) Catalog. Website, http://www.globalcmt.org/CMTfiles.html, Accessed May 7, 2009.

Hatcher, R.D., Jr. 1972. Developmental model for the southern Appalachians. GSA Bulletin 83, 2735-2760.

Hatcher, R.D., Jr., W.A. Thomas, P.A. Geiser, A.W. Snoke, S. Mosher and D.V. Wiltschko. 1989. Alleghenian orogen. In Hatcher, R.D., Jr., W.A. Thomas and G.W. Viele (Eds.), The Appalachian-Ouachita orogen in the United States. Geological Society of America, The Geology of North America F-2, Chapter 5, 233-318.

Hauser, E.C. 1996. Midcontinent rifting in a Grenville embrace. In van der Pluijm, B.A. and P.A. Catacosinos (Eds.), Basement and basins of eastern North America. Geological Society of America Special Paper 308, 67-75.

Heaman, L.M. and B.A. Kjarsgaard. 2000. Timing of eastern North American kimberlite magmatism: continental extension of the Great Meteor hotspot track? Earth and Planetary Science Letters 178, 253-268.

Herrmann, R.B. 1978. A seismological study of two Attica, New York earthquakes. Bulletin of the Seismological Society of America 68, 641-651.

Hildenbrand, T.G. and J.D. Hendricks. 1995. Geophysical Setting of the Reelfoot Rift and Relations between Rift Structures and the New Madrid Seismic Zone. U.S. Geological Survey Professional Paper 1538-E.

Hinze, W.J., R.L. Kellogg and N.W. O'Hara. 1975. Geophysical studies of the basement geology of southern peninsula of Michigan. AAPG Bulletin 59, 1562-1584.

Hoehn, M.H. 1991. An integrated geophysical study of the Grenville province in the greater Lake Erie region. M.S. thesis, Purdue University.

Hoffman, P.F. 1988. United plates of America, the birth of a craton: early Proterozoic assembly and growth of Laurentia. Annual Review of Earth and Planetary Science 16, 543-603.

Hoffman, P.F. 1989. Precambrian geology and tectonic history of North America. In Bally, A.W. and A.R. Palmer (Eds.), The geology of North America: an overview. Geological Society of America, The Geology of North America A, 447-512.

Howell, P.D. and B.A. van der Pluijm. 1990. Early history of the Michigan basin: subsidence and Appalachian tectonics. Geology 18, 1195-1198.

Howell, P.D. and B.A. van der Pluijm. 1999. Structural sequences and styles of subsidence in the Michigan basin. GSA Bulletin 111, 974-991.

Hughes, S. and J.H. Luetgert. 1991. Crustal structure of the western New England Appalachians and the Adirondack Mountains. Journal of Geophysical Research 96, 16471-16494.

Hynes, A., A. Indares, T. Rivers and A. Gobeil. 2000. Lithoprobe line 55: integration of out-of-plane seismic results with surface structure, metamorphism, and geochronology, and the tectonic evolution of the eastern Grenville Province. Canadian Journal of Earth Sciences 37, 341-358.

Idriss, I.M. 2008. An NGA empirical model for estimating the horizontal spectral values generated by shallow crustal earthquakes. Earthquake Spectra 24, 217-242.

INTERA. 2011. Descriptive Geosphere Site Model. Intera Engineering Ltd. report for the Nuclear Waste Management Organization NWMO DGR-TR-2011-24 R000. Toronto, Canada.

Jacobi, R.D. and J. Fountain. 1993. The southern extension and reactivations of the Clarendon-Linden fault system. Geographie Physique et Quaternaire 47, 285-302.

Jacobi, R.D. and J. Fountain. 2002. The character and reactivation history of the southern extension of the seismically active Clarendon-Linden Fault System, western New York State. Tectonophysics 353, 215-262.

Jacobi, R.D., C.F.M. Lewis, D.K. Armstrong and S.M. Blasco. 2007. Popup field in Lake Ontario south of Toronto, Canada: indicators of late glacial and postglacial strain. The Geological Society of America, Special Paper 425, 129-147.

Johnson, L.R. and W. Silva. 1981. The effects of unconsolidated sediments upon the ground motion during local earthquakes. Bulletin of the Seismological Society of America 71, 127-142.

Johnston, A.C. 1996a. Seismic moment assessment of earthquakes in stable continental regions—I: instrumental seismicity. Geophysical Journal International 124, 381-414.

Johnston, A.C. 1996b. Seismic moment assessment of earthquakes in stable continental regions—II: historical seismicity. Geophysical Journal International 125, 639-678.

Johnston, A.C., D.J. Reinbold and S.I. Brewer. 1985. Seismotectonics of the Southern Appalachians. Bulletin of the Seismological Society of America 75, 291-312.

Johnston, A.C., K.J. Coppersmith, L.R. Kanter and C.A. Cornell. 1994. The Earthquakes of Stable Continental Regions: Final Report Submitted to Electric Power Research Institute (EPRI): TR-102261. Palo Alto, California.

Kamo, S.L., T.E. Krogh and P.S. Kumarapeli. 1995. Age of the Grenville dyke swarm, Ontario-Quebec: implications for the timing of Iapetan rifting. Canadian Journal of Earth Sciences 32, 273-280.

Keefer, D.L. and S.E. Bodily. 1983. Three-point approximations for continuous random variables. Management Science 29, 595-609.

Keller, G.R., E.G. Lidiak, W.J. Hinze and L.W. Braile. 1983. The role of rifting in the tectonic development of the mid-continent, U.S.A. Tectonophysics 94, 391-412.

Kellett, R.L., A.E. Barnes and M. Rive. 1994. The deep structure of the Grenville Front: a new perspective from western Quebec. Canadian Journal of Earth Sciences 31, 282-292.

Kim, W.-Y, S. Dineva, S. Ma and D. Eaton. 2006. The 4 August 2004, Lake Ontario, earthquake. Seismological Research Letters 77, 65-73.

Klitgord, K.D., D.R. Hutchinson and H. Schouten. 1988. U.S. Atlantic continental margin; Structural and tectonic framework. In Sheridan, R.E. and J.A. Grow (Eds.), The Atlantic continental margin, U.S. Geological Society of America, The Geology of North America I-2, 19-55.

Kumarapeli, P.S. 1985. Vestiges of Iapetan rifting in the craton west of the northern Appalachians. Geoscience Canada 12, 54-59.

Kumarapeli, P.S. 1993. A plume-generated segment of the rifted margin of Laurentia, southern Canadian Appalachians, seen through a completed Wilson cycle. Tectonophysics 219, 47-55.

Kumarapeli, P.S. and V.A. Saull. 1966. The St. Lawrence Valley system: a North American equivalent of the East African Rift Valley system. Canadian Journal of Earth Sciences 3, 639-658.

Lamontagne, M. and G. Ranalli. 1996. Thermal and rheological constraints on the earthquake depth distribution in the Charlevoix, Canada, intraplate seismic zone. Tectonophysics 257, 55-69.

Lamontagne, M. and G. Ranalli. 1997. Faults and spatial clustering of earthquakes near La Malbaie, Charlevoix seismic zone, Canada. Seismological Research Letters 68, 337-352.

Lamontagne, M., P. Keating and S. Perreault. 2003. Seismotectonic characteristics of the lower St. Lawrence seismic zone, Quebec: insights from geology, magnetics, gravity, and seismics. Canadian Journal of Earth Sciences 40, 317-336.

Larsen, C.E. 1985. Lake level, uplift, and outlet incision, the Nipissing and Algoma great lakes. In Karrow, P.F. and P.E. Calkin (Eds.). Quaternary Evolution of the Great Lakes, Geological Association of Canada, Special Paper 30, 63-76.

Lemieux, Y., A. Tremblay and D. Lavoie. 2003. Structural analysis of supracrustal faults in the Charlevoix area, Quebec: relation to impact cratering and the St-Laurent fault system. Canadian Journal of Earth Sciences 40, 221-235.

Lewis, C.F.M., G.D.M. Cameron, E.L. King, B.J. Todd and S.M. Blasco. 1995. Structural contour, isopach and feature maps of Quaternary sediments in western Lake Ontario. Atomic Energy Control Board Report, INFO-0555.

Li, A., D.W. Forsyth and K.M. Fischer. 2003. Shear velocity structure and azimuthal anisotropy beneath eastern North America from Rayleigh wave inversion. Journal of Geophysical Research 108. 1-24.

Lucius, J.E. and R.R.B. Von Frese. 1988. Aeromagnetic and gravity anomaly constraints on the crustal geology of Ohio. Geological Society of America Bulletin 100, 104-116.

Lund, B. and J.O. Naslund. 2009. Glacial isostatic adjustment: implications for glacially induced faulting and nuclear waste repositories. In C.B. Connor, N.A. Chapman and L.J. Connor (Eds.), Volcanic and tectonic hazard assessment for nuclear facilities. Cambridge University Press, 142-155.

Ma, S. and D.W. Eaton. 2007. Western Quebec seismic zone (Canada): clustered, midcrustal seismicity along a Mesozoic hot spot track. Journal of Geophysical Research 112. B06305, 1 - 16.

Ma, S. and G. Atkinson. 2006. Focal depths for small to moderate earthquakes ($m_N < 2.8$) in western Quebec, southern Ontario, and northern New York. Bulletin of the Seismological Society of America 96, 609-623.

Ma, S., D.W. Eaton and J. Adams. 2008. Intraplate seismicity of a recently deglaciated shield terrane: a case study from northern Ontario, Canada. Bulletin of the Seismological Society of America 98, 2828-2848.

Macheridas, A. 2002. The development of a moment-magnitude based earthquake catalog for the northeastern United States. M.Sc. Thesis. Boston College, U.S.

Mazzotti, S. and J. Adams. 2005. Rates and uncertainties on seismic moment and deformation in eastern Canada. Journal of Geophysical Research 110.

McFall, G. H. and A. Allam, 1990. Neotectonic investigations in southern Ontario: Prince Edward County – Phase I: Atomic Energy Control Board. Technical Report INFO-0343.

McFall, G.H. 1993. Structural elements and neotectonics of Prince Edward County, southern Ontario. Geographie Physique et Quaternaire 47, 303-312.

McFall, G.H. and A. Allam. 1991. Neotectonic investigations in southern Ontario: Prince Edward County – Phase II: Atomic Energy Control Board. Technical Report INFO-0343-2.

McGuire, R.K., W.J. Silva and C.J. Costantino. 2001. Technical Basis for Revision of Regulatory Guidance on Design Ground Motions: Hazard- and Risk-Consistent Ground Motion Spectra Guidelines. NUREG/CR-6728, U.S. Nuclear Regulatory Commission, Washington, D.C.

McGuire, R.K., W.J. Silva and C.J. Costantino. 2002. Technical Basis for Revision of Regulatory Guidance on Design Ground Motions: Development of Hazard- and Risk-Consistent Seismic Spectra for Two Sites. U.S. Nuclear Regulatory Commission NUREG/CR-6769.

McHone, J.G. 1996. Constraints on the mantle plume model for Mesozoic Alkaline intrusions in northeastern North America. The Canadian Mineralogist 34, 325-334.

McQuest Marine Sciences Ltd. 1995. The geophysical survey of Lake Ontario in 1993: report prepared for the Atomic Energy Control Board, Ottawa, Canada. AECB Project No. 2.243.3.

Mereu, R.F., D. Epili and A.G. Green. 1990. Pg Shingles: preliminary results from the onshore GLIMPCE refraction experiment. Tectonophysics 173, 617-626.

Mereu, R.F., D. Wang, O. Kuhn, D.A. Forsyth, A.G. Green, P. Morel, G.G.R. Buchbinder, D. Crossley, E. Schwarz, R. duBerger, C. Brooks and R. Clowes. 1986. The 1982 COCRUST seismic experiment across the Ottawa-Bonnechere graben and Grenville Front in Ontario and Quebec. Geophysical Journal International 84, 491-514.

Mereu, R.F., H.W. Asmis, B. Dunn, J. Brunet, D. Eaton, S. Dineva and A. Yapp. 2002. The seismicity of the western Lake Ontario area: results from the Southern Ontario Seismic Network (SOSN), 1992-2001. Seismological Research Letters 73, 534-551.

Metzger, A.G., J.G. Armbruster and L. Seeber. 2000. Documentation, Location and Size-Estimation of “New” Historical Earthquakes in the Central United States: Continuation. Final technical report, U.S. Geological Survey Contract No. 1434-HQ-97-GR-03064.

Milkereit, B., D.A. Forsyth, A.G. Green, A. Davidson, S. Hanmer, D.R. Hutchinson, W.J. Hinze and R.F. Mereu. 1992. Seismic images of a Grenvillian terrane boundary. Geology 20, 1027-1030.

Moench, R.H. and J.N. Aleinikoff. 2002. Stratigraphy, geochronology, and accretionary terrane settings of two Bronson Hill arc sequences, northern New England. Physics and Chemistry of the Earth 27, 47-95. Republished (because of editorial errors) in 2003: Physics and Chemistry of the Earth 28, 113-160.

Mohajer, A., N. Eyles and C. Rogojina. 1992. Neotectonic faulting in metropolitan Toronto: implications for earthquake hazard assessment in the Lake Ontario region. Geology 20, 1003-1006.

Mohajer, A.A. 1993. Seismicity and seismotectonics of the western Lake Ontario region. Geographie Physique et Quaternaire 47, 353-362.

Morgan, W.J. 1983. Hotspot tracks and the early rifting of the Atlantic. Tectonophysics 94, 123-139.

Murphy, J.B. and J.D. Keppie. 2005. The Acadian orogeny in the northern Appalachians. International Geology Review 47, 663-687.

O'Dowd, C.R., D. Eaton, D. Forsyth and H.W. Asmis. 2004. Structural fabric of the Central Metasedimentary Belt of southern Ontario, Canada, from deep seismic profiling. Tectonophysics 388, 145-159.

Onasch, C.M. and C.F. Kahle. 1991. Recurrent tectonics in a cratonic setting: an example from northwestern Ohio. Geological Society of America Bulletin 103, 1259-1269.

Ontario Geological Survey. 1991. Bedrock geology of Ontario – southern sheet. Map 2544, Scale 1:1,000,000.

OPG. 2001. Southern Ontario Seismic Network – Seismic Hazard Resolution Project. Ontario Power Generation Report N-REP-02004-10003, Rev. 00. Toronto, Canada.

Ouassaa, K. and D. Forsyth. 2002. Interpretation of seismic and potential field data from western New York State and Lake Ontario. Tectonophysics 353, 115-149.

Ouassaa, K., D. Forsyth and D. White. 2002. The 2000 Southern Ontario Seismic Project. Geological Survey of Canada, Current Research Report 2002-E9.

Pehme, P. and M. Melaney. 2010. Borehole Geophysical Logging in DGR-1 and DGR-2. Intera Engineering Ltd. Report TR-07-08 Rev.3. Ottawa, Canada.

Petersen, M.D., A.D. Frankel, S.C. Harmsen, C.S. Mueller, K.M. Haller, R.L. Wheeler, R.L. Wesson, Y. Zeng, O.S. Boyd, D.M. Perkins, N. Luco, E.H. Field, C.J. Wills and K.S. Rukstales. 2008. Documentation for the 2008 update of the United States national seismic hazard maps. U.S. Geological Survey, Open-File Report 2008-1128.

Pomeroy, P.W., D.W. Simpson and M.L. Sbar. 1976. Earthquakes triggered by surface quarrying—the Wappingers Falls, New York, sequence of June, 1974. Bulletin of the Seismological Society of America 66, 685-700.

Poole, W.H., B.V. Sanford, H. Williams and D.G. Kelley. 1970. Geology of southeastern Canada. In Douglas, R.J.W. (Eds.), Geology and Economic Minerals of Canada. Geological Survey of Canada Economic Geology Report No. 1, 228-304.

Powell, C.A., G.A. Bollinger, M.C. Chapman, M.S. Sibol, A.C. Johnston and R.L. Wheeler. 1994. A seismotectonic model for the 30-kilometer-long Eastern Tennessee seismic zone. Science 264, 686-688.

Pratt, T., R. Culotta, E. Hauser, D. Nelson, L. Brown, S. Kaufman, J. Oliver and W. Hinze. 1989. Major Proterozoic basement features of the eastern midcontinent of North America revealed by recent COCORP profiling. Geology 17, 505-509.

Puffer, J.H. 2002. A late neoproterozoic eastern Laurentian superplume: location, size, chemical composition, and environmental impact. American Journal of Science 302, 1-27.

Rankin, D.W. 1976. Appalachian salients and recesses: late Precambrian continental breakup and the opening of the Iapetus Ocean. Journal of Geophysical Research 81, 5605-5619.

Rankin, D.W., J.R. Chiarenzelli, A.A. Drake, Jr., R. Goldsmith, L.M. Hall, W.J. Hinze, Y.W. Isachsen, E.G. Lidiak, J. McLelland, S. Mosher, N.M. Ratcliffe, D.T. Secor, Jr. and P.R. Whitney. 1993. Chapter 5—Proterozoic rocks east and southeast of the Grenville front: in Reed, J.C., Jr., M.E. Bickford, R.S. Houston, P.K. Link, D.W. Rankin, P.K. Sims and W.R. Van Schmus (Eds.), Precambrian: Conterminous U.S. Geological Society of America, The Geology of North America C-2, 335-461.

Rimando, R.E. and K. Benn. 2005. Evolution of faulting and paleo-stress field within the Ottawa graben, Canada. Journal of Geodynamics 39, 337-360.

Rivers, T. 1997. Lithotectonic elements of the Grenville province: review and tectonic implications. Precambrian Research 86, 117-154.

Rivers, T. and D. Corrigan. 2000. Convergent margin on southeastern Laurentia during the Mesoproterozoic: tectonic implications. Canadian Journal of Earth Sciences 37, 359-383.

Rivers, T., J. Martignole, C.F. Gower and A. Davidson. 1989. New tectonic divisions of the Grenville Province, southeast Canadian Shield. Tectonics 8, 63-84.

Rocher, M., A. Tremblay, D. Lavoie and A. Campeau. 2003. Brittle fault evolution of the Montréal area (St Lawrence Lowlands, Canada): rift-related structural inheritance and tectonism approached by palaeostress analysis. Geological Magazine 140, 157-172.

Roden-Tice, M.K. and R.P. Wintsch. 2002. Early Cretaceous normal faulting in southern New England: evidence from apatite and zircon fission-track ages. The Journal of Geology 110, 159-178.

Roden-Tice, M.K. and S.J. Tice. 2005. Regional-scale mid-Jurassic to Late Cretaceous unroofing from the Adirondack Mountains through central New England based on apatite fission-track and (U-Th)/He thermochronology. The Journal of Geology 113, 535-552.

Roden-Tice, M.K., D.P. West, Jr., J.K. Potter, S.M. Raymond and J.L. Winch. 2009. Presence of a long-term lithospheric thermal anomaly: evidence from apatite fission-track analysis in northern New England. The Journal of Geology 117, 627-641.

Roden-Tice, M.K., S.J. Tice and I.S. Schofield. 2000. Evidence for differential unroofing in the Adirondack Mountains, New York State, determined by apatite fission-track thermochronology. The Journal of Geology 108, 155-169.

Roest, W.R. 1995. Interpretation of aeromagnetic and gravity anomalies in the Precambrian Shield of southern Ontario. Program, List of Participants and Abstracts from the Atomic Energy Control Board Workshop on Seismic Hazard Assessment in Southern Ontario, Ottawa, Ontario, June 19-21, INFO-0604-1, C11-C22.

Rondenay, S., M.G. Bostock, T.M. Hearn, D.J. White, H. Wu, G. Sénéchal, S. Ji and M. Mareschal. 2000. Teleseismic studies of the lithosphere below the Abitibi-Grenville lithoprobe transect. Canadian Journal of Earth Sciences 37, 415-426.

Root, S. and C.M. Onasch. 1999. Structure and tectonic evolution of the transitional region between the central Appalachian foreland and interior cratonic basins. Tectonophysics 305, 205-223.

Ruff, L., R. LaForge, R. Thorson, T. Wagner and F. Goudaen. 1994. Geophysical Investigations of the Western Ohio-Indiana Region. Final Report, NUREG/CR-3145, Vol. 10, RA.

Rutty, A.L. and A.R. Cruden. 1993. Pop-up structures and the fracture pattern in the Balsam Lake area, southern Ontario. Geographie Physique et Quaternaire 47, 379-388.

Sadigh, K., C.-Y. Chang, N.A. Abrahamson, S.J. Chiou and M.S. Power. 1993. Specification of long-period ground motions: updated attenuation relationships for rock site conditions and adjustment factors for near-fault effects. Proceedings of ATC-17-1 Seminar on Seismic Isolation, Passive Energy Dissipation, and Active Control, San Francisco, California, March 11-12, 2, 59-70.

Sanford, B.V. 1993. Stratigraphic and structural framework of upper Middle Ordovician rocks in the Head Lake–Burleigh Falls area of south-central Ontario. Geographie Physique et Quaternaire 47, 253-268.

Sanford, B.V. 1995. Stratigraphy and structure of Paleozoic rocks beneath western Lake Ontario. Atomic Energy Control Board Report, INFO-0613.

Sanford, B.V., F.J. Thompson and G.H. McFall. 1985. Plate tectonics—a possible controlling mechanism in the development of hydrocarbon traps in southwestern Ontario. Bulletin of Canadian Petroleum Geology 33, 52-71.

Sbar, M.L. and L.R. Sykes. 1973. Contemporary compressive stress and seismicity in eastern North America: an example of intra-plate tectonics. Geological Society of America Bulletin 84, 1861-1882.

Seeber, L. and J. Armbruster. 1995. Seismogenesis and structure in the Lake Erie–Lake Ontario region of the U.S. from a global perspective. Program, List of Participants and Abstracts from the Atomic Energy Control Board Workshop on Seismic Hazard Assessment in Southern Ontario, Ottawa, Ontario, June 19-21, INFO-0604-1, D5-D20.

Seeber, L. and J.G. Armbruster. 1991. The NCEER-91 Earthquake Catalog: Improved Intensity-Based Magnitudes and Recurrence Relations for U.S. Earthquakes East of New Madrid. NCEER-91-0021, National Center for Earthquake Engineering Research.

Seeber, L. and J.G. Armbruster. 1993. Natural and induced seismicity in the Lake Erie–Lake Ontario region: reactivation of ancient faults with little neotectonic displacement. Géographie Physique et Quaternaire 47, 363-378.

Sella, G.F., S. Stein, T.H. Dixon, M. Craymer, R.S. James, S. Mazzotti and R.K. Dokka. 2007. Observation of glacial isostatic adjustment in “stable” North America with GPS. Geophysical Research Letters 34, L02306.

Senior Seismic Hazard Analysis Committee (SSHAC). 1997. Recommendations for Probabilistic Seismic Hazard Analysis: Guidance on Uncertainty and Use of Experts. U.S. Nuclear Regulatory Commission, NUREG/CR-6372.

Silva, W., N. Gregor and R. Darragh. 2003. Development of regional hard rock attenuation relations for central and eastern North America, mid-continent and Gulf Coast areas. Unpublished report by Pacific Engineering and Analysis.

Silva, W.J. 1976. Body waves in a layered anelastic solid. Bulletin of the Seismological Society of America 66, 1539-1554.

Silva, W.J. 1992. Factors controlling strong ground motions and their associated uncertainties. In Seismic and Dynamic Analysis and Design Considerations for High Level Nuclear Waste Repositories, ASCE 132-161.

Silva, W.J. 1997. Characteristics of vertical strong ground motions for applications to engineering design. In Friedland, I.M., M.S. Power and R.L. Mayes (Eds.), Proceedings of the FHWA/NCEER Workshop on the Representation of Seismic Ground Motion for New and Existing Highway Facilities. Technical Report NCEER-97-0010.

Silva, W.J. and K. Lee. 1987. WES RASCAL Code for Synthesizing Earthquake Ground Motions. State-of-the-Art for Assessing Earthquake Hazards in the United States series Report 24, U.S. Army Engineers Waterways Experiment Station, Miscellaneous Paper S-73-1.

Silva, W.J., N. Abrahamson, G. Toro, and C. Costantino. 1996. Description and Validation of the Stochastic Ground Motion Model. Unpublished report submitted to Brookhaven National Laboratory, Associated Universities, Inc.. Upton, New York.

Silva, W.J., T. Turcotte and Y. Moriwaki. 1986. Soil Response to Earthquake Ground Motions. EPRI Research Project RP 2556-07, Electric Power Research Institute. Palo Alto, California.

Silverman, B.W. 1986. Density Estimation for Statistics and Data Analysis. Chapman and Hall. London, England.

Slattery, S. 2011. Neotectonic Features and Landforms Assessment. Nuclear Waste Management Organization Report NWMO DGR-TR-2011-19 R000. Toronto, Canada.

Sleep, N.H. 1990. Monteregian hotspot track: a long-lived mantle plume. Journal of Geophysical Research 95, 21983-21990.

Smith, W.E.T. 1962. Earthquakes of eastern Canada and adjacent areas 1534-1927. Publications of the Dominion Observatory, Ottawa 26.

Smith, W.E.T. 1966. Earthquakes of eastern Canada and adjacent areas 1928-1959. Publications of the Dominion Observatory, Ottawa 32.

Somerville, P., N. Collins, N. Abrahamson, R. Graves and C. Saikia. 2001. Ground Motion Attenuation Relations for the Central and Eastern United States: Final Report to U.S. Geological Survey. URS Group, Inc., Pasadena, California.

Sonley, E., and G.M. Atkinson. 2005. Empirical relationship between moment magnitude and Nuttli magnitude for small-magnitude earthquakes in southern Canada. Seismological Research Letters 76, 752-755.

St. Louis University Earthquake Center. Website http://www.eas.slu.edu/Earthquake_Center. Accessed on February 12, 2010.

St. Seymour, K. and P.S. Kumarapeli. 1995. Geochemistry of the Grenville dyke swarm: role of plume-source mantle in magma genesis. Contributions to Mineralogy and Petrology 120, 29-41.

St.-Julien, P., A. Slivitsky and T. Feininger. 1983. A deep structural profile across the Appalachians of southern Quebec. In Hatcher, R.D., Jr., H. Williams and I. Zeitz (Eds.), Contributions to the tectonics and geophysics of mountain chains. Geological Society of America, Memoir 158, 103-111.

Stark, T.J. 1997. The East Continent Rift complex: evidence and conclusions. In Ojakangas, R.W., A.B. Dickas and J.C. Green (Eds.), Middle Proterozoic to Cambrian rifting, central North America. Geological Society of America Special Paper 312, 253-266.

Sterling, S. 2010. Bedrock Formations in DGR-1 and DGR-2. Intera Engineering Ltd. Report TR-07-05 Rev.3. Ottawa, Canada.

Stock, C. and E.G.C. Smith. 2002. Adaptive kernel estimation and continuous probability representation of historical earthquake catalogs. Bulletin of the Seismological Society of America 92, 904-912.

Street, R.L. and F.T. Turcotte. 1977. A study of northeastern North American spectral moments, magnitudes, and intensities. Bulletin of the Seismological Society of America 67, pp. 599-614.

Thomas, R.L., J.L. Wallach, R.K. McMillan, J.R. Bowley, S. Frape, D. Keyes and A.A. Mohajer. 1993. Recent deformation in the bottom sediments of western and southeastern Lake Ontario and its association with major structures and seismicity. Geographie Physique et Quaternaire 47, 325-335.

Thurston, P.C. 1992a. Archean geology of Ontario: introduction. In Thurston, P.C., H.R. Williams, R.H. Sutcliffe and G.M. Stott (Eds.), Geology of Ontario. Ontario Geological Survey, Special Volume 4, Part 1, Ch. 4, 73-78.

Thurston, P.C. 1992b. Proterozoic geology of Ontario: introduction. In Thurston, P.C., H.R. Williams, R.H. Sutcliffe and G.M. Stott (Eds.), Geology of Ontario. Ontario Geological Survey, Special Volume 4, Part 1, Ch. 13, 543-546.

Toro, G.R. 1981. Biases in Seismic Ground Motion Prediction. Ph.D. Thesis. Massachusetts Institute of Technology, U.S.

Toro, G.R., N.A. Abrahamson and J.F. Schneider. 1997. Model of strong ground motions from earthquakes in central and eastern North America: best estimates and uncertainties. Seismological Research Letters 68, 41-57.

Trehu, A.M., K.D. Klitgord, D.S. Sawyer and R.T. Buffler. 1989. Atlantic and Gulf of Mexico continental margins. In Pakiser, L.C. and W.D. Mooney (Eds.), Geophysical framework of the continental United States. Geological Society of America Memoir 172, 349-382.

Tremblay, A. and N. Pinet. 2005. Diachronous supracrustal extension in an intraplate setting and the origin of the Connecticut Valley—Gaspé and Merrimack troughs, northern Appalachians. Geological Magazine 142, 7-22.

Tremblay, A. and S. Castonguay. 2002. Structural evolution of the Laurentian margin revisited (southern Quebec Appalachians): implications for the Salinian orogeny and successor basins. Geology 30, 79-82.

Tremblay, A. and Y. Lemieux. 2001. Supracrustal Faults of the St. Lawrence Rift System between Cap-Tourmente and Baie-Saint-Paul, Quebec. Geological Survey of Canada, Current Research 2001-D15.

Tremblay, A., B. Long and M. Massé. 2003. Supracrustal faults of the St. Lawrence rift system, Québec: kinematics and geometry as revealed by field mapping and marine seismic reflection data. Tectonophysics 369, 231-252.

Tremblay, A., G. Ruffet and S. Castonguay. 2000. Acadian metamorphism in the Dunnage zone of southern Qu´ebec, Northern Appalachians: 40Ar/39Ar evidence for collision diachronism. GSA Bulletin 112, 136–46.

Tuttle, M. 2006. Paleoseismic investigation of long-term rates of large earthquakes in the Charlevoix and proposed Rabaska site areas, Preliminary report. Prepared for Rabaska, Inc., October 9.

Tuttle, M.P. and G.M. Atkinson. 2010. Localization of large earthquakes in the Charlevoix seismic zone, Quebec, Canada, during the past 10,000 years. Seismological Research Letters 81, 140-147.

Tuttle, M.P., K. Dyer-Williams and N.L. Barstow. 2002. Paleoliquefaction study of the Clarendon-Linden fault system, western New York state. Tectonophysics 353, 263-286.

U.S. Nuclear Regulatory Commission (U.S. NRC). 2007. Regulatory Guide 1.208: A Performance-Based Approach to Define the Site-Specific Earthquake Ground Motions.

van der Pluijm, B.A. and K.A. Carlson. 1989. Extension in the Central Medisedimentary Belt of the Ontario Grenville: timing and tectonic significance. Geology 17, 161-164.

Van Schmus, W.R. 1992. Tectonic setting of the Midcontinent Rift System. Tectonophysics 213, 1-15.

Van Schmus, W.R., M.E. Bickford and A. Turek. 1996. Proterozoic geology of the east-central Midcontinent basement. In van der Pluijm, B.A. and P.A. Catacosinos (Eds.), Basement and Basins of Eastern North America, Geological Society of America Special Paper 308, 7-32.

Van Tyne, A.M. 1975. Clarendon-Linden structure, western New York. New York Geological Survey Open File Report, Albany, 1-10.

Wallach, J.L. 1990. Newly discovered geological features and their potential impact on Darlington and Pickering. Atomic Energy Control Board Report, INFO 0342.

Wallach, J.L. 1995. Characteristics of the Niagara-Pickering and Georgian Bay linear zones and their implications for a large magnitude earthquake in the vicinity of the Darlington and Pickering nuclear power plants, near Toronto. Program, List of Participants and Abstracts from the Atomic Energy Control Board Workshop on Seismic Hazard Assessment in Southern Ontario, Ottawa, Ontario, June 19-21. INFO-0604-1, C1-C5.

Wallach, J.L. and A.A. Mohajer. 1990. Integrated geoscientific data relevant to assessing seismic hazard in the vicinity of the Darlington and Pickering nuclear power plants. Proceedings of the Canadian Geotechnical Conference, Prediction and Performance in Geotechnique, October 10-12, 2, 679-686.

Wallach, J.L. and R.L. Thomas. 1996. Southern limit of the St. Lawrence fault zone and its seismic hazard implications for communities adjacent to Lake Ontario. Geological Society of America Abstracts with Programs, Northeastern Section, 108.

Wallach, J.L., A.A. Mohajer and R.L. Thomas. 1998. Linear zones, seismicity, and the possibility of a major earthquake in the intraplate western Lake Ontario area of eastern North America. Canadian Journal of Earth Sciences 35, 762-786.

Weichert, D.H. 1980. Estimation of the earthquake recurrence parameters for unequal observation periods for different magnitudes. Bulletin of the Seismological Society of America 70, 1337-1346.

Wells, D.L. and K.J. Coppersmith. 1994. New empirical relationships among magnitude, rupture length, rupture width, rupture area, and surface displacement. Bulletin of the Seismological Society of America 84, 974-1002.

West, D.P., Jr. and M.K. Roden-Tice. 2003. Late Cretaceous reactivation of the Norumbega fault zone, Maine: evidence from apatite fission-track ages. Geology 31, 649-652.

Wheeler, R.L. 1995. Earthquakes and the cratonward limit of Iapetan faulting in eastern North America. Geology 23, 105-108.

Wheeler, R.L. 1996a. Sources of seismic hazard near the eastern Great Lakes. Geological Society of America Abstracts with Programs, Northeastern Section, 110.

Wheeler, R.L. 1996b. Earthquakes and the southeastern boundary of the intact Iapetan Margin in eastern North America. Seismological Research Letters 67, 77-83.

Wheeler, R.L. and A.C. Johnston. 1992. Geologic implications of earthquake source parameters in central and eastern North America. Seismological Research Letters 63, 491-514.

White, D.J., D.A. Forsyth, I. Asudeh, S.D. Carr, H. Wu, R.M. Easton and R.F. Mereu. 2000. A seismic-based cross-section of the Grenville orogen in southern Ontario and western Quebec. Canadian Journal of Earth Sciences 37, 183-192.

White, D.J., R.M. Easton, N.G. Culshaw, B. Milkereit, D.A. Forsyth, S. Carr, A.G. Green and A. Davidson. 1994. Seismic images of the Grenville Orogen in Ontario. Canadian Journal of Earth Sciences 31, 293-307.

Whitmeyer, S.J. and K.E. Karlstrom. 2007. Tectonic model for the Proterozoic growth of North America. Geosphere 3, 220-259.

Winardhi, S. and R.F. Mereu. 1997. Crustal velocity structure of the Superior and Grenville provinces of the southeastern Canadian Shield. Canadian Journal of Earth Sciences 34, 1167-1184.

Wu, P. and P. Johnston. 2000. Can deglaciation trigger earthquakes in N. America? Geophysical Research Letters 27, 1323-1326.

Youngs, R.R. and K.J. Coppersmith. 1985. Implications of fault slip rates and earthquake recurrence models to probabilistic seismic hazard estimates. Bulletin of the Seismological Society of America 75, 939-964.

Zartman, R.E. 1977. Geochronology of some alkalic rock provinces in eastern and central United States. Annual Review of Earth and Planetary Sciences 5, 257-286.

Zelt, C.A., D.A. Forsyth, B. Milkereit, D.J. White, I. Asudeh and R.M. Easton. 1994. Seismic structure of the Central Metasedimentary Belt, southern Grenville province. Canadian Journal of Earth Sciences 31, 243-254.

Zhu, T.-F. and L.D. Brown. 1986. Consortium for continental reflection profiling Michigan surveys: reprocessing and results. Journal of Geophysical Research 91, 11477-11495.

Zoback, M.L. 1992. Stress field constraints on intraplate seismicity in eastern North America. Journal of Geophysical Research 97, 11761-11782.

Zoback, M.L., S.R. Nishenko, R.M. Richardson, H.S. Hasegawa and M.D. Zoback. 1986. Mid-plate stress, deformation, and seismicity. In Vogt, P.R. and B.E. Tucholke (Eds.), The western North Atlantic region. Geological Society of America, The Geology of North America M, 297-312.

Zoback, M.L. and M.D. Zoback. 1991. Tectonic stress field of the continental United States. In Pakiser, L.C. and W.D. Mooney (Eds.), Geophysical framework of the continental United States, Boulder Colorado. Geological Society of America Memoir 172, 523-541.

8. ABBREVIATIONS AND ACRONYMS

AEF	Annual Exceedance Frequencies
ANSS	Advanced National Seismic Systems
CAB	Composite Arc Belt
CABBZ	Composite Arc Belt Boundary Zone
CENA	Central and Eastern North America
CEUS	Central and Eastern United States
CGB	Central Gneiss Belt
CMB	Central Metasedimentary Belt
CMBBZ	Central Metasedimentary Belt Boundary Zone
COCORP	Consortium for Continental Reflection Profiling
COCRUST	Canadian Consortium for Crustal Reconnaissance Using Seismic Techniques
DGR	Deep Geologic Repository
ECC	Extended Continental Crust
ECGH	East Continent Gravity High
ECRB	East Continent Rift Basin
EGBL	Erie–Georgian Bay Lineament
EHLZ	Erie-Huron Linear Zone
GBLZ	Georgian Bay Linear Zone
GFTZ	Grenville Front Tectonic Zone
GIA	Glacial Isostatic Adjustment.
GLIMPCE	Great Lakes International Multidisciplinary Program on Crustal Evolution
GMH	Great Meteor Hotspot
GMPE	Ground Motion Prediction Equations
GPS	Global Positioning System
GSC	Geological Survey of Canada
HLEL	Hamilton – Lake Erie Lineament
IRM	Iapetan Rifted Margin

MRS	Midcontinent Rift System
NAZ	Northern Appalachians
NBCC	National Building Code of Canada
NEDB	National Earthquake Data Base
NPLZ	Niagara-Pickering Linear Zone
PSHA	Probabilistic Seismic Hazard Assessment
SCR	Stable Continental Regions
SHEEF	Seismic Hazard Earthquake Epicentre File
SLRS	St. Lawrence Rift System
SSC	Seismic Source Characterization
SSHAC	Senior Seismic Hazard Advisory Committee
UHRS	Uniform Hazard Response Spectrum
WAU	Western Adirondack Uplift
WNA	Western North America

APPENDICES

THIS PAGE HAS BEEN LEFT BLANK INTENTIONALLY

APPENDIX A: EARTHQUAKE CATALOGUE

See enclosed CD

THIS PAGE HAS BEEN LEFT BLANK INTENTIONALLY

APPENDIX B: SPECTRAL MATCH DESIGN TIME HISTORIES

See enclosed CD